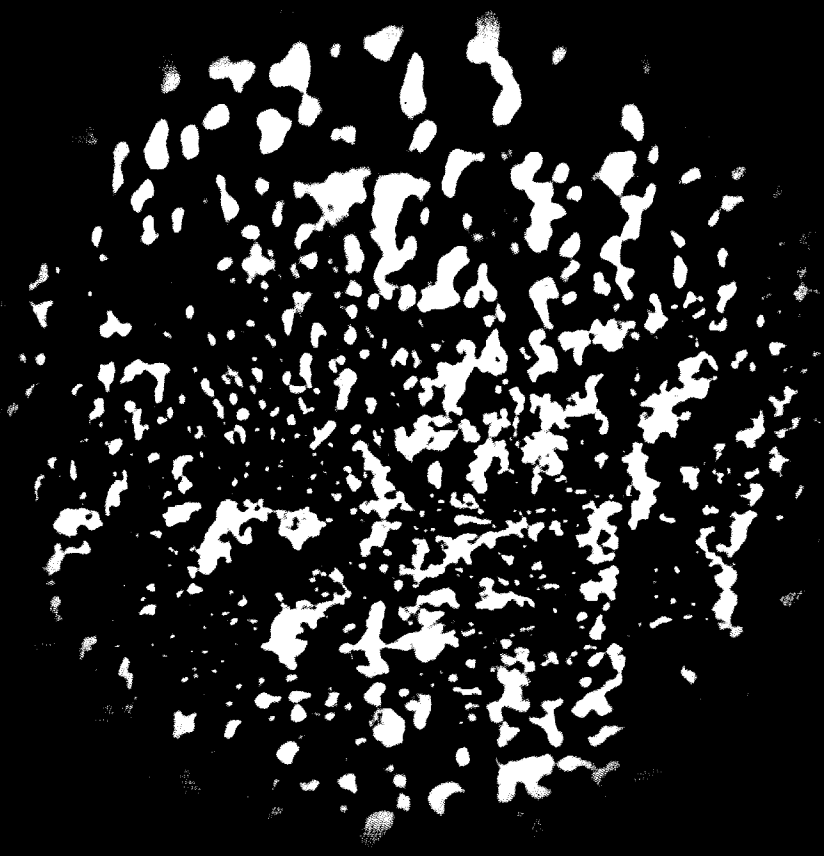
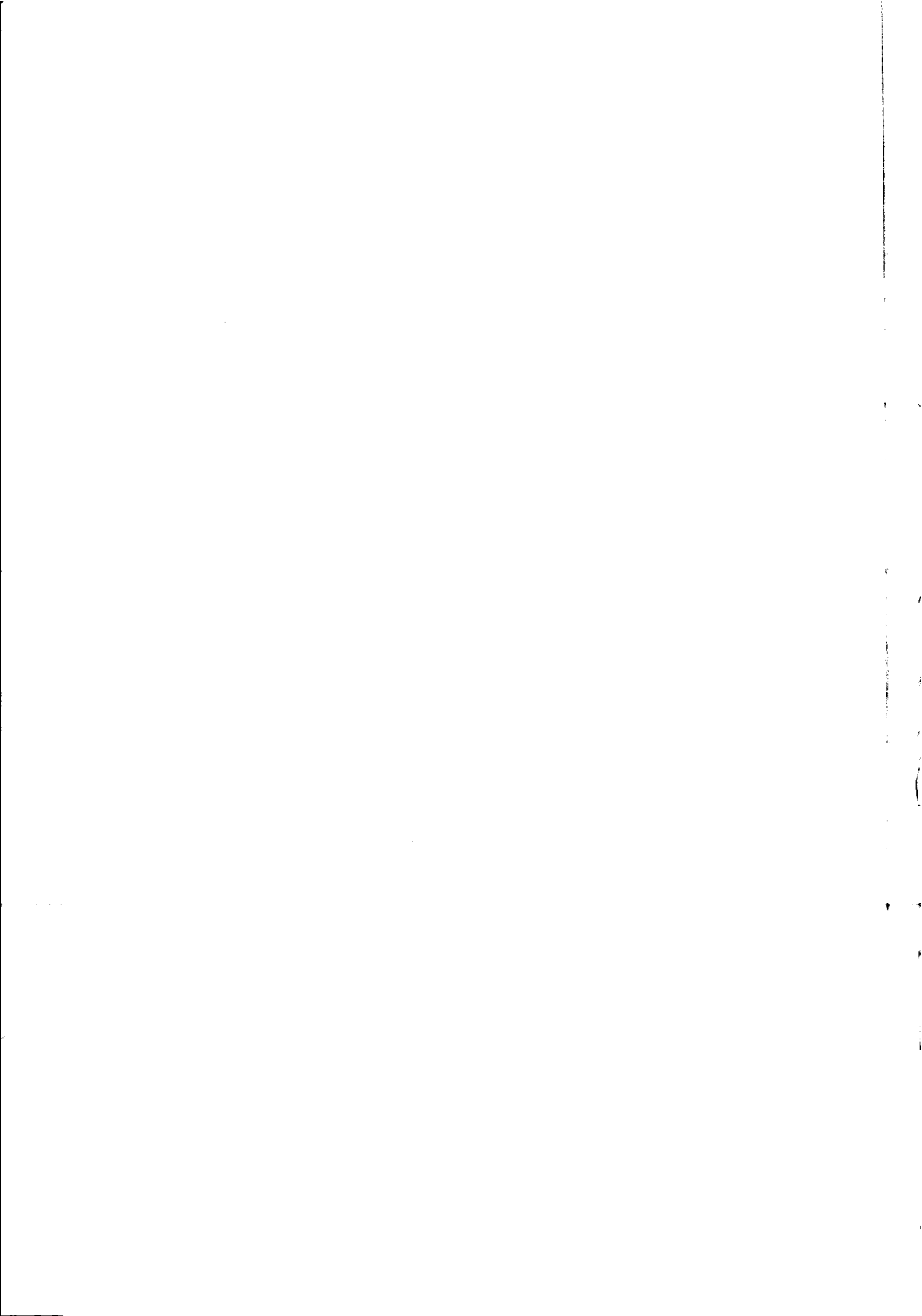


Fouling and Bioprotection of Metals



Rik Breur



Stellingen

behorende bij het proefschrift

Fouling and Bioprotection of Metals

1. Zonder kennis van biologische verschijnselen is het onmogelijk tot een goed begrip te komen van de toepassingsmogelijkheden van metalen in zeewater.
2. Als er leven wordt gevonden op Mars, dan is de kans groot dat dit afkomstig is van de Aarde.
(D.C. White et al., *Utilization of biomarkers to define microbial communities in biofilms and as contaminants of spacecraft searching for extraterrestrial life, Proc. 2nd European Union COST520 workshop on Biofouling and Materials, Sion (Zwitserland) 1999 pp. 41-69*)
3. De hoge kritische stroomdichtheid in supergeleidende $YBa_2Cu_3O_{7-\delta}$ films wordt veroorzaakt door mispassingsdislocaties die ontstaan door spanningsrelaxatie. Mispassingsdislocaties verhinderen namelijk de beweging van de gequantiseerde magnetische fluxlijnen en voorkomen daardoor de dissipatie van energie.
(J.M. Huijbregtse, *Proefschrift VU Amsterdam 2001 hoofdstuk 4*)
4. Het corrosiewerend effect van gedoteerd geleidend polypyrrool moet worden toegeschreven aan het "zelfopofferend" dedoteren van het polypyrrool.
5. Zoals Little e.a. hebben aangetoond, zegt de aanwezigheid van grote concentraties bacteriën op lokaal gecorrodeerde metalen niets over het al dan niet microbiologische karakter van de corrosie.
(B.J. Little et al., *Diagnosing microbiologically influenced corrosion, Proc. 7th Int. Symp. on Electrochemical Methods in Corrosion Research, Budapest 2000 lezing nr. E 192*)
6. Een kwalificatie van metalen naar hun gevoeligheid voor spleetcorrosie kan het beste worden uitgevoerd met kunstmatig zeewater.
7. Elektrochemische impedantiespectroscopie is een uitgelezen techniek om on-line corrosiemonitoring mee te bedrijven.
8. Het gebruik van bacteriën in corrosiebescherming zal leiden tot duurzame zelfreparerende deklagen.
9. Genetische manipulatie is voor de mensheid de enige mogelijkheid om op de lange termijn te overleven.
10. Veel van de publicistische acties van Greenpeace lijken eerder gericht op het verkrijgen van financiering, dan op de primaire zorg voor een schoner milieu en een duurzamer samenleving.
11. Formules in publicaties bevatten vaak fouten, een auteur kan daarom zijn formules beter zelf afleiden, in plaats van blindelings te vertrouwen op de literatuur.
12. Gezien de dominante rol van multinationals op het leven van alledag en het feit dat het leven niet uitsluitend om geld draait, is het verstandig om in de directies van deze grote bedrijven een meerderheid aan ingenieurs te benoemen.
13. De huidige bestrijding van MKZ is inhumain en uit de tijd. MKZ kan veel effectiever, preventief worden bestreden door in veestallen goede luchtfilters te installeren.

Propositions

Belonging to the dissertation

Fouling and Bioprotection of Metals

1. Without knowledge of biological phenomena, it is impossible to fully understand the applicability of metals in seawater.
2. If life is found on Mars, its most probable source of origin is Earth.
(D.C. White et al., *Utilization of biomarkers to define microbial communities in biofilms and as contaminants of spacecraft searching for extraterrestrial life*, Proc. 2nd European Union COST520 workshop on Biofouling and Materials, Sion (Switzerland) 1999 pp. 41-69)
3. The high critical current density in superconducting $\text{YBa}_2\text{Cu}_3\text{O}_{7-\delta}$ films is caused by misfit dislocations, which arise from stress relaxation. Misfit dislocations prevent the motion of the quantumized magnetic flux lines, and thus prevent the dissipation of energy.
(J.M. Huijbregtse, *PhD-thesis VU Amsterdam 2001 chapter 4*)
4. The corrosion protection of doped conductive polypyrrole must be ascribed to "self-sacrificial" dedoping of the polypyrrole.
5. As Little et al. have shown, the presence of a high concentration of bacteria at locally corroded metals does not necessarily imply that the corrosion process is of microbiological origin.
(B.J. Little et al., *Diagnosing microbiologically influenced corrosion*, Proc. 7th Int. Symp. on Electrochemical Methods in Corrosion Research, Budapest 2000 lecture no. E 192)
6. The ranking of metals regarding their sensitivity to crevice corrosion is done best with artificial seawater.
7. Electrochemical impedance spectroscopy is an outstanding technique for the on-line monitoring of corrosion.
8. The use of bacteria in corrosion protection will lead to sustainable self-repairing coatings.
9. Genetic engineering will in the end be the only way to survive for humanity.
10. The actions of Greenpeace often turn into fund raising media events. Its initiatives should instead all be focused on its prime task, the care for a cleaner environment and a more sustainable society.
11. Equations in publications often contain errors. Therefore an author can better derive her/his equations from scratch, rather than to put full trust in the literature.
12. In view of the dominant influence of multinationals on the society and the very fact that there is much more to live for than mere money making, it is advisable to have a majority of engineers in the boards of such companies.
13. The present control of foot and mouth disease is inhuman and outdated. The spread of FMD can be curbed much better preventatively by installing high quality air filters in the stables of farms.

Rik Breur
14 December 2001

3803111
766572
310290

Fouling and Bioprotection of Metals

**Monitoring and Control of Deposition Processes
in Aqueous Environments**

TR3799



TNO Industrial Technology

Cover:

Carbon steel covered with a bacterial biofilm with corrosion protective properties (Fig. 4.38)

Fouling and Bioprotection of Metals

**Monitoring and Control of Deposition Processes
in Aqueous Environments**

Aangroei en biologische bescherming van metalen

Monitoring en sturing van aangroeiprocessen in waterige milieus

PROEFSCHRIFT

ter verkrijging van de graad van doctor
aan de Technische Universiteit Delft,

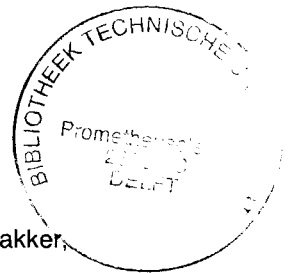
op gezag van de Rector Magnificus prof. ir. K.F. Wakker,
voorzitter van het College voor Promoties,

in het openbaar te verdedigen op vrijdag 14 december 2001 om 10.30 uur

door

Hendrik Jacobus Arie BREUR

materiaalkundig ingenieur,
geboren te Arnhem.



Dit proefschrift is goedgekeurd door de promotoren:

Prof. dr. ir. J. van Turnhout

Prof. dr. J.H.W. de Wit

Samenstelling promotiecommissie:

Rector Magnificus,

Prof. dr. J.H.W. de Wit,

Prof. dr. ir. J. van Turnhout,

Prof. dr. ir. M.C.M. van Loosdrecht

Prof. dr. P.L. Bonora

Prof. dr. J. Davenport

Prof. dr. W.F. Bogaerts

Ir. G.M. Ferrari

voorzitter

Technische Universiteit Delft, promotor

Technische Universiteit Delft, promotor

Technische Universiteit Delft

Università degli Studi, Trento, Italië

University College Cork, Ierland

Katholieke Universiteit Leuven, België

TNO Industrie

Copyright © 2001 by H.J.A. Breur.

All rights reserved

No part of the material protected by this copyright notice may be reproduced or utilised in any form or by any means, electronic or mechanical, including photocopying, recording or by any information storage retrieval system, without permission from the author.

ISBN 90-9015351-9

Printed in The Netherlands

Table of Contents

1	Introduction.....	1
1.1	Background and General Introduction.....	1
1.2	Outline of the Thesis.....	3
1.3	References.....	4
2	Biofouling on Surfaces.....	5
2.1	Introduction.....	5
	2.1.1 Biofouling Basics.....	6
	2.1.2 Biofouling Communities.....	7
	2.1.3 Barnacle Fouling Mechanisms.....	12
2.2	Sequence and Seasonality of Biofouling.....	15
	2.2.1 Introduction.....	15
	2.2.2 Experimental.....	15
	2.2.3 Results.....	17
	2.2.4 General Discussion.....	24
2.3	Modelling of Biofouling.....	25
	2.3.1 Introduction.....	25
	2.3.2 Data Handling.....	25
	2.3.3 Model Selection.....	30
	2.3.4 Modelling.....	35
	2.3.5 General Discussion.....	57
2.4	Conclusions.....	58
2.5	References.....	69
3	Fouling in Heat Exchangers.....	61
3.1	Introduction.....	61
	3.1.1 Deposition Mechanisms.....	62
	3.1.2 Corrosion Processes Underneath Deposits.....	64
3.2	Biofouling on Copper Alloys.....	65
	3.2.1 Introduction.....	65
	3.2.2 Properties of Cunifer Alloys in Seawater.....	67
	3.2.3 Barnacle Assay Experiments.....	69
	3.2.4 Field Trials.....	73
	3.2.5 General Discussion.....	82
3.3	Inorganic Fouling in Heat Exchangers.....	83
	3.3.1 Introduction.....	83

3.3.2	Electrochemical Impedance Spectroscopy Studies of Corrosion and Scaling Mechanisms	84
3.3.3	Experimental Set-up	86
3.3.4	Electrochemically Induced Scaling	88
3.3.5	Thermally Induced Scaling	98
3.3.6	General Discussion	106
3.4	Conclusions	107
3.5	References	108
4	Bioprotection	111
4.1	Introduction	111
4.1.1	Effects of Microfouling on Water Chemistry at the Interface	113
4.1.2	Effects of Biofilms on Corrosion	115
4.1.3	Microbiological Corrosion Prevention	116
4.2	Biological Phosphating Processes	117
4.2.1	Introduction	117
4.2.2	Experimental	118
4.2.3	Results	120
4.3.4	General Discussion	142
4.3	Protective Biofilms	143
4.3.1	Introduction	143
4.3.2	Experimental	143
4.3.3	Results	144
4.3.4	General Discussion	148
4.4	Anticorrosive Bioadditives	149
4.4.1	Introduction	149
4.4.2	Experimental	149
4.4.3	Results	150
4.4.4	General Discussion	157
4.4	Conclusions	158
4.5	References	159
5	Conclusions and Future Research	163
	General Summary	165
	Samenvatting	167
	Nawoord	169
	Curriculum Vitae	170

1 Introduction

Summary

Deposition processes occur on every surface exposed to a biologically or chemically active environment. In general, the deposition deteriorates the surface and is called fouling. Both organic and inorganic fouling are possible, from algal fouling on stone and dental plaque problems occurring on teeth to scaling in heat exchangers and soot deposition on buildings. The research focuses on deposition processes in aqueous environments.

In the second part of the chapter, an outline of the thesis is given and the specific areas of research are defined. Three main topics are addressed: biofouling on surfaces, fouling and its effects in heat exchangers and bioprotection.

1.1 Background and General Introduction

Deposition processes occur on surfaces exposed to a biologically or chemically active environment. In most cases, deposition processes are detrimental for the surface on which they occur: one can think of dental plaque [1-3], of the scaling of heater elements in washing machines or the growth of mussels and other macro-organisms on the piling of oil platforms.

Algal fouling on buildings is an example of biological fouling. As soon as the algae start colonising the stone surface, they start producing compounds in order to increase their adhesion to the surface. These compounds are commonly acidic, degrading the surface [4-6]. Inorganic fouling is occurring on buildings as well. In industrial and rural areas, buildings turn grey and black due to exhaust gasses. Since these fouling processes are unacceptable both from the aesthetic point of view and for the structural integrity of the buildings, countermeasures are necessary. One way to deal with the fouling is removing the dirt when it gets too bad. Another option is to use special coatings, designed to prevent fouling. Examples are anti-graffiti coatings [7] and self-cleaning coatings [8].

Another area where fouling occurs is the aqueous environments. Here, the fouling processes are quite diverse. Both biofouling and inorganic fouling can occur. Especially biofouling is much more diverse in an aqueous environment. Depending on factors like temperature, water flow and water make-up, many different organisms can colonise a surface. The research carried out for this thesis has been focussed on aqueous deposition processes.

Well-known examples of the deteriorating effects of biofouling are the increase in fuel consumption and the decrease in maximum obtainable speed of ships and the blocking of heat exchanger tubes leading to overheating of e.g. engines and process streams [9-12]. Other fouling problems occur e.g. in the use of underwater sensing and imaging technology. These kinds of equipment are very sensitive to fouling, since already small amounts of biofouling can result in degrading image or data quality to a low, useless level [13]. It is obvious that these processes should be prevented.

One of the important inorganic fouling processes occurring in aqueous environments is scaling: the deposition of calcareous deposits, often takes place on hot surfaces like heater elements (washing machines) and heat exchangers [14]. Due to the formation of the scales, the heat transfer rate decreases resulting in less efficient processes and even corrosion and subsequent breakdown of the equipment. For this reason, e.g. the use of scaling inhibitors in cooling water is in many cases inevitable [15, 16].

The examples mentioned above are all fouling processes deteriorating surfaces and the major part of this thesis will deal with these problematic processes. However, examples exist in which the 'fouling' deposit protects the surface. For example, several researches claim the prevention of macrofouling due to specific microfouling [17]. Furthermore, microbiologically influenced or induced corrosion could be prevented when harmless micro-organisms colonise a surface before harmful species appear [18]. Pritchard et al. [19] suggested the use of organic layers. Volkland et al. [20] claim that protective phosphate layers can be built by special bacterial species. These recent findings led to a new approach in the protection of metals. These 'bioprotection' processes can lead to novel organic and inorganic protective layers of biological origin.

1.2 Outline of the thesis

The aim of this research was: *investigate the interactions between metals and the environment resulting in fouling and use the knowledge obtained to develop methods to prevent the effects of fouling or turn the fouling into a beneficial deposition process, resulting in methods to protect the metals.*

The investigations have been divided into three parts.

1. An investigation of the general temporal biofouling process on surfaces submerged in seawater. Though the general processes and biofouling species are known, the amount of data on succession throughout the season is limited. The data on the sequence and seasonality of the biofouling process has further enabled us to set-up preliminary models for the biofouling process. Previous modelling has mostly been restricted to microfouling systems.
2. The investigation of biological and inorganic fouling in heat exchangers. Fouling influences the heat transfer in heat exchangers and is therefore an undesired phenomenon. Furthermore, corrosion processes can be enhanced or induced due to fouling. Inorganic fouling has been studied in fresh cooling water systems and biofouling has been investigated in seawater carrying systems.
3. Bioprotection processes. Some of the biological deposition processes can have a positive influence on the corrosion resistance of materials. Investigations have been performed to find out the mechanisms of protective layer formation.

1.3 References

- 1 D.J. Bradshaw and P.D. Marsh, Analysis of pH-driven disruption of oral microbial communities in vitro, *Caries-Research*, Vol. 32 No. 6 (1998) pp. 456-462
- 2 M. Marek, Interactions between dental amalgams and the oral environment, *Advances in Dental Research*, Vol. 6 (1992) pp. 100-109
- 3 B. Grosogoeat, F. Laurent, G. Benay, J.P. Magnin, F. Dalard, L. Reclaru, M. Lissac, J.J. Rameau, Microorganismes et corrosion endobuccale, *Forum Biodeterioration des Materiaux*, 2-3 October 1997, Ottrott, France
- 4 L.F. Rodrigues, A.M. Mauricio, A.M.G. Pacheco, P.S.D. Brito, L.A. Aires-Barros, The Response of an Electrochemical Sensor to Stone-decay Factors in Marine Environments, *Proceedings of Euromat '98*, 22-24 July 1998, pp 383-392
- 5 E.A. Pires, C.M. Rangel, S. Turgoose, R.C. Newman, Monitoring Stone Decay in Simulated Oceanic Environment, *Proceedings of Euromat '98*, 22-24 July 1998, pp 393-402
- 6 M. Rautureau, Chemical Physic State and Biological-Reactivity of Rock-Atmosphere Interface, *Forum Biodeterioration des Materiaux*, 2-3 October 1997, Ottrott, France
- 7 A. Biedermann, Leicht zu reinigende und selbstreinigende glatte Oberflächen, *Keramische Zeitschrift* Vol. 51 No. 10 (1999) pp. 874-878
- 8 V. Romeas, P. Pichat, C. Guillard, T. Chopin, C. Lehaut, Self-cleaning properties of TiO₂-coated glass: Degradation, under simulated solar light, of palmitic (hexadecanoic) acid and fluoranthene layers deposited on the glass surface, *Journal de Physique-IV*, Vol. 9 No.3 (1999) pp. 247-252
- 9 G.S. Bohlander, Biofilm effects on drag: measurements on ships, *Proceedings of Polymers in a Marine Environment*, 23-24 Oct. 1991, Paper 16
- 10 A. Milne, Roughness and drag from the marine paint chemist's viewpoint, *International Workshop on Marine Roughness and Drag*, 29 March 1990, London, Paper 12
- 11 H.A. Jenner, Driehoeksmosselen en aangroei problemen, *H₂O*, No. 18 (1985) pp. 2-6
- 12 W.G. Characklis, N. Zelver and M. Turakhia, Microbial Films and Energy Losses, *Proceedings of the Symposium on Marine Deterioration*, 1981, pp. 75-81
- 13 A. Kerr, M.J. Cowling, C.M. Beveridge, M.J. Smith, A.C.S. Parr, R.M. Head, J. Davenport and T. Hodgkiess, The Early Stages of Marine Biofouling and its Effect on Two Types of Optical Sensors, *Environment International*, Vol. 24 No. 3 (1998) pp. 331-343
- 14 C.A. Branch and H.M. Müller-Steinhagen, Influence of Scaling on the performance of shell-and-tube heat exchangers, *Heat Transfer Engineering*, Vol. 12 No. 2 (1991) pp. 37-45
- 15 Alan Marshall, A new 'total organic' approach for the control of corrosion and deposition in cooling water systems, *Corrosion Prevention & Control*, December 1987, pp. 159-162
- 16 S. Patel and A.J. Nicol, Developing a cooling water inhibitor with multifunctional deposit control properties, *Materials Protection*, June 1996, pp. 41-47
- 17 C. Holström and S. Kjelleberg, The effects of external biological factors on settlement of marine invertebrate and new antifouling technology, *Biofouling*, Vol. 8 (1994) pp. 147-160
- 18 J.S. Potekhina, N.G. Sherisheva, L.P. Povetkina, A.P. Pospelov, T.A. Rakitina, F. Warnecke and G. Gottschalk, Role of microorganisms in corrosion inhibition of metals in aquatic habitats, *Applied Microbiology and Biotechnology*, Vol. 52 No. 5 (1999) pp. 639-646
- 19 A. Pritchard, Biofilms: beneficial or corrosive?, *Proceedings of the 2nd COST 520 Workshop*, 9-12 June 1999, Sion, Switzerland
- 20 H.P. Volkland, H. Harms, K. Knopf, O. Wanner and A.J.B. Zehnder, Corrosion inhibition of mild steel by bacteria, *Biofouling*, Vol. 15 No. 4 (2000) pp. 287-297

2 Biofouling on Surfaces

Summary

The purpose of the research presented in this chapter is to increase the insight in the biological fouling processes occurring in coastal areas. Firstly, the effects of season and location on biofouling have been investigated on glass slides. Next, the results from these investigations were used for setting up a general biofouling model which could be used by installations and equipment end-users to estimate the strength of the antifouling method they ought to use for specific seasons and locations.

From the study towards seasonality of biofouling processes, differences were present in the level of biofouling between Millport (Scotland), Den Helder (The Netherlands) and Cascais (Portugal). Besides the deployment place, deployment date of the samples could account for a large part of these differences. This conclusion emphasises the fact that, depending on time of year and place of deployment, biofouling is more or less damaging for equipment and the antifouling methods used could be adjusted.

Modelling the biofouling for the Den Helder case showed the rather simple relations between the surface coverage of different fouling organisms. Based on the logistic growth model, mathematical models were set-up for eight broad categories of fouling organisms and it was shown that, using deployment date and time of exposure as main parameters, the coverage with the organisms could be predicted.

2.1 Introduction

For preventing biofouling and its consequences, knowledge of the biofouling process is of the utmost importance. Moreover, especially in the case of biofouling, the fouling rate is very much determined by the season. In summer, the water is full of biological activity. Growth rates are higher in warm water, as a consequence, also the number of organisms settling and growing on surfaces is much larger than in winter, when organisms have less energy for growth and reproduction. As a result, antifouling measures needed for preventing biofouling are less in winter than in summer.

Most end-users cannot permit any fouling, because of the large (economic) consequences. For example a single mussel could block a tube in a heat exchanger, eventually resulting in leakage due to erosion corrosion [1-2]. Therefore, despite the fact that biofouling is less in winter than in summer, the measures taken are often the same throughout the year. This may result in unnecessary release of biocides into the environment.

Manufacturers and users of equipment (underwater cameras, sensors for pH, turbidity, oxygen, etc.) would benefit very much from a more detailed description of biofouling in coastal areas. However, they are in general not biologists and therefore would have a difficulty in interpreting biological data. A model describing the biofouling process based on a few easily measured parameters like temperature and light intensity would be of much greater help to them. Such model would enable them to predict the amount of biofouling occurring when using equipment for a certain period of time. However, due to the lack of environmental and biofouling data, such general model does not exist. Models are limited to one species, for example algae or bacteria [3-7]. More information exists on general biological growth modelling. Several models were derived in the literature to describe the growth of species and the interaction between species [48, 49].

Research presented in this chapter addresses both the lack of biofouling data on temporal changes and the lack of a general model describing sequence and seasonality of biofouling in coastal areas. First part of the research, section 2.2, provides data on the biofouling process in three different European coastal zones: Scotland, The Netherlands and Portugal. Data were collected throughout the biofouling season of 1997. The second part of the research, section 2.3, uses the part of the data collected in The Netherlands to develop a general temporal biofouling model. The remainder of the introduction gives an overview of the basics in biofouling and of the main species involved in the biofouling process. Moreover, a more detailed description of the behaviour of barnacles is given, because of their important contribution to the biofouling process in North Atlantic and North Sea coastal areas.

2.1.1 Biofouling Basics

The adhesion of a primary population of micro-organisms to marine surfaces has been studied intensively. Clean surfaces placed in the sea adsorb bacteria within hours. Once the attachment process is initiated, an irreversible ecological succession occurs, leading to the development of a mature microbial community. The predominant organisms are bacteria, algae, and protozoa enmeshed in a thick layer of bacterial slime. Dead cells and other debris accumulate in the matrix of slime, providing a continuous nutrient source.

Formation of the primary biofilm appears to involve five stages [8, 9]:

1. an initial conditioning stage;
2. attraction of motile bacteria;
3. reversible adsorption of both motile and non-motile bacteria;
4. an irreversible stage of attachment mediated by bacterial polymers;
5. a final stage of development of a secondary microflora and subsequent settlement and growth of macrofouling species.

The first four stages occur very rapidly and are complete within hours; the secondary population may take days or weeks to develop. The first stages are schematically drawn in figure 2.1.

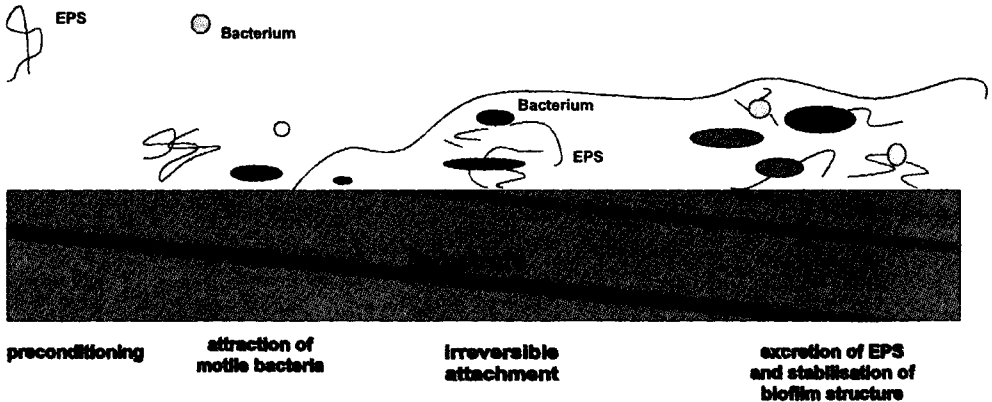


Figure 2.1: Schematic representation of the steps towards development of a mature biofilm (EPS: extracellular polymeric substances)

1. **Conditioning stage.** The surface of objects placed in seawater is immediately coated with a monolayer of material floating in the water. This conditioning film is usually composed of high molecular weight glycoproteins. The film-forming substances are contributed from two major sources:

a) Spontaneous adsorption of biological macromolecules originally in solution or in suspension in the seawater.

b) Polysaccharide slimes secreted by the pioneer attaching microbial organisms.

Significant specificity seems to be shown for both these processes, in that the adsorbing macromolecules and early-attached organisms are not necessarily the most abundant components in the adjacent aqueous boundary layers.

2. Attraction of motile bacteria. All motile bacteria apparently have chemoreceptors. These receptors allow them to move along chemical gradients. Bacteria are attracted to a wide range of organic chemicals that accumulate on marine surfaces, including polypeptides, amino acids, sugars and all the organic matter of the conditioning film.
3. Reversible adsorption. The bacteria are held at some distance from the surface by electrical double-layer repulsion energies. In this reversible phase of biofilm formation, the bacteria are held only weakly at the solid surface; they exhibit Brownian motion and are liable to shear flow.
4. Irreversible attachment. This irreversible step occurs following the production of extracellular polymers by the bacteria. Synthesis of these extracellular fibers allows the bacteria to bridge the electrical repulsion barrier between the material surface and the bacterial cell, and these fibrils, polysaccharides or glycoproteins, attach the bacteria firmly to the surface. The formed primary film grows, utilising nutrients flowing past it, and at the same time bacteria produce large quantities of polymers, enabling them to trap debris and other micro-organisms. The first organisms to colonise "conditioned" surfaces are rod-shaped chemoheterotrophic bacteria, which can readily use organic nutrients adsorbed to the solid substratum [10].
5. Development of secondary microflora and macrofouling settlement. Ultimately, a second microbial population develops. The rate of development depends on the nutrient status of the water: in open ocean waters a secondary population may take weeks to develop, whereas in warm coastal waters a rich film develops within days.

Even though the general process of biofouling described here appears to be independent of the type of surface, the physical and chemical character of the substratum is one of the most important factors in determining which specific organisms will be involved in the fouling and how firm the attachment becomes. Furthermore, environmental conditions, such as pH, oxidation-reduction potential, temperature, presence of growth inhibitory or lytic agents, affect the microenvironment, the species which attach, and perhaps the subsequent colonisation.

2.1.2 Biofouling Communities

As pointed out in the previous section, biofouling consists of several consecutive steps. After initial colonisation with micro-organisms, macro-organisms take over. The fouling with macro-organisms also shows a certain sequence in the development. This sequence and its dependence on season are the subject of the studies presented in this chapter. In this section, the broad categories of fouling communities that can be present at a surface are treated. Barnacles are treated more fully in section 2.1.3, because of their importance regarding the effects of biofouling on surfaces in temperate marine systems.

Micro-organisms

Bacteria are in general the dominant micro-organisms present on submerged surfaces. The bacteria produce extracellular polysaccharides and polypeptides (forming a slime) which mostly favours attachment of further bacteria and other micro-organisms like fungi, microalgae, protozoa, macroalgae and invertebrates [11-13]. Since diatoms require light for photosynthetic activity, their presence in the biofilm will be largely restricted to the eutrophic zone. Slime forming

bacteria are always present in the water, but their succession is dictated by the amount of organic materials and the temperature. Figure 2.2 shows two examples of biofilms on special glasses.

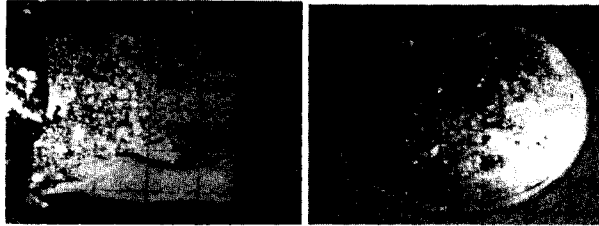


Figure 2.2: Biofilms on glass

The environment of micro-organisms that live in a biofilm is completely different from that of planktonic organisms. In a biofilm organisms are more or less immobilised, embedded in a slimy matrix of *extracellular polymeric substances (EPS)*. This biofilm consists of 80-95% water. The organic proportion is dominated by EPS while the cell material itself only makes up a small fraction. Figure 2.3 shows pictures of bacteria loosely attached to the surface and bacteria embedded in EPS.

Analysis of the chemical composition showed that a biofilm consists of no less than 15 amino acids. The biofilm also contains the monosaccharids *glucose* and *ribose* and the fatty acids *palmitine*, *stearine* and *oleine*. In addition particulate matter such as *clay*, *humic substances* and *corrosion products* could be embodied in the biofilm [13, 14].

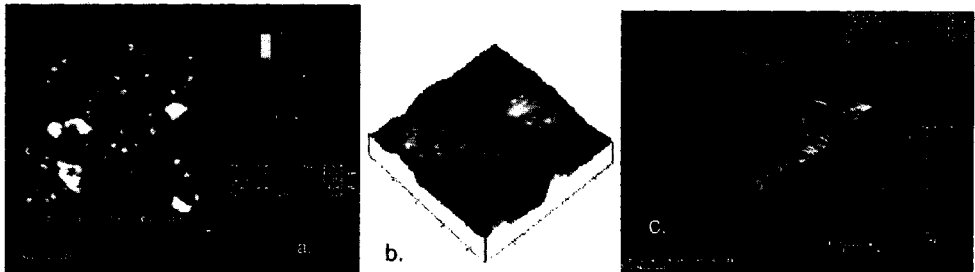


Figure 2.3: Atomic Force Microscopy pictures of biofilm bacteria: a. bacteria loosely attached to the surface; b. close-up 3D image of a; c. Bacteria embedded in EPS.

Temperature is an important factor in the development of a biofilm. In the temperature range from 5 to 60°C for example the surface of a **heat exchanger** will always carry biofilms [13]. The activity increases with temperature, but at high temperatures it is likely that organisms will be killed. At intermediate temperatures growth and reproduction can be quite rapid (bacteria may divide every 20 minutes at optimum growth conditions [15]). Unfortunately, the temperature of many open recirculating cooling water systems falls near the optimum for maximum cell activity [11].

Diatoms

Diatoms are single celled organisms [21]. They make a glass house of silica consisting of two valves that fit into each other like a little pillbox, Figure 2.4. The colour of the living tissue is yellow-brown instead of the green we know of other creatures that use light as a source for energy. Due to their need for light as energy source, they are found in the eutrophic zone. They occur from early spring until the end of autumn.

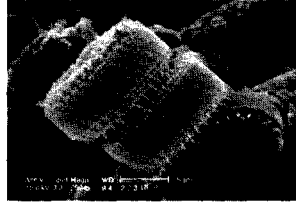


Figure 2.4: Centric diatoms

In marine waters a variety of body shapes is possible. Figure 2.5 shows some of the possible options. They can occur as single cells (a, b, f), as chains (c, d) and stalked (e).

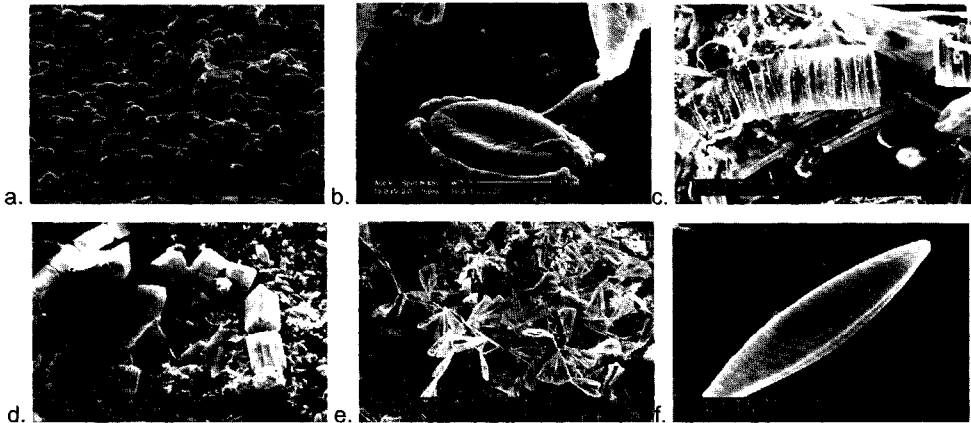


Figure 2.5: Marine diatoms. a. *Cocconeis* spp.; b. *Cocconeis* sp. embedded in mucilage; c. *Fragilaria* sp.; d. *Grammatophora* sp.; e. *Licmophora* sp.; f. *Navicula* sp..

Some diatoms are able to move. The pennates are the best movers. The mechanism for this is still not well understood but it seems that through the slit alongside the cell (the raphe) tiny microfibrils protrude. With these they can move over a substrate. Other diatoms excrete a mucilage to stick to the surface, Figure 2.5b.

Seaweeds

Seaweeds are aquatic plants that contain chlorophyll, a green pigment that enables them to capture energy from light [34]. They exist in three colours: green, brown and red. In the brown ones, the green pigment is masked by the brown pigment fucoxanthin and in the red ones by the red pigment phycoerythrin. Brown algae do not flourish in warm waters and are therefore relatively scarce in the Mediterranean. Red algae flourish in temperate and warm waters.

Bivalve molluscs

The mussel *Mytilus edulis* and the saddle oyster, *Pododesmus patelliformis*, are very common in the central and northern North Sea. In order to survive and reproduce, these animals attach themselves with byssus threads on hard surfaces. *M. edulis* settles in the range from the mean water level to about -25m and *P. patelliformis* settles at all elevations [16]. Figure 2.6 shows a picture of mussels on a copper-nickel panel galvanically coupled to steel.



Figure 2.6: *Mytilus edulis* on a copper-nickel panel galvanically coupled to steel.

Saddle oysters, together with solitary tubeworms, are one of the first organisms to settle on newly installed or cleaned objects [16]. Though these oysters are overgrown and suffocated by colonial species within two or three years, dead shells remain attached for several years [16].

Zebra mussels (*Dreissena polymorpha*) are the only freshwater mussels able to attach themselves with byssus threads on hard surfaces. Subsequently, the mussels grow on vertical structures and resist high currents. The accumulation of Zebra mussels in heat exchangers can cause increased flow resistance and colonies clog water intakes. Zebra mussels are common in the Netherlands in fresh and brine water, and need flowing water to thrive. The upper chlorine level for these organisms lies between 500-1.110 mg/l and they will resist short periods with higher concentrations. Marine harbours with a large influx of fresh water could create good conditions for Zebra mussels. Most problems, however, occur at factories that use fresh and brine water for their cooling system [1].

Barnacles

Barnacles (Figure 2.7) cause major fouling problems in the marine environment. Observations in the past [17] show that attachment of barnacles on vessels occurs most readily in harbours and when they are subjected to relatively low water movement. Heat exchangers that are not in use create the same hydrodynamic conditions and settlement is most likely to occur at these moments.

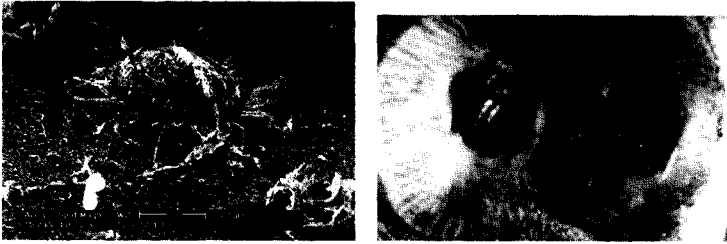


Figure 2.7: a. SEM picture of juvenile barnacle (*Balanus crenatus*) b. adult barnacles (*Balanus amphitrite*)

The tropical barnacle *Balanus amphitrite* (Figure 2.7b) is very common in European harbours and estuaries in the Mediterranean Sea. In sublittoral waters isolated populations may occur in the cooling water of energy stations. In these mentioned waters *Balanus amphitrite* is an important macro-fouling organism [18]. In other marine waters, other barnacle species are more important, e.g. *Balanus crenatus* in the North Sea (Figure 2.7a).

Tubeworms

The serpulid tubeworms are typified by the secretion of a calcareous tube, which makes them important fouling organisms. As with most other fouling organisms, settlement occurs preferentially in tropical waters. Though tubeworms are widely spread, fouling of these organisms is most marked in the Mediterranean and the Indian Ocean [20].

Only the serpulids *Pomatoceros triqueter*, *Hydroides norvegica*, *Merciella enigmatica* and *Spirobis* spp. are frequently reported as fouling organisms. The solitary tubes of the tubeworms *P. triqueter* and *H. norvegica* are usually scattered over all surfaces from the mean low water level to the mud level. *P. triqueter*, *H. norvegica* and *M. enigmatica* are common on ships hulls, buoys and dock structures in large masses. *H. norvegica* tolerates polluted conditions well and is moderately resistant to antifouling paints. *P. triqueter* is very sensitive to antifouling paints but tolerates exposition to heavy seas. *Spirobis* spp. generally prefer settlement on rocks in shallow waters, though some species were found on test surfaces as well [20].

Figure 2.8 shows young tubeworms on a bivalve collected in the Adriatic Sea near Hvar (Croatia). Mono-specific dominance by these species is very uncommon and most of these animals are smothered by colonial organisms after three or four years [16].

Ascidians

A round or spherical body surrounded by a jelly-like coating typifies ascidians [35]. The body can be hard and soft and they can live both solitary and in colonies. Ascidians are suspension feeders and for this reason, there are two siphons: an oral through which the water enters and an atrial through which the water leaves the body. In colonial species, the individuals join the atrial opening.

Ascidians are found on a variety of places until 100m depth. They grow on different surfaces, like rocks, stones, seaweeds and pilings. Figure 2.9 shows both a solitary species (*Molgula manhattensis*) and a colonial species (*Botryllus schlosseri*).



Figure 2.8: Tubeworms on a shell in the Adriatic sea near Hvar.

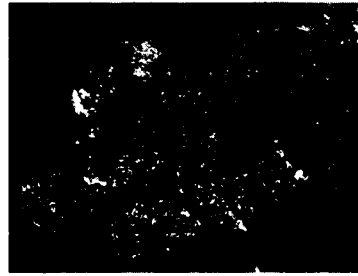


Figure 2.9: Ascidian species: *Molgula manhattensis* (left top); and *Botryllus schlosseri* (right).

Bryozoa

Bryozoa are small, colonial animals and are found mainly in marine environments [35]. The colonies can grow along the surface or upright. The individual 'zoids' are in general smaller than 1 mm. The whole colony can consist of thousands of zoids. Each zoid has a cuticulus, which is strengthened by a calcareous material. It collects its food, micro-organisms like bacteria and diatoms, with a small tentacle. Bryozoa are found on substrates like rocks, seaweed, stones and shells. Figure 2.10 shows a species of bryozoa found in the North Sea on top of a mussel.



Figure 2.10: Bryozoa (enlargement 2x)



Figure 2.11: Hydrozoa (*Obelia* sp.)

Hydrozoa

Most hydrozoa are colonial animals [35]. The colonies are formed out of groups of polyps arising from a single stolon linking them together and anchoring them to the substratum. They are easily mistaken for seaweeds, due to their branched appearance. Hydrozoa are sublittoral species and attach to various surfaces like seaweeds, stones and rocks. Figure 2.11 shows an *Obelia* sp..

2.1.3 Barnacle Fouling Mechanisms

Of the fouling organisms described in the previous section, barnacles are the most troubling to marine industries, because they are persistent, difficult to repel or remove and are present throughout the fouling season. For this reason, many studies have been directed towards this type of organism. A more in depth discussion of the behaviour of this organism is given here.

Barnacles are born as free swimming larvae called nauplii. They pass through six naupliar stages and one cyprid stage. The larvae do not eat in the cyprid stage, but consume the gained reserves of the previous stages. In the cyprid stage the barnacle has to find a suitable surface to

settle. There are at least four distinct adhesion mechanisms occurring successively during settlement and further development of the barnacle [19]:

1. During the presettlement exploratory phase the cyprid larva "walks" on its two antennules which stick temporarily by attachment organs (Figure 2.12). The attachment organs are covered with small cuticular hairs. The organs also contain sense organs (which may be chemo- or mechano receptors), a large cement duct from the main cement glands, and small antennular cement glands. Only the small antennular cement glands are likely to be involved in adhesion.
2. During fixation a relatively large volume of larval bioadhesive is discharged through pores in the two attachment organs from the major cement glands. This large volume of cement usually embeds both antennules and the immediate region of the cypris ventral surface so preventing further translation.
3. Immediately after transformation, the cyprid cement glands are transformed into adult cement glands together with the cyprid ducts. Up to a week after metamorphosis, the basal area of the "pinhead" barnacle becomes applied to the substratum. The origin of the cement surrounding the basal area is not known. This cement is much weaker than cyprid cement and could not be transported to the base of the young barnacle. The glands can therefore not produce it.
4. During further development of the barnacle, secondary cement glands are formed. The ducts of these glands open through the base of the barnacle. They form rings of cement between the base and the substratum and replace all the other mechanisms in the adult.

The sensory equipment of the cyprid with which it selects its habitat has been the subject of intensive research. Most challenging are observations concerning the influence of adsorbed materials. It has been demonstrated that proteins (arthropodin) layers increase settlement [19]. Even a monolayer of proteins enables settlement. The cyprid only responds to adsorbed proteins, in solution these materials have no effect. In its search for a suitable surface to settle, the barnacle prefers hollow above sphere shaped surfaces and rough above smooth surfaces. Surfaces with a low surface energy are avoided by barnacles. Though barnacles are able to settle on surfaces with low energy, the adhesion force between the baseplate and the substratum will be low [19].

The mechanisms involved in selecting a habitat are not fully understood. Nott and Foster [22] showed that the attachment organ has open ended receptors thought to be chemosensory. If the attachment organ is placed on a potential substratum, it releases enzymes that break down the adsorbed protein layer. The formed amino-acids could then be recognised with the chemo receptors. Based on these amino-acids, the substrate will be approved or rejected by the cyprid.

Crisp [19] thought it would be more likely that the cyprid uses the mechanoreceptors to determine the force that is needed to pull of the attachment organ from the surface. This way the cyprid determines if the substratum is suitable for settlement.

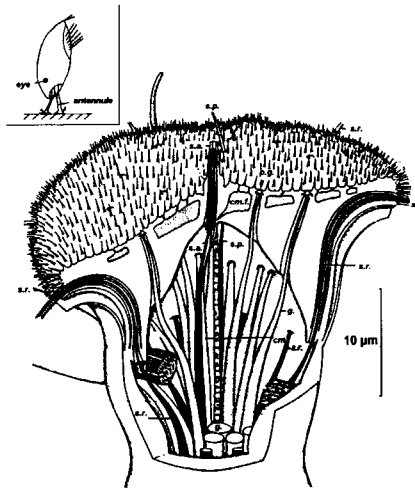


Figure 2.12: The attachment organ of the antennule of the cyprid *Semibalanus balanoides* [19]. The position of the antennule on the cyprid is shown in the upper left.

s.a.	axial sense organ	g.	antennular gland
cm.	cement duct	s.p.	postaxial sense organ
cm.r.	radial canal of cement duct	s.r.	radial sense organ
p.g.	pore of antenular gland		

Beside the physical and chemical properties of the substratum, the presence of other barnacles also has influence on the selected habitat [23]. The presence of other individuals is determined by the number of cyprids that have explored the substratum. When cyprids are exploring a potential substratum, they leave "fingerprints" that consist of a sticky protein substance. This substance will adhere stronger on substrates with a high surface energy. Therefore, more protein is left on the surface during exploration. The number of cyprids that have explored the surface increases with the number fingerprints left behind, which is an indication for a favoured substratum.

Attachment of barnacles on vessels occurs most readily when subjected to relatively small water movement. In an experiment, a rotating disc immersed in the sea and glasstubes were used to determine the limiting velocities for attachment of three barnacle species [17]. These limiting velocities lie between 0.5-0.9 knots (0.93-1.7 km/h) for *B. amphitrite*, between 0.4-0.7 knots (0.74-1.3 km/h) for *B. eburneus* and above 1.1 knots (2.0 km/h) for *B. improvisus*. The water current has also effect on the growth rate of the attached barnacles. The growth rate was found to be increased by water currents less than 1.5 knots and decreased at higher velocities. The negative effects of water currents were found to decrease with increasing age of the settled barnacles. Six hours after attachment, the growth rate was reduced to one-third of normal at 1.5 knot, and completely stopped at 3 knots. Five days after attachment, currents ranging from 3.3-8 knots prevented growth. The detachment of barnacles appeared to some extent where growth rate was reduced and even more where growth was completely stopped.

2.2 Sequence and Seasonality of Biofouling

2.2.1 Introduction

Studies of microbial fouling processes have been directed at the industrial environments where fouling problems include increased corrosion rates and the clogging of filters and pipelines [24-25]. Research undertaken as a consequence of these biofouling problems has led to an initial understanding of the processes involved in the development of fouling biofilm communities [26-28].

However, few studies have investigated the development of fouling microbial biofilms in the marine environment [29-31]. Information about the expected biofouling pressure at a range of diverse sites would be extremely useful to end-users of antifouling methods allowing them to determine the type and level of antifouling protection required for a particular mission.

The purpose of this study was to determine the sequence and extent of biofouling likely to develop on installations and equipment during use in the euphotic zone of coastal waters. The specific aim of the work was to describe the development of biofouling assemblages on surfaces at three contrasting coastal sites throughout the fouling season in order to predict the fouling pressure.

2.2.2 Experimental

Experimental Locations

Experiments were undertaken at three sites representing different coastal environments in; Scotland (Keppel Pier, Millport), The Netherlands (Den Helder harbour) and Portugal (Bay of Cascais near Lisbon), see Figure 2.13.



Figure 2.13: Study sites of the biofouling investigations in Millport (Scotland), Den Helder (The Netherlands) and Cascais (Portugal)

Keppel Pier (55°45'0N 4°55'8W) is the University Marine Biological Station (UMB) pier at Millport. This location is close inshore, exposed to south-westerly winds and tidal currents: the channel bed is sandy with a few large boulders ($z_{\max} = 7\text{m}$). UMB was considered to be representative of a cool temperate moderately exposed coastal area. The marine environment of the Clyde Sea area has been more fully described elsewhere [32].

Experiments in the Netherlands were carried out on a raft in the harbour of Den Helder (52° 56' N and 4° 46' E) in the North sea at the entrance of the Wadden Sea. The depth of the harbour at the raft site is 8m. Tidal motion and water currents generated water flow around the raft. Turbidity in the water column is high, Secchi depths varied between circa 0.8 and 1.5 meters. Wave action at this site is very low due to the sheltered nature of the harbour. This site represented a warm temperate sheltered site with high turbidity.

At the IST site in Cascais Bay (38°41'41N 09°25'00W) experiments were deployed from a metal frame suspended from buoys in the sea at a constant depth of 1.5 meters. The rig was moored approximately 40 meters from the shore. Cascais is on an exposed area of the Atlantic coast of Portugal, the site is subject to high wind and wave action, although this is mainly during the winter. The seabed consists of rocks and sand. The water was turbid throughout the study and visibility was estimated to vary between 0.5 and 1 meter.

Materials and Methods

Glass microscope slides were used as the substrata deployed during the study because of its inert character, influencing the adhesion processes as less as possible. Methods were standardised as far as possible. Inevitably, practical considerations reflecting differences between the three deployment sites and also the laboratory facilities of the collaborating institutes required there to be slight changes but these were kept to a minimum.

Between May and November 1997, glass slides (76x26 mm²) were exposed at the UMB and TNO sites. The glass slides were slotted into cuts in rubber bungs that held the slides vertically. Five bungs were tied onto a rope approximately 0.2 meters apart. For the first 5 sets of slides, TNO co-ordinated deployments exactly with those being undertaken at UMB. Deployment of the sixth set was delayed at UMB by one week because of practical problems, deployments at the TNO site continued with the original schedule. IST was unable to meet the first deployment due to technical difficulties: deployments of slides at this site began in June. At this site, slides were attached to a custom-built metal frame suspended from a raft instead of using the rubber bung method.

Slides deployed at the UMB site were subjected to wave action and tidal fluctuations but always remained within the upper 4 m of the water column, throughout the experiments the turbidity at this site was low, Secchi depth was consistently greater than 5m. Turbidity was considerably higher at the TNO and IST sites, to account for the higher attenuation of light, slides at these sites were suspended in the top 2 meters of the water column.

A set of 80 slides was deployed every four weeks at each of the sites. Every week three slides were collected for bacterial counts and three replicate slides were collected for estimations of biofouling by algae and macrobiota, all the slides were selected at random. The collected slides were dip rinsed in 0.2µm sterile filtered seawater (SF) to remove loosely adhered material, the material remaining was fixed by immersing the slides in 20ml/l glutaraldehyde. Water temperature was also recorded at each site throughout the study.

Enumeration of Bacterial Cells

Accumulation of bacterial cells on the glass surfaces was estimated using epifluorescence microscopy. At UMB the glutaraldehyde fixed slides were stained by the fluorochrome 4',2-Diamidino-2-phenylindole dihydrochloride (DAPI:), at TNO and IST Acridine Orange (AO: 0.2 g in 200 ml distilled water), an alternative fluorochrome stain, was used. Both stains were sterile filtered before being used. Prior to the study both stains were assessed at UMB and found to be comparable.

Bacterial cells were enumerated at $\times 1000$ magnification using epifluorescent microscopes. A minimum of 400 cells or 30 fields of view were counted. Bacterial counts were stopped when the density of cells or complexity of the biofilm prevented individual cells from being discriminated.

Estimation of Eukaryotic Fouling

Visual examination and bright field microscopy were used to assess unfixed samples. After an initial visual examination the samples were examined with a magnification of $\times 100$. First any macrofouling on the slides was investigated and the percentage cover estimated. The main groups of organisms were identified. This 'canopy' layer was then removed if appropriate and the microfouling assemblage underneath investigated. Percentage coverage was estimated for the main taxonomic groups found, the use of unfixed samples allowed workers to gain a better understanding of the hydrated nature of the biofilm however using this approach it was not possible to identify taxa to the species level.

Surface coverage was estimated using the *Brown-Blanquet scale* [42], which divides surface coverages in five areas, as listed in Table 2.1

Table 2.1: Surface coverage and the corresponding BBS-values [42]

Braun Blanquet scale	Surface coverage (%)
0	Scarce
1	0-5
2	5-25
3	25-50
4	50-75
5	75-100

Scanning Electron Microscopy was used to further assess the microfouling communities.

2.2.3 Results

The occurrence of species varied markedly among the three sites. Figure 2.14 shows a horizontal bar chart with the occurrence of the main species recorded.

Fouling in The Netherlands shows the largest diversity. All nine categories of fouling organisms show a time period in which their presence leads to a pronounced surface coverage. At IST this only five of the nine species were recorded and at UMB all species were recorded, but only for seven species, a pronounced coverage was found. Below, the fouling is described for the three sites, divided into microbiota and macrobiota.

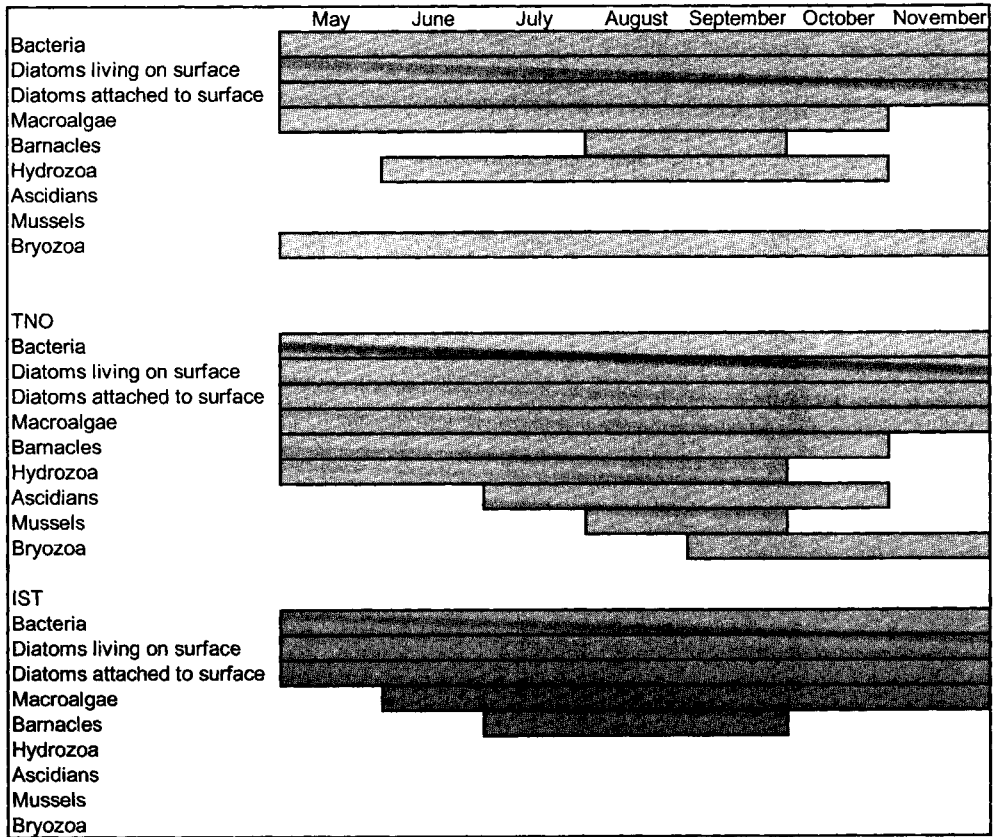


Figure 2.14: Occurrence of the main species recorded for the three sites during the fouling season

Microbiota

Bacteria were the first organisms to colonise the glass surfaces in large numbers at each of the three sites. Epifluorescence microscopy allowed the bacterial cells to be broadly separated by morphology into rod, coccoid and filamentous forms, although no attempt was made to identify the strains present. In general as the biofilm accumulated rod shaped bacteria became the most abundant type. Filamentous forms, often growing away from the surface, became more prevalent as the biofilm matured. The bacteria showed exponential rates of increase and the biofilms at all sites, quickly became too complicated to allow accurate enumeration of the cells to be made (>50,000 cells mm⁻²).

Within 12 hours of immersion colonisation of the slide surfaces by diatoms was observed. At the UMB site the 'surface dwelling' diatoms showed some small differences in percentage cover depending on the time of deployment. Throughout the sampling period the percentage cover rarely exceeded 25% and less than 5% cover by individual diatoms was more usual. The most significant period of community development for this group at Keppel Pier was from late June until early July when surfaces had up to 75% coverage. All the common 'surface diatom' cells were pennate diatoms and included a number of highly motile species including some *Navicula* spp. and *Nitzschia* spp.

Initial colonisation normally took place in the first one to two weeks of deployment. At UMB, adhered diatoms were highly significant members of the fouling community from August onwards, *Cocconeis* spp. accounted for most of this high cover. A number of slides had greater than 75% cover during this period although it took a minimum of 4 weeks for cover to get above 5%. These species also left 'footprints' after the cells had become dislodged which would affect the transmission of light. The footprints were formed from particulate matter and bacterial cells adhered to the mucilage that had surrounded the cells at the surface; presumably exuded by the cells for attachment (Figure 2.15).

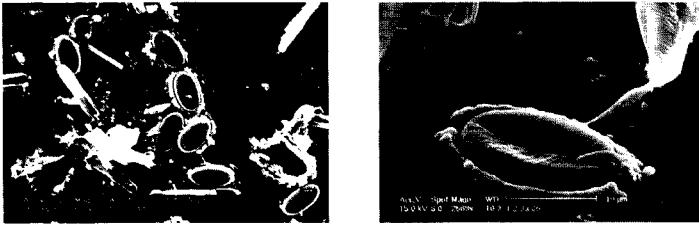


Figure 2.15: Diatoms embedded in mucilage

Colonisation at the other two sites was more rapid than in Scotland (Table 2.2). During the summer at Cascais (first 4 deployments) the glass surfaces were heavily colonised (BBS 4) within 2 weeks and many samples were fully colonised by single diatoms (BBS 5) after an immersion period of four weeks. Within two weeks of deployment slides at the TNO site were fully colonised by single diatoms of all different types, see e.g. Figure 2.4 and 2.5, BBS 5 (except for the starting point 22nd of November, it then takes at least three weeks). For the first four sets of slides, the coverage decreased rapidly to BBS 1 as the slides became colonised by barnacles. When barnacles were absent colonisation by these diatoms remained very high (BBS 5), as the biofilm developed a loosely attached layer of diatoms was observed to grow over the first layer at the surface of the glass. In comparison with the summer fouling communities the development of diatom fouling on the surfaces deployed in November was much slower which was probably due to the lower water temperature. However, colonisation up to BBS 5 was still present. The variety in species decreased: only one single pennate type was present (Figure 2.5a).

Filamentous forms commonly became established at surfaces within one week and could account for high localised cover on slides at UMB and TNO. However, filamentous diatoms are never able to fully colonise a surface. Most of the filaments observed *in situ* grew away from the surface rather than across it. On slides exposed at the Den Helder between June and August the colonisation pattern was similar to that seen for 'single diatoms' (initial increase followed by a decrease due to macrofouling). Filamentous diatoms were most prominent during the middle part of the experiment when the water temperature and light levels were high. At Cascais, the general development of a filamentous diatom community was slow, 4 weeks after deployment, cover was less than 25% (BBS 2). Slides deployed in November showed even less fouling by filamentous species which may have reflected a more turbulent environment.

Macrobiota

Table 2.3 summarises the Braun-Blanquet data for the macroalgal fouling at each site during the study period. Percentage cover of these seaweeds was low at the UMB site, growth rates being faster during the summer although rarely developing into plants of significant size. At the TNO and IST sites where water temperatures were higher biofouling by macroalgae was faster and more significant. However, growth was not directly reflected in increased surface coverage, because the seaweed grew away from the surfaces. The most common algae were *Chlorophyta* including *Cladophora* spp., *Enteromorpha* sp. and *Ulothrix* spp.. Examples of the *Rhodophyta* included flat bladed and filamentous types but these species did not develop sufficiently for identifications. Occasionally encrusting red algae were also observed on slides at UMB.

In the early stages of the immersion, red algae were slow to establish. Surfaces were usually immersed for over three weeks before plants were observed (microscopy). Filamentous forms were the only examples of the *Phaeophyceae* colonising the slides, populations developed on surfaces within the first two weeks of immersion. At Den Helder large quantities were observed during the early stages of fouling (up to BBS 5) but as the biofouling community developed amounts declined (to BBS 3). During the second, third and fourth deployment periods, the percentage cover decreased after an initial period of high cover due to competition for space with other fouling species leading to detachment of plants or reduction by grazing. Fouling by macroalgae at the Cascais site on slides was rapid, heavy growth was consistently established during the period of exposure. *Chlorophyceae* and *Phyophyceae* began to appear on the samples after 1 week and after 5 weeks seaweeds had fully colonised many of the samples (BBS 5). Species of red algae were only occasionally found on the slides in the Bay of Cascais.

Barnacles were the only macroinvertebrate recorded at every site (Table 2.4). At Keppel Pier one species of barnacle (*Chthamalus montagui* Southward) was recorded on the slides in late summer. Immediately prior to the study *Semibalanus balanoides* (Linnaeus) cyprids had been settling in April but this species was absent from slides deployed in the joint study. Each species showed marked periodicity in the timing of the cyprid settlement that reflected the reported life histories and settlement behaviour of these animals. Fouling by barnacles was more significant at the other two sites. During the first three exposure periods at Den Helder, barnacles (*Balanus* sp.) fully colonised the samples (BBS 5). Surfaces immersed during the fourth deployment exhibited less fouling by barnacles than on the slides deployed earlier in the season, BBS 4. In the final period, no barnacles settled. At the IST site no such periodicity of barnacle settlement was observed during the period of study. Barnacles were first observed on the slides 5 weeks after deployment (BBS=1). It took 8 weeks for the percentage cover of barnacles to exceed 75%, when the surfaces were considered to be fully colonised (BBS 5).

Hydrozoa were significant colonising organisms for much of the sampling period at UMB and TNO. At UMB slides were colonised by *Obelia longissima* and a *Tubularian* sp. a mixed community persisted through June. By July *Obelia* was rarely found and colonies of *Tubularia* sp. accounted for over 75% (BBS 5) of the biofouling cover on slides during August. Recruitment and development took a minimum of 2 weeks for colonies to become sufficiently established to be observed during sampling. Hydrozoan recruitment was low in the late summer/autumn period which allowed other species to colonise the slides. In October a mixed hydrozoan community once again developed rapidly, after only 5 weeks cover was recorded at BBS 4. Hydrozoan colonies (*Obelia* sp.) were present on slides from the Den Helder site between May and October, growth was found to be most prolific in July. No new settlement was observed on slides after August.

Low levels of annelids (*Serpulidae*: *Pomatoceros* sp.) were recorded throughout the sampling period on slides immersed at Keppel Pier. Following deployment of a surface it took at least 5

weeks for recruitment and growth resulting in cover above 1%. This species grew in encrusting calcareous tubes that were difficult to remove.

Small mussels were found at irregular intervals during the study at UMB, a more sustained pattern of fouling was observed at the TNO site (*Mytilus edulis*) but percentage cover was generally low. These animals are mobile and attachment was not permanent at UMB, although slides deployed at the start of August did suffer a period of prolonged settlement during September. At TNO most mussels are found on top of a barnacle layer. This seemed to imply that mussel adhesion on glass itself was too loose.

Bryozoa colonised slides at UMB throughout the period of the joint study. Two types of bryozoa were recorded a hard net-like bryozoan resembling *Electra* sp. and a soft *Alcyonidium* like species. Both species when observed covered significant areas of the slides. The hard encrusting *Electra* sp. mat was very difficult to remove once established. At the TNO site bryozoa were only observed from the end of September onwards, the settlement period would appear to have been short since slides deployed in October (20/10) were not colonised by bryozoa. Growth of established colonies continued until the final slides were recovered in December.

Ascidians (*Molgula manhattensis* and colonial species *Botryllus schlosseri*) grew on the slides in Den Helder harbour from August until November although no new settlement occurred after September. During August and September ascidians accounted for over 75% cover (BBS 5) on slides deployed for at least four weeks. Cover was lower in October and November, BBS 3 and BBS 1 respectively. In general growth of ascidians was not significant during the first four weeks of immersion. Ascidians were scarcely found on slides deployed at Keppel Pier and were never recorded on slides at Cascais.

A number of organisms were only recorded colonising slides on rare occasions, these included cup corals, a *Lasaea* like species, fungi and yeasts. The biofouling communities also included several groups of mobile active organisms associated with the biofilm covered surfaces, these organisms included ciliates, gastropods, nematodes, copepods, nudibranchs, starfish, sea urchins and various unidentified larvae.

2.2.4 General Discussion

In this study, glass slides provided a clean, relatively inert standard surface for immersion at each site. Recruitment processes were likely to be very important during the initial stages of biofilm development, and in particular, the availability of cells in the water column capable of settling on the surface. This study investigated the early development of biofouling communities on surfaces under a range of environmental conditions. Novel information about the accumulation of biofouling on surfaces was quantified.

The colonisation of surfaces at the three sites followed the expected pattern, which has been described in earlier studies [8, 9]. Within a few hours of immersion bacteria and a few solitary diatoms were found to have already reached and colonised the surfaces. An initial development of microbial biofilm was repeated at every site for each new set of surfaces deployed, although differences in the species composition of the assemblage were expected the main groupings remained the same. There was a strong relationship between the deployment site and the rate of biofouling. This effect is likely to have been due to environmental factors and recruitment processes. Water temperature was considered to be a strong candidate, the slowest development of a biofouling community was observed at Keppel Pier, which also had the lowest water temperature.

A more detailed analyses of the data from Keppel Pier and Den Helder harbour showed a significantly higher rate of fouling accumulation at the TNO site than at Millport [33]. Rate and level of biofouling were also shown to be affected by the timing of the deployments.

Water temperature and light levels are important environmental factors that are likely to affect the type of biofilm that develops and the speed with which biofilm accumulates. During the joint study biofouling development was fastest at the warm water sites. Both at the Bay of Cascais site where the water temperature from June to October ranged between 16.5-22°C, and the TNO site where it was 14.3-22.8°C algal fouling developed more rapidly than at the Keppel pier site where the temperature was lower (10.5-21°C). This assertion is supported by regression analysis of the amount of bacteria present in the biofilms accumulating on glass surfaces deployed at the UMB site after one week showed a significant effect of water temperature supporting these findings [33].

The biofouling at Cascais followed a clear pattern, in the first 1-2 weeks a bacterial and diatom dominated community quickly developed, the biofouling continued leading to a macrofouling community dominated by barnacles and green and brown macroalgae. More complex patterns of fouling community dynamics were seen at the TNO and UMBSM sites. Periodic changes in the abundance of different groups of organisms and species was recorded at the both these sites during the study. The periodicity of some populations of biofouling organisms is most obviously seen amongst the dominant macrofouling fauna, of which the changes in the barnacle and hydrozoan communities are good examples. Barnacle populations were reported to consistently dominate the biofouling community at the Bay of Cascais site. During the summer barnacles often fully colonised samples at the TNO site, but numbers declined later in the year and no cyprid settlement was recorded on the final set of samples. In contrast cyprid settlement at Keppel Pier showed very distinct periodicity.

The hydrozoan colonies observed at Keppel Pier and Den Helder were extremely competitive on glass surfaces, dominating the biofouling community for periods, out competing other macrofouling organisms for space. At high fouling intensity a fibrous mat of stolons criss crossed the surface and made the organisms difficult to remove.

The more complex pattern of fouling community development at the Den Helder harbour is subject of the next section. A general model is derived for the temporal changes.

2.3 Modelling of Biofouling

2.3.1 Introduction

Due to the lack of data on the macrofouling process and its sequence and seasonality, there is a lack of models on biofouling and the scarce models that exist are in most cases dealing with bacterial fouling [5-7]. Some examples of models on algal blooms are also available [3-4]. However, no mathematical models were found on marine macrofouling modelling. Since mathematical models would be useful for example for equipment end-users to estimate and predict the chance of biofouling problems, it was decided to use the data obtained at TNO during the experiments described in section 2.2 for the development of a model for biofilm growth in temperate marine waters.

2.3.2 Data Handling

As was described in section 2.2, a multitude of organisms can be present on a biofouled surface and the settlement and growth of the species depend on time of year and presence or absence of other species, in competition for the surface space. Based on the observations combined with the data, a general biofouling interaction model can be derived. Figure 2.16 shows the main categories of organism present. A multitude of interactions are possible between the organisms. The general characteristics of the growth patterns and the interaction between the species, as observed during the field study at TNO, are summarised in Table 2.5.

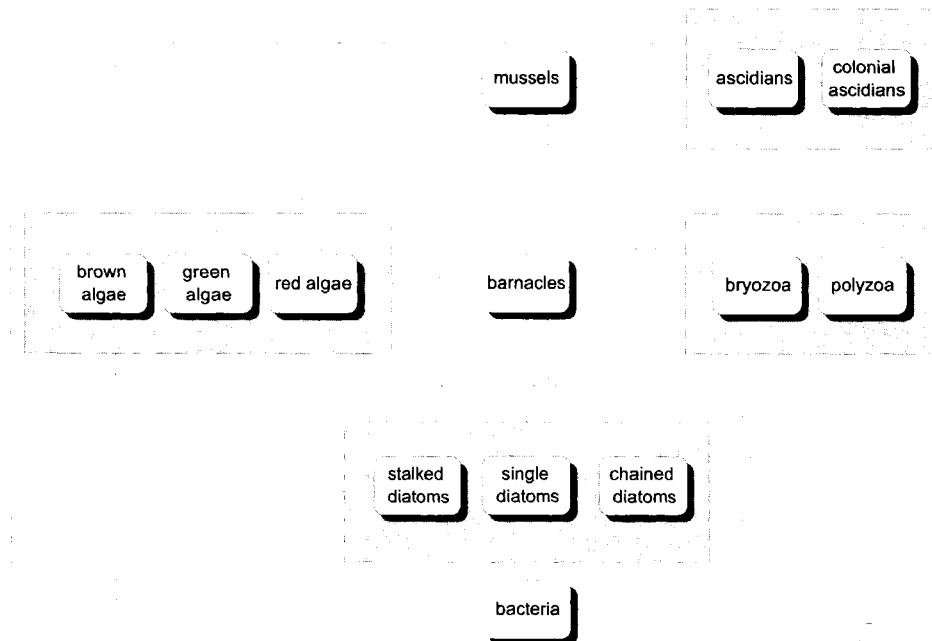


Figure 2.16: General model for biological surface colonisation at Den Helder

Table 2.5: General characteristics of the growth of species throughout the fouling season

Species	Description of fouling pattern
Bacteria	Bacteria are the first colonisers of the surface. Depending on the season, the number increases in the first weeks. The influence of the amount of bacteria on the succeeding macrofouling process could not be determined
Barnacles	In the first four periods a nice S-curved shape with a maximum coverage of 100% is found for barnacle growth. In the fifth period, a peak is found after which the coverage drops again. In the final periods, hardly any barnacle coverage is present. Barnacles are obviously not hindered by other fouling organisms in their settlement on the surface.
Single diatoms	The growth of single diatoms is characterised by a strong initial coverage with a maximum coverage up to 100% after ca. two weeks. Depending on the barnacle growth (repression) a subsequent exponential decay is present.
Chained diatoms	Chained diatoms are present in small numbers. The growth pattern resembles the pattern for single diatoms.
Stalked diatoms	Stalked diatoms are only scarcely present. They occur throughout the fouling season, but a general pattern seems not to be present.
Green algae	Green algae are present throughout the season. Macroalgae occur mostly during summer (June-August). Microalgae occur as well in the rest of the season. Coverage is low, due to the growth manner: attachment at one place and extensive growth into the water.
Brown algae	Brown algae are also present throughout the season. Coverage is higher and lasts longer in Spring and Autumn, due to the lower repressive action of other organisms.
Red algae	Red algae are especially present in the end of the fouling season, but only at low coverage (<5%)
Polyzoa	During the first three periods, polyzoa are present up to 50% coverage. The fouling diminishes after several weeks. Barnacle coverage might play a role.
Mussels	Mussels are only present during July and August. They settle on surfaces fully colonised by barnacles.
Ascidians	Ascidians show a behaviour resembling barnacle coverage. However, the fouling pressure is present in a shorter period and 100% coverage is reached less often.
Colonial ascidians	Coverage with colonial ascidians is difficult to predict. It depends quite a lot on the coverage with other organisms.
Bryozoa	Bryozoa arise during the late season (September) and reached 70% coverage maximum. No obvious interactions with other species were observed.

To obtain practically applicable models from the exposure of the glass samples, simplifications of the data have been necessary. The first simplification rests in the fact that for practical application of a model, the model has to account for the worst case scenario. It has to be certain that the fouling that occurs is **never worse** than the fouling predicted by the model. Therefore for each species at every evaluation point, the highest surface coverage percentage has been taken as a basis for the modelling.

Another simplification that was made was to omit the organisms that never occurred in surface coverage above 5%. Although they might play an important role in the processes taking place, the contribution to the biofilm coverage is minimal. Furthermore, three categories for the different algal species and three for the different diatom species have been joined in algal fouling and diatom fouling. Finally, bacterial biofouling was omitted, since the bacterial fouling will always evolve and will only be the basis for the fouling layer. The influence of bacterial fouling can be large (think of microbial corrosion). In Figure 2.17, the scheme of the simplified interactions is given.

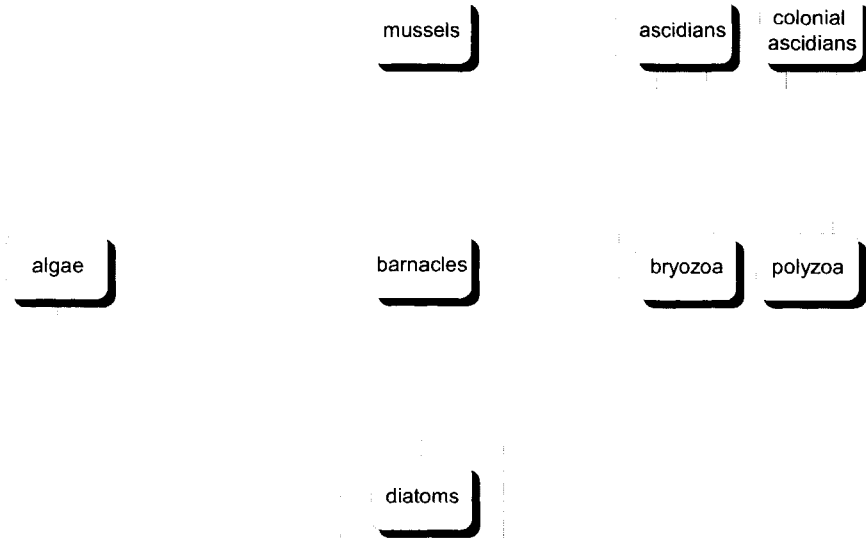
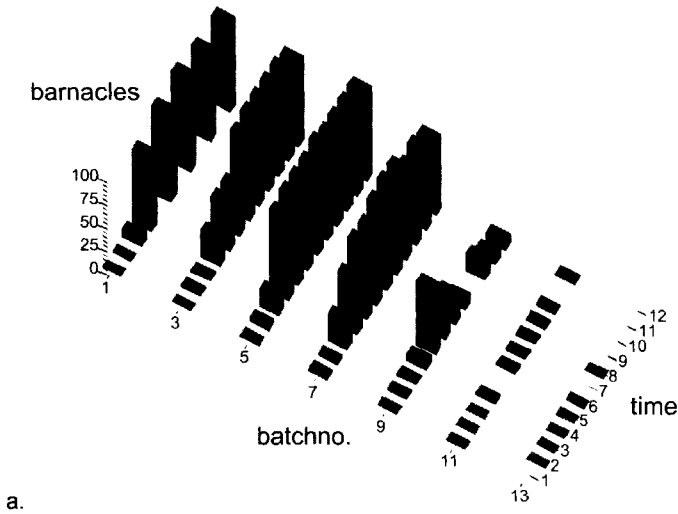
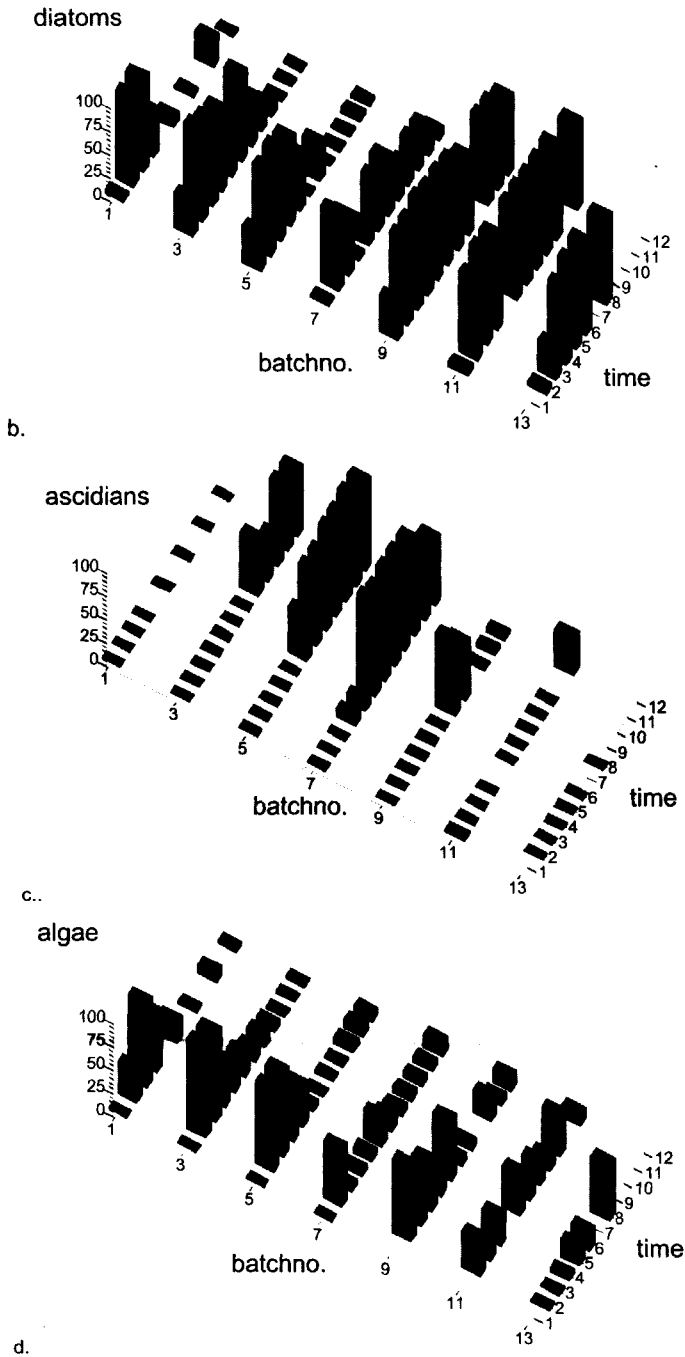
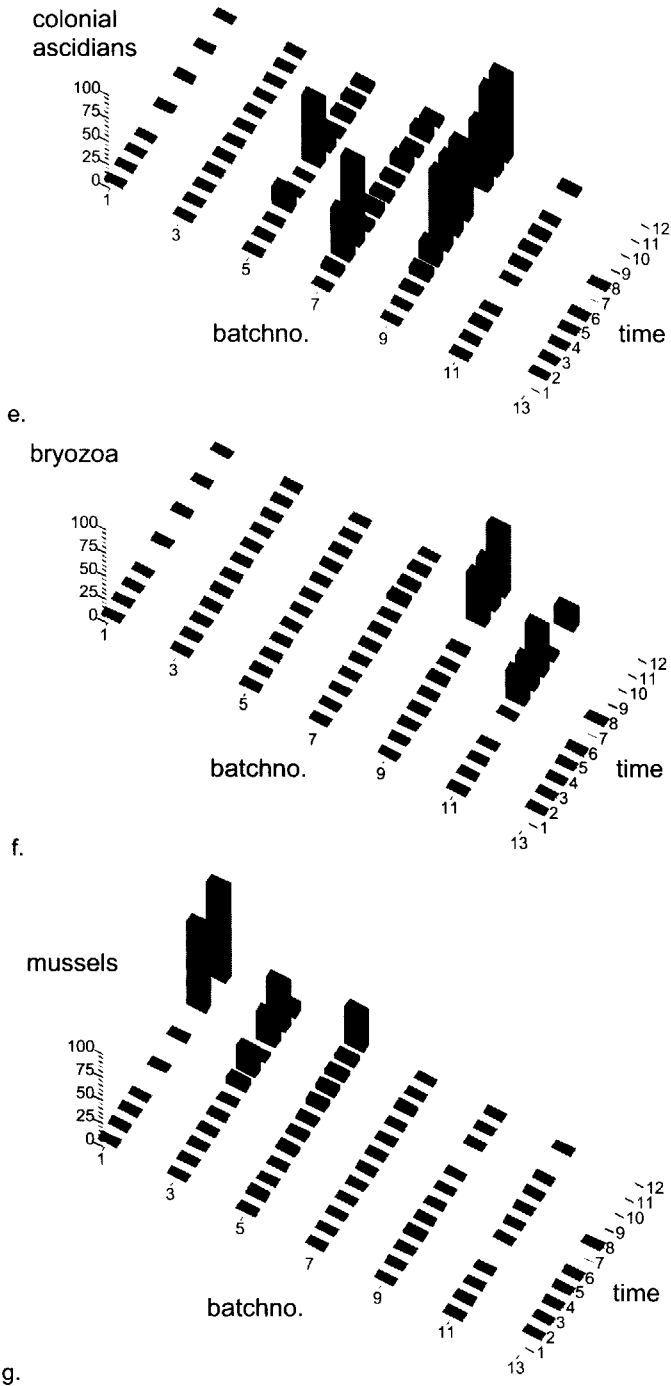


Figure 2.17: Schematic representation of the main fouling organisms and their possible interactions in the build-up of fouling layers.

Figure 2.18 shows the modified data, based on the categories presented in Figure 2.17 and adjusted for a worst case scenario, graphically. At each deployment, two batches were deployed. For the evaluation, these two batches are merged into one, explaining the missing even batch numbers.







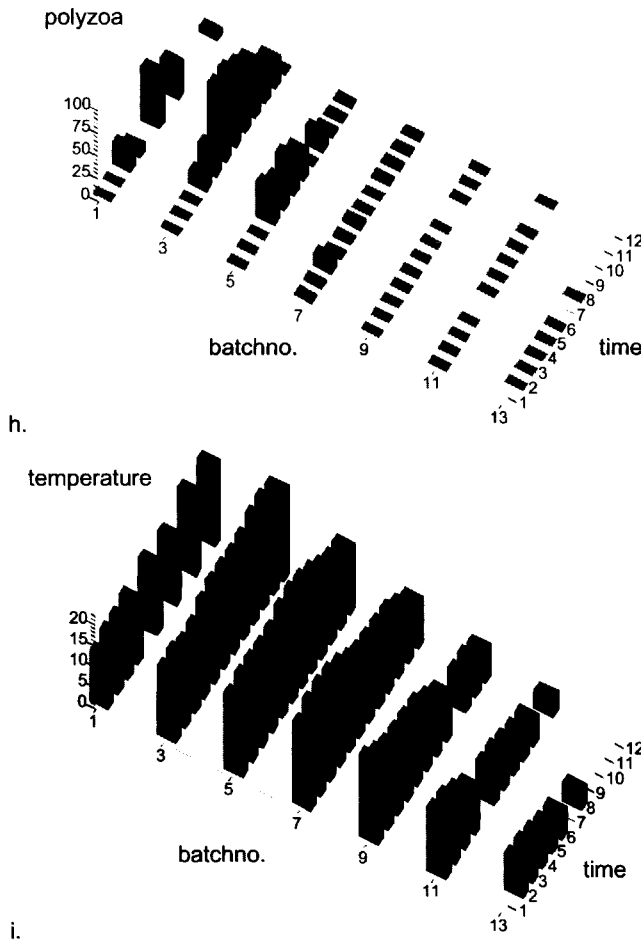


Figure 2.18: Experimental data modified to represent a worst-case for the fouling problem: a. barnacles; b. diatoms; c. ascidians; d. algae; e. colonial ascidians; f. bryozoa; g. mussels; h. hydrozoa; i. temperature (time is given in weeks, coverage in %coverage, temperature in °C).

2.3.3 Model Selection

To obtain useful models, first a base model has to be selected which is used to modify for our purposes. There are several items that the model has to address.

- Incubation time. Before growth starts, there is a certain time period, which the organisms need to settle and adjust to their new situation. This delay time depends on the type of organism, the season, etc.
- Growth rate. Different organisms grow at a different rate. Therefore, growth rate needs to be a parameter that can be adjusted.
- Maximum coverage. When growth starts, it cannot be infinite. A certain maximum coverage of the surface has to be met. This is not necessarily 100% coverage. Depending on season and species, it can be in a range between 0 and 100%.

- Interaction between organisms. Because of the limited space for settlement and growth, the different species will interact: stronger species can out compete the weaker ones and also grazing and predating will take place.
- Environmental parameters. The time of year is very important in regard to the environmental conditions. In winter, water temperature is low and growth rates and settlement frequency are low. Because of the limited biological growth, organic nutrient concentrations are also low. Furthermore, decay of organism concentration could occur.

These conditions can be met by several growth models [48, 49]:

- Gompertz

$$y'(t) = a \cdot \exp(-\exp(b - gt))$$

a = maximum of population
b = delay in start of population growth
g = growth rate
t = time

Used for modelling of growth of for instance individuals and in oncology research (cancer research [36, 37]).

- Avrami

$$y(t) = a(1 - \exp(-(k(t - t_0))^n))$$

a = maximum of population
k = population growth rate
*t*₀ = delay in start of population growth
t = time
n = power (*n* ≥ 1)

Used commonly for spherulitic growth of polymer crystals [38, 39].

- Logistic

$$C_x(t) = \frac{C_{\max}}{1 + \left(\frac{C_{\max}}{C_0} - 1\right)e^{-rt}}$$

C_x(t) = coverage with organism *x*
C_{max} = maximum surface coverage
C₀ = initial surface coverage
r = growth rate
t = time

Commonly used for growth of populations, limited by environmental factors like nutrients or space. The model is an extension of the exponential growth model [40, 41].

All of these models are able to describe S-curve growth as we have observed it. Other well known growth models, like the Monod-model [43]

$$\mu = \frac{\hat{\mu}S}{K_s + S}$$

μ = specific growth rate coefficient
 $\hat{\mu}$ = maximum growth rate coefficient
 S = concentration of limiting nutrient
 K_s = Monod coefficient

are less applicable, since they cannot meet all of the conditions that were set (the Monod-model, for instance, does not contain a lag-phase in the growth).

Since we are searching for simple models in this exploring modelling study, we have chosen logistic growth, which is easy to use and the parameters are clearly addressing the variables that need to be addressed. Furthermore, it is widely applied in other areas of population biology.

Logistic Growth

The logistic growth model has been developed by Verhulst [44] as an extension of the exponential growth model

$$\frac{dN}{dt} = rN \text{ or } N = N_0 e^{rt}$$

N = population size
 r = net growth rate
 t = time

to account for the fact that growth is limited (due to e.g. limited availability of nutrients) and a population will show a maximum size, the maximum sustainable population. This implies that the growth rate, which is the difference between the development and decay rates

$$r = g - d$$

r = growth rate
 g = development rate
 d = decay rate

will become zero, due to the fact that growth will decline, due to the limiting growth condition, and the decay rate will increase, due to the increased population size. Two equations are defined:

$$g = g_0 - k_g N$$

g = development rate
 g_0 = initial development rate
 k_g = development rate decline factor
 N = population size

$$d = d_0 + k_d N$$

d = decay rate
 d_0 = initial decay rate
 k_d = decay rate increase factor
 N = population size

Substituting for r , g and d , we get:

$$\frac{dN}{dt} = (r_0 - (k_g + k_d)N)N$$

$$r_0 = (g_0 - d_0)$$

When the population size stabilises, we get for the maximum sustainable population K :

$$(k_g + k_d) = \frac{r_0}{K}$$

K = maximum sustainable population

This leads us to the logistic growth equation in differential form:

$$\frac{dN}{dt} = r_0 N \left(1 - \frac{N}{K}\right) \quad (2.1)$$

N = population size
 K = maximum sustainable population
 r_0 = initial growth rate
 t = time

When the population size N approaches the maximum sustainable population K , the increase in population in time will decline to zero.

Integrating this equation with boundary condition

$$N(0) = N_0$$

gives us the Logistic growth model in integrated form

$$N(t) = \frac{K}{1 + \left(\frac{K}{N_0} - 1\right)e^{-r_0 t}} \quad (2.2)$$

$N(t)$ = population size
 K = maximum sustainable population
 N_0 = initial population size
 r_0 = initial growth rate
 t = time

If we put

$$e^{r_0 t_0} = \frac{K}{N_0} - 1 \quad \text{or} \quad t_0 = \frac{1}{r_0} \ln\left(\frac{K}{N_0} - 1\right) \quad (2.3)$$

we can rewrite the logistic equation to

$$N(t) = \frac{K}{1 + \exp(-r_0(t - t_0))} \tag{2.4}$$

N(t) = population size
K = maximum sustainable population
r₀ = initial growth rate
t₀ = delay time
t = time

the delay time *t₀* is a measure for the start-up of population growth.

Interacting Species

During the field study, decay occurred on several occasions for the organisms after initial growth to the maximum sustainable population. As we have observed that the most important factor is the presence of another organism, this parameter is now brought into the model. This can be done in several ways:

- Use 'predator-prey' relationships, e.g. Lotka-Volterra, which is based on the logistic growth model (describing intraspecific competition) [45, 46].

In this model, the population sizes of two species are related through two equations:

species 1:

$$\frac{dN_1}{dt} = r_1 N_1 \left(\frac{K_1 + N_1 + \alpha_{12} N_2}{K_1} \right)$$

N₁ = population size of species 1
N₂ = population size of species 2
r₁ = growth rate of species 1
K₁ = maximum sustainable population of species 1
α₁₂ = impact of one species 2 organism on the population size of species 1
t = time

species 2:

$$\frac{dN_2}{dt} = r_2 N_2 \left(\frac{K_2 + N_2 + \alpha_{21} N_1}{K_2} \right)$$

N₁ = population size of species 1
N₂ = population size of species 2
r₂ = growth rate of species 2
K₂ = maximum sustainable population of species 2
α₂₁ = impact of one species 1 organism on the population size of species 2
t = time

The disadvantage of this approach is that there are no pure predator-prey relationships in our study and furthermore the different species show different interactions, which would make the models complex and not easy to handle and interpret.

- Incorporate the decay or growth limitations in the Logistic equations

Within the logistic growth model, growth is limited due to certain parameters. Examples of these parameters are: amount of nutrients present, space, etc.. In our case, space is a basic limiting factor: although the organisms can grow away from the surface, the borders of the glass slide are determining the maximum population on it. Therefore, instead of calculating the maximum number on the slides, the maximum surface coverage is calculated.

Depending on the amount and types of other organisms present, the available surface for an organism to grow on decreases or increases. For example, it was observed that mussels only grow on top of a barnacle layer. Therefore, when the coverage with barnacles increases, the maximum available surface for mussels increases.

The opposite is true for diatoms. The surface fraction covered by barnacles can hardly be covered by diatoms. Since barnacles obtain a much firmer attachment, these will repress the diatoms. Therefore, as the barnacle coverage increases, the maximum available surface fraction for diatoms decreases.

2.3.4 Modelling

Before starting the modelling it was envisaged that a data set of a single season would probably not form a basis for conclusive models with full interactions between the species. This was, however, not the aim of the study. It represents a pilot study to find simple models with only the main interactions between different species. No attempt was made to look into physiological growth mechanisms. The models used are based on the commonly used logistic growth model, equation 2.2, which results in a S-curved growth. Instead of using numbers to express the population size, we use surface coverage as a measure of population size, since surface coverage is the most relevant and moreover, using surface coverage enables us to compare the growth of the different species more directly. This is shown in equation 2.5.

$$C_x(t) = \frac{C_{x,max}}{1 + \left(\frac{C_{x,max}}{C_{x,0}} - 1\right)e^{-rt}} \quad (2.5)$$

$C_x(t)$ = coverage with species x (%)
 $C_{x,max}$ = maximum surface coverage with species x (%)
 $C_{x,0}$ = initial surface coverage with species x (%)
 r = growth rate (weeks⁻¹)
 t = time (weeks)

Due to the interactions presented in Table 2.5, adaptations and/or expansions to the model were made, which are presented below. Each organism is treated separately. For each batch the curves were fitted using the non-linear regression method of SPSS version 10.0.5. Non linear regression was carried out with sequential quadratic programming. The values for the fit parameters C_{max} , and r_0 are graphically displayed as well. Furthermore, the delay time t_0 (c.f. equations 2.3 and 2.4) is shown graphically for each batch and each species:

$$t_0 = \frac{1}{r_0} \ln\left(\frac{C_{x,max}}{C_{x,0}} - 1\right) \tag{2.6}$$

t_0 = delay time before growth start (weeks)
 $C_{x,max}$ = maximum surface coverage with species x (%)
 $C_{x,0}$ = initial surface coverage with species x (%)
 r_0 = growth rate (weeks⁻¹)

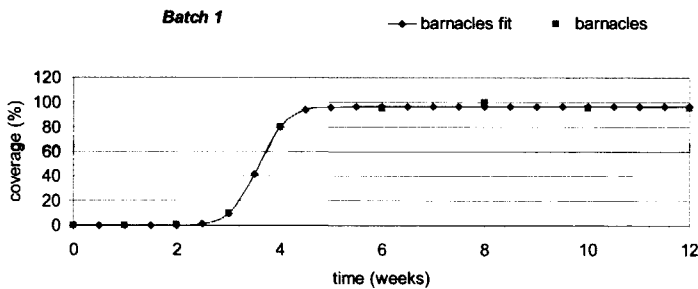
Barnacles

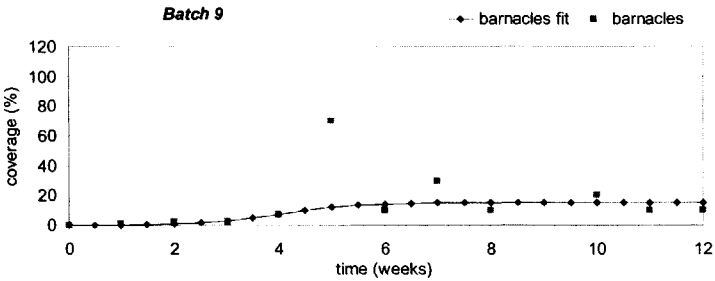
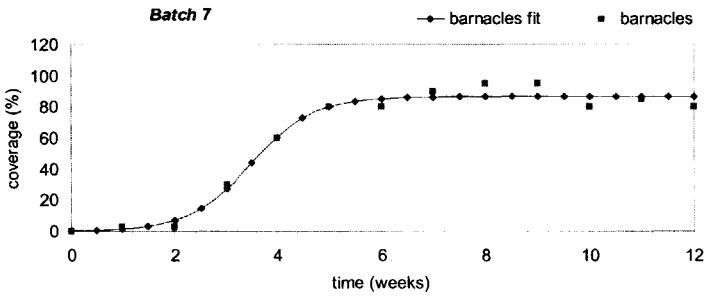
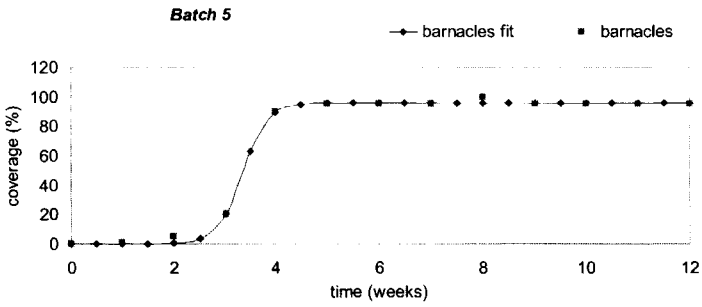
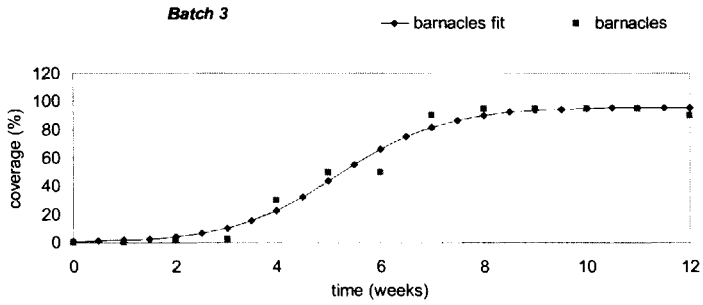
As was stated in Table 2.5, barnacles are strong fouling organisms, apparently not repressed by other organisms. Changes in growth pattern are mainly caused by the fouling season. Therefore the logistic growth model holds without adaptations, equation 2.7.

$$C_b(t) = \frac{C_{b,max}}{1 + \left(\frac{C_{b,max}}{C_{b,0}} - 1\right)e^{-r_0 t}} \tag{2.7}$$

$C_b(t)$ = coverage with barnacles (%)
 $C_{b,max}$ = maximum surface coverage with barnacles (%)
 $C_{b,0}$ = initial surface coverage with barnacles (%)
 r_0 = growth rate (weeks⁻¹)
 t = time (weeks)

Figure 2.19 represents the curves fitted on the data for the six batches where barnacle growth occurred. Except for batch 9, the fitted curves give a very good match to the data. The reason for the poor fit for batch 9 has to do with the decrease in temperature of the seawater. Below a certain temperature, the growth potential decreases rapidly (death rate will exceed the growth rate).





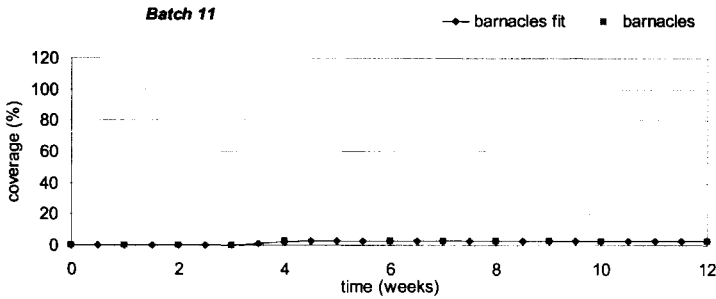


Figure 2.19: Results of modelling of barnacle growth for six batches

Figure 2.20 shows the values for the model parameters C_{max} and r_0 . Furthermore, t_0 is calculated as an indication of the delay time before growth starts, equation 2.8:

$$t_0 = \frac{1}{r_0} \ln\left(\frac{C_{b,max}}{C_{b,0}} - 1\right) \tag{2.8}$$

- t_0 = delay time before growth start (weeks)
- $C_{b,max}$ = maximum surface coverage with barnacles (%)
- $C_{b,0}$ = initial surface coverage with barnacles (%)
- r_0 = growth rate (weeks⁻¹)

Initially, the maximum coverage is high and the delay in growth and the growth rate are low. This is in good agreement with practice, from which the barnacle growth starts in spring and barnacles will cover all immersed structures until the autumn.

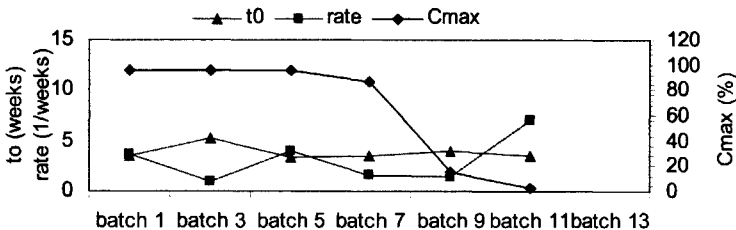


Figure 2.20: Parameter values for the barnacle growth model

Diatoms

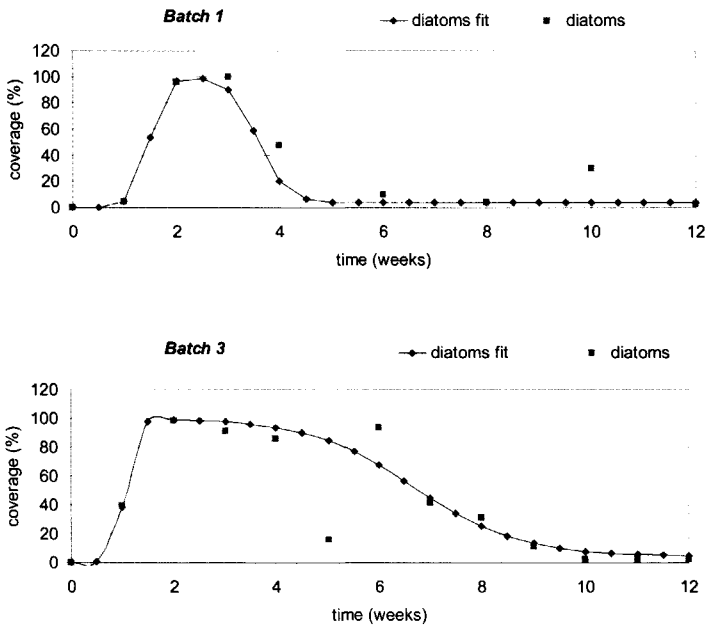
Diatoms are present throughout the fouling season and their presence is mainly influenced by the occurrence of other fouling organisms, which repress the diatoms. The main organism relevant for the repression is the barnacle. Although diatom growth is possible on top of the barnacle, in general coverage is low. Therefore the logistic growth model is adjusted. Just the fraction of the surface not covered by barnacles is available for diatom growth, equation 2.9.

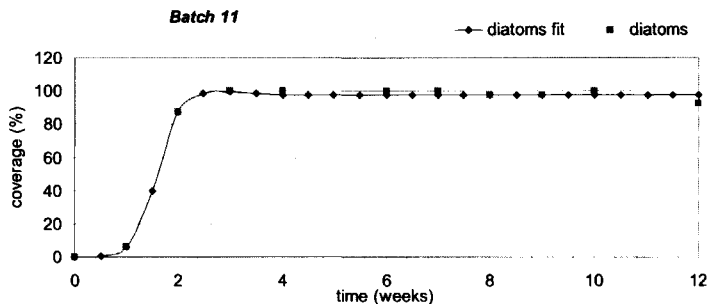
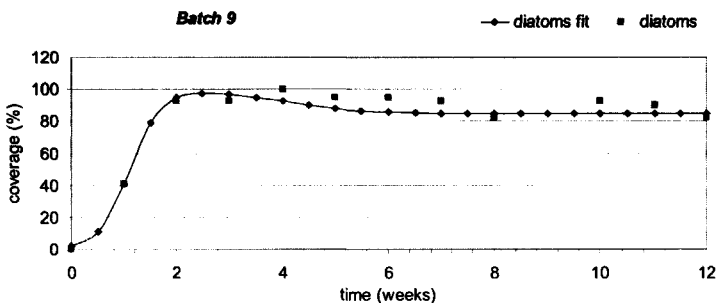
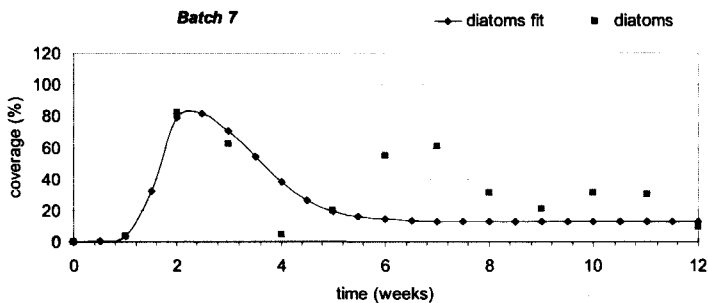
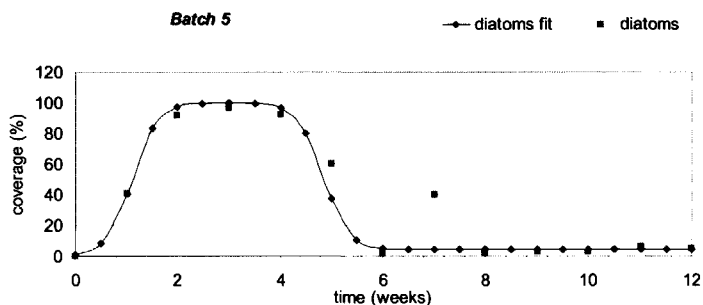
$$C_d(t) = \frac{C_{d,max} (1 - 0.01 \cdot C_b(t))}{1 + \left(\frac{C_{d,max} (1 - 0.01 \cdot C_b(t))}{C_{d,0}} - 1 \right) e^{-r_0 t}} \tag{2.9}$$

- $C_d(t)$ = coverage with diatoms (%)
- $C_b(t)$ = coverage with barnacles (%)
- $C_{d,max}$ = maximum surface coverage with diatoms (%)
- $C_{d,0}$ = initial surface coverage with diatoms (%)
- r_0 = growth rate (weeks⁻¹)
- t = time (weeks)

Figure 2.21 shows the curves fitted to the data for diatom coverage. Both the incline and decline in surface coverage are properly modelled. The coverage repression by barnacles can clearly be observed. This effect diminishes at the end of the season. In this period, diatom fouling can cover the whole surface area until the end of the exposure period.

One adaptation had to be made to the model. For each organism, the highest cover percentage is used, because we deal with a worst case approach. Hence, the highest diatom coverage is presented in conjunction with the highest barnacle coverage. If this highest barnacle coverage is used to model the decline in diatom coverage, it will result in the lowest diatom coverage. In fact, the decline in diatom coverage starts too soon. Therefore, the barnacle coverage function used to model the diatom coverage in equation 2.9 was adjusted with a delay of two weeks.





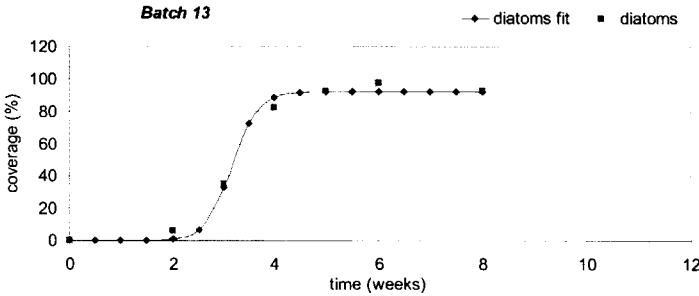


Figure 2.21: Results of modelling of diatom growth for seven batches

Figure 2.22 shows the values for the model parameters C_{max} and r_0 for the different batches. It is clear that the parameters hardly change during the fouling season and thus the growth of diatoms appears to be hardly influenced by the time of the year. As a measure of the delay before growth starts, t_0 is calculated according to equation 2.10:

$$t_0 = \frac{1}{r_0} \ln\left(\frac{C_{d,max}}{C_{d,0}} - 1\right) \tag{2.10}$$

- t_0 = delay time before growth start (weeks)
- $C_{d,max}$ = maximum surface coverage with diatoms (%)
- $C_{d,0}$ = initial surface coverage with diatoms (%)
- r_0 = growth rate (weeks⁻¹)

In this case, it is not completely correct to calculate t_0 in this manner, since the factor in the denominator of equation 2.9 is not a constant due to the influence of $C_b(t)$. However, it still gives a good indication of the delay time. Note that $C_b(0)$ is small.

t_0 is a little higher at the end of the season, this effect is likely to increase in winter, leading to very low overall coverage. Growth rate is higher in spring. This is in good agreement with the observation of a dense multi species biofilm, especially in spring.

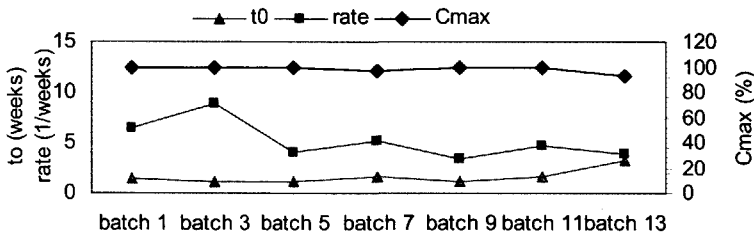


Figure 2.22: Parameter values for the diatom growth model

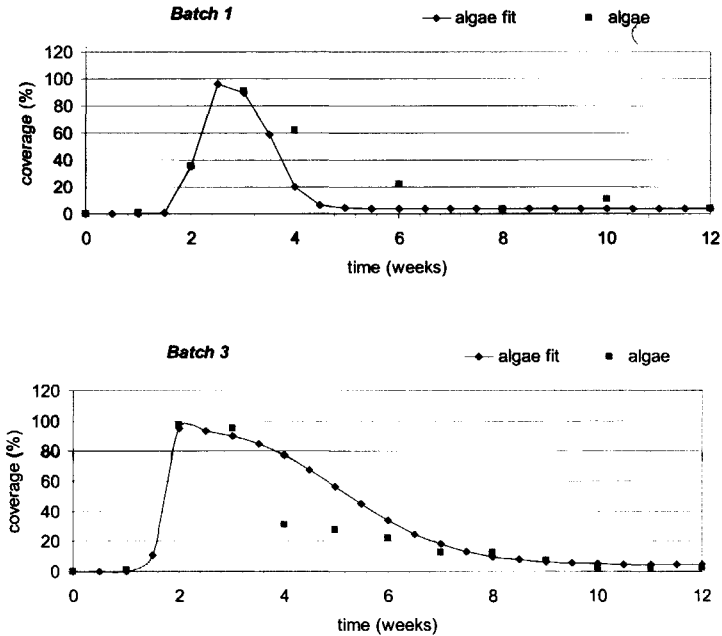
Macro-algae

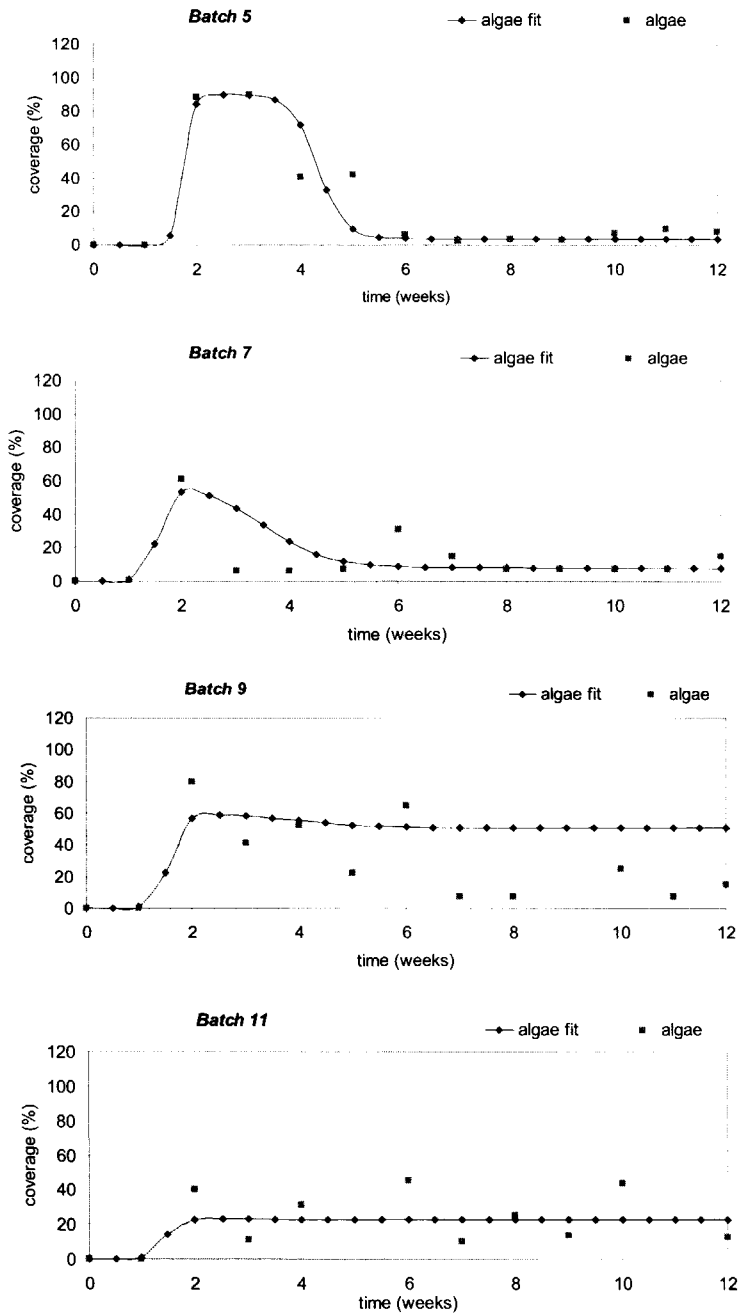
As is the case for diatoms, also macro-algae are mainly out competed by the growth of barnacles. Therefore the same adaptation to the logistic growth model was made, equation 2.11.

$$C_a(t) = \frac{C_{a,max}(1 - 0.01 \cdot C_b(t))}{1 + \left(\frac{C_{a,max}(1 - 0.01 \cdot C_b(t))}{C_{a,0}} - 1 \right) e^{-r_0 t}} \tag{2.11}$$

- $C_a(t)$ = coverage with algae (%)
- $C_b(t)$ = coverage with barnacles (%)
- $C_{a,max}$ = maximum surface coverage with algae (%)
- $C_{a,0}$ = initial surface coverage with algae (%)
- r_0 = growth rate (weeks⁻¹)
- t = time (weeks)

Figure 2.23 shows the results for fitting this model to the worst-case data. Except for some data points, the model is able to predict the general trend in the data. Largest deviations are found in the data for batch 7, where after a peak in week 2, the algae coverage diminishes in week 3, 4 and 5.





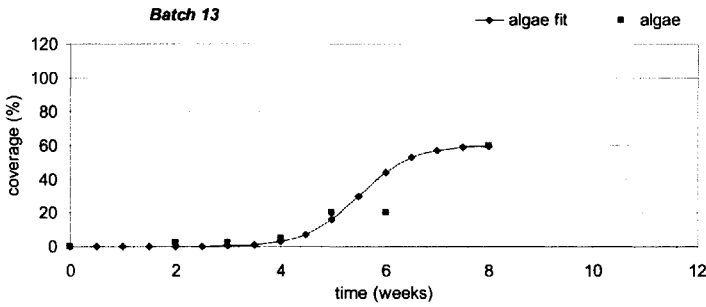


Figure 2.23: Results of modelling of algae growth for seven batches

Figure 2.24 shows the parameter values for the algal growth model. t_0 is calculated using equation 2.12, with the same restriction as t_0 for diatoms, equation 2.10.

$$t_0 = \frac{1}{r_0} \ln\left(\frac{C_{a,max}}{C_{a,0}} - 1\right) \tag{2.12}$$

- t_0 = delay time before growth start (weeks)
- $C_{a,max}$ = maximum surface coverage with algae (%)
- $C_{a,0}$ = initial surface coverage with algae (%)
- r_0 = growth rate (weeks⁻¹)

It can be seen that algae growth is faster and coverage is higher in the beginning of the fouling season. This is in agreement with the fact that light levels in the water are higher during spring and the fact that predation by fish and epi-benthic organisms is low.

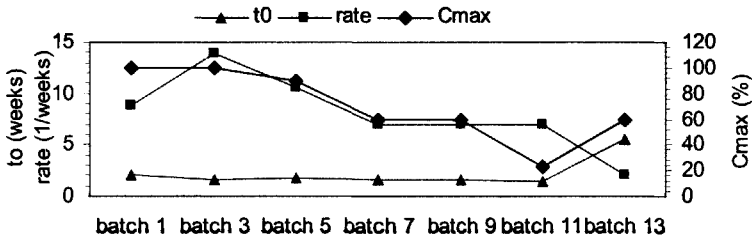


Figure 2.24: Parameter values for the algal growth model

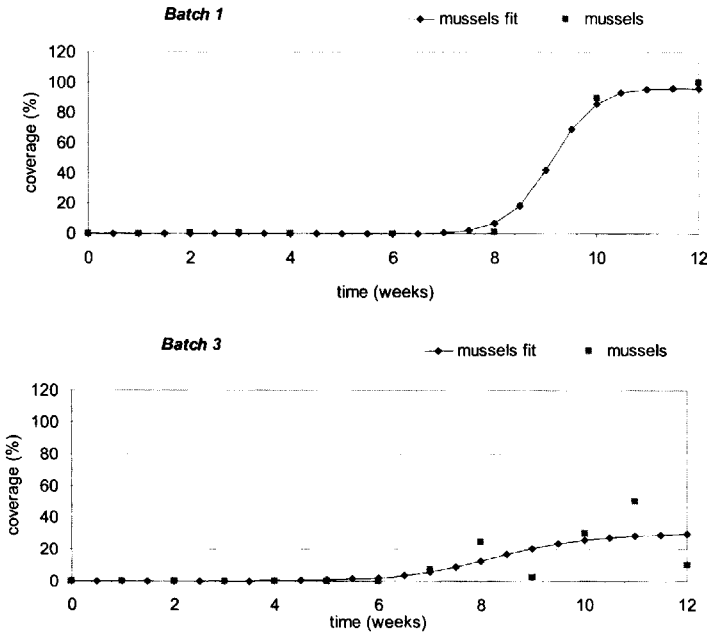
Mussels

Mussels were only able to colonise the surfaces in three of the batches, this probably has to do with a certain recruitment periodicity. In the other cases they did not develop. It was shown that mussels needed a solid base to settle and grow on and therefore in our case they only appeared on barnacle covered areas, since adhesion to the glass slides is poor. The growth model is adjusted for this effect, equation 2.13.

$$C_m(t) = \frac{C_{m,max} (0.01 \cdot C_b(t))}{1 + \left(\frac{C_{m,max} (0.01 \cdot C_b(t))}{C_{m,0}} - 1 \right) e^{-r_0 t}} \tag{2.13}$$

$C_m(t)$ = coverage with mussels (%)
 $C_b(t)$ = coverage with barnacles (%)
 $C_{m,max}$ = maximum surface coverage with mussels (%)
 $C_{m,0}$ = initial surface coverage with mussels (%)
 r_0 = growth rate (weeks⁻¹)
 t = time (weeks)

Figure 2.25 shows the fit results. The coverage increased up to 100% in the first batch. In later batches this didn't happen any more, either due to the decreased growth rate (batch 3) or due to the increased delay time (batch 5).



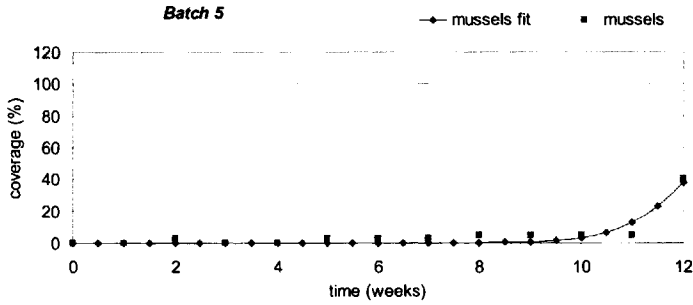


Figure 2.25: Results of modelling of mussel growth for three batches

Figure 2.26 shows the values of the parameters in the fits. t_0 is calculated as an indication for delay time using equation 2.14. Again, t_0 is only an indication of the delay time, due to the influence of $C_b(t)$.

$$t_0 = \frac{1}{r_0} \ln\left(\frac{C_{m,max}}{C_{m,0}} - 1\right) \tag{2.14}$$

- t_0 = delay time before growth start (weeks)
- $C_{m,max}$ = maximum surface coverage with mussels (%)
- $C_{m,0}$ = initial surface coverage with mussels (%)
- r_0 = growth rate (weeks⁻¹)

Due to the different effects that cause the differences in surface coverage and the fact that mussels only occurred during three batches, no general trends are present in the parameters, except for the increase in delay time.

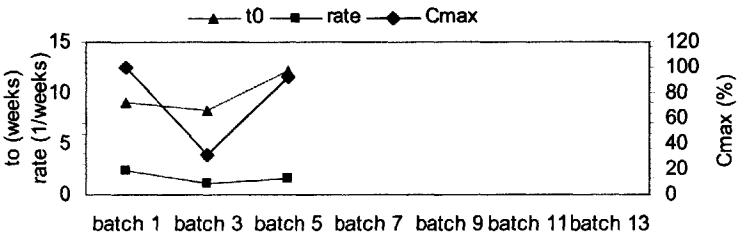


Figure 2.26: Parameter values for the mussel growth model

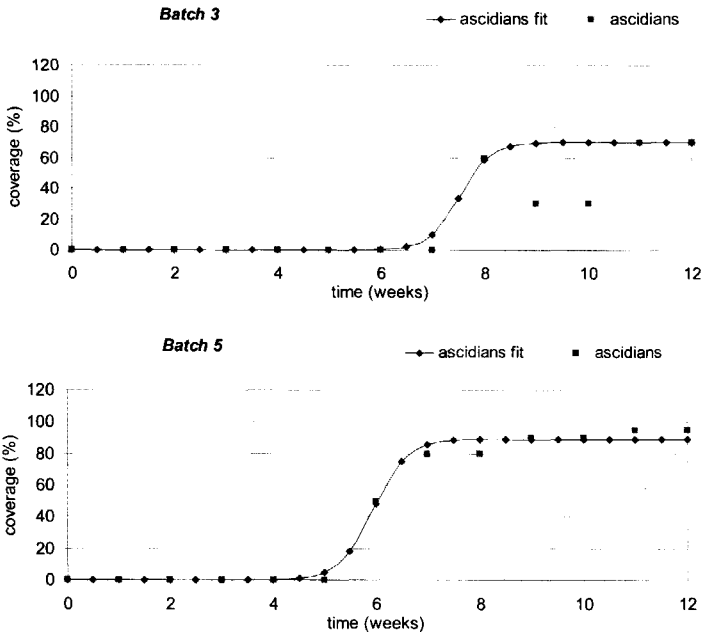
Ascidians

Ascidians are strong settlers, like the barnacles. Their settlement is hardly influenced by other species. Therefore, the logistic growth model can be applied without adaptations, equation 2.15.

$$C_{asc}(t) = \frac{C_{asc,max}}{1 + \left(\frac{C_{asc,max}}{C_{asc,0}} - 1 \right) e^{-r_0 t}} \tag{2.15}$$

$C_{asc}(t)$ = coverage with ascidians (%)
 $C_{asc,max}$ = maximum surface coverage with ascidians (%)
 $C_{asc,0}$ = initial surface coverage with ascidians (%)
 r_0 = growth rate (weeks⁻¹)
 t = time (weeks)

Figure 2.27 shows the results of the curve fitting using this growth model. As can be seen, the model is able to predict the data values accurately. For batches 7 and 9, a decrease in coverage is present in the end of the curves. This is, as was the case in batch 9 for the barnacles, due to the rapid change in environment towards the winter. The ascidians are no longer able to sustain themselves and death rate will exceed the growth rate. This change is most easily measured in a decrease in temperature.



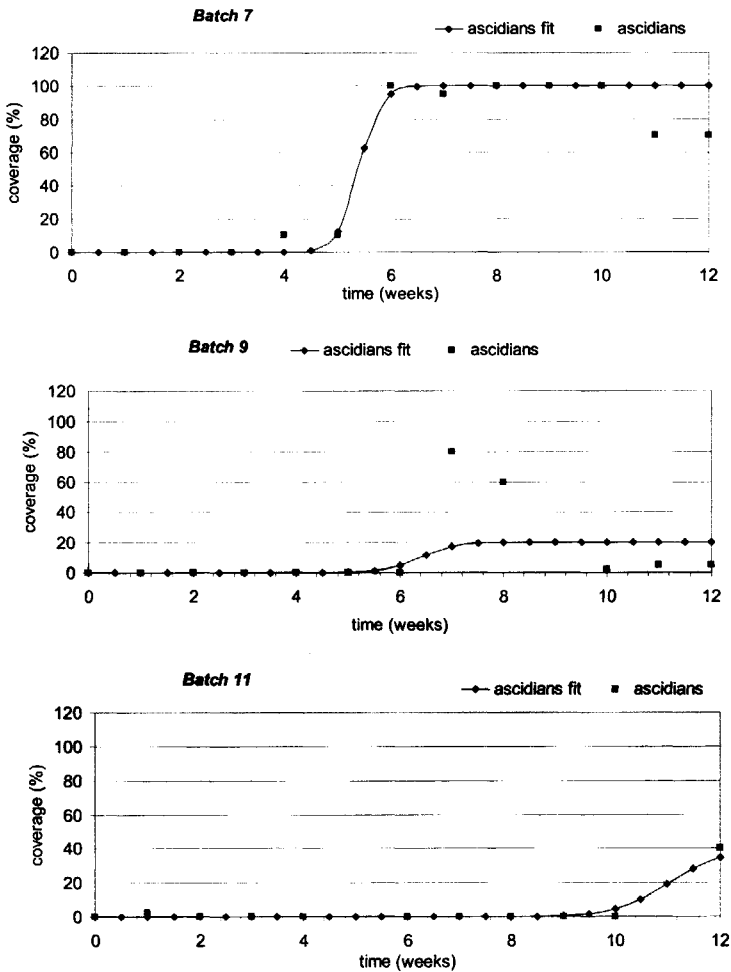


Figure 2.27: Results of modelling of ascidian growth for five batches

Figure 2.28 shows the parameter values for the models and the delay time t_0 as calculated using equation 2.16:

$$t_0 = \frac{1}{r_0} \ln\left(\frac{C_{asc,max}}{C_{asc,0}} - 1\right) \tag{2.16}$$

t_0 = delay time before growth start (weeks)

$C_{asc,max}$ = maximum surface coverage with ascidians (%)

$C_{asc,0}$ = initial surface coverage with ascidians (%)

r_0 = growth rate (weeks⁻¹)

Obvious is the increase in growth rate and decrease in delay time during summer. Furthermore, the maximum surface coverage increases during the season till the end of summer. Due to the increased death rate and decreased growth rate from this point onwards, the maximum sustainable population decreases sharply.

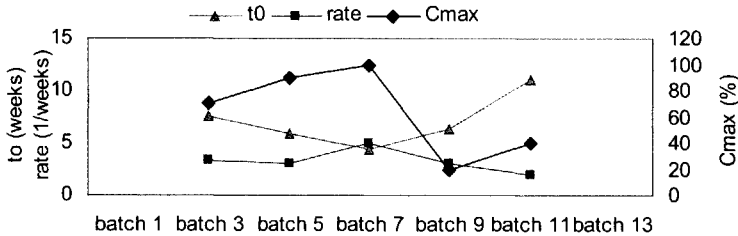


Figure 2.28: Parameter values for the ascidian growth model

The effect observed at the end of the fouling season, a sharp decrease in growth potential which we contribute mainly to the decrease in temperature, is a direct effect that can be explained by the fact that for many biological processes, a minimum, optimum and maximum temperature exist for the growth rate of organisms. This effect has for example been modelled by Logan [43, 47, 50] with an equation relating the growth rate to temperature. The equation from literature is slightly adjusted to give a form in which all parameters have a physiological meaning, equation 2.17¹.

$$r(T(t)) = r_{max} \left[\frac{(T(t) - T_{min})^2}{(T(t) - T_{min})^2 + (T_h - T_{min})^2} - \exp\left\{ \frac{T(t) - T_{max}}{T_{max} - T_{opt}} \right\} \right] \quad (2.17)$$

$r(T(t))$ = growth rate (weeks⁻¹)

$T(t)$ = temperature (°C)

r_{max} = maximum growth rate (weeks⁻¹)

T_{min} = lower growth limiting temperature (°C)

T_h = "half-saturation" temperature (°C)

T_{max} = upper growth limiting temperature (°C)

T_{opt} = optimum growth temperature (°C)

t = time (weeks)

Other types of temperature dependence of the growth rate are discussed by McMeekin, Hastings and Shimoni [48, 49, 51].

To incorporate the temperature dependent specific growth rate of equation 2.17, we have to return to the logistic growth equation in differential form, equation 2.1. Since the temperature is changing in time and the specific time dependence is not known, it is not possible any more to find an analytical solution for the integrated growth rate. Therefore we leave the integral in the equation and integrate the $r(T(t))$ numerically using the trapezoidal rule in order to find estimates for the temperature dependent ascidian coverage, equation 2.18.

¹ Note that the Logan-equation given in Haefner [43] is in fact incorrect.

$$C_{asc}(t) = \frac{C_{asc,max}}{1 + \left(\frac{C_{asc,max}}{C_{asc,0}} - 1\right)e^{-\int r(T(t))dt}} \tag{2.18}$$

$C_{asc}(t)$ = coverage with ascidians (%)
 $C_{asc,max}$ = maximum surface coverage with ascidians (%)
 $C_{asc,0}$ = initial surface coverage with ascidians (%)
 $r(T(t))$ = time dependent growth rate (weeks⁻¹)
 t = time (weeks)

If we take $r_{max} = 3.6 \text{ weeks}^{-1}$; $T_{max} = 30^{\circ}\text{C}$; $T_h = 16^{\circ}\text{C}$; $T_{min} = 3^{\circ}\text{C}$; $T_{opt} = 25^{\circ}\text{C}$, we are able to predict the growth of the ascidians quite accurately, with the T(t)-profile of Figure 2.18i, in those cases where the effect of temperature was present, see Figure 2.29. The calculated r-profile is given in Figure 2.30.

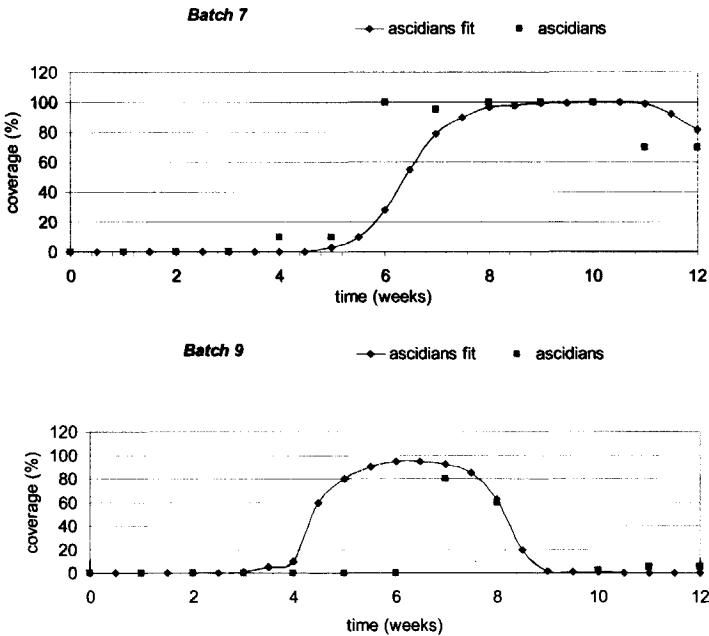


Figure 2.29: Results of modelling of ascidian growth for two batches including the effect of temperature decrease on the growth rate.

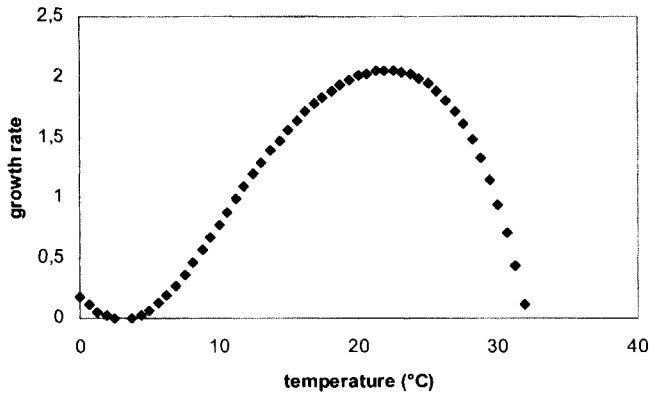


Figure 2.30: r -profile as a function of temperature, as calculated using equation 2.17. $r_{max} = 3.6 \text{ weeks}^{-1}$; $T_{max} = 30^\circ\text{C}$; $T_h = 16^\circ\text{C}$; $T_{min} = 3^\circ\text{C}$; $T_{opt} = 25^\circ\text{C}$

Polyzoa

Polyzoa are influenced by barnacles, mussels and ascidians. Especially mussels and ascidians can repress polyzoan growth, most likely due to competition for space. This has to be taken into account in the model, equation 2.19 (not taking into account the decline in ascidian coverage in batch 7 and 9). For multispecies repression, it is not possible to use just the fraction of total coverage, since the coverage is not cut off at 100%. Therefore the total coverage was divided by a certain total coverage C_{total} , which varied depending on the amount of repressing species present. Here C_{total} is 200%.

$$C_p(t) = \frac{C_{p,max} \left(1 - \frac{C_b(t) + C_{asc}(t)}{C_{total}(t)}\right)}{1 + \left(\frac{C_{p,max} \left(1 - \frac{C_b(t) + C_{asc}(t)}{C_{total}(t)}\right)}{C_{p,0}} - 1\right) e^{-r_0 t}} \tag{2.19}$$

- $C_p(t)$ = coverage with polyzoa (%)
- $C_b(t)$ = coverage with barnacles (%)
- $C_{asc}(t)$ = coverage with ascidians (%)
- C_{total} = maximum total coverage (%)
- $C_{p,max}$ = maximum surface coverage with polyzoa (%)
- $C_{p,0}$ = initial surface coverage with polyzoa (%)
- r_0 = growth rate (weeks^{-1})
- t = time (weeks)

Figure 2.31 shows the data and the fits for the model. Both the growth and the decay are modelled properly. Figure 2.32 shows the values for the model parameters C_{max} and r_0 . Furthermore an indication for the delay in growth start is found in t_0 , equation 2.20. Due to the influence of $C_b(t)$ and $C_{asc}(t)$, it can only be regarded as an indication of the delay.

$$t_0 = \frac{1}{r_0} \ln\left(\frac{C_{p,max}}{C_{p,0}} - 1\right) \tag{2.20}$$

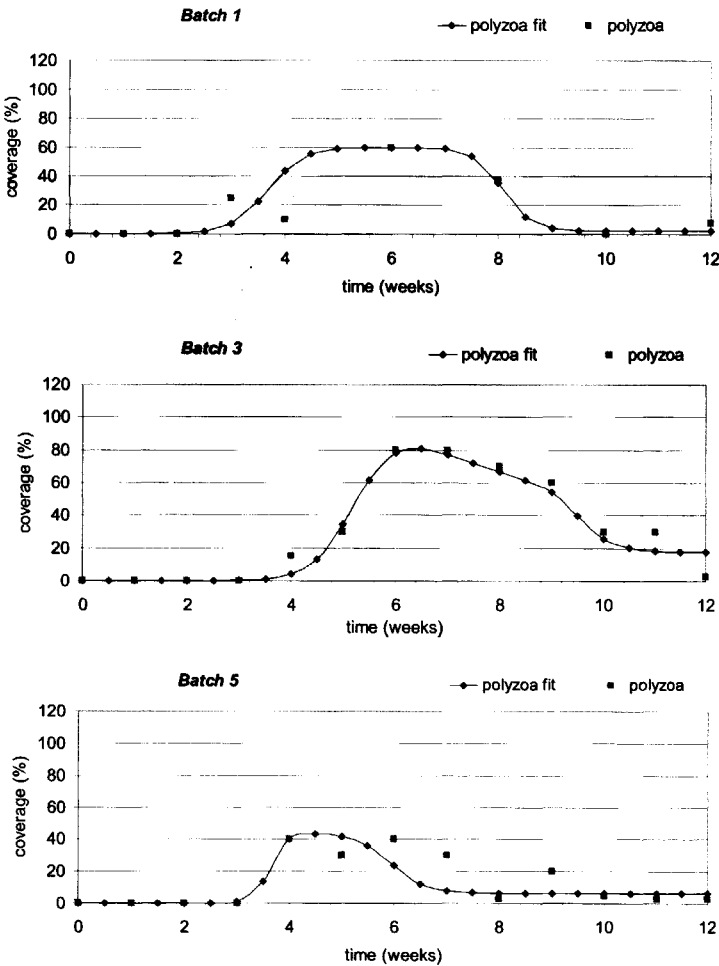
t_0 = delay time before growth start (weeks)

$C_{p,max}$ = maximum surface coverage with polyzoa (%)

$C_{p,0}$ = initial surface coverage with polyzoa (%)

r_0 = growth rate (weeks⁻¹)

The maximum coverage increases initially but it decreases after batch 3. This is in agreement with the practical observation of a peak in the polyzoan presence during spring. The increased growth rate was partially an effect of the increased water temperature and the more plentiful food supply.



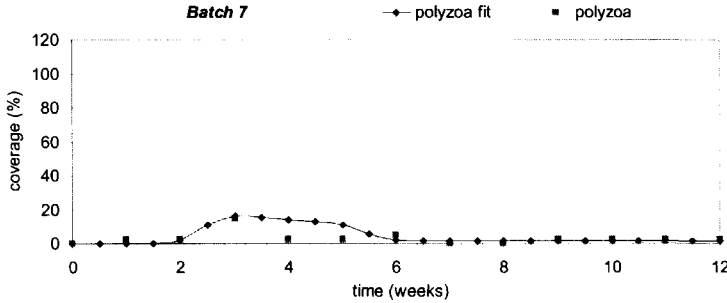


Figure 2.31: Results of modelling of polyzoa growth for four batches

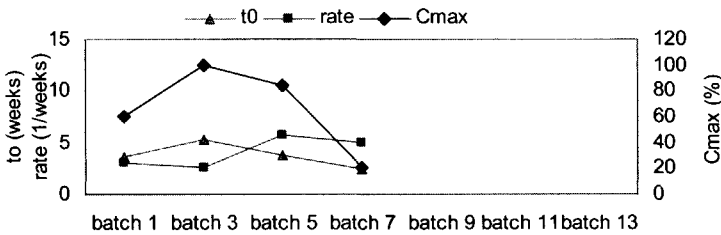


Figure 2.32: Parameter values for the polyzoa growth model

Colonial ascidians (*Botryllus schlosseri*).

As is the case for the polyzoa, colonial ascidians can be repressed by different organisms as well. Especially the barnacles and the ascidians are of importance. The growth model is adapted in a similar way as for the polyzoa, equation 2.21.

$$C_{col}(t) = \frac{C_{col,max} \left(1 - \frac{C_b(t) + C_{asc}(t)}{C_{total}(t)}\right)}{1 + \left(\frac{C_{col,max} \left(1 - \frac{C_b(t) + C_{asc}(t)}{C_{total}(t)}\right)}{C_{col,0}} - 1\right) e^{-r_0 t}} \tag{2.21}$$

- $C_{col}(t)$ = coverage with colonial ascidians (%)
- $C_b(t)$ = coverage with barnacles (%)
- $C_{asc}(t)$ = coverage with ascidians (%)
- C_{total} = maximum total coverage (%)
- $C_{col,max}$ = maximum surface coverage with colonial ascidians (%)
- $C_{col,0}$ = initial surface coverage with colonial ascidians (%)
- r_0 = growth rate (weeks⁻¹)
- t = time (weeks)

As is visible in Figure 2.33, the models can fit the data, except for batch 5. Although, due to the absence of colonial ascidians in week 5 and 6, the fit is rather poor.

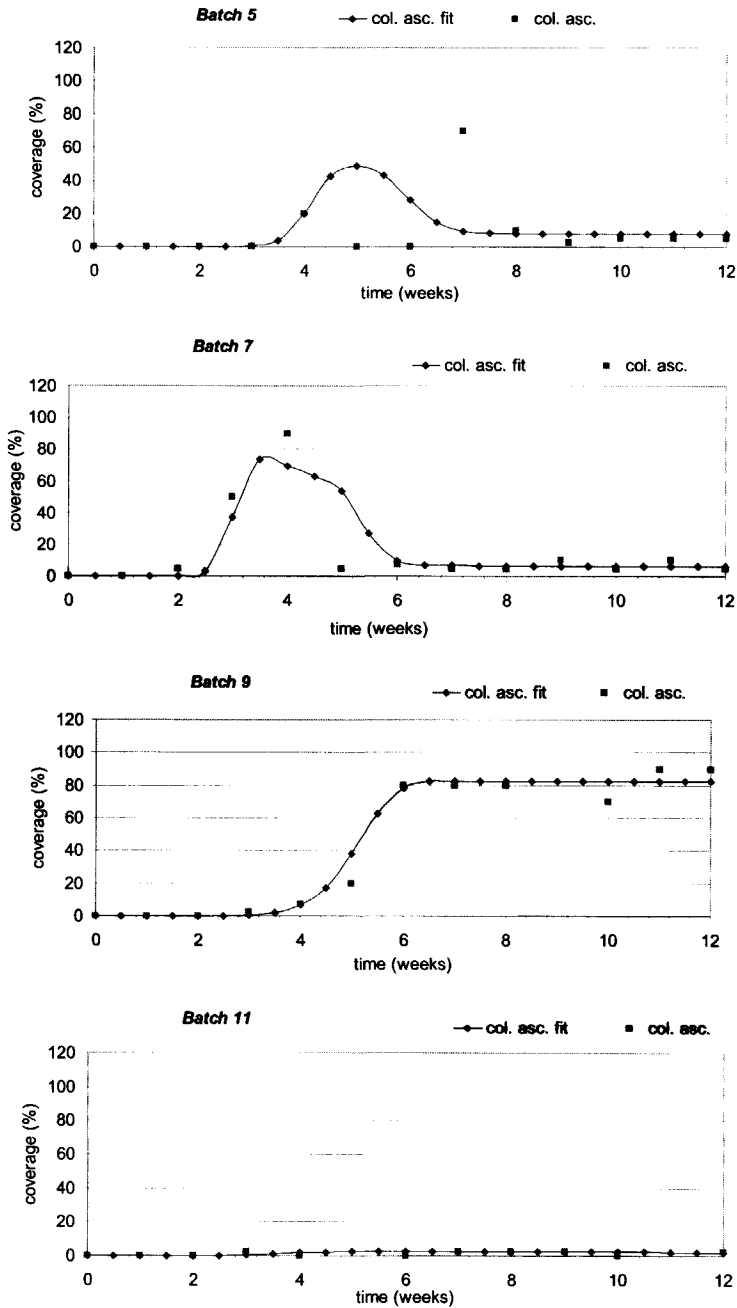


Figure 2.33: Results of modelling of Colonial ascidians growth for four batches

Figure 2.34 shows the values for the model parameters C_{max} and r_0 . t_0 is calculated as an indication of delay time, equation 2.22. Again, due to the influence of $C_b(t)$ and $C_{asc}(t)$, it is only an indication of the delay time. Maximum coverage is more or less constant during the period the Colonial ascidians are present, indicating that the organisms can cover the whole surface, if no other species would be present.

$$t_0 = \frac{1}{r_0} \ln\left(\frac{C_{col,max}}{C_{col,0}} - 1\right) \tag{2.22}$$

t_0 = delay time before growth start (weeks)
 $C_{col,max}$ = maximum surface coverage with colonial ascidians (%)
 $C_{col,0}$ = initial surface coverage with colonial ascidians (%)
 r_0 = growth rate (weeks⁻¹)

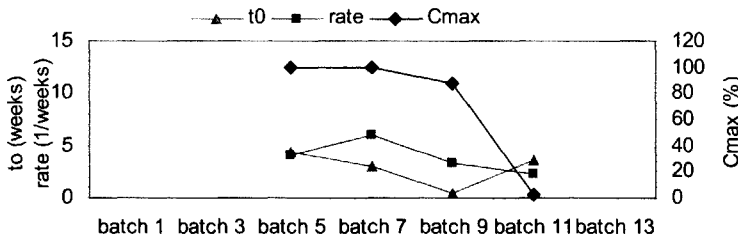


Figure 2.34: Parameter values for the colonial ascidians growth model

Bryozoa

Bryozoa were only present late in the season and therefore no significant interactions could be observed with e.g. barnacles or ascidians. The logistic growth model is applicable again, equation 2.23.

$$C_{bryo}(t) = \frac{C_{bryo,max}}{1 + \left(\frac{C_{bryo,max}}{C_{bryo,0}} - 1\right)e^{-r_0 t}} \tag{2.23}$$

$C_{bryo}(t)$ = coverage with bryozoa (%)
 $C_{bryo,max}$ = maximum surface coverage with bryozoa (%)
 $C_{bryo,0}$ = initial surface coverage
 r_0 = growth rate (weeks⁻¹)
 t = time (weeks)

Figure 2.35 shows the model fits to the data. Improving the fits could be possible only when more data would be available. Figure 2.36 shows the parameter values for the models with t_0 as delay time calculated using equation 2.24. The peak in maximum coverage combined with the low value for the delay are due to the very short period in which the bryozoa can grow (due to absence of other organisms to repress bryozoa growth).

$$t_0 = \frac{1}{r_0} \ln\left(\frac{C_{bryzo,max}}{C_{bryzo,0}} - 1\right) \tag{2.24}$$

t_0 = delay time before growth start (weeks)
 $C_{bryzo,max}$ = maximum surface coverage with bryozoa (%)
 $C_{bryzo,0}$ = initial surface coverage with bryozoa (%)
 r_0 = growth rate (weeks⁻¹)

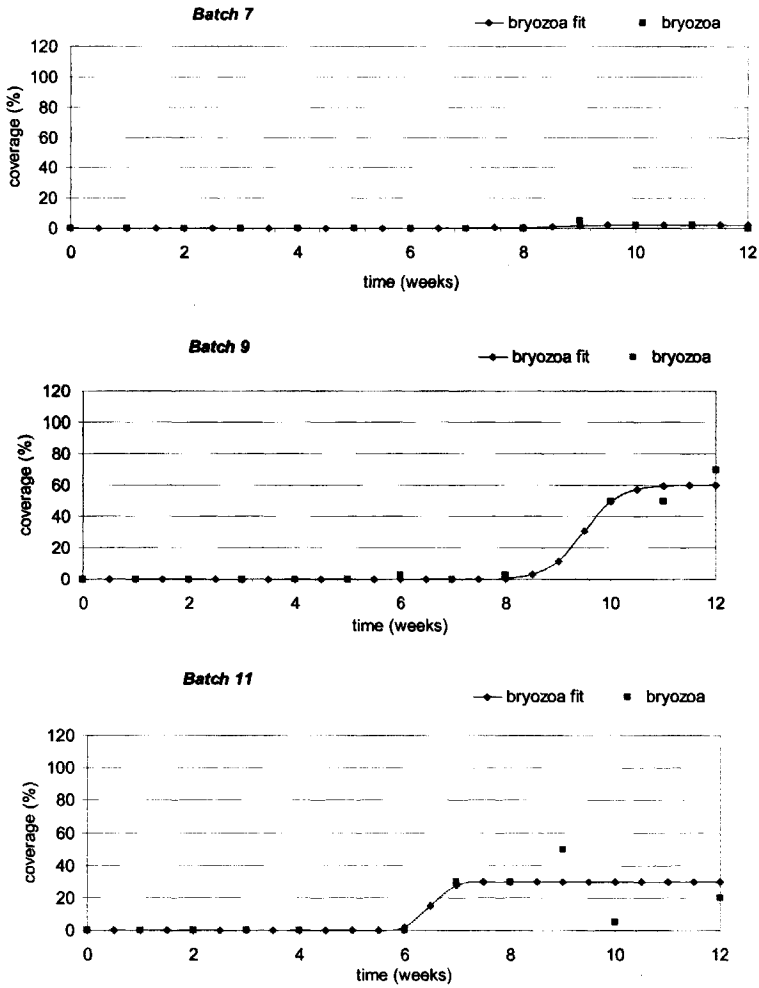


Figure 2.35: Results of modelling of bryozoa growth for three batches

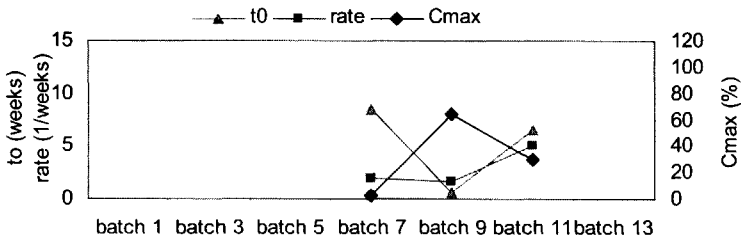


Figure 2.36: Parameter values for the bryozoa growth model

2.3.5 General Discussion

Based on the data presented, it can be concluded that the increases of the dominant populations in a biofouling community could be adequately modelled using the often applied logistic growth model. Although no exact information was obtained from the parameter values, the changes could qualitatively be explained and the models appear suitable for predictions regarding fouling.

The effect of seasonal changes could in most cases be seen as a change in the growth rate parameter. For barnacles and ascidians, this was not enough. In the autumn, the change in environmental conditions, clearly evident in a decrease in seawater temperature, was so large that the coverage decreased towards the end of the exposures. This decline can be explained by the increase in death rate and decrease in development rate. To account for this effect in the models, we have incorporated a temperature effect in the growth rate, suggested by Logan, which comprises a minimum, optimum and maximum growth temperature. With this addition to the model, it turned out to be possible to fit the decline in coverage quite good.

Though we are aware that temperature is not the only parameter that directly influences the growth potential, it has been selected here, since it was the only parameter for which accurate data were readily available. Other parameters like light intensity, amount of nutrients in the water, etc. could have as much influence as the temperature. Their effects will most likely show a seasonal pattern comparable to the pattern observed for the temperature.

The models presented here were only able to show the development and decay. However, for practical applicability one should also be able to predict the settlement during the season. This has not yet been possible, based on the available data. A much more in-depth study of the environment would be required to see which parameters (e.g. water temperature, dissolved oxygen content, silt content) are the main factors influencing the growth initiation processes.

2.4 Conclusions

This chapter focussed on the process of biofouling on surfaces in marine environments. The sequence in fouling communities and the dependency on time of the year of deployment and deployment site were investigated. Three sites were incorporated in the study, Den Helder (The Netherlands, Millport (Scotland) and Cascais (Portugal). The site with the heaviest fouling pressure and the most diverse fouling pattern was the Den Helder site. The data collected on the fouling process in Den Helder were used to develop mathematical models, which could eventually serve the end-users of installations and equipment in the marine environments to use appropriate antifouling procedures.

It can be concluded from the analysis given in section 2.2 that both deployment date and site are crucial parameters determining the fouling burden. Especially the differences between Den Helder and Millport could show this. Furthermore, it was evident that the generally assumed model for biofilm development was valid in all three cases, the time period of development being dependent on the time of year. The biofilms are, especially in summer, rapidly overgrown by macrobiota.

For the Den Helder site it could further be concluded that the deployment date influenced the resulting dominant fouling organisms strongly. For example mussels, ascidians and polyzoa are incapable of overgrowing one another and therefore if one of these species is present, it is likely to become the dominant species.

The modelling in section 2.3 showed that it is possible to estimate the fouling rate of organisms. To this end, logistic growth was assumed, adjustment of three parameters in the logistic growth model was sufficient to describe the growth patterns. Besides these factors, temperature plays an essential role. For all but one class of organisms, the effect of temperature could be accounted for by changes in the model parameters. However, for predicting ascidian growth, the model had to be adjusted rigorously to account for a strong seasonal effect in the growth rate.

2.5 References

- 1 H.A. Jenner and J.P.M. Mommen, Driehoeksmosselen en aangroei problemen, *H₂O*, Vol. 18 No. 1 (1985) pp. 2-6
- 2 D.B. Harwood, D.J. Buda, Zebra mussel control experiences at Detroit Edison Harbor Beach Power Plant, Proceedings of the 1994 International Joint Power Generation Conference, 2-6 October 1994, Phoenix, USA, pp. 13-17
- 3 G. Bendoricchio, G. Coffaro and C. de Marchi, A trophic model for *Ulva rigida* in the Lagoon of Venice, *Ecological Modelling*, Vol. 75-76 (1994) pp. 485-496
- 4 C. Solidoro, G. Pecelik, R. Pastres, Davide Franco and C. Dejak, Modelling macroalgae (*Ulva Rigida*) in the Venice lagoon: Model structure identification and first parameters estimation, *Ecological Modelling*, Vol. 94 (1997) pp. 191-206
- 5 O. Wanner and P. Reichert, Mathematical modelling of mixed-culture biofilms, *Biotechnology and Bioengineering*, Vol. 49 (1996) pp. 172-184
- 6 Y. Tan, Z. Wang and K.C. Marshall, Modeling substrate inhibition of microbial growth, *Biotechnology and Bioengineering*, Vol. 52 (1996) pp. 602-608
- 7 C. Picioreanu, Multidimensional modeling of biofilm structure, Ph.D.-thesis, 1999, TU Delft, Delft, The Netherlands
- 8 W.G. Characklis, K.C. Marshall, *Biofilms*, 1990, Wiley, New York
- 9 G. Bitton, K.C. Marshall, *Adsorption of microorganisms to surfaces*, 1980, Wiley, New York
- 10 W.A. Corpe, Secretion of adhesive polymers and attachment of marine bacteria to surfaces, *Proceeding of the Third International Biodegradation Symposium*, 1976, pp. 433-442
- 11 E.A. Foumeny and P.J. Heggs, *Heat Exchange Engineering. volume 2 compact heat exchangers techniques of size reduction*, 1991, Horwood, New York
- 12 M.T.S. Lutterbach and F.P. França, Biofilm formation in water cooling systems, *World Journal of Microbiology & Biotechnology* Vol. 12 (1996) pp. 391-394
- 13 E. Heitz, H.C. Flemming and W. Sand, *Microbially influenced corrosion of materials; scientific and engineering aspects*, 1996, Springer, Berlin, Germany
- 14 L.M.G. Wolfs, Literatuurstudie over het hechtingsmechanisme van aangroeiende organismen, TNO-report V-87-336, 1987
- 15 R. Edyvean, I.W. Eames and R. Brook, Corrosion problems of water cooled condensers. In: *Heat Exchange Engineering volume 2: Compact Heat Exchangers Techniques of Size Reduction*, 1991, Horwood, New York
- 16 J.R. Lewis and A.D. Mercer, *Corrosion and Marine Growth on Offshore Structures*, 1984, Horwood, Aberdeen, UK
- 17 F.G.W. Smith, Effect of water currents upon the attachment and growth of barnacles, *Biol. Bull. Mar. Biol.*, Vol. 90, pp. 51-70
- 18 P.R. Willemsen, Handleiding voor het kweken van de zeepok *Balanus amphitrite*, Internal TNO-report (1995)
- 19 D.J. Crisp, G. Walker, G.A. Young and A.B. Yule, Adhesion and Substrate Choice in mussels and Barnacles, *Journal of Colloid and Interface Science*, Vol. 104 No. 1 (1985)
- 20 OECD, *Catalogue of Main Marine Fouling Organisms (vol 3): Serpulids*, 1967, OECD, Paris, France
- 21 <http://biology.about.com/science/biology/gi/dynamic/offsite.htm>
- 22 J.A. Nott, B.A. Foster, On the structure of the antennular attachment organ of the cypris larva of *Balanus Balanoides*, *Phil. Trans. Royal Society*, Vol. 256 No. B803 (1969) pp. 105-134
- 23 E.W. Knight-Jones and D.J. Crisp, Gregariousness in barnacles in relation to the fouling of ships and to anti-fouling research, *Nature*, Vol. 171 No. 4364 (1953) pp. 1109-1110
- 24 W.G. Characklis, *Microbial Biofouling Control*. In *Biofilms* (eds. W. G. Characklis and K. C. Marshall), 1990, John Wiley & Sons, New York, pp. 585-633
- 25 W.G. Characklis, *Biofilms and microbial fouling*, *Advances in Applied Microbiology*, Vol. 29 (1983) pp. 93-138

- 26 W.G. Characklis, Microbial Biofouling Control. In Biofilms (eds. W. G. Characklis and K. C. Marshall), 1990, John Wiley & Sons, New York, pp. 585-633
- 27 S.P. Denyer, S.P. Gorman and M. Sussman, Microbial Biofilms: Formation and Control, 1993, Blackwell Scientific Publications, Oxford, UK
- 28 H.M. Lappin-Scott and J.W. Costerton, Plant and Microbial Biotechnology Research Series Volume 5: Microbial Biofilms, 1995, Cambridge Press, Cambridge, UK
- 29 R.E. Baier, Initial events in microbial film formation, Marine Biodeterioration: An Interdisciplinary Study, 1984, Naval Institute Press, Annapolis, USA, pp. 57-62
- 30 B.J. Little, Succession in microfouling, Marine Biodeterioration: An Interdisciplinary Study, 1984, Naval Institute Press, Annapolis, USA, pp. 63-67
- 31 M.J. Anderson, Variations in biofilms colonizing artificial surfaces: seasonal effects and effects of grazers, Journal of the Marine Biological Association of the United Kingdom, Vol. 75 (1995) pp. 705-714
- 32 J.A. Allen, P.R.O. Barnett, J.M. Boyd, R.C. Kirkwood, D.W. Mackay and J.C. Smyth, The environment of the Estuary and Firth of Clyde, Proceedings of the Royal Society of Edinburgh B, 1986, The Royal Society of Edinburgh, Edinburgh, UK
- 33 R.M. Head, H.J.A. Breur Head, S. Campos, P. Sebastiao, J. Hills, J. Davenport, C. Guedes Soares, G.M. Ferrari, J.C. Thomason, Biofouling on glass surfaces at three contrasting shallow water sites and implications for optical sensor performance, in prep.
- 34 A. Campbell, Hamlyn Guide: Seashores and shallow seas of Britain and Europe, 1994, Hamlyn, London, UK
- 35 J.D. Fish and S. Fish, A Student's Guide to the Seashore, 1996, Cambridge University Press, Cambridge, UK
- 36 S.C. Ferreira Jr., M.L. Martins and M.J. Vilela, Growth model for primary cancer (II). New rules, progress curves and morphology transitions, Physica-Acta; Statistical Mechanics and its Applications, Vol. 272 No. 1 (1999) pp. 245-256
- 37 R. Chignola, D. Liberati, E. Chiesa, C. Anselmi, R. Foroni, S. Sartoris, A. Brendolan, G. Tridente and G. Andrighetto, Non-parametric method for the analysis of experimental tumour growth data, Medical and Biological Engineering and Computing, Vol. 37 No. 4 (1999) pp. 537-542
- 38 G.O.R. van Ekenstein and Tan Y.Y. Alberda, Crystallization and melt behaviour of isotactic poly((4- α , α -dimethyl-benzyl)phenyl methacrylate), Polymer. Vol. 38 No. 22 (1997) pp. 5605-5610
- 39 R. Phillips and J.A.E. Manson, Prediction and analysis of nonisothermal crystallization of polymers, Journal of Polymer Science, Part B: Polymer Physics, Vol. 35 No. 6 (1997) pp. 875-888
- 40 L.P. Ooijkaas, R.M. Buitelaar, J. Tramper and A. Rinzema, Growth and sporulation stoichiometry and kinetics of *Coniothyrium minitans* on agar media, Biotechnology and Bioengineering, Vol. 69 No. 3 (2000) pp. 292-300
- 41 E.B. Daae and A.P. Ison, Simple structured model describing the growth of *Streptomyces lividans*, Biotechnology and Bioengineering, Vol. 58 No. 2-3 (1998) pp. 263-266
- 42 J. Braun-Blanquet, Pflanzensoziologie ed. 3, Springer, 1964, New York, USA
- 43 J.W. Haefner, Modelling Biological Systems, Chapman & Hall, 1996, New York, USA
- 44 P.F. Verhulst, Notice sur la loi que la population suit dans son accroissement, Corr. Math. et Phys., Vol. 10 (1938) pp. 113-121
- 45 V. Volterra, Variazioni e fluttazioni del numero d'individui in specie animali conviventi, Mem. Acad. Sci. Lincei, No. 2 (1926)
- 46 A.J. Lotka, Elements of Physical Biology, Williams & Wilkins, 1925, Baltimore, USA
- 47 J.A. Logan, Toward an expert system for development of pest simulation models, Environmental Entomology, Vol. 17 (1988) pp. 359-376
- 48 T.A. McMeekin, J.N. Olley, T. Ross and D.A. Ratkowsky, Predictive Microbiology: theory and application, Research Studies Press, 1993, Taunton, UK
- 49 A. Hastings, Population Biology: Concepts and Models, Springer, 1997, New York
- 50 J.L. Jenkins, J.A. Powell, J.A. Logan and B.J. Bentz, Low seasonal temperatures promote life cycle synchronization, Bulletin of Mathematical Biology, Vol. 63 (2001) pp. 573-595
- 51 E. Shimoni and T.P. Labuza, Modeling pathogen growth in meat products: future challenges, Trends in Food Science & Technology, Vol. 11 (2000) pp. 394-402

3 Fouling in Heat Exchangers

Summary

This chapter discusses various fouling problems that can occur inside heat exchangers. After a short introduction in the general phenomena, two specific cases are discussed. The first case is the biological fouling on copper alloys. Though these alloys ought to have sufficient antifouling properties, this actually does not hold in several practical cases. Problems arise especially due to galvanic couplings to other metals and due to cathodic protection systems. The second case addresses scaling in fresh water cooling systems. Scaling occurs at warm areas in heat exchangers due to the inverse solubility of CaCO_3 . Scaling decreases the heat transfer through the heat exchanger walls. Furthermore, underneath these layers, corrosion problems arise.

Regarding the biofouling development on Cunifer alloys, a fouling potential was determined which is the potential below which the settlement of specific fouling organisms was possible. A relation between this potential and the electrochemical behaviour of the alloys in seawater was investigated. Furthermore, field trials with galvanically coupled plates of Cunifer to zinc and carbon steel in practically relevant surface area proportions showed the danger of coupling towards the intrinsic antifouling properties of Cunifer alloys.

It was shown that, even in the immunity area of the alloys where copper dissolution is minimal, antifouling properties can still be sufficient. Regarding settlement mechanism, this points to a chemical substrate selection mechanism for the organisms.

Regarding scaling in heat exchangers, a set-up has been designed to be able to measure corrosion and scaling phenomena on heated electrodes. Using this set-up, electrochemical impedance spectroscopy was used to characterise the processes. It was shown that the response of different scales shows a different effect in the impedance plots. A dense scale showed an increase in charge transfer resistance whereas a less dense layer did not show this increase. Furthermore, it was possible to determine the onset of pitting, which is especially interesting for application in corrosion monitoring strategies.

3.1 Introduction

A specific case in which fouling deteriorates surfaces is the surface of heat exchangers. In general, the first effect of fouling is a reduced heat transfer through the walls of a heat exchanger. Fouling layers show most times low heat conductivity and the heat has to cross a thicker layer due to the presence of the fouling layer. The secondary effect of fouling is that corrosion and/or erosion processes can be enhanced. For example the presence of barnacles inside a tube will cause turbulent flow behind the barnacle, causing erosion. When scaling occurs, the temperature of the metal underneath the scaling will increase, differential aeration cells can occur and pitting can be initiated.

Both biological and inorganic fouling have been investigated. For biofouling, the effect of coupling fouling resistant metals to other metals has been investigated, section 3.2. Barnacle assay experiments were carried out to assess the effect of change in potential on the settlement of barnacle larvae for two specific copper alloys: CuNi10Fe and CuNi30Fe. The same alloys were used for a field trial to assess the effect of coupling these alloys to zinc and steel which happens commonly in practise. Regarding inorganic fouling, the specific case of scaling in fresh cooling water is investigated; section 3.3. Due to heat transfer, scaling occurs preferentially on the warm spots of tube materials.

The main corrosion problem in cooling water heat exchangers is corrosion under fouling deposits. Generally it occurs as a form of localised attack due to the fact that the electrochemical environment underneath the deposit is different from the electrochemical environment at the rest

of the surface. In principle the mechanisms leading to under deposit corrosion are known. A short summary of the mechanisms is described in sections 3.1.1 and 3.1.2.

3.1.1 Deposition Mechanisms

Several processes can give rise to fouling of immersed surfaces: particulate deposition, crystallisation, freezing, corrosion, chemical reaction and biofouling. In this section, the three most important to cooling water heat exchangers will be dealt with. These are particle deposition, crystallisation/scale formation and biological growth. These will be dealt with in subsequent order [1].

Particle Deposition

In a lot of cases particle deposition plays a dominant role in the fouling process. Physical and chemical processes taking place in the flow can give rise to the formation of particles depositing at the walls of tubes due to relatively quiescent conditions.

In the case of cooling water, for example, the solubility of CaCO_3 depends largely on temperature. When the temperature rises, the solubility decreases and supersaturation can occur. CaCO_3 can then precipitate and the particles can deposit at the surface. Deposition is possible both directly due to crystal formation at the surface and indirectly due to precipitation in the water and subsequent transport to the surface.

Also in biofouling, the microbes causing slime formation have to be transported to the surfaces to enable them to attach to the surface. In many cases, the same types of transport are responsible:

1. Diffusive transportation. Due to concentration differences, particles from regions of higher concentrations will tend to move to areas with lower concentrations.
2. Brownian motion. Particles will have a random motion within the solutions. In some cases the random motion results in collisions with the walls and conglomeration at the surface may take place when the particles stick to the surface.
3. Momentum forces. Due to non-laminar flow, particles can have a momentum component directed towards the wall. This component can cause collisions of particles with the wall and the particles can stick to the surface.
4. Thermophoresis. Due to temperature differences, smaller particles tend to move to cooler regions. In fact, it is a result of the higher kinetic energy of molecules in warmer regions relative to the kinetic energy of particles in cooler areas. The warm side of the particle will be bombarded stronger than the cool side and therefore the particle will tend to move to a cooler region.
5. Settling forces. For example the gravitational force can cause settling of deposits. Since for heat exchangers, the flow is generally quite high, these forces will not play an important role. Except of course for periods when the cooling system is not operational, when flow is stopped and particles have the time to settle.

For all of the above mentioned transport mechanisms, the driving force has to be sufficiently large to cause the particles to collide with the surface, because the particle has to pass through the laminar flow layer at the surface to reach the surface.

After the transport of the particles to the surface, they need to stick to the surface. Not all of the particles will be able to stick to the surface. The drag of the flow has to be overcome for a reasonable time period. The chance that a particle will stick to the surface, the sticking probability, is less than unity and will depend on factors like type of flow, flow rate, temperature, size and nature of the particles and the physical character of the surface.

Crystallisation and Scale Formation

One condition is always necessary for crystallisation to occur: supersaturation. When a solution is in equilibrium with the solid phase of the solute, the solution is called saturated. When, for example due to temperature changes the solubility decreases rapidly, the solution becomes supersaturated: it contains more solute than the equilibrium value. Supersaturation can occur due to both temperature rises and temperature drops. In general, the solubility of compounds rises as temperature increases. However, several examples exist (e.g. CaCO_3 , $\text{Ca}(\text{PO}_4)_2$) of compounds with inverse solubility: their solubility decreases with increasing temperature. In the case of cooling water, especially inverse solubility products like CaCO_3 give rise to problems in the case of cooling water systems due to the scale formation.

The moment supersaturation occurs, nuclei will start to form and crystals will grow at the nucleation spots. Two different types of crystal growth can occur: diffusion limited and reaction rate limited. Which type occurs will of course depend on factors like the strength of the supersaturation, the amount of mixing in the solution and the nuclei density.

Scaling can either appear as hard layers, mainly consisting of calcium carbonates, or as soft gel-layers mainly consisting of calcium phosphates. The hard calcium carbonate scaling is deleterious for the heat transfer resistance. Depending on the structure, the calcium phosphate layers hardly affect the heat transfer and protect carbon steel from corroding. However, when the phosphate layers grow too thick, the heat transfer resistance can rise after all.

Biological Growth

Biological growth can be split up in two categories: microbiological and macrobiological growth. Macrobiological growth includes e.g. the growth of algae, mussels and barnacles. Bacteria, diatoms, fungi etc. are microbiological organisms. These two categories have specific effects on the surfaces they have fouled:

- Microbiological species can have quite diverse effects on materials, ranging from passive influence by changing the (electrochemical) environment to active influence by using metal atoms for their metabolism. Especially bacteria are organisms that can actively use the metals. Most of the other organisms are only capable of changing the environment.
- For corrosion processes in fresh water heat exchangers, especially the micro-organisms are of importance. These will form a biofilm on the walls of the heat exchanger. The direct consequence is that the heat transfer rate will be lowered. Also the electrochemical environment will change. Although most of the water in biofilms can freely diffuse through the biofilm, the concentration of for example oxygen will be influenced: oxygen will be used in the metabolism of the aerobic micro-organisms.
- The concentration of oxygen can even become low enough for anaerobic bacteria to develop. Several of the anaerobic bacteria are known to use metal ions in their metabolic processes and are thus able to remove metal directly. More commonly occurring are anaerobic bacteria using sulphur instead of oxygen for their metabolism. *Sulphate reducing bacteria (SRB)* are in most cases the cause of microbial corrosion.
- Macrobiological species can cause reduction and eventually blockage of the water flux through the heat exchanger tubes. The reduction of the flux reduces the maximum amount of cooling water flowing through the heat exchanger and thus has a direct influence on the cooling capacity. Furthermore, when macrofouling species like barnacles and mussels get into the narrow tubes of the heat exchanger, blockage can occur, but already before blockage a deleterious effect is present: erosion corrosion. The macrofouling causes distortion of the regular flow pattern and flow gets more turbulent. Especially behind the macrofouling species, this turbulence can cause erosion corrosion.

3.1.2 Corrosion Processes Underneath Deposits

In the previous section, the various mechanisms leading to fouling of heat exchangers were described. Only the processes that are of importance to cooling water systems were dealt with. The fouling on the walls of the heat exchangers enhances different corrosion processes. An overview of the corrosion processes that can take place is given below.

Pitting Corrosion

Pitting corrosion is a form of corrosion occurring due to the fact that a protective noble layer on top of a less noble base material is damaged and is not repaired. The less noble material will start to work as cathode to protect the noble layer. At the damaged spot metal ions will rapidly dissolve and a pit will grow.

Pitting corrosion mainly occurs on passivating steels in solutions containing halogen ions. Since for the make-up of cooling water, surface water is started with, several additions are needed to protect the materials. One of the additions, to prevent biological growth, is the addition of active chlorides. These chlorides increase the materials susceptibility to pitting corrosion. Pitting corrosion occurs underneath damaged protective layers and therefore materials like stainless steel are susceptible to this phenomenon. The process of pitting corrosion is sensitive to temperature changes, a critical pitting temperature determines the lowest temperature at which pitting occurs.

Galvanic Corrosion

Galvanic corrosion can occur when dissimilar metals are electrically connected. In general this type of corrosion can be avoided by insulating the metals. However, interactions of the micro-organisms with the metal often result in changes of the corrosion potential of the metal. Therefore microbiology can also give rise to galvanic corrosion effects. Furthermore, in practical applications, coupling is inevitable or required. E.g. in submarines, for safety precautions, all metal parts need to be connected to prevent sparking due to possible potential differences.

Under Deposit Corrosion

Under deposit corrosion is caused by the change in electrochemical environment underneath the fouling. In most cases the change in oxygen concentration is a predominant factor. Due to the depletion of oxygen, the corrosion potential underneath the deposit drops and thus gets less noble than the surrounding material. The material under the deposit becomes anodic and metal ions start to dissolve.

Another cause of under deposit corrosion, which can act in heat exchangers, is corrosion under biofilms. In this case a biological deposit is formed and the presence of this deposit causes the electrochemical environment to change. Aerobic bacteria use the oxygen present in the water fraction of the biofilms reducing the oxygen concentration. Besides the change in electrochemistry, it is also possible that the organisms use the metal of the wall material in their metabolism. Both these cases are called microbial corrosion.

In case corrosion takes place underneath scaling, it seems obvious to speak of under deposit corrosion. However, this might not be right on several occasions, because the corrosion is not necessarily caused by a change in chemical environment. The scale on top of the tube material increases the heat transfer resistance between tube material and water. This implies that the temperature of the tube material increases, which inherently increases the sensitivity to corrosion. The deposit is not truly the cause this form of corrosion. It is just the reason for the temperature increase.

Concluding Remarks

A number of deposition processes and corrosion processes can take place inside heat exchangers. The most complex ones take place underneath fouling deposits. It was mentioned that the general under deposit corrosion mechanisms could not simply explain the processes taking place underneath the deposits. More factors are of influence.

It is realised that the temperature plays a dominant role in the process. Scale formation takes place at the heated sections of the heat exchangers due to the inverse solubility of several calcium salts. Also biofouling can be enhanced by temperature increases. Most biofilm forming species prefer warm sites to settle and grow. For these reasons corrosion sensitivity is largest at the heated areas. The effect will even be enhanced due to the lower heat transfer rate at fouled areas, which will further increase the temperature. Finally the increase in temperature due to the heating can enhance the kinetics of the corrosion processes.

3.2 Biofouling on Copper Alloys

3.2.1 Introduction

Corrosion and fouling of heat exchangers, used on ships in seawater, is recognised as a major problem for a long time. In the late 1950s failure of seawater cooled heat exchangers of newly built vessels often necessitated stops at sea [2]. The larger vessels were equipped with larger heat exchangers, which made a higher flow rate of the cooling water through the tubes necessary. Due to this higher flow rate, the aluminium brass tubes were subject to severe impingement attack, which perforated the tubes within six months.

In order to overcome these failures a lot of research has been performed on this subject. A solution to this problem was found in two ways:

- Placing of sacrificial iron anodes in the condenser tubes, which also included release of ferrous sulphate ions.
- Replacing the heat exchanger tubes with a more suitable material

In this way copper-nickel (CuNi10 and CuNi30) and later nickel-based (Monel 400) alloys were developed. These alloys suffer from corrosion and fouling as well, but perform much better than the alloys used before.

The performance of these alloys seems to depend on various parameters. Below the most important ones are summarised:

- Flow rate of the cooling water
- Pollution of the seawater
- Temperature of the seawater inside the heat exchanger tubes
- Design of the heat exchanger system (narrow passages, elbows, etc.)
- Bacterial growth in the seawater (which a.o. depends on the season)
- Galvanic coupling with other metals
- Oxygen concentration in the seawater

Some of the above-described parameters are in control of nature and cannot be influenced by mankind. However, other parameters can (easily) be adapted to prevent corrosion and fouling.

Four alloys are most commonly used in marine heat exchanger applications:

- Nickel-Aluminium bronze (AB2) (UNS C95810)
- Monel 400 (UNS N04400)
- CuNi10 (UNS C70600)
- CuNi30 (UNS C71500)

These alloys are widely used as heat exchanger materials in large marine vessels. The composition of the alloys is given in Table 3.1.

Table 3.1: Composition of four widely used heat exchanger alloys

Alloy	UNS code	Cu	Ni	Al	Fe	Sn	Mn
Ni-Al bronze	C95810	Balance	5.0	9.5	4.8	<0.1	<3.0
Monel 400	N04400	30.5	65.2		1.3		0.98
CuNi10	C70600	87.9	10.1	<0.005	1.32	0.014	0.485
CuNi30	C71500	68.7	29.7	<0.005	0.52	<0.01	0.382

Pure copper has not been used extensively in a marine environment, but provides the basic properties of the modern marine copper alloys [3]:

- General corrosion resistance in seawater
- Resistance to stress corrosion cracking and crevice corrosion
- Resistance to marine biofouling
- Excellent ductility and fabrication characteristics
- High thermal conductivity

The various alloying additions provide:

- Additional strength and corrosion fatigue resistance
- Resistance to erosion and impingement attack
- Improved resistance to corrosion in both clean and polluted seawater
- Appropriate casting and wrought fabrication characteristics.

Nowadays aluminium bronze and copper-nickel alloys represent the two most important copper alloy groups for marine applications [3]. Aluminium bronzes combine high mechanical strength and low corrosion rates at high flow rates [4]. Nickel-aluminium bronzes exhibit the highest resistance to cavitation damage of all copper alloys and, are therefore extensively used for large ship propellers, heavy-duty impellers and casings of pumps and turbines. For heat exchanger tubes, especially CuNi10Fe and CuNi30Fe are used.

Besides their good corrosion resistance in seawater, copper alloys show intrinsic antifouling behaviour due to the slow dissolution of copper ions. However, in practice cases occur where copper alloys are galvanically coupled to other metals. Due to these couplings, the potential changes and the copper dissolution is influenced. Most couplings are with steel and zinc and therefore the coupling generally lowers the potential. This indicates that the dissolution of copper is lower. In some cases, the dissolution is even lower than necessary to provide enough toxic effect for marine organisms.

This section deals with these fouling processes on Cunifer alloys. After an initial theoretical evaluation of the corrosion behaviour of copper alloys, two experimental series are treated. The first involves a barnacle assay experiment to evaluate the settlement of barnacles at different potentials; the second deals with a field trial experiment in which the practical couplings have been investigated for their potential problems regarding fouling.

3.2.2 Properties of Cunifer Alloys in Seawater

Mechanical Properties

The addition of nickel in copper alloys increases the strength and durability of copper alloys and decreases the corrosion rate. A disadvantage of early copper-nickel alloys was their poor resistance to erosion corrosion. Addition of iron to the alloy composition has improved the erosion corrosion resistance. The addition is set to 1.0-1.8 wt% for CuNi10Fe and to 0.4-0.7 wt% for CuNi30Fe alloys [5].

Due to the solid solution of copper and nickel, the structure of the alloy is homogeneous and simple [6]. These alloys are superior to other copper alloys in their resistance against acidic solutions and are well resistant to stress corrosion cracking and impingement attack [7]. CuNi30Fe shows the best resistance to general corrosion in seawater of all commercially available copper alloys. CuNi10Fe is, however, often used in practice because of its good corrosion resistance combined with attractive lower costs. Both alloys are very common materials for condensers and heat exchangers.

Corrosion Behaviour

In aqueous environments, copper oxide (Cu_2O) is the main component of the protective film formed on the alloys. The film is stuck to the surface and shows parabolic growth kinetics [8]. Figure 3.1 shows the possible chemical reactions at the surface in aqueous environments. This diagram implies that the corrosion process is not always uniform and the dissolution rate of copper can change along the surface [9, 10].

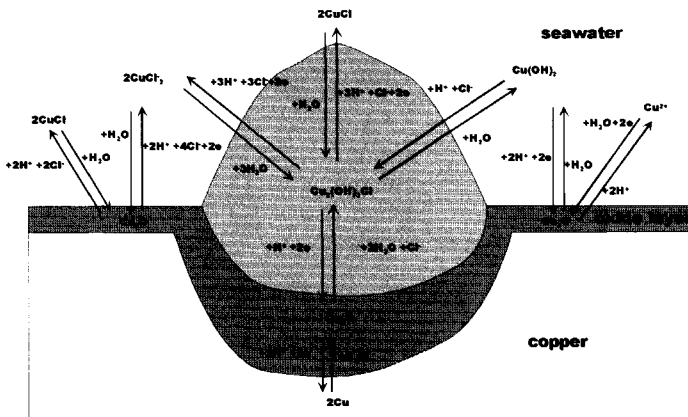


Figure 3.1: Chemical model for the corrosion reactions of copper in seawater [11]

The reactions occurring at the Cunifer surface can easiest be explained using the (simplified) Pourbaix-diagram, shown in Figure 3.2. The behaviour of the two alloys is much alike. The only obvious difference in the diagrams is the shift of the border of the passive area. For CuNi10Fe this border is around pH 8.6 and for CuNi30Fe it is around 7.8. This indicates that in natural seawater with pH around 7.8, the alloys might behave differently: CuNi10Fe will cannot passivate and will therefore build up a protective Cu_2O layer more slowly; CuNi30Fe on the other hand could show passivation and could more rapidly build up the protective layer. Due to the stable oxide of copper, both alloys will show similar corrosion rates at long term exposure (6 to 8 weeks) [12, 13].

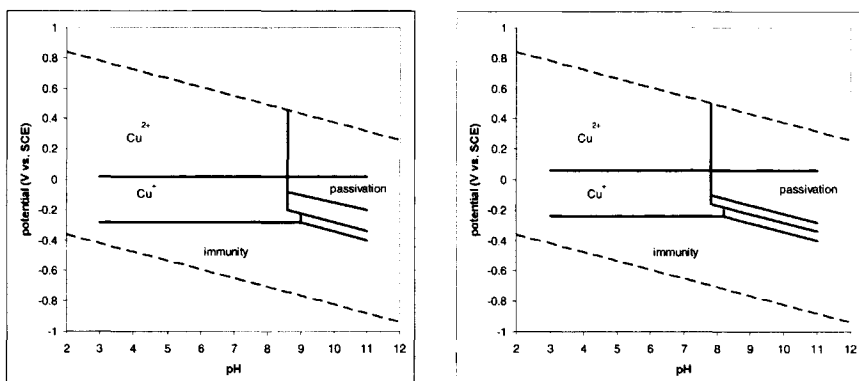
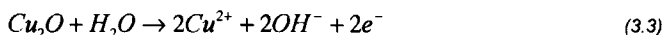
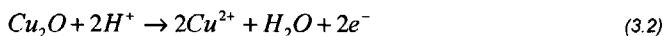
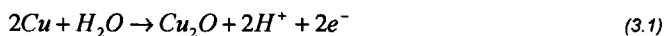


Figure 3.2: Simplified Pourbaix diagram for CuNi10Fe (a) and CuNi30Fe (b) in seawater (25°C, [Cl⁻]=19.1 g/l, [O₂]=6.4 g/l) [15]

The immunity area is approximately the same for CuNi10Fe and CuNi30Fe and is situated below -250mV (vs. SCE). This potential is less noble than the one, which would normally set for the alloys in seawater.

Antifouling Properties of Copper

The antifouling properties of copper and copper alloys are very useful for the designers of marine equipment. Copper has a toxic effect on many marine organisms. The bivalent Cu²⁺ ion is able to influence the enzyme and respiration system. This ion is released according the equations 3.1 to 3.3.



The effectivity of copper is influenced by many parameters, amongst others the condition and age of the organism, chemical seawater composition, presence of other biocides and the concentration of copper ions. For most organisms a concentration of several milligrams per litre is enough to show mortal effects.

In the literature, different values can be found for the minimum corrosion rate to provide enough resistance against fouling. Lennox et al. [14] claim that a minimum corrosion rate of 5 mg/dm²/day would be sufficient, while Swain et al. [9] claim that already 1 mg/dm²/day would be enough.

Efird et al. [6] have exposed CuNi10Fe and CuNi30Fe for 14 years to seawater in different circumstances. They measured the corrosion resistance and the antifouling performance in the tidal zone for flowing and stagnant water. The corrosion rates were between 1 and 2 μm/year (0.25-0.5 mg/dm²*day) and decreased even after 14 years. The fouling resistance was still satisfactory after this period for both alloys.

3.2.3 Barnacle Assay Experiments

Introduction

As was pointed out in the previous section, copper alloys show an intrinsic antifouling behaviour. Normally, due to general corrosion, a stable oxide surface layer develops (reaction 3.1). The protection by the oxide layer results in a decrease of the corrosion rate in time. The copper oxide can react and form dissolved Cu^{2+} , see reactions 3.2 and 3.3, which is very toxic to macro-organisms that cause fouling.

Thus, as long as there is a high enough concentration of copper ions, i.e. corrosion, the alloy will be protected against fouling. However, this will only be true in case the metal is exposed at its open corrosion potential (OCP). In many cases, coupling exists between different metals used and often metals are protected against general corrosion with impressed current cathodic protection systems. For this reason, the electrochemical potential of the metals is lower than the OCP and the corrosion will decrease. This implies, however, that the dissolution of copper is lower and could become too low for the metal to have intrinsic corrosion properties. For example, the curve for protection against corrosion could be as indicated in Figure 3.3. The intrinsic protection against fouling, however, is based on the principle of general corrosion. So, as the general corrosion decreases due to the impressed potential, the chance on fouling will increase, see Figure 3.3. In general this curve is sigmoidal, as is the case for growth curves.

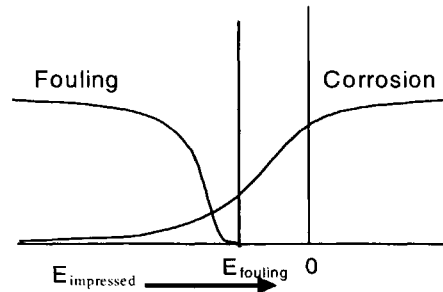


Figure 3.3: Curves of fouling and corrosion as a function of the impressed potential. The maximum protection is situated where both fouling and corrosion are low, i.e. at the crossing of the curves

Because any fouling is damaging and can form the basis for other fouling, fouling should be completely prevented. Therefore, the potential at which fouling is just not possible on the surface, is of main interest. Expressed in copper concentrations, this value is called the EC100 value, meaning the concentration (or in this case the potential) at which 100% effect, i.e. total settlement prevention, is obtained. This potential is named the fouling potential. This potential is determined using a barnacle assay for CuNi10Fe and CuNi30Fe.

Experimental

In order to estimate the fouling potential, a barnacle settlement assay with *Balanus amphitrite* was conducted. Hereby, we determine at which potential barnacles are able to settle on samples of CuNi10Fe and CuNi30Fe, the fouling potential.

For CuNi10Fe, the assay is performed in two test series with four test units in duplicate. The set-up is shown in Figures 3.4 and 3.5 [16]. Cyprid larvae are inserted in the perspex tube with a diameter of 2.4 cm. The exposed surface CuNi10Fe is 4.5 cm². The tests are conducted in duplicate. Two test units, with equal potential, are placed in a single container. The seawater

level in all units is refreshed in drops to prevent electrical earthing of the set-up. To prevent the loss of barnacle larvae, the holes in the perspex-tube are covered with a 55 μm mesh.

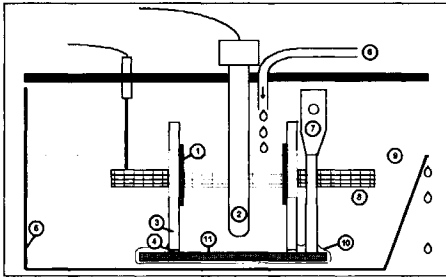


Figure 3.4: Schematic representation of the measuring unit, with: 1) the 55 μm mesh, 2) Ag/AgCl reference electrode, 3) perspex(PMMA)-tube, 4) silicon paste, 5) container, 6) sea water inlet, 7) working electrode contact, 8) platinum electrode, 9) water level, 10) insulation and 11) the work electrode: CuNi10Fe sample.



Figure 3.5: Photographical representation of a single measuring unit used in the settlement assay.

The first series is used to find the range in which the fouling potential is situated. In the first test, the potential of the CuNi10Fe sample remained constant at 0, -200, -500 and -900 mV vs. Ag/AgCl. Based on the results of the first series the range of potentials for the second series is selected.

After one week of pre-exposure to seawater, approximately 60 cyprid larvae are added to all the test units. After three days the larvae settlement is examined. Upon settlement of one or more of the larvae, the impressed potential in this particular situation is considered lower than the fouling potential and vice versa. A second experimental trial around the first estimate of the fouling potential determines the fouling potential more precisely.

For CuNi30Fe, more experiments have been carried out with the same test set-up. However, in this case duplicate-measurements were carried out in separate containers. Furthermore the pre-exposure time was less constant than in the experiments with CuNi10Fe, due to a discontinuity of the availability of cyprid larvae. Based on the results, an estimate of the fouling potential was made again.

Results

Table 3.2 shows the results of the experiments on CuNi10Fe. The results of the first test series show that at a potential of -500mV settlement is still possible, while at -200 mV no settlement occurs and the activity of the few surviving larvae is low. The duplicates of the -500 and -900 mV, which had a lower refresh rate, show that the refresh rate is also an important factor for settlement. A lower refresh rate results in build up of toxic copper ions. This build up causes the larvae to be less active and settlement is reduced. From the first series it can be concluded that the fouling potential lies between -200 and -500 mV (vs Ag/AgCl). Based on these results, the second series is chosen to cover the -200 and -500 mV area at 100 mV intervals.

The second series shows the same results for the -200 and -500 mV samples. There is also settlement at -400 mV while at -300 mV none of the larvae settled. This results in a fouling potential between -300 and -400 mV.

Table 3.2: Settlement results for CuNi10Fe of both series. The initial number of cyprids used in each test unit is displayed between brackets

Potential (mV vs. Ag/AgCl)	series 1		series 2	
	1	2	1	2
0	[59] no settlement, dead larvae	[72] no settlement, dead larvae	-	-
-200	[60] no settlement, few surviving larvae, 1 floating barnacle	[73] no settlement, dead larvae	[61] no settlement, dead larvae	[52] no settlement, few surviving larvae
-300	-	-	[74] no settlement, active larvae	[54] no settlement, active larvae
-400	-	-	[67] 1 settled barnacle, active larvae	[72] 2 settled barnacles, active larvae
-500	[76] 6 settled barnacles, active larvae	[58] 3 settled barnacles, less active larvae then 1 (lower refresh rate)	[62] 4 settled barnacles, mostly active larvae	[47] 4 settled barnacles, mostly active larvae
-900	[69] 8 settled barnacles, active larvae	[91] 5 settled barnacles, less active larvae then 1 (lower refresh rate)	-	-

For CuNi30Fe, four series were carried out. Table 3.3 shows the results of the settlement assay. In the first series, low potentials were used. At all three potentials tested, settlement occurred. Settlement was strongest at -1100 mV (vs. Ag/AgCl), however, also at -400 mV, settlement occurred. At -1100 mV scaling took place. In the most scaled region, the larvae did settle but had not been able (yet) to transform into juvenile barnacles.

During the second trial, two potentials were selected; at -850 mV settlement occurred as expected; at -250 mV no settlement occurred. This indicates that the fouling potential should be between -250 and -400 mV (vs. Ag/AgCl).

During the third trial, again two potentials were selected; at -850 mV settlement occurred as expected; at -250 mV no settlement occurred. This indicates that the fouling potential should be between -300 and -400 mV (vs. Ag/AgCl).

During the fourth trial, three potentials were selected and 316 AISI stainless steel was used as a reference. The potentials were selected to narrow down the range in which the fouling potential could be. However, no settlement occurred at potentials between -250 and -400 mV. The stainless steel sample showed a lot of barnacles could settle and the quality of the larvae has not influenced the test.

Table 3.3: Settlement results for CuNi30Fe. The initial number of cyprids used in each test unit is displayed between brackets

Exp.no.	Cell no.	Potential (mV vs. Ag/AgCl)	Pre-exposure (days)	Larvae settled	remark	
1	1	-850	15	[73] 18 settled	Scale deposition	
	2			[75] 6settled		
	4	-1100		[>300] >150 settled		
	5	-400		[66] 18 settled		
2	6	Glass	7	[82] 28 settled		
	1			-850		[77] 2 settled
	2	-850		[65] 17 settled		
	4	Glass		[64] 18 settled		
3	5	-250	41	[68] 0 settled	Larvae in cell 2 are less active	
	6	-250		[64] 0 settled		
	1	-850		[150] 21 settled		Larvae in cell 6 are less active
	2	-850		[51] 1 settled		
4	5	-300	18	[108] 0 settled		
	6	-300		[59] 1 settled		
	1	-250		[136] 0 settled		
	2	-250		[98] 0 settled		
	3	-325		[94] 0 settled		
	4	-325		[118] 0 settled		
AISI 316	OCP	0	[108] 0 settled	[98] 0 settled		
			[>150] >50 settled			

Discussion

Based on the results of the barnacle assay experiments it can be concluded that the fouling potentials are between -300 and -400 mV (vs. Ag/AgCl) and -250 and -400 mV (vs. Ag/AgCl) for CuNi10Fe and CuNi30Fe respectively. Furthermore, the experiments with CuNi30Fe showed the effect of pre-exposure. During the 3rd experiment, one barnacle was able to settle on the sample exposed at -300 mV (vs. Ag/AgCl). Pre-exposure was long enough (41 days) for a stable Cu_2O layer to form, decreasing the amount of copper dissolving. During the fourth experiment the pre-exposure time was 15 days and no settlement was possible even at -400 mV (vs. Ag/AgCl).

For practical application of the results, one should keep in mind that the fouling of even one barnacle could lead to damage of the system. Especially tubes of heat exchangers are vulnerable, since erosion corrosion could easily occur behind a settled barnacle. Therefore the upper limit should be used in practical installations.

Another remarkable result is present in the data for CuNi10Fe. In the potential region between active settlement of the larvae and killing, the larvae remain active but refrain from settling on the unifer surface. In this area, copper dissolution is smaller than the rate required for toxic

antifouling properties. Therefore it is suggested that the settlement is highly influenced by the surface properties (electrochemical double layer). Furthermore this is a further indication that the antennulas of the barnacles contain chemoreceptors (section 2.1.3), since the copper concentration is too low to be toxic.

The fact that the antifouling properties appear to be sufficient at potentials below the OCP could have a practical spin-off. CuNi30Fe is used because of its better mechanical properties at high flow velocities than CuNi10Fe. Corrosion is too rapid for the latter alloy. However, decreasing the potential slightly could slow the corrosion down. In this way, the antifouling properties can be preserved and the system can retain its integrity for a longer period. This could lead to a *reduction* in costs, since CuNi30Fe is more expensive than CuNi10Fe.

3.2.4 Field Trials

Introduction

As was mentioned in section 3.2.2 and as was obvious from the results of section 3.2.3, the intrinsic antifouling properties of copper alloys can be deteriorated to a large extent by changes in the electrochemical potential. However, in several practical applications, coupling of metals cannot be prevented or is obligatory. To estimate the chance of troubles resulting from the coupling, field trials were carried out. Furthermore, the lab-trials only showed the effects of potential on the settlement of barnacles. To get a better overview of the effects on marine organisms, field trials have been carried out to investigate the effects. Couplings to practical relevant metals were made: zinc and carbon steel.

Experimental

Panels of CuNi10Fe and CuNi30Fe were exposed freely and coupled to carbon steel (in different sizes) and zinc, as is shown in Table 3.5. Carbon steel panels were prepared in three sizes: small: 1/5 times surface area of CuNi; same size; large: 5 times surface area CuNi. Coupling to zinc was done using zinc anodes screwed to the panels. Two plastic PVC reference panels were exposed as well.

Electrical connections between the panels are made of insulated copper wires. Connections at the panels are insulated using steel filler. The steel filler was coated with Sigma Novaguard to further prevent corrosion of the connections. Panels were attached to the rack using nylon bolts. CuNi-panels were exposed at the same depths as far as possible to prevent differences in fouling burden due to differences in light intensity.

Experiments were carried out at the raft of TNO in Den Helder as was described in section 2.2.2.

Table 3.4: Overview of the panels in the field trials. Coupling between panels is shown with a black line.

	1	2	3	4	5	6	7	8
A				B. Ref.	10. CuNi10 + Zinc			
B								
C	1. CuNi10	3. CuNi10	5. CuNi10			12. CuNi30	15. CuNi30	17. CuNi30
D			6. CuNi30	B. Ref.	11. CuNi30 + Zinc	13. CuNi30		
E								
F								

Five inspections were carried out according to the scheme of Table 3.5. During three of the inspections, also the electrochemical potential was measured to have some information on the electrochemical state of the system and to be able to relate the fouling pattern to the Pourbaix diagram.

Table 3.5: Inspection scheme

	Inspection date (2000)	Visual inspection	OCP measurement
0.	24 th of May	-	-
1.	7 th of June	Yes	Yes
2.	20 th of June	Yes	No
3.	19 th of July	Yes	Yes
4.	17 th of August	Yes	No
5.	25 th of August	Yes	Yes

Results

Figure 3.6 shows the whole rack with panels at the first inspection (2 weeks exposition). On all samples, including the references, some microfouling (bacteria and diatoms) were present. No macrofouling had occurred yet. Obvious are the large corroded areas on the steel panels, due to the protective action for the CuNi panels. Also the zinc anodes are heavily corroded and a thick layer of zinc salts is already present.

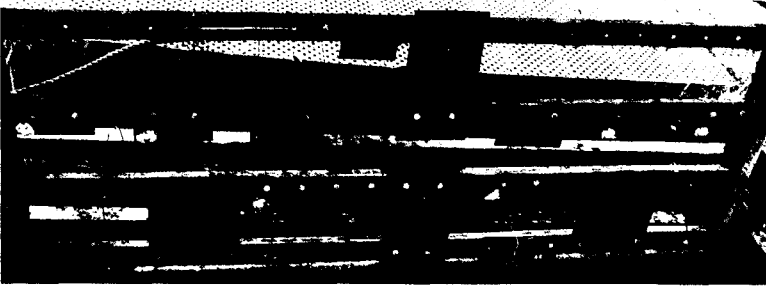


Figure 3.6: First inspection of panels

At the second inspection (Figure 3.7), again microfouling was present. Furthermore a lot of juvenile barnacles were present at the (not corroded areas of the) steel panels, Figure 3.8 and the reference panels. Furthermore some barnacles were present at panes 10 and 11, Figure 3.9 and 3.10. No macrofouling was present on the CuNi samples at OCP and coupled to steel, e.g. Figure 3.11.



Figure 3.7: Second inspection of panels



Figure 3.8: Second inspection: steel panels

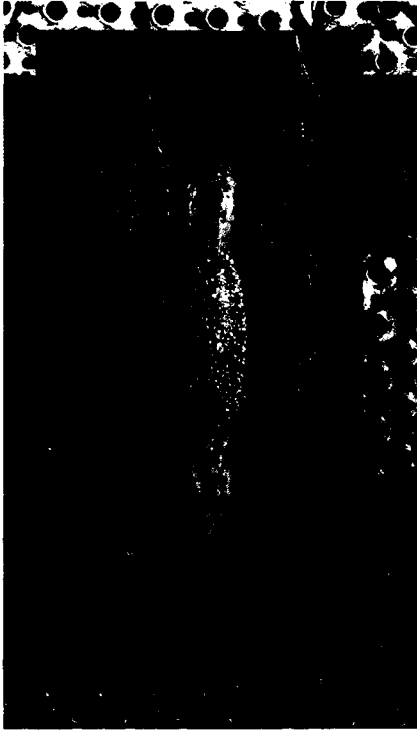


Figure 3.9: Second inspection: CuNi10 (plate) coupled to zinc (anode, attached on the CuNi-plate)

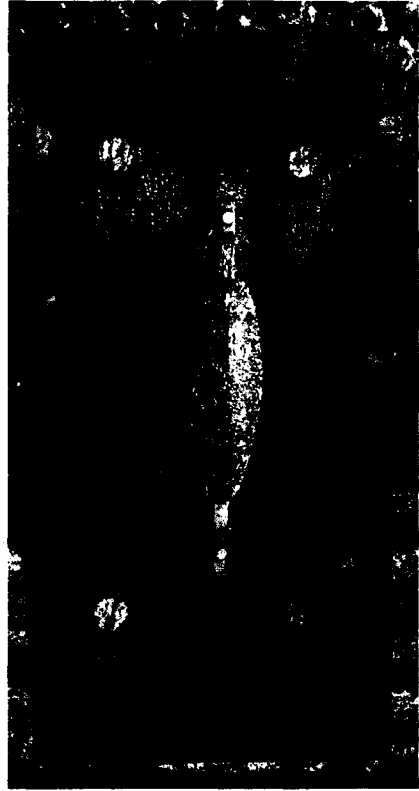


Figure 3.10: Second inspection: CuNi30 (plate) coupled to zinc (anode, attached on the CuNi-plate)



Figure 3.11: Second inspection: CuNi10 coupled to steel (CuNi-plates shown)

At the third inspection, Figure 3.12, fouling became worse. Macrofouling covered the reference samples entirely, Figure 3.13. Besides barnacles, also some ascidians and algae were present. Fouling at the coupled samples increased quite rapidly as well. Figure 3.14 shows a large steel panel, which is, at the not corroded areas, almost fully covered with barnacles. Figure 3.15 shows the CuNi10Fe panel coupled to this steel panel. Also here quite some barnacles are present. No ascidians were able to settle. The same behaviour was present for the other five combinations of CuNi and steel. Slightly more barnacles were covering the CuNi30Fe samples but no marked differences were present.



Figure 3.12: Third inspection: whole rack



Figure 3.13: Third inspection: reference sample (panel 8)

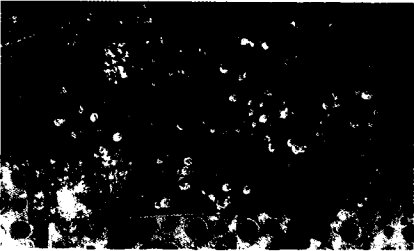


Figure 3.15: Third inspection: CuNi10 sample (panel 3)

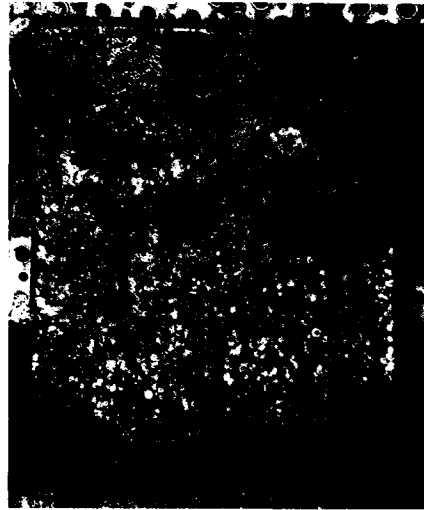


Figure 3.14: Third inspection: large steel sample (panel 4)

For the panels coupled to zinc, fouling was comparable to fouling on the other CuNi samples. More barnacles were present at the surface of the CuNi30 sample, Figure 3.17. Remarkable in Figures 3.16 and 3.17 is the area around the zinc anode. No macrofouling is noticed here. This can be attributed to the toxic effect of zinc salts. The deposition of these toxic salts prevents the adhesion of macrofouling species. The freely exposed samples remained free of fouling, Figures 3.18 and 3.19.



Figure 3.16: Third inspection: CuNi10 coupled to zinc (panel 10)

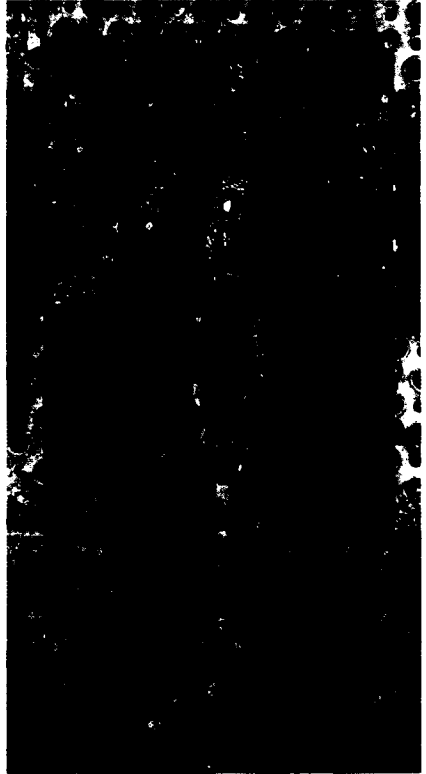


Figure 3.17: Third inspection: CuNi30 coupled to zinc (panel 11)



Figure 3.18: Third inspection: CuNi10 (panel 5)



Figure 3.19: Third inspection: CuNi30 (panel 12)

At the fourth inspection, Figure 3.20, all samples coupled to steel were completely covered with different kinds of organisms, a.o. barnacles (*Balanus crenatus*), ascidians, colonial ascidians (*Botryllus schlosseri*), and algae. Examples are given in Figures 3.21 and 3.22. The intrinsic antifouling properties are completely annulled. Also the steel samples are completely covered by several species, e.g. Figures 3.23 and 3.24. Again the corroded areas are free of fouling.



Figure 3.20: Fourth inspection: whole rack



Figure 3.21: Fourth inspection: CuNi30 (panel 15)



Figure 3.22: Fourth inspection: CuNi30 (panel 17)



Figure 3.23: Fourth inspection: steel sample same size (panel 14)



Figure 3.24: Fourth inspection: large steel sample (panel 16)

For the samples coupled to zinc, also numerous different species are present, Figures 3.25 and 3.26. Again, the CuNi30Fe sample is slightly heavier fouled than the CuNi10Fe sample. The freely exposed samples remained free of fouling as expected, Figures 3.27 and 3.28.



Figure 3.25: Fourth inspection: CuNi10 coupled to zinc (panel 10)



Figure 3.26: Fourth inspection: CuNi30 coupled to zinc (panel 11)



Figure 3.27: Fourth inspection: CuNi10 (panel 5)



Figure 3.28: Fourth inspection: CuNi30 (panel 12)

At the fifth inspection, no changes were present, Figure 3.29.

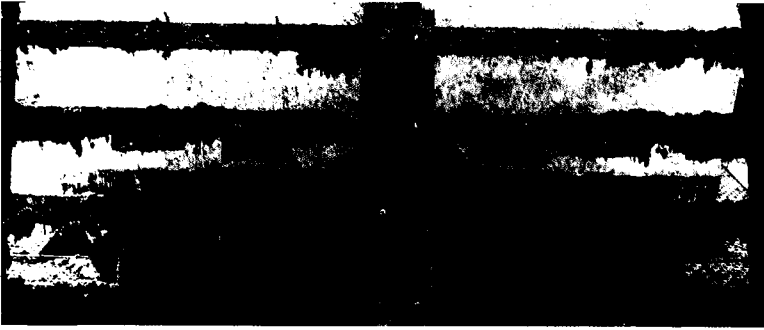


Figure 3.29: Fifth inspection: whole rack

Table 3.6 shows the values of the electrochemical potential as measured during the 1st, 3rd and 5th inspection. Interesting is the increase in potential at the 3rd inspection for all samples coupled to steel. This is caused by the rapid increase in coverage between the 1st and 3rd inspection. Non-corroded steel areas are almost entirely fouled. The potentials of the coupled Cunifer-samples are all below the fouling potential as determined in section 3.2.3 (ca. -350mV vs Ag/AgCl). In the end all potential values are even in the immunity range for these alloys (Figure 3.2). The fouling on the galvanically coupled samples can therefore easily be explained.

For the freely exposed samples (panel 5 and 12), the potentials are in the same range for the first two measurements. The potential doesn't decrease into the immunity range. The fact that no macrofouling was possible implies that the determination of a fouling potential is in fact an oversimplification. Though the corrosion rate is slow at these potentials (a.o. through the formation of a stable Cu₂O layer), corrosion is still fast enough to create a surface condition, which is non-desirable for macrofouling species. This is in good agreement with the observation in section 3.2.3, where barnacle larvae remained active, but did not settle on the Cunifer surface. In a field trial, the larvae have a number of sites where they can settle and they will go to other sites.

Table 3.6: Electrochemical potential (mixed potentials) of the panels

Panel combination	E_{corr} 1 st inspection mV (vs. Ag/AgCl)	E_{corr} 3 rd inspection mV (vs. Ag/AgCl)	E_{corr} 5 th inspection mV (vs. Ag/AgCl)
1 / 2	-560	-420	-650
3 / 4	-570	-440	-690
5	-170	-450	-450
6 / 7	-520	-380	-640
10	-710	-740	-950
11	-700	-620	-940
12	-300	-340	-400
13 / 14	-590	-220 ¹	-650
15 / 16	-580	-440	-690
17 / 18	-470	-340	-650

¹ Value is too noble. Probably measurement is wrong, potential of the coupled sample can never be more noble than the potential of the freely exposed sample.

Discussion

Initially, the general fouling behaviour is according to the expectations: some microfouling, no macrofouling. As the potential decreases and drops below the fouling potential, it was expected that fouling would occur. Indeed, at the third inspection, macrofouling species are present and fouling increases until complete colonisation is a fact.

In some cases, CuNi10Fe did show less fouling than CuNi30Fe, as was anticipated based on the higher copper concentration in the alloy. The differences are, however, not very large. However, this can be explained by the general observation in literature [15] that the corrosion behaviour of CuNi10Fe and CuNi30Fe is the same for longer exposure periods to seawater. Though this is not expected based on Pourbaix-diagrams, since CuNi10Fe is in the active corrosion region, whereas CuNi30Fe is in the passive region in seawater (pH approximately 7.8), this is due to the formation of Cu_2O as corrosion product in both the passive and active region. Furthermore, it is stated that the surface of CuNi10Fe is enriched with nickel as corrosion proceeds.

The behaviour of the samples exposed at OCP is not as expected beforehand. In the first period, the potential is high (-170mV vs. Ag/AgCl) and copper dissolution is large enough to prevent larvae from settling. However, at the third inspection, the potential has decreased to a value below the determined "fouling potential" and thus it should be expected that macrofouling will occur. This is not the case. On one hand, this can be explained by the slow regeneration of the Cu_2O layer, which has formed at the surface. On the other hand, the absence of fouling can be explained by the fact that many macro-organisms have a selection mechanism for the surface where they settle. A low concentration of toxic Cu^{2+} ions (e.g. in the electrochemical double layer) could be enough for the organisms to decide to settle elsewhere. In the lab-trials, the organisms have a less wide choice of settlement surface.

3.2.5 General Discussion

The preceding section focussed on the biofouling problems that can occur on Cunifer, a material commonly used for marine heat exchangers. The material is used for its good combination of mechanical properties with heat transfer rate and intrinsic antifouling properties. However, as is shown in this section, fouling can result on Cunifer alloys due to careless use. On one hand, it is often impossible to prevent all galvanic couplings. On the other hand, in some cases the coupling is obligatory for safety precautions.

A barnacle assay study showed the effects of electrochemical potential on the settlement of barnacle larvae. A "fouling potential" was determined (between -300 and -400mV vs. Ag/AgCl for CuNi10Fe and between -250 and -400mV vs. Ag/AgCl for CuNi30Fe) and moreover, it was shown (for CuNi10Fe) that a region exists in which fouling is prevented without killing the barnacle larvae, suggesting that the settlement surface selection is in this case electrochemically driven.

The coupling of Cunifer to zinc and steel was investigated in a field study to qualify the effects. It was shown that both CuNi10Fe and CuNi30Fe are liable to fouling. Differences in antifouling properties between CuNi10Fe and CuNi30Fe are only present in the initial exposure period. The differences fade away rapidly due to the similar build-up oxide layer.

Furthermore, it was shown that even though OCP is an important factor, it is not the only determining factor. Surface conditions and stability of the oxide layer are of importance as well. This was obvious from the exposure at OCP, since the potential dropped below the fouling potential, but still no macrofouling was present.

3.3 Inorganic Fouling in Heat Exchangers

3.3.1 Introduction

Heat exchangers form an essential part of many industrial processes and very often use water as cooling agent. Depending on the type and position in the process, the water composition can be very diverse. For example, some heat exchangers have a critical cooling function in the process they control. In this case, the cooling water needs to be conditioned to a large extent and in general, closed loop cooling systems are used, e.g. critical parts of nuclear power stations. In other situations, the cooling is less critical and water make-up does not need to be controlled that precisely, e.g. ship engine. In that case, water can be picked up from the environment.

In those cases where environmental water is used, several compounds are present in the water that can result in deterioration of the heat transfer due to the deposition of compounds on the walls of the heat exchanger. This fouling process might even lead to the deterioration of the complete heat exchanger due to corrosion damage occurring underneath the deposits. Corrosion damage can result in unexpected shutdowns, when leaks in the systems occur and it can result in hazardous situations in case of toxic process streams. Nowadays, maintenance schedules are quite strict to be sure no leaks will occur. However, this implies a frequent check of the systems resulting in relatively high outage times. The present research has the aim to investigate the phenomena electrochemically, in order to (eventually) find ways to monitor the processes in situ. This would result in a lower check frequency and thus leads to lower maintenance costs. In the specific case treated within this section, a fresh water cooling system is regarded consisting of AISI 316L stainless steel tubes.

Two experimental series have been carried out which will be treated in this section. These experimental series have been done in a specially designed set-up, described in section 3.3.3. In the first experimental series, scaling was induced electrochemically by lowering the potential (section 3.3.4); in the second series, scaling was induced thermally (section 3.3.5). Both processes were analysed using electrochemical impedance spectroscopy.

Before the experiments are discussed, a short literature survey is given regarding the use of EIS in scaling research. As was mentioned EIS is used for the electrochemical investigations. Both pitting and crevice corrosion can occur and both of them are localised phenomena. Moreover, conductivity of the scales is poor, so d.c.-techniques are inappropriate. Therefore, advanced electrochemical techniques are needed to predict the corrosion phenomena. Electrochemical impedance spectroscopy has turned out to be a very useful tool, as was reported by e.g. Keddah et al. [18] and as will be shown by the experimental results presented in this chapter.

3.3.2 Electrochemical Impedance Spectroscopy Studies of Corrosion and Scaling Mechanisms

Introduction

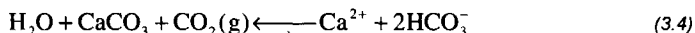
Scaling is a deposition process, which is strongly dependent on temperature and pH. The effect of pH is generally observed in heat exchangers. The effect of pH is observed in cathodic protection systems: oxygen reduction to hydroxide is enhanced by the impressed low potential of the cathodic protection system. The resulting increase in pH favours the deposition process. Although the potential changes applied in electrochemical measurement techniques are generally much lower than those in cathodic protection, they will influence the scaling process and also the scaling layer formed on the surface. Therefore, to monitor scaling and scaling induced corrosion, one should select an electrochemical technique which uses low to moderate potential changes. The techniques suitable for the investigation of the fouling processes are therefore limited. At best, one should have no influence of the measurement technique at all.

A technique that gives a large amount of information on all kinds of electrochemical processes and is also suggested to be applicable for localised corrosion processes, is electrochemical impedance spectroscopy. It has been shown that scaling can be monitored, including morphology and scaling rate. C. Gabrielli, M. Keddari and co-workers [18, 24, 25-28] have performed most of the work done in this area. They have also shown, in a specific case, that pitting corrosion could be detected [21].

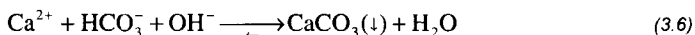
The study of the fouling process can be split into two parts: studying scaling and studying the consequences of scaling. Both processes will show different responses in the results of impedance measurements. Firstly, the scaling process and the interpretation will be dealt with. Subsequently, localised corrosion phenomena are treated.

EIS for Studying Scaling

The main scaling phenomenon is the deposition of calcium carbonate. This process is enhanced by temperature increase due to the inverse solubility of CaCO_3 , which can be explained by reaction 3.4:



When the temperature increases, CO_2 will evaporate more easily and the equilibrium will shift left, inducing deposition of CaCO_3 . The scaling process is also influenced by electrochemistry, specifically the oxygen reduction process, according to reactions 3.5 and 3.6:



When the potential is decreased, the amount of electrons available at the surface will increase and the equilibrium in reaction 3.5 will shift to the right hand side. Due to the increased concentration reaction 3.6 shifts to the right as well. This means an enhanced scaling.

The group of researchers mentioned above has used EIS to investigate the electrode surface during the scaling process. They have set-up a model for the blocking of the electrode by calcite crystals and have verified their model experimentally. Calcite deposits at room temperature at potentials below -1.2 V (SSE) (-1.850 V vs. SHE). They were able to show the build-up of a diffusion barrier for oxygen [25] and they could show differences in surface coverage. Estimations can be drawn from the EIS measurements under certain conditions about the

fraction of the surface covered by a scale [24]. Furthermore it was possible to estimate the deposition rate of scaling in case of thermally activated scaling and showed that the impedance response of the deposits was different [28]. This is especially important for situations in which scaling occurs at open circuit potential, e.g. due to thermal scaling. Under such conditions, d.c.-measurements cannot resolve the scaling rate. In EIS, the rate can be estimated from the impedance response. The calcareous deposit blocks progressively the active surface, resulting in an increase of the magnitude of the impedance response. The impedance could be regarded as resulting from a diffusion controlled transfer process (diffusion layer thickness for oxygen). The impedance of such response of such a system is as follows:

$$Z(\omega) = R_{ct} \left(1 + k \frac{\tanh \delta \sqrt{j\omega/D}}{\sqrt{j\omega D}} \right) \quad (3.7)$$

R_{ct} = charge transfer resistance
 k = reaction rate constant
 δ = diffusion layer thickness (Debye length)
 D = diffusion coefficient of the active species

The increase in δ directly gives the scaling rate. Since $Z(\omega)$ is measured and R_{ct} can be derived by fitting the measurement using equivalent circuits, the scaling rate can indeed be determined from the impedance measurement.

EIS in Studying Localised Corrosion

Although the technique of EIS has not generally been applied to localised corrosion phenomena, several authors have already suggested the use of this technique for studying localised corrosion phenomena [19, 20, 22, 23]. Oltra et al. [21] claim the ac-measurement technique EIS has several advantages over dc-techniques commonly used for studying localised corrosion phenomena. Firstly, changes in the passive film during the incubation of pitting cannot be shown with dc-measurements. Furthermore, during the pitting, it is impossible for dc-measurements to determine the rate-determining step during pit growth.

Oltra et al [21] have used EIS-measurements to study stable pit formation. They claim that pit initiation can be registered. Figure 3.30 shows the difference in impedance response for a blank, i.e. not pitted, Ni-plated steel and the same sample with a laser-initiated pit. Furthermore, the pitting surface area can be estimated. Limitations are found in the fact that the surface geometry of the pit changes continuously, as does the distribution of the ac-current in the electrolyte.

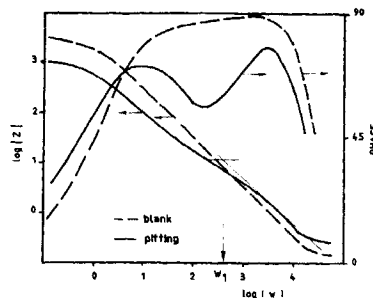


Figure 3.30: Evolution of the impedance spectra on a model pit. Blank: Ni-plated steel electrode without any localised corrosion; pitting: a 0.025cm diameter hole is formed in the previous electrode by a laser beam before immersion in the electrolyte.

The pitting phenomena reported here, are based on modelled pits and are not happening under a deposit, and are furthermore controlled to a large extent and therefore transposing the results of these experiments to the case we will deal with is not allowed. Furthermore, in case of pitting, a non-stationary situation is present in the system and uncontrolled changes are occurring. Impedance spectroscopy is designed for stationary or slowly changing systems because of the length of the measurements. Strictly speaking, EIS-analysis is therefore not allowed. However, the results do show that possibilities exist to use EIS for the purpose of monitoring pitting corrosion. Experimental trials are necessary to show the usefulness in this case.

3.3.3 Experimental Set-up

As was shown in the previous section, EIS shows a high potential to be used successfully in studying localised corrosion and scaling and eventually monitoring the processes. To perform an accurate study, the experimental conditions need to be as close to reality as possible. For the set-up, this leads to the following demands:

- Heat cross-flow through the sample to accurately simulate the scaling deposition
- Dimensions of the sample should enable accurate EIS
- Symmetrical electrode setting
- Replaceable working electrode
- Visual examination of sample during experiments

Based on these demands, a versatile set-up has been designed as is schematically drawn in Figure 3.31. With this robust set-up, it is possible to investigate the effects of scaling and corrosion processes both electrochemically and visually.

The lab-sensor has been designed in PMMA. The probe part can be screwed in and out as far as necessary to level it in the same height as the rest of the cell. The probe can be ground and still be levelled. The sample surface is made of AISI 316L, two thermocouples are inserted for measuring a temperature profile through the probe. This profile is used to estimate the surface temperature and to regulate the heating element on the back of the probe. The heating is done with a resistance and d.c.-current to prevent inductive effects which could disturb the electrochemical measurements.

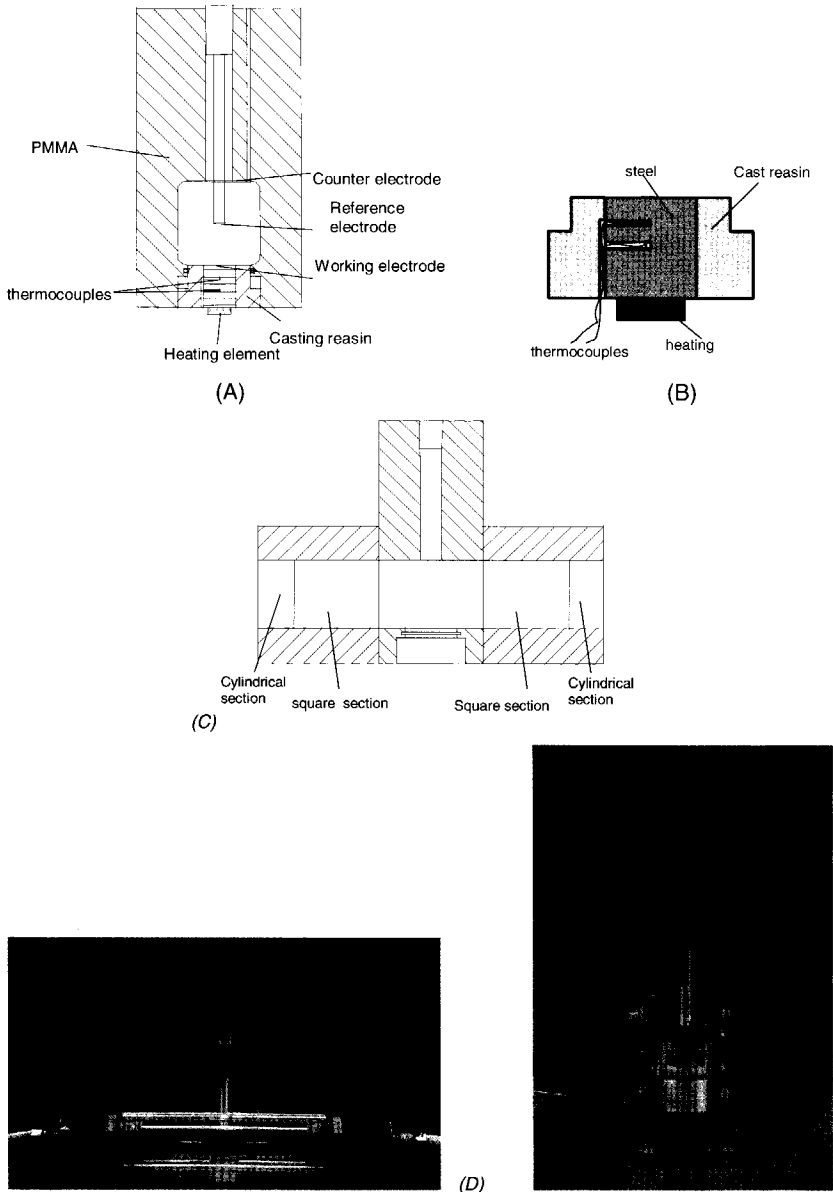


Figure 3.31: Schematic drawings of the cooling water sensor. (A) measurement section, (B) working electrode and heating section, (C) complete set-up, (D) pictures of complete set-up

3.3.4 Electrochemically Induced Scaling

With the sensor described in section 3.3.3, experimental trials have been carried out for 900 hours [31]. This section deals with the experimental procedures, results and interpretation of the measurements and an initial idea on monitoring to formulate an algorithm for the monitoring strategy.

Experimental Procedure

The experiments were carried out with a flow through system containing 30 litre of cooling water according to NEN7420 [17], including 10 ppm 1-hydroxy ethylidene diphosphonic acid for scaling inhibition and excluding kaoline and ethanol to prevent biological growth. The water was heated to a temperature of ca 40°C. The temperature of the water was measured at the outlet of the measurement cell. The throughput of the pump used was ca. 8 l/h, which gives an average flow speed of 1.4 cm/s at the sensor surface.

The probe surface was heated to ca. 60°C, which was regulated by a computer using National Instruments Labview software. EIS was performed using a potentiostat (Solartron 1250) and a frequency response analyser (Solartron 1260). Measurement frequencies ranged from 0.01 to 50000 Hz. For the analysis of the impedance data, Boukamp software was used [29] to fit equivalent electrical circuits, corresponding to the physically changing system. These fits are performed using a Non-Linear Least Squares fit procedure. When the errors in the fit do not show a marked frequency dependence, the fit is accurately describing the system and no processes are left out. A more detailed description of the fit procedures is given e.g. by Van Westing [30].

General Observations During Electrochemically Induced Scaling

Figure 3.32 shows the corrosion potential as a function of time as it was measured before each EIS measurement. Initially, the potential is 50-100 mV vs. Ag/AgCl. However, after ca. 150 hours, the potential decreases sharply. This is caused by the initiation of crevice corrosion, as was visually observed, see Figure 3.33.

Although the crevice formed is in fact an unexpected problem and is unacceptable for the sensor, it was decided to continue the experiments. In fact the occurrence of the crevice enabled the monitoring of crevice corrosion which was one of the aims of the sensor. It should be reminded that the crevice corrosion occurring in this case is different from the crevice corrosion that occurs underneath a scaling layer, but it was in fact interesting to investigate the possibility of monitoring this corrosion phenomenon. It has, however to be reminded during the analysis of the results that the crevice may have influenced the rest of the results.

After approximately 340 hours, still no scaling was present yet. It turned out not to be possible to initiate scaling thermally. This was probably due to the presence of 10-20 ppm of phosphonate which is more than generally added to inhibit scaling on cool spots which arises from the evaporation of CO₂ shifting the equilibrium in equation 3.1 to the left. Therefore, it was decided to induce scaling electrochemically. The potential was set to -1.0 V (vs. sat. Ag/AgCl). The scaling started rapidly and was quite homogeneous. After circa 100 hours of polarisation, the scale covered most of the surface and the potential was released again. After a certain period, pitting initiated. This can be seen in the scattered potential curve after about 500h, and was observed visually as well. Several pits formed as is shown in Figure 3.34.

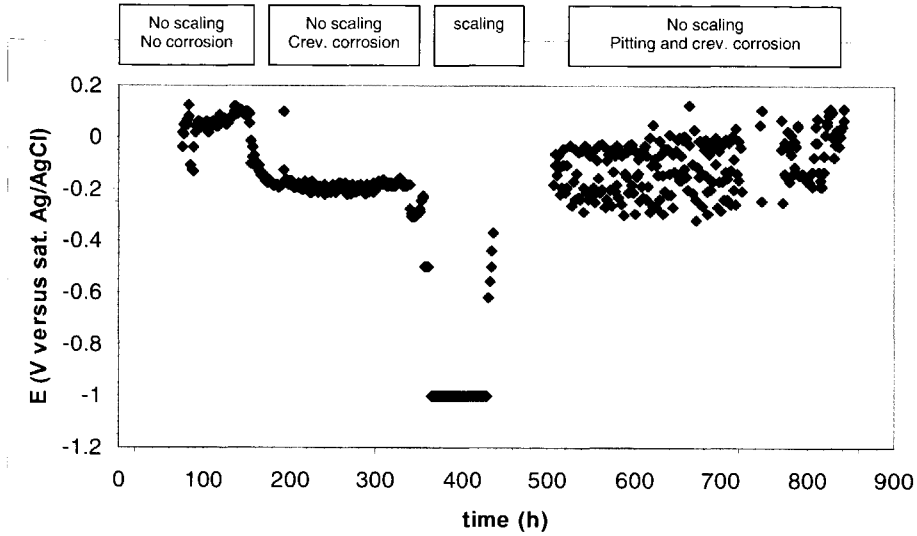


Figure 3.32: OCP of the sample during the experimental cycle, measured before each EIS measurement.

Optical Microscopy and SEM-analysis

Figure 3.34 shows a light microscopy image of the scaled image with several pits present. Pits of several magnitudes have been analysed with EDX. The wt% of the most interesting elements related to the corrosion spots are presented in Table 3.7.

Table 3.7: EDX weight percentages of several elements at locations on the corroded sample.

Spot in Figure 3.34	Wt% of elements					
	Ca	Cl	O	Fe	Cr	Ni
A	17	12	n.d.	41	16	4.5
B	12	1.6	n.d.	69	3.9	4.1
C	6.9	n.d.	32	50	1.4	1.8
D	0.8	n.d.	24	61	11	1.4

Interesting is the high amount of chloride present in the smallest pit. This indicates that the pit is highly active. When the pit grows, the chloride content decreases, which is a result of the regeneration of deposited chlorides due to the fact that oxides are more stable. The chloride ions are moving to other places, e.g. newly formed pits, since their presence is not necessary any longer for electroneutrality. Furthermore it is obvious that, as the pits grow, the amount of Ca in the corrosion product decreases, which implies that the growing corrosion pit removes the scale.

Figure 3.35 shows pictures of the large corrosion pit after removal of the corrosion products. Examining the sample, it was noticed that many small pits could be observed as well.

The scale itself has been investigated using SEM. As was stated by Gabrielli et al. [28], the crystal structure of scales formed at low potentials is rhombohedral (calcite). Figure 3.36 indeed shows this characteristic crystal structure. Finally, it can be observed that the layer is quite dense: between the rhombohedral crystals, a dense layer of CaCO_3 is present.

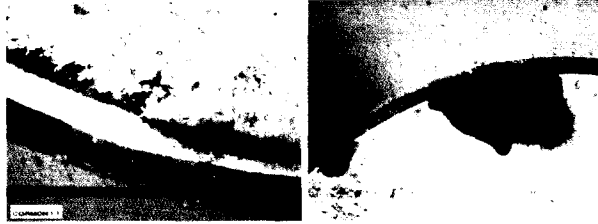


Figure 3.33: Crevice corrosion on the side of the sensor surface.

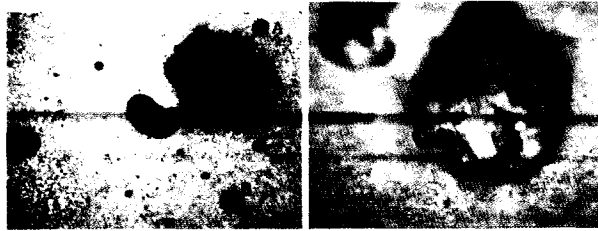


Figure 3.34: Pitting corrosion on the sensor surface.

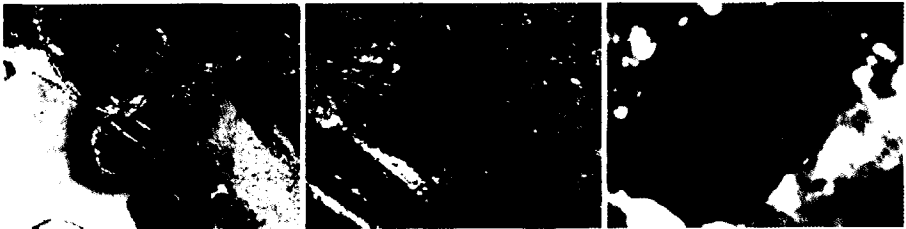


Figure 3.35: Pictures (enlargement 1, 4 and 6x) of the large corrosion pit as was shown with scale in Figure 3.34.

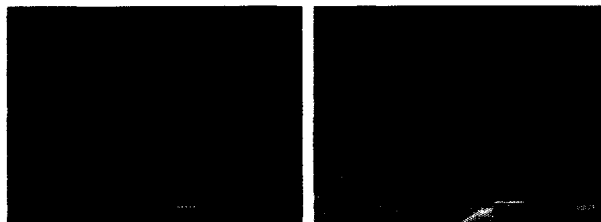


Figure 3.36: Calcite crystal structure of CaCO_3 scale at two locations on the sample (enlargement 2200 and 3000x).

Impedance Analysis Electrochemically Induced Scaling

Based on the general observations by visual observations and OCP-monitoring during the experimental cycle, it is expected that the analysis will result in four different regions:

1. No corrosion, no scaling

In the initial phase of the experiments, no scaling occurred and the cooling water composition is stable. Therefore, the electrochemical double layer is expected to remain unchanged (C_{dl} , R_{ct}). Furthermore, the passive layer is continuously regenerated (C_{pass} , R_{pass}). Figure 3.37 shows the expected equivalent impedance model of the system.

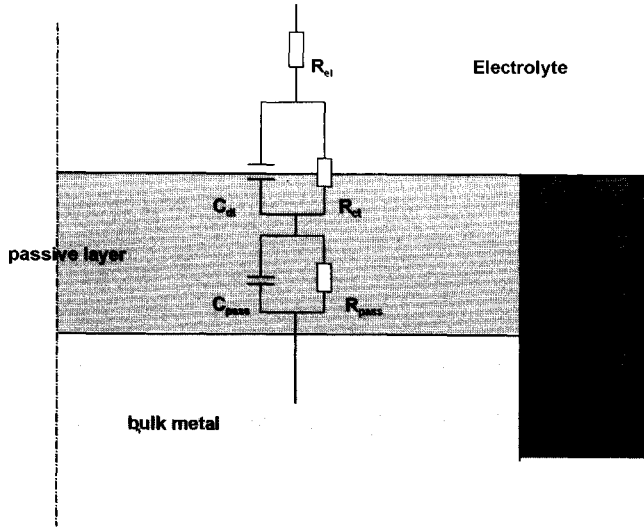


Figure 3.37: Hypothetical circuit model of impedance response with no corrosion and no scaling.

2. No scaling, crevice corrosion at the edge of the probe

The crevice corrosion at the edge of the sample is expected to give a separate contribution to the impedance signal (C_{corr} , R_p), either due to the corrosion reaction or due to the capacitive behaviour of the corrosion products as a result of charge transport in this layer. Three time constants are therefore expected in this region, see Figure 3.38. In principle, the R_{ct} and C_{dl} should be drawn in the crevice as well, however, for the sake of clarity of the Figure, it is omitted.

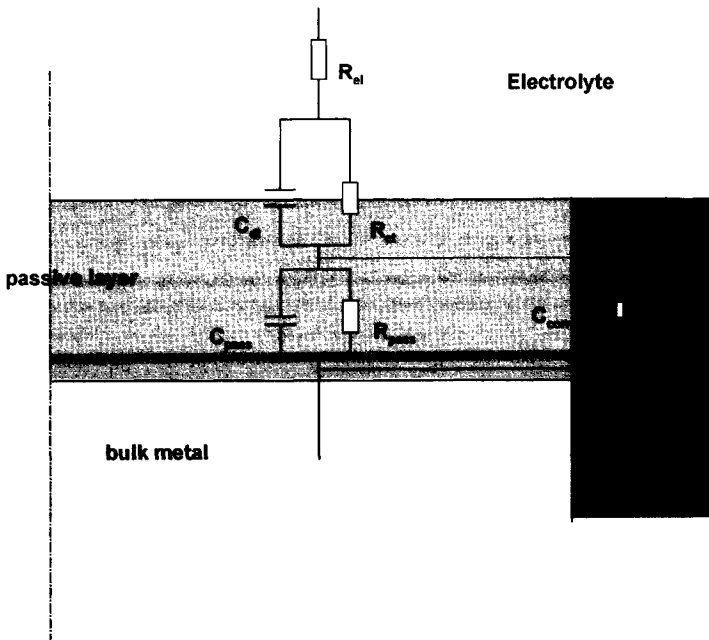


Figure 3.38: Hypothetical circuit model of impedance response with crevice corrosion and no scaling.

3. Impressed potential. No corrosion, scaling

In this region, it is expected that the crevice corrosion is suppressed and therefore will not be visible in the impedance signal any more. Furthermore, an increase in the oxygen diffusion path length due to the formation of a porous scaling layer will increase the impedance of the diffusion path. The passive layer contribution to the signal is still expected to be present. Finally, a contribution of the scaling layer itself can be expected (C_{scale} , R_{scale}). However, this latter contribution will emerge at high frequencies and will not be visible below 10 kHz. Figure 3.39 shows the equivalent circuit elements of the expected impedance response.

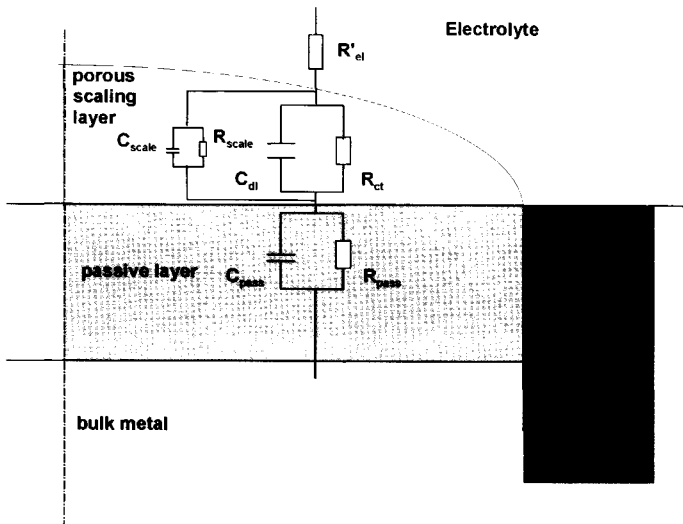


Figure 3.39: Hypothetical circuit model of impedance response without corrosion and electrochemically induced scaling.

4. No scaling, pitting and crevice corrosion

When the potential has returned to the OCP, scaling is not expected any more and therefore the diffusion path should be constant. However, pitting starts and at the pitting spots, the scale is slowly removed, which could lead to a decrease in the oxygen diffusion path length. Furthermore, pitting corrosion can add a time constant to the EIS signal (C_{pit} , R_{pit}), the expected crevice corrosion time constant should reappear again and the passive layer will probably still be visible. Figure 3.40 shows the equivalent circuit elements of the expected impedance response.

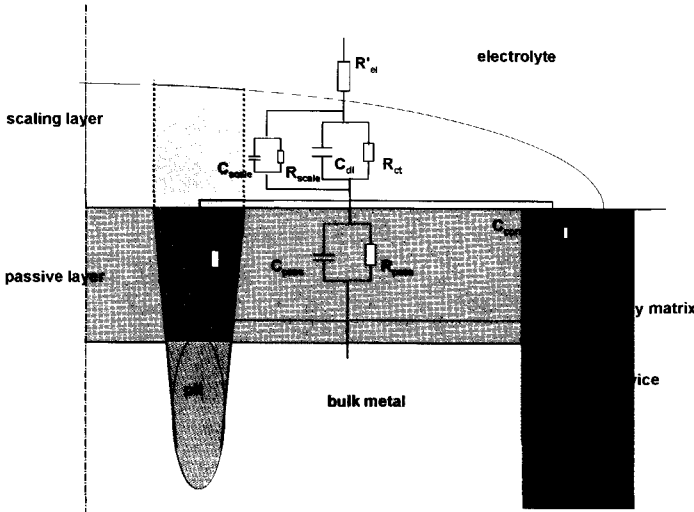


Figure 3.40: Hypothetical circuit model of impedance response with pitting and crevice corrosion and no scaling.

For the analysis, the data were split in four regions. Characteristic Bode-plots are shown in Figure 3.41. Characteristic Nyquist-plots are depicted in Figure 3.42. Although for the physical understanding of the phenomena, capacitances have been used in the schematic drawings, in practice a deviation of capacitive behaviour is occurring. The impedance changes:

$$Z = \frac{1}{j\omega C} \rightarrow Z = \frac{1}{(j\omega)^n Y_0}$$

The behaviour approaches true capacitive behaviour for $n = 1$. Other commonly found values for n are 0.4-0.6 for diffusion processes (0.5 for ideal infinite length diffusion), 0.8 for corrosion reactions and >0.9 for coatings. Figure 3.38 gives an overview of the Y_0 -values, n -values and the resistances found during the analysis.

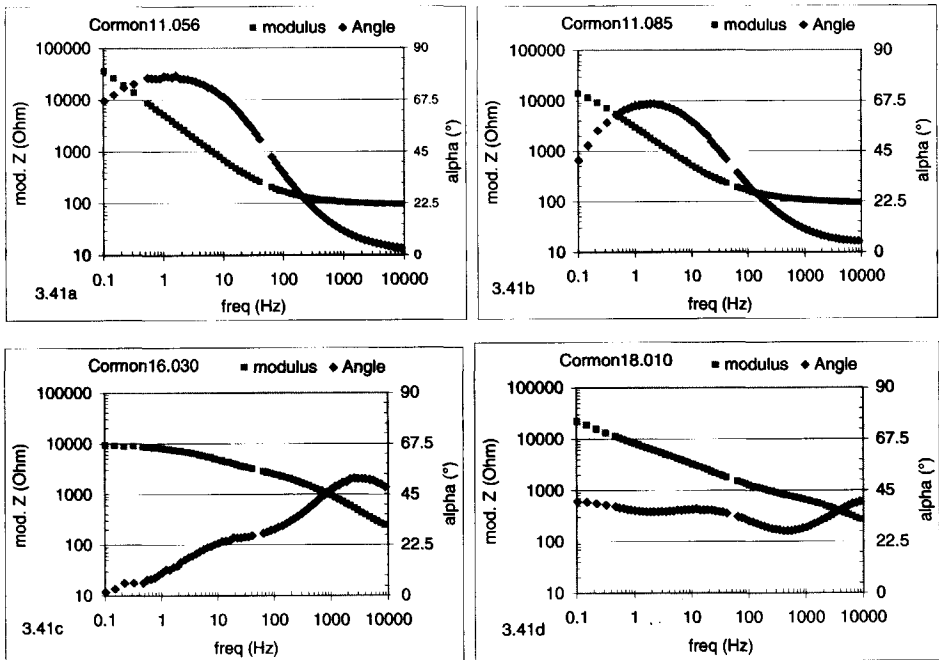


Figure 3.41: Characteristic Bode-plots for the four different regions observed during the exposure of AISI316 to fresh cooling water and heating of the sample. a: no scaling, no corrosion; b: no scaling, crevice corrosion at the edge of the probe; c: impressed potential, scaling, no corrosion; d: no scaling, pitting and crevice corrosion.

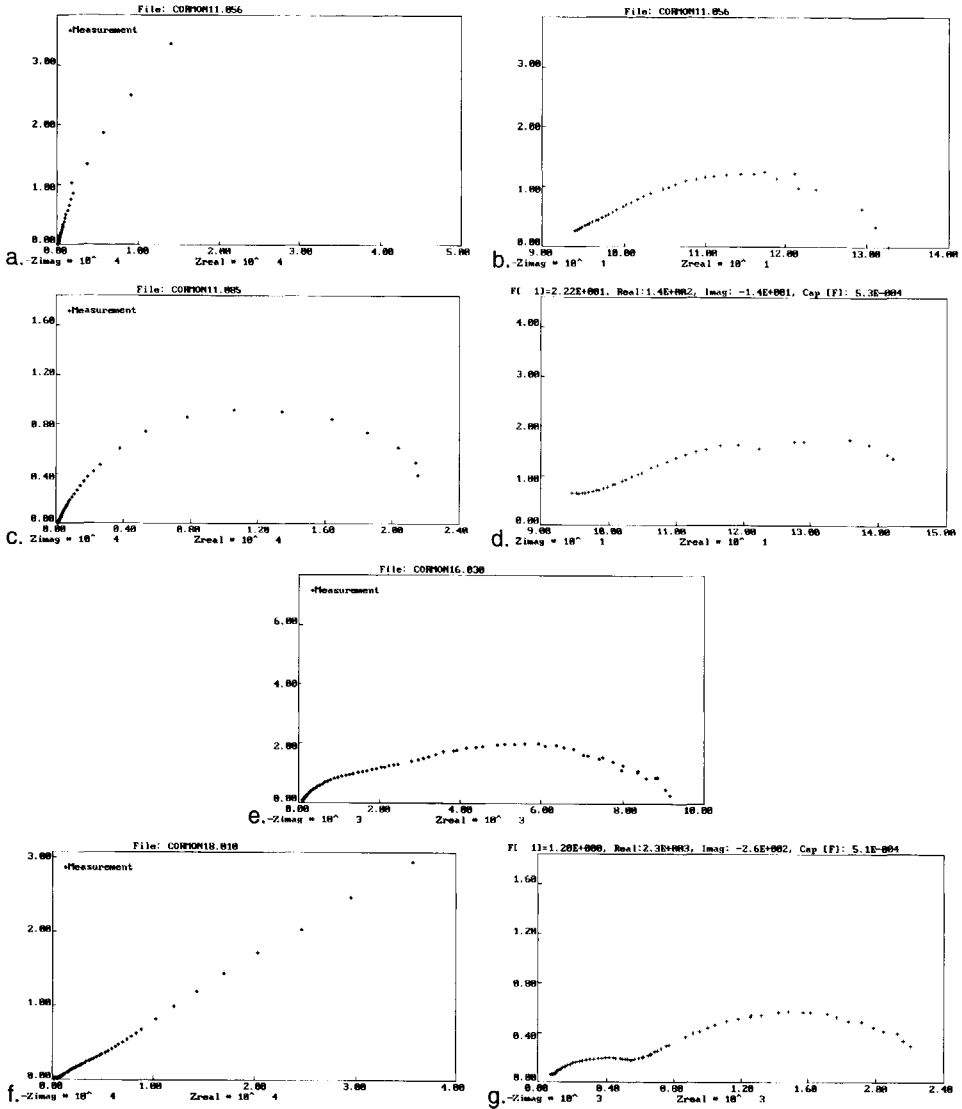


Figure 3.42: Characteristic Nyquist-plots for the four different regions observed in the experimental trials. a: no scaling, no corrosion (0.1-50,000Hz); b: no scaling, no corrosion (25-15,000Hz); c: no scaling, crevice corrosion at the edge of the probe (0.1-50,000Hz); d: no scaling, crevice corrosion at the edge of the probe (22-10,000Hz); e: impressed potential, scaling, no corrosion (0.1-50,000Hz); f: no scaling, pitting and crevice corrosion (0.1-50,000Hz); g: no scaling, pitting and crevice corrosion (1.2-50,000Hz).

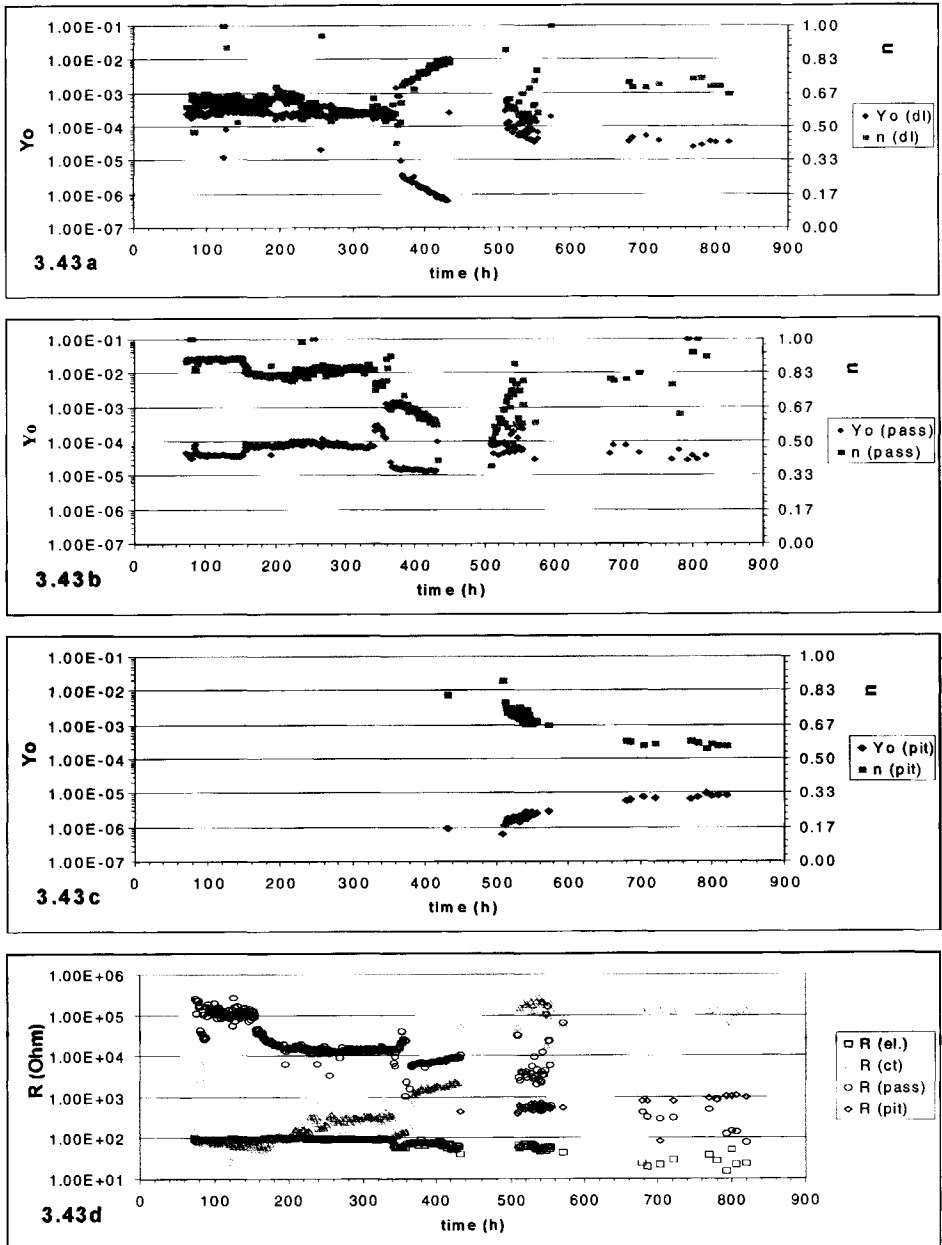


Figure 3.43: Impedance plots for the whole experimental period of the exposure of AISI316 to fresh cooling water and heating of the sample. a: $Y_{o, dl}$ and n_{dl} ; b: $Y_{o, pass}$ and n_{pass} ; c: $Y_{o, pit}$ and n_{pit} ; d: R_{el} , R_{pit} , R_{ct} , R_{pass} .

Discussion

During the first 150 hours (EIS during the last 80 hours), two time constants are present, related to the electrochemical double layer and the passive layer. They are present in series: $R_{el}(R_{ct}Q_{dl})(R_{pass}Q_{pass})$. Both are stable.

After approximately 150 hours, as was pointed out in the general observations, the potential decreases rapidly to a new stationary value about 300 mV below the initial value, due to crevice corrosion. This step is visible in the EIS analysis as follows:

- A decrease in the n-value of the passive layer. This decrease in n-value (from 0.9 to 0.8) indicates a deterioration of the passive layer or could be due to the contribution of crevice corrosion, which would yield an n-value of ca. 0.8.
- It is expected that from now on this time constant is dominated by this crevice corrosion process and the passive layer is not visible within this frequency domain any more. The decrease in R_{pass} is also indicating the dominance of the crevice corrosion over the passive layer resistance.
- An increase in Y_o . The crevice is filled with corrosion products, which have a charge storage capacity resulting in an increase in the capacitive response.
- The crevice corrosion is not resulting in a separate time constant. The time constant related to the double layer does not change markedly.

After approximately 290 hours, still no scaling was present. To induce scaling, the potential was set to $-1.0V$ (versus sat. Ag/AgCl). Scaling initiated and a (more or less) homogeneous layer of calcite was formed. The first observation to be made in the impedance data is the jump in the values of the various parameters. It was of course expected that the impressed potential would have a marked effect because it directly influences the oxygen reduction to hydroxide, The increase in layer thickness shows up in several parameters:

- An increase in resistance R_{ct} , which is, at this stage merely a diffusion resistance of the scaling layer. This resistance will increase due to the layer build-up.
- A decrease in the double layer Y_o . The scale is partially blocking the surface. At those places where the scale is strongly adhering to the surface, the electrochemical activity will diminish, resulting in a smaller capacitance of the double layer.
- The $Y_{o, pass}$ dominated by the crevice corrosion is slightly decreasing and the n-value drops slowly from the value of a corrosion process (0.8) to lower values more characteristic of a diffusion process. These changes indicate that the corrosion products are stable and are being covered by a diffusion barrier: the scaling layer.

When the impressed potential is removed, quite rapidly a third time constant shows up. During this phase, the OCP was scattering to a large extent and also pitting was visible after a while. Based on these observations, it is likely that the pitting process is responsible for the third time constant. Based on the physical model describing the process, it can be expected that the pitting process would occur in a time constant parallel to the passive layer and in series with the double layer capacitance/diffusion resistance: $R_{el}(R_{ct}Q_{dl})(Q_{pass}(R_{pass}(R_{pit}Q_{pit})))$. However, fitting a series of measurements did not give proper results. Therefore, an alternative circuit was used for the fitting, i.e. three time constants in series with each other, $R_{el}(R_{ct}Q_{dl})(R_{pass}Q_{pass})(R_{pit}Q_{pit})$. This circuit gave much better fit results. This series model can be explained by the fact that it is likely that the passive layer time constant has shifted to frequencies above 10kHz and is therefore no longer visible. The three time constants in series can account for the scaling layer diffusion barrier ($(R_{ct}Q_{dl})$), the pitting corrosion ($(R_{pass}Q_{pass})$) and the build-up of corrosion products inside the pit ($(R_{pit}Q_{pit})$).

3.3.5 Thermally Induced Scaling

Experimental Procedure

A second experimental trial has been carried out to confirm the observations and interpretation of section 3.3.4. Experiments lasted 4000 hours. The experimental settings were the same as described previously, with some changes:

- EIS was in this case performed using a potentiostat (Solartron 1255) and a frequency response analyser (Solartron 1270).
- Measured frequencies ranged from 0.01 to 500.000Hz.
- Time period between two measurements was increased to 5 hours
- Flow rate of cooling water was increased from 8l/h to 80 l/h
- Scaling inhibitor was omitted from the cooling water to enhance scale formation

General Observations during Thermally Induced Scaling

Figure 3.44 shows the OCP of the system as a function of time, measured before each EIS measurement. Compared to the potential in the previous series, the potential is lower at the beginning. During the first 400 hours, this can be explained by the lower sample temperature, the heating was not turned on yet. As soon as the heating is switched on, a thin deposition layer will be formed, resulting in the increase in potential. The next 1000 hours ($t = 500$ to 1500 hours), the scale increases in thickness. However no further influence on the potential is present. After 1900 hours, crevice corrosion occurs like was the case in the previous series. Potential decreases towards values which were present in the previous series (-200mV vs. Ag/AgCl). However, the potential is much less stable in this case.

After 600 hours, the measurements were stopped ($t = 2600$ h). No pitting had occurred yet. Therefore it was decided to initiate pitting artificially. At $t = 3000$ h, 500ml hypochlorite was added to the cooling water. The potential did increase, however, the effect was too large: the medium deteriorated. Therefore another way was used to induce pitting. A potential of 1V vs. Ag/AgCl was impressed for three hours. When pits were visual, the impressed potential was removed and EIS measurements were carried out ($t = 3700 - 4000$ hours).

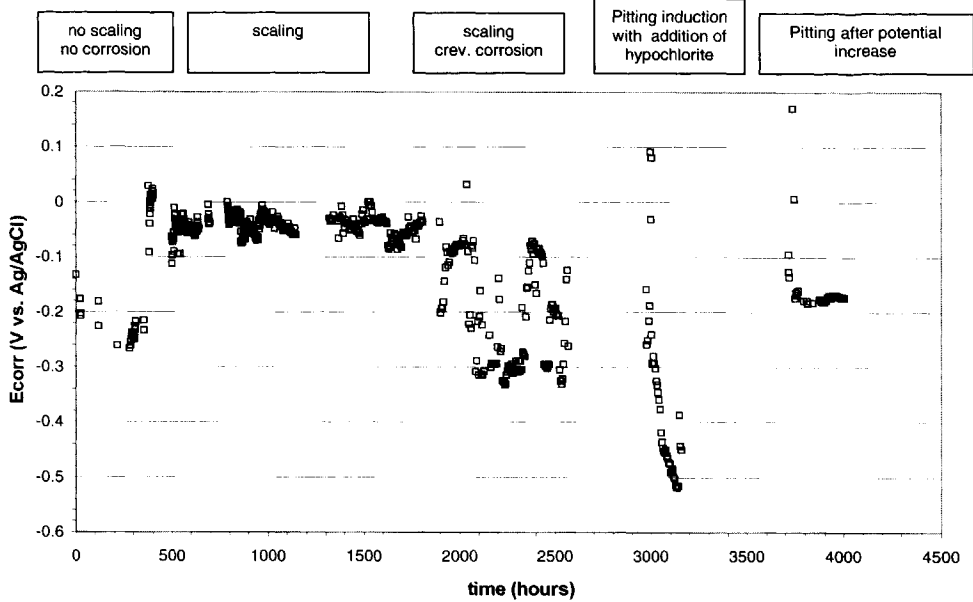


Figure 3.44: OCP of the sample during the experimental cycle, measured before each EIS measurement

Optical Microscopy and SEM-analysis

Figure 3.45a shows a picture of the sample surface after the full experimental cycle. Three pitting areas are visible and also the crevice corrosion spot can be observed. Figure 3.45b shows a close-up of the crevice corrosion. Figure 3.46 shows the biggest pit (left one in Figure 3.45a). For the second picture, the scale was removed. As can be seen, the pit is very small relative to the area showing corrosion products.

Figure 3.47 shows two SEM pictures of the pitted area. The rod-shaped particles in the close-up turned out to be MnS (EDX-analysis). Figure 4.48 shows the scale covering the whole surface. The scale structure is quite different from the one formed electrochemically in the first experimental trial (Figure 3.36). The structure is much less dense and only a thin layer is completely covering the surface.

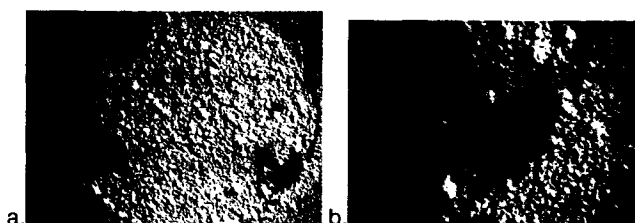


Figure 3.45: a: Image of the sample surface after the experiment (enlargement 0.63x); b: Close-up of the crevice corrosion spot (enlargement 2x).

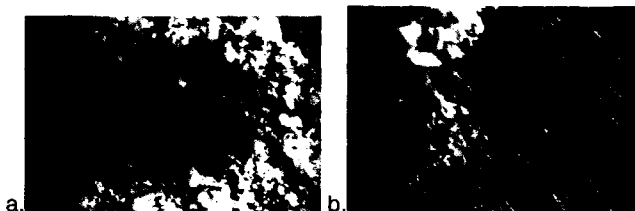


Figure 3.46: Images of a pit on the sample surface before (a) and after (b) removal of the scale (enlargement 6x)



Figure 3.47: SEM-images of the pit, shown in figure 3.46 (enlargement 350 and 1300x)



Figure 3.48: SEM-image of the scale present on the sample surface after the experiments (enlargement 400x)

Impedance Analysis

Based on the general observations, microscopy and OCP-analysis, it is expected that the analysis of the impedance data can be divided in four areas.

1. No corrosion, no scaling

Initially, no scaling or corrosion processes are occurring. As was the case for the first experimental series, a contribution to the impedance of a stable double layer (C_{dl} , R_{ct}) and a stable passive layer (C_{pass} , R_{pass}) is expected, see Figure 3.37.

2. No corrosion, scaling

Secondly, scaling is covering the surface area. As was discussed before and was suggested by Gabrielli et al. [25 to 28], the effect of a scaling layer will be present in an increased diffusion path for oxygen, resulting in an increased charge transfer resistance, R_{ct} . Furthermore, blocking of the surface will decrease the electrochemical activity which could result in a decreased capacitive behaviour, C_{dl} . Furthermore, a high frequency response of the scaling layer could be observed (C_{scale} , R_{scale}). Figure 3.49 shows the expected components of the system.

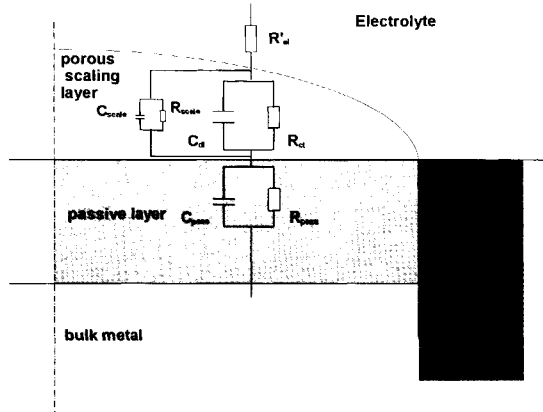


Figure 3.49: Hypothetical model of impedance response with no corrosion and thermally induced scaling.

3. Crevice corrosion, scaling

After the layer is completely covering the surface, crevice corrosion occurs. As was explained in the previous section, this could lead to a contribution to the impedance as a result of the corrosion reaction, but more likely due to the presence of corrosion products (C_{corr} , R_p), see Figure 3.50.

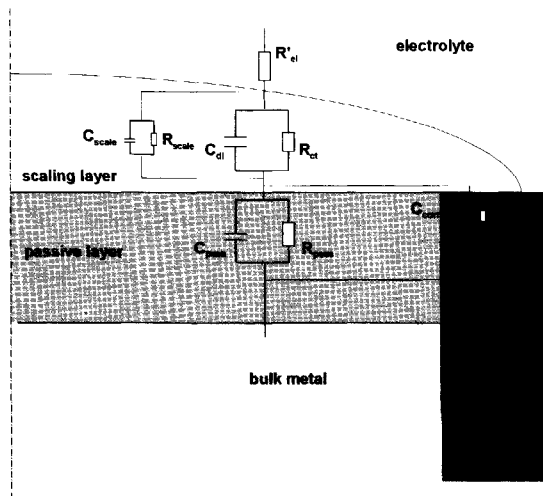


Figure 3.50: Hypothetical model of impedance response with crevice corrosion and thermally induced scaling.

4. Scaling, pitting and crevice corrosion

In the fourth area, pitting occurs alongside scaling and crevice corrosion. Therefore, a similar behaviour is expected in this area as was deduced in the previous section. A contribution of the pitting will arise in a separate time constant (C_{pit} , R_{pit}), see Figure 3.40.

For the analysis of the impedance data, the experiments were split in four regions, Figure 3.51 shows six characteristic Bode-plots. In the first three plots, no obvious differences are present. For the fourth plot, with developed crevice corrosion, a change is present especially in the low-frequency area. The behaviour is more resistive and less capacitive. Moreover, the modulus of the impedance has decreased. In the fifth plot, the impedance modulus increases at the low frequency area again and turns slightly more capacitive again. In the sixth plot, where pitting is present, a clearly different behaviour is observed which can be retraced to a third time constant.

Figure 3.52 shows the values of the Y_0 -, n - and R -values found in the EIS analysis. For the analysis, series circuits of the time constants showed the best fit results, as was the case in the first experimental trial.

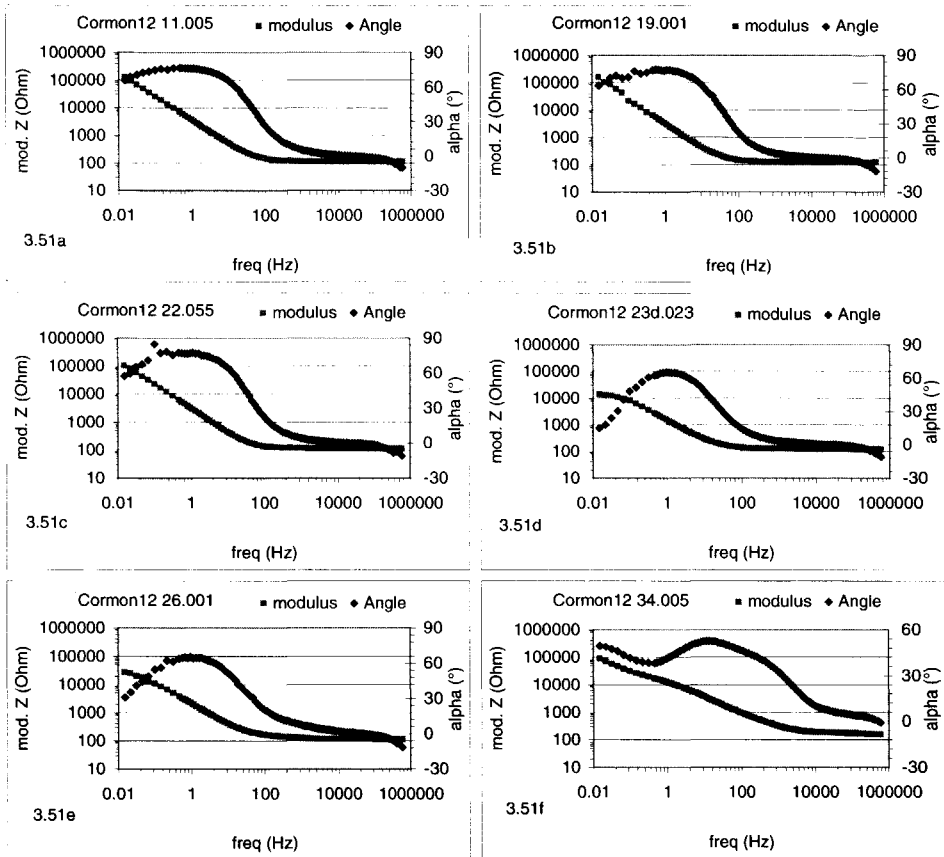


Figure 3.51: Six characteristic Bode-plots for thermally induced scaling trial:
 a. Initial impedance behaviour without scaling or corrosion
 b. Impedance behaviour with scaling, without corrosion
 c. Impedance behaviour with scaling at the onset of crevice corrosion
 d. Impedance behaviour with scaling and crevice corrosion
 e. Impedance behaviour with scaling and further developed crevice corrosion
 f. Impedance behaviour with scaling, crevice corrosion and pitting

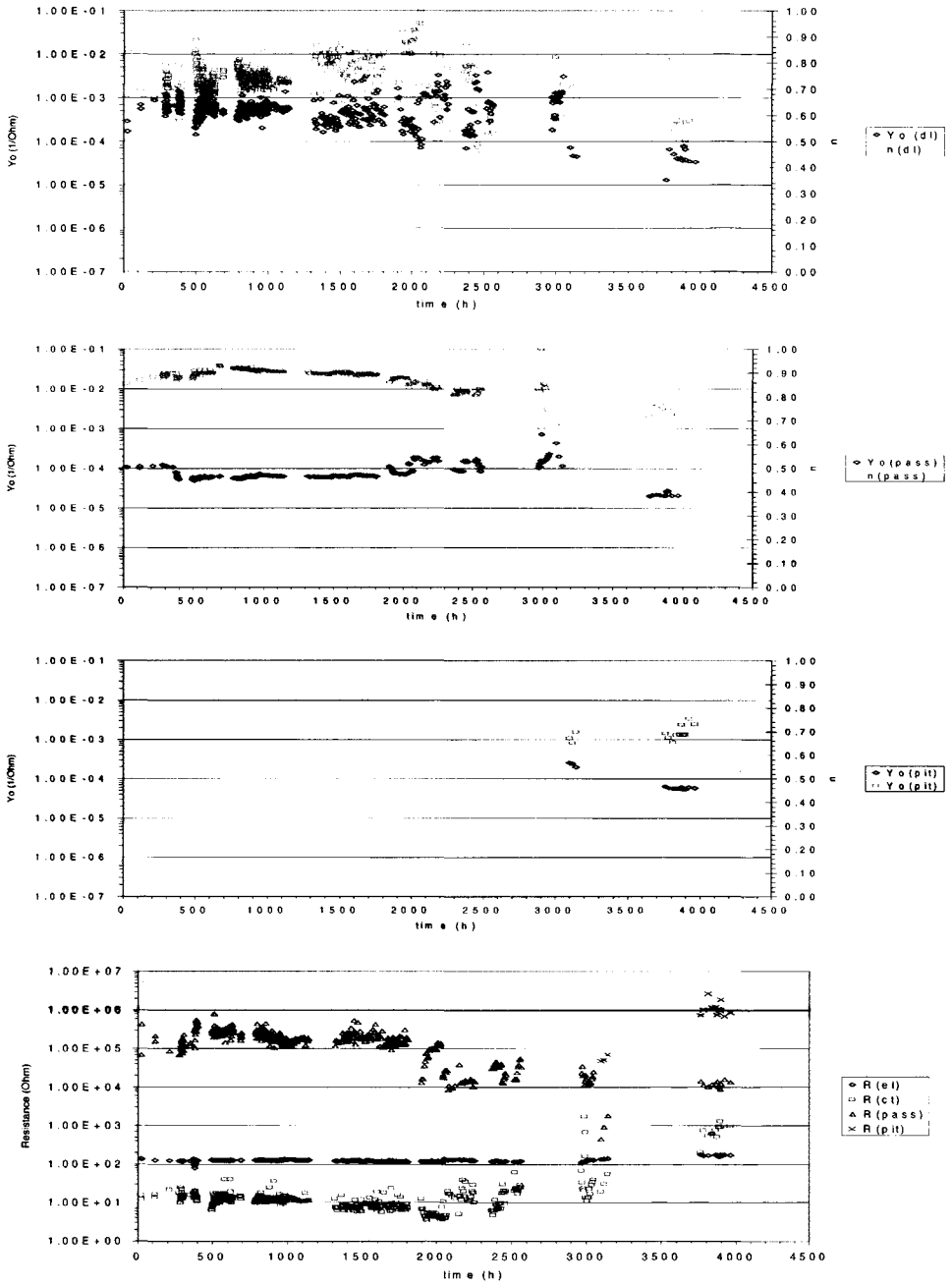


Figure 3.52: Impedance plots for the whole experimental period during thermally induced scaling and subsequent corrosion. a: $Y_{0,d}$ and $n_{(d)}$; b: $Y_{0,pass}$ and $n_{(pass)}$; c: $Y_{0,pit}$ and $n_{(pit)}$; d: R_{elt} , R_{pit} , R_{ct} , R_{pass} .

Discussion

$Y_{o,dl}$ decreases slightly during the formation of the scaling layer, which could be the result of the partial blocking of the electrode surface. The n -value increases from 0.7 in the beginning to 0.8 at the onset of crevice corrosion. When crevice corrosion has started, the n -value decreases again to 0.6, a value characteristic of diffusion controlled processes.

In the pitting area ($t = 3700$ to 4000 h), n_{dl} has decreased further, implying that also in this region diffusion of ions through the scaling layer is a rate-determining step. The $Y_{o,dl}$ and n_{dl} are scattering to a large extent. This is an effect of the high correlation (>0.9) for these parameters.

R_{ct} is more or less constant during the scale formation, suggesting that the scaling layer does not increase the resistance against charge transfer. This is in agreement with the observation that the scale shows an open/porous structure.

$Y_{o,pass}$ is constant during the scaling process and increases slightly in the crevice corrosion area. n_{pass} decreases to 0.8 when crevice corrosion occurs, suggesting again, as was stated in the previous section, that the passive layer no longer determines this time constant. Instead it is determined by crevice corrosion. Figure 3.53 further justifies this suggestion. In this Figure, the first plot shows the full frequency range impedance diagram. The second plot shows the diagram with the low-frequency time constant subtracted. As can be observed, the remaining impedance cannot accurately be fitted with one semi-circle. Another time constant is apparently present. For the remainder of the impedance measurements, this distinction between these time constants could not be made. The interaction is too close.

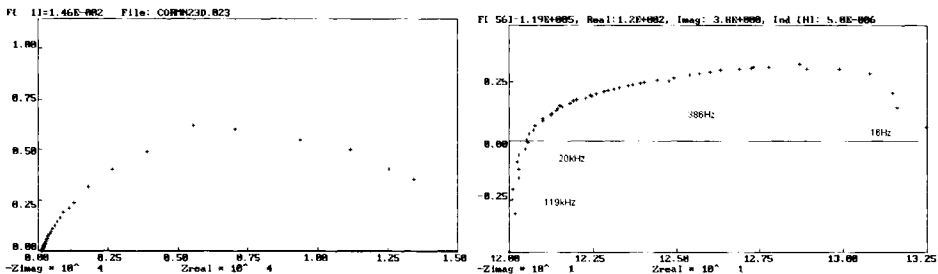


Figure 3.53: Impedance plots for an EIS measurement in the crevice corrosion region. A: full frequency range; b: low frequency time constant subtracted.

R_{pass} hardly changes throughout the experiments. This implies that, even when crevice corrosion occurs and the resistance is more related to the corrosion process, no marked change is present.

The values for the parameters related to the pitting process do not show a specific development with time. However, this might imply that when the impressed potential was removed, pitting did not proceed and, as was mentioned previously, the capacitive behaviour of the corrosion products was measured.

3.3.6 General Discussion

As was shown by the two experimental trials presented in the two previous sections, it is possible to detect pitting using impedance measurements. The second series acknowledged the suppositions made in the first analysis to be able to describe the data. Furthermore, it was obvious that the model used, a simple series model of three time constants in the most complex situation, was enough to explain the data.

The values of all modelled parameters in the two experimental series are of the same order of magnitude in the two different series. This strengthens the analysis. Also the correlations between the time constants was low when a series model was used in both cases. Therefore it is assumed that the series model is a good approximation of what is physically happening.

It was also shown that, based on the developments in R_{ct} , a scaling layer could be characterised. In the first series, a dense layer was built up, whereas in the second series a porous layer was formed. This was seen in a stable R_{ct} for the second series and an increasing R_{ct} during scaling during the first analysis.

The fact that pitting can thus be detected leads to the optional use of EIS measurements in monitoring corrosion processes underneath scaling layers. It was shown that an additional time constant arises due to pitting. Detecting this time constant with EIS-measurements in practice would show that cleaning of the heat exchanger is necessary to prevent excessive corrosion damage.

3.4 Conclusions

This chapter dealt with two specific heat exchanger situations. The first concerned cunifer systems which are used for marine applications. The second concerned stainless steel used in fresh water cooling systems. For both systems, fouling can occur in practice and the consequences were dealt with in this chapter.

For cunifer alloys it was made clear that, though intrinsically these alloys are well resistant against corrosion, care should be taken in their practical use. Coupling to other metals deteriorates the antifouling performance. It was shown that the performance could last even in the immunity areas of the alloys. Based on this fact, it was concluded that the attachment mechanisms of macrofouling species is driven more by surface condition than by concentration of toxic compounds in solution. A low concentration of toxins in the boundary layer can be enough to prevent fouling.

For scaling of stainless steel and the corrosion processes underneath the scaling, it was concluded that electrochemical impedance measurements are a strong and useful tool in detecting both scaling and corrosion. Furthermore it was concluded that different types of scaling layers are distinguishable, based on their impedance response.

Another conclusion that can be drawn from the impedance analysis is that the use of constant phase elements in studying localised phenomena is very useful, since a continuous analysis can be given with the same time constants throughout the process. When the character of the process determining a time constant changes, this will be visible in the n -value of the constant phase element. In case more specific circuit elements would have been used, the models would not fit any more when the character of a time constant changes.

3.5 References

- 1 T.R. Bott, Fouling in heat exchangers, 1995, Elsevier, Amsterdam, The Netherlands
- 2 E.B. Shone and G.C. Grim, Experience with seawater-cooled heat transfer equipment, MER, March 1986, pp. 20-23
- 3 B.B. Moreton, Copper alloys in marine environments today and tomorrow - Part I, Corrosion Prevention and Control, December 1985, pp. 122-125
- 4 A. Schüssler and H.E. Exner, The corrosion of nickel-aluminium bronzes in seawater - I. Protective layer formation and the passivation mechanism, Corrosion Science, Vol. 34 No. 11 (1993) pp. 1793-1802
- 5 A.S.M. Handbook volume 2: Properties & Selection: Nonferrous Alloys and Special-Purpose Materials, 1992, ASM International, USA, pp. 339-340
- 6 K.D. Eford and D.B. Anderson, Sea water corrosion of 90-10 and 70-30 Cu-Ni: 14 year exposures, Materials performance (1975) pp. 37-40
- 7 A.S.M. Handbook Volume 13: Corrosion, 1992, ASM International, USA, pp. 610-625
- 8 K.A. Chandler, Marine and Offshore Corrosion, 1985, Butterworths, London, UK, pp. 126-129
- 9 G.W. Swain, R.A. Farrar and S.P. Hutton, The use of controlled copper dissolution as an anti-fouling system, Journal of Materials Science, Vol.17 (1982) pp. 1079-1094
- 10 B.J. Little and F.B. Mansfeld, The corrosion behavior of stainless steels and copper alloys exposed to natural sea water, Werkstoffe und Korrosion, Vol. 42 (1991) pp. 331-340
- 11 G. Bianchi, G. Fiori, P. Longhi and F. Mazza, "Horse shoe" corrosion of copper alloys in flowing sea water, Corrosion, Vol. 34 (1978) pp. 396-406
- 12 F.P. IJseling, Invloed van de potentiaal op de vorming van corrosieproducten op CuNi10Fe in zee water, KIM corrosielaboratorium (1986)
- 13 F.P. IJseling, J.M. Krougman, L.J.P. Drolenga, 5th. International Congress on Marine Corrosion and Fouling, Barcelona (1980) paper 146
- 14 T.J. Lennox, M.H. Peterson and R.E. Groover, De-alloying of copper alloys and response to cathodic protection in quiescent sea water, Materials Protection and Performance, Vol. 10 No. 7 (1971) 31-37
- 15 K.D. Eford, Potential-pH diagrams for 90-10 and 70-30 Cu-Ni in sea water, Corrosion, Vol. 31 (1975) 77-83
- 16 J.J. Kleikers, Het effect van kathodische bescherming op de aangroeiende eigenschappen van CuNi30Fe in zee water, KIM afstudeerscriptie, December 1999
- 17 NEN 7420, Industrieel koelwater; Bepaling van de effectiviteit van koelwaterconditionerings-programma's onder standaardomstandigheden, September 1996, Nederlands Normalisatie-instituut, Delft, The Netherlands
- 18 R. Oltra and M. Keddad, Application of EIS to Localised Corrosion, Electrochimica Acta, Vol. 35 No. 10 (1990) pp. 1619-1629
- 19 M.W. Kendig and F. Mansfeld, Proceedings of the Fall Meeting of the Electrochemical Society, Vol.82 No. 2 (1982) p. 105
- 20 M.G.S. Ferreira and J.L. Dawson, Journal of the Electrochemical Society, Vol. 132 (1982) p. 760
- 21 R. Oltra and M. Keddad, Application of EIS to Localised Corrosion, Electrochimica Acta, Vol. 35 No. 10 (1990) p. 1619-1629
- 22 F. Mansfeld, S. Lin, K. Kim and H. Shih, Pitting and surface modification of SiC/Al, Corrosion Science, Vol. 27 No. 9 (1987) p. 997-1000
- 23 B. Elsener and H. Boehni, 1st International Symposium on EIS, 1989, Extended Abstract C2.13
- 24 J.M. Blengino, M. Keddad, J.P. Labbe and L. Robbiola, Physico-chemical characterisation of corrosion layers formed on iron in a sodium carbonate-bicarbonate containing environment, Corrosion Science, Vol. 37 No. 4 (1995) pp. 621-643
- 25 C. Deslouis, C. Gabrielli, M. Keddad, A. Khalil, R. Rosset, B. Tribollet and M. Zidoune, Impedance Techniques at Partially Blocked Electrodes by Scale Deposition, Electrochimica Acta, Vol. 42 No. 8 (1997) pp. 1219-1233

- 26 C. Gabrielli, M. Keddam, A. Khalil, R. Rosset and M. Zidoune, Study of calcium carbonate scales by electrochemical impedance spectroscopy, *Electrochimica Acta*, Vol. 42 No. 8 (1997) pp. 1207-1218
- 27 C. Gabrielli and M. Keddam, Contribution of electrochemical impedance spectroscopy to the investigation of the electrochemical kinetics, *Electrochimica Acta*, Vol. 41 No. 7/8 (1996) pp. 957-965
- 28 C. Gabrielli, M. Keddam, G. Maurin, H. Perrot, R. Rosset and M. Zidoune, Estimation of the deposition rate of thermal calcareous scaling by the electrochemical impedance technique, *Journal of Electroanalytical Chemistry*, Vol. 412 (1996) pp. 189-193
- 29 B.A. Boukamp, Manual AC-impittance data analysis system 'Equivalent Circuit', University of Twente, 1989, Enschede, The Netherlands
- 30 E.P.M. van Westing, Determination of coating performance with impedance measurements, PhD-Thesis, TU Delft, 1992, Delft, The Netherlands
- 31 H.J.A. Breur, E.P.M. van Westing, J.H.W. de Wit, J.C. Verhoef, J. van Turnhout, G.M. Ferrari, Electrochemical Impedance Measurements with Heated Electrodes for the Study of Fouling in Heat Exchangers, EMCR2000 Conference, June 2000, Budapest, Hungary



4 Bioprotection

Summary

The aim of the work presented in this chapter was to investigate the possibilities for using microbiological processes to prevent corrosion. If this is possible, the research can lead to a whole new class of environmentally friendly anticorrosion products, with the additional benefit that they will be based on renewable resources.

To investigate the possibilities, three different experimental routes have been followed. First, biological phosphating processes are discussed. It turned out to be possible to obtain phosphate layers, which show a protective effect for carbon steel. The bacteria are shown to be responsible for a layer build up in a controlled and homogeneous way.

Second, the formation of stable, protective biofilms was investigated. It is shown that it is possible to grow a homogeneous biofilm with relatively low bacterial content, resulting in an increased polarisation resistance. This could eventually lead to a living auto-recovery anticorrosion system, able to renew itself when damage occurs.

Third, bacterial polysaccharides were investigated for their effect on corrosion resistance. It is shown that marked increases in corrosion resistance are possible due to the formation of dense passive layers on the carbon steel surface. This approach turned out to be the most viable for further development into anticorrosive bioadditives to coatings or pre-treatment processes.

4.1 Introduction

Metal surfaces are commonly protected from environmental influences by (in)organic coatings combined with a suitable pre-treatment. Heavy metals have proven to be very efficient. In the past, anticorrosive pigments like chromates and lead oxide were incorporated in organic paints. Chromates are also used as component of pre-treatments. However, health and environmental concern has led to a ban on lead oxides and a restriction on the use of chromates. Further restrictions, a.o. toward zinc and heavy metal phosphating are envisaged. Therefore, a need exists to develop alternatives to these conventional pre-treatments.

Micro-organisms are able to influence the electrochemical status of metals. In general the influence has a deteriorative effect, known as microbially influenced or microbially induced corrosion [1]. Often, sulphur-reducing bacteria play a crucial role in this form of corrosion. They are able, under anaerobic conditions, to produce sulphides, which accelerate the corrosion processes. Moreover, they can produce acidic and basic compounds and differential aeration cells can occur because of aerobic bacteria using up the oxygen in parts of the surface biofilm.

Microbial biofilms develop on virtually every surface that is exposed to water. These organic layers that form after bacteria attach to and replicate on a surface, have been defined as consisting of cells immobilised on a substratum and frequently embedded in an organic polymer matrix of microbial origin. The presence of a biofilm on a metal surface can create chemical conditions vastly different from those of the ambient environment, influencing the electrochemical properties of the substrata. Thus, factors that vary little in the open ocean (such as pH, dissolved oxygen, peroxide, and the heavy metal manganese and iron) can vary dramatically at the metal-biofilm interface. *Microbial influenced corrosion (MIC)* is considered as being one particular example of the general phenomena of metal-microbe interactions.

For many years, research into MIC focused on *sulphate-reducing bacteria (SRB)* and *manganese-oxidising bacteria (MOB)*, which have shown to enhance metal surfaces dissolution by metabolic deposition of corrosive compounds. Recently it has become evident that several

other organisms may drive corrosion. For passive metals, one of the most noticed consequence of this interaction is a shift of the open-circuit potential of in the noble direction, increasing the risk of pitting corrosion. The structural and physiological heterogeneity of natural biofilms is mainly indicated as responsible for the corrosive effect, by formation of differential aerated areas and by heterogeneous deposition of bio-products. However, biofilms occur widely, and although the amount of cases of MIC is rising as engineers become more widely aware of its existence and learn how to test for it, it is becoming clear that not all biofilms are corrosive. On the contrary, it has been shown that under some circumstances, especially in laboratory tests, the coverage of such biofilms can inhibit corrosion.

For example, Volkland et al. [2] have shown the formation of *vivianite* ($\text{Fe}_3(\text{PO}_4)_2 \cdot 8\text{H}_2\text{O}$) by several bacterial strains (among which *Rhodococcus* sp. and *Pseudomonas* sp.). In regular phosphating processes, similar layers are formed and therefore, these layers could have a similar protective effect. Furthermore, amongst others Jayaraman et al. [3] and Pedersen et al. [4] have investigated the influence of aerobic biofilms, consisting of e.g. *Pseudomonas fragi*, *Escherichia coli* and *Serratia marcescens*, on the corrosion rate of metals. Part of the decrease in corrosion rate observed could be attributed to the consumption of oxygen by the bacteria. This finding was confirmed by experiments with fixed biofilms. Nevertheless, this mechanism could not account for the full effect. In some cases, corrosion inhibition was observed with fixed biofilms, though less pronounced than with living ones. It was suggested that the protective mechanism was related to extracellular polysaccharides formed during the metabolism of the bacteria. These polysaccharides could be used as corrosion inhibitors or as pre-treatment processes.

Recently, another approach towards this kind of biomineralisation is applied as well. In this case, the biofilm is regarded as a special type of coating [8]. An advantage of a biofilm over a conventional coating could be the inherent binding force and the inherent oxygen consumption resulting in an oxygen barrier layer. Disadvantages would be the internal conductivity, the amount of water (approximately 98%) and the rapid diffusion of ions through the "pseudo" coating. As is the case for regular coatings, the problems arising from biofilms occur when they are inhomogeneous or damaged. However, if it turns out to be possible to create a stable biofilm system, the living biofilm can protect the metal by an "auto-recovery" system acting when the layer is damaged. The biofilm will grow again on the bare spots. The mechanism of this auto-recovery system can be regarded in close analogy to that of chromate layers. These owe their protective function to such properties as well: chromates can leach out of the layer to repair it. Thus far, environmentally friendly alternatives to chromates like molybdate- and cerate layers don't have this property yet.

Another use of biofilm-metal interactions can result from the effect of biofilms on stainless steels in seawater. Especially the influence of micro-organisms in the shift of the electrochemical potential to more noble values has been investigated. Despite numerous investigations, the exact mechanism of this ennoblement is still under discussion [5]. One of the possible explanations is the formation of a noble manganese oxide (MnO_2) layer by micro-organisms. In case an inhomogeneous layer is formed, a galvanic cell arises which enhances corrosion. A homogeneous layer, on the other hand, could give corrosion prevention [6]. Permanganate pre-treatments, resulting in a manganese oxide layer are already under investigation to form an alternative for chromate layers. Controlled layer formation is, as in other alternatives, the main difficulty. Biological deposition processes might solve this problem.

As is clear from the findings presented here, several options exist to use micro-organisms in corrosion protection methods. They can be divided in four different classes as is shown in Figure 4.1. A distinction can be made between 'direct' and 'indirect' protection options. Direct means working with bacteria and 'living layers', indirect means production of bacterial products and use of these products in anticorrosion products. Within the scope of this chapter, four options have been investigated. Section 4.2 deals with biological phosphating processes using bacteria to

deposit phosphates. Section 4.3 deals with protective biofilms, investigating the effect of homogeneously formed biofilms on corrosion resistance. The indirect strategies are treated in section 4.4. Since it is difficult to incorporate bacterial products in coatings, these options are combined into one research strategy: the effect of the compounds, i.e. polysaccharides, is studied in solution.

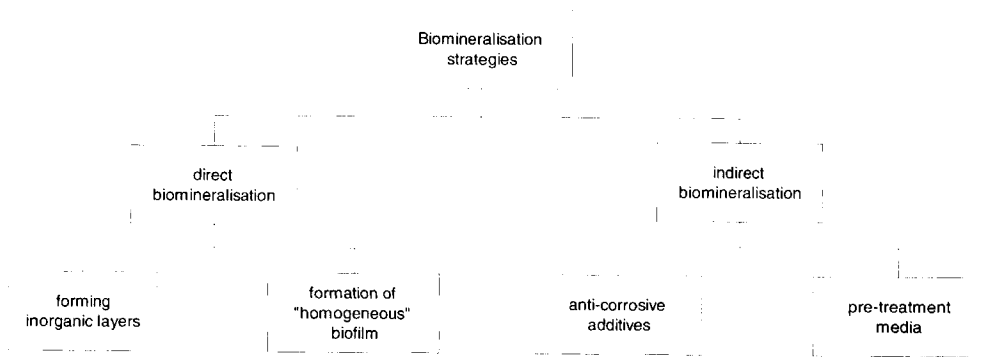


Figure 4.1: Overview of possibilities to obtain bioprotection with bacteria and/or their products

Before turning to the practical investigations of bioprotection, some theoretical background is given in the remainder of the introduction.

4.1.1 Effects of Microfouling on Water Chemistry at the Interface

Water chemistry is different for each type of water. Seawater, for example, contains much more salts than fresh water and waste water, for example, contains much more organic nutrients than surface water. In addition to these differences, micro-organisms can exert a local effect when they are present in the form of a biofilm. These effects can be even more pronounced than the general effects. Since the variety of biofilms in seawater is large and more research has been done on biofilms in seawater than in any other water types, many of the examples given here are sea water related.

Oxygen Variations.

The presence of a microbial biofilm on a metal surface can create chemical conditions at the metal-film interface that are vastly different from those of the ambient environment, for instance as in the case of dissolved oxygen. Surface waters, where corrosion often takes place, are usually saturated with oxygen at a value depending on the water temperature and salinity. These values vary from less than 5 ml/l in warm saline waters to over 10 ml/l in cold fresh water. The effect such variations can have on the corrosion rate of many materials is widely recognised.

Much larger variations than these, however, can be produced on the metal surface by a microbial film. Even in cases where the oxygen concentration in the water is at air saturation, the oxygen concentration at the metal surface under a microbial film can be zero. In bringing this about, the biofilm acts both as a physical oxygen diffusion barrier and as an active oxygen sink in which the living bacteria consume oxygen during respiration.

pH Variations

In contrast to the case for dissolved oxygen, pH variations of sea water are quite small due to buffering of the water. PH values range from 8.1 to 8.3 in open ocean surface water, to little less than 7.6 in deep water. In coastal and estuarine waters, pH values from 7.8 to 8.0 are fairly common. Such pH variations are hardly significant to corrosion in seawater with two exceptions, first, in the formation and stability of calcareous deposits, and second, on the pitting corrosion of aluminium alloys. Changes in pH under marine biofilms, however, can again be much larger and more important. Values as low as 5 can be expected under aerobic biofilms containing acid producing bacteria. Even more acid pH values, in the range of 1 to 2, can be expected under discrete biodeposits [46].

Metabolically induced variations. Some microbes are capable of directly producing acids such as formic, succinic, acetic and sulphuric, while others are involved in metabolising nitrogen compounds. Some can reduce nitrates, which can act as good corrosion inhibitors, to nitrite or nitrogen. Some can oxidise sulphur or sulphides to sulphate and ultimately to sulphuric acid. Others, particularly the anaerobic SRB, can reduce sulphates to sulphides, often producing corrosive H_2S as an end product. Certain types of bacteria are directly involved in the oxidation of metal ions. Particularly damaging are those fresh water bacteria that oxidise ferrous and manganese ions to ferric and manganic.

With their metabolic activity bacteria are also able to precipitate different kind of oxides on the metal surface. Some of these mechanisms will be presented in the further sections.

Surface coverage variations. The effect of these and other organisms on corrosion depends not only on their metabolic capabilities, but also on the numbers and distribution of organisms on the metal surface. A range of individual bacteria is typical of the film that forms on metals immersed in natural temperate seawaters for less than about 12h. This type of film, with very small total surface coverage, is unlikely to have much of an effect on corrosion. As the film grows, however, it spreads over the surface, due to the production of the characteristic *extracellular polymeric substances (EPS)*. This extracellular polysaccharide may provide nearly complete surface coverage. The film can also form in more discrete colonies or biodeposits, leaving much of the surface uncovered. In both cases, complete film or discrete deposit, the biofilm is able to produce a localised environment at the metal surface that is utterly different from that of the bulk water. Moreover, when the surface coverage is incomplete, the film will produce both oxygen and other chemical concentration cells, thus increasing the likelihood of localised corrosion. In natural waters, where many species of micro-organisms are present, it is common to find them working in consort, that is, one organism will create a set of environmental conditions in which another organism can flourish and grow. A classic example is the creation, in a nominally aerated environment, of an anaerobic microenvironment under a mature film or colony. The aerobic organisms in the outer part of the film have created conditions favourable for the growth of the anaerobic SRB below them.

The electrochemistry of corrosion can also change the chemistry at the metal-water interface, and this can either encourage or inhibit biofilm formation. Corrosion can encourage bacterial attachment and growth by producing chemical compounds that the organisms can use as nutrients or energy sources. Conversely, electrochemistry can produce chemical compounds that will inhibit biofilm formation. E.g., cathodic protection can produce enough OH^- ions to shift the pH at the metal surface to values above 10. Values more basic than about pH 9.5 are detrimental to most marine bacteria. Another inhibitory chemical is hydrogen peroxide, which is produced as a transitory intermediate during many oxygen reactions involved in corrosion .

4.1.2 Effects of Biofilms on Corrosion

General mechanisms of biofilms affecting metal corrosion can be:

- Creation of differential aeration through a patchy distribution of microbial colonies;
- Barrier properties for the passage of charged species across the biofilm matrix;
- Modification of the medium conductivity;
- Chelation of certain metal ions by the EPS;
- Alteration of the corrosion inhibitor's stability at the metal surface;
- Metal deposition by metabolic bacterial activity;

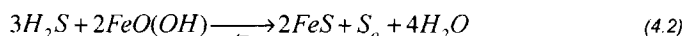
These mechanisms, by which biofilms influence the rate of the general corrosion reactions, depend on diverse environmental conditions and generally proceed simultaneously.

Two MIC-phenomena are most widely known: Acid corrosion due to SRB-growth and stainless steel pitting corrosion due to ennoblement.

Corrosive Effects of Sulphate Reducing Bacteria

Sulphate reducing bacteria (SRB) stimulate corrosion mainly in mild steels as a consequence of their activities within mixed species biofilms. Despite the anaerobic nature of SRB, maximal corrosive activity is demonstrated where there is access to oxygen and the biofilm develops a characteristic aerobic-anaerobic (O_2/AnO_2) interface, as it is often the case in the bottom of marine biofilms.

The primary contribution of SRB to the corrosion process is the production of hydrogen sulphide. At least a portion of this sulphide arises directly from the oxidation of hydrogen formed at the cathode of the electrochemical corrosion cell. They will metabolically produce H_2S near the surface, while iron is oxidised at the anodic site, with the final result of production of HS^- and S_0 aggressive compounds:



Iron sulphide corrosion products (reaction 4.1) may be either protective or corrosive. Where they are in the form of a tightly adherent thin film or tarnish, they protect the underlying steel in a manner directly analogous to the oxide film that constitutes the corrosion resistance of stainless steel. In most cases, however, such films are unstable and their rupture gives rise to extremely active corrosion cells between the iron sulphide (cathode) and the exposed steel surface (anode). Thick, loosely adherent iron sulphide deposits act to stimulate corrosion in the same manner as outlined for ruptured protective films.

Biofilm Induced Shift in Corrosion Potential

The corrosion potentials (E_{corr}) of several passive metals that a variety of investigators has tested become nobler with time as a microbial film builds up. Mollica and Trevis [35] were the first to report this type of result, and many others have published similar data [5, 36, 40]. The open circuit corrosion potential becomes nobler by 400 to 500mV or more as the natural population film grows. The initial delay time of less than one day varies up to about 15 days depending on geographical location, water temperature and flow conditions. That this effect is directly attributable to the microbial film has been shown in many different ways.

Furthermore it was shown, that the delay time increased, and the degree of ennoblement decreased by increasing the flow speed of water past the surface [35]. Increasing the flow speed

retards formation of the microbial film. It has also been shown that the ennoblement can be prevented by raising the water temperature sufficiently (to 40°C) to inactivate the bacteria. This does not mean there will be no microbial effects on corrosion at elevated temperatures. Little et al. [37] have shown that thermophilic bacteria can stimulate corrosion at temperatures up to at least 80°C.

Scotto et al. [43] published the important result that the ennoblement disappeared when a respiration inhibitor, sodium azide, was added to the water. This result implies that the mere physical presence of the bacterial film does not cause the effect, but it is related in some way to an active metabolic process.

On metals that do not form passive films, corrosion potential corrosion ennoblement has not been observed.

There have been several proposals for the mechanism of potential ennoblement by the biofilm. These include

- 1) catalytic enhancement of the reversible oxygen potential reaction by organo-metallic complexes [43] or bacterially produced enzymes [44];
- 2) modification of the oxygen reaction response to a change in pH under the biofilm [38, 39];
- 3) the introduction of new cathodic reactions not involving oxygen;
- 4) an increase in the exchange current density (i_0) for the oxygen reaction [40].

4.1.3 Microbiological Corrosion Prevention

The bacterial iron biomineralisation is a diverse and widespread phenomenon that results from cellularly mediated physiological processes. Transmission electron microscopy examination of bacterial cells, growing naturally in fresh water and marine environments, reveals that they can precipitate a variety of iron minerals like ferrihydrite and iron hydroxysulphate [23]. These precipitates modify the near surface water chemistry of submerged metals, influencing the rate and type of corrosion reactions.

Biologically controlled biomineralisation is a completely regulated process whereby the organism precipitates essential mineral phases within its pre-formed framework. Because the site at which a mineral forms is isolated from the external environment by a barrier through which ions cannot freely diffuse, mineralisation may proceed under thermodynamically unfavourable conditions.

Biologically induced biomineralisation is the dominant process among bacteria, with biominerals commonly generated as secondary by-products from interactions between the activity of the micro-organisms and their surrounding environment. Minor perturbations such as the introduction of biologically produced metabolic end-products (e.g., OH^- , CO_2 , H^+ and NH_3), the release of cations by the cell, or the development of a charged surface can all induce the nucleation of minerals with crystal habits similar to those produced by precipitation from inorganic solutions.

Some bacteria show an extreme selectivity in binding one metal from a range of competing cations to fulfil essential physiological functions, whereas other bacteria react to dissolved ions as if they were an open ion exchange resin, presumably a function of living in a concentrated solution where salts abound. In this regard, it is not surprising that biofilms are considered ideal cation scavengers, often accumulating quantities of metals comparable to those of cation exchange resins.

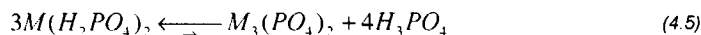
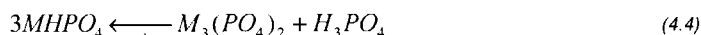
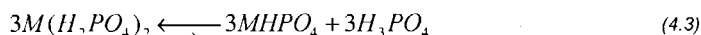
4.2 Biological Phosphating Processes

4.2.1 Introduction

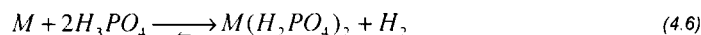
Phosphating is the most commonly applied pre-treatment process. Since the first patent on this type of process in 1869 [45], the process has developed to a very efficient and fast method for metal pre-treatment. Process times have decreased from 2-2.5 hours down to 60-90 seconds and spray processes, allowing much bigger products to be pre-treated have replaced bath processes. Furthermore, the processing temperature has decreased continuously and nowadays, process temperatures of 25-35°C are commonly used.

The mechanism on which phosphate processes rely is based on the solubility of metal phosphates [34]. Orthophosphoric acid, H_3PO_4 , is a tribasic acid with dissociation constants $K_1 = 0.7101 \times 10^{-2}$; $K_2 = 7.99 \times 10^{-8}$ and $K_3 = 4.8 \times 10^{-13}$. Therefore, only the first dissociation step will be complete in practice. From this fact arise the solubility properties of metal phosphates: primary phosphates are in general soluble, secondary phosphates are either unstable or not soluble and tertiary phosphates are insoluble. The formation of phosphate layers is taking advantage of the solubility of the primary phosphates and the insolubility of the tertiary ones.

Solutions of primary heavy metal (most commonly Zinc) phosphates can react to form secondary and tertiary phosphates and free orthophosphoric acid through the following reactions:



These reactions are influenced by pH and temperature. When a metal surface is hung in such a solution, the metal will dissolve and form a primary metal phosphate, using up some of the free H_3PO_4 .



Reactions 4.3 to 4.5 will shift to the right to compensate the loss of free acid. The secondary and tertiary phosphates formed will deposit on the surface.

The layer deposition can be accelerated by three means: addition of heavy metal salts (especially Cu and Ni); addition of oxidising agents (e.g. nitrates); physical means (spraying processes deposit layers more rapidly than immersion processes).

Besides these heavy metal (including Fe) phosphating processes, several options exist for heavy metal free phosphating processes, based on phosphates of sodium, potassium or ammonium. In these processes, the iron dissolving from the exposed surface is built in in the phosphate layer. The essential difference with the heavy metal phosphate coating processes being the solubility of all (including secondary and tertiary) phosphate salts. These coatings are referred to as lightweight iron phosphate coatings.

A big advantage of these lightweight phosphate processes is the omission of heavy metals. Another advantage is the less acidic pH needed for these processes: pH of the solutions can be between 4-6 (heavy metals: 1.5-3.5). However, acidic conditions prevail and the properties of the lightweight phosphating processes are far less good compared to heavy metal phosphate processes.

Volkland et al. [2] found conditions under bacterial activity where phosphate formation was found under even milder conditions. Mild steel coupons were incubated in cultures of three different aerobic bacteria in the presence of phosphates and afterwards exposed to a corrosive aqueous medium. When the steel was incubated together with growing, biofilm forming bacteria, which had a direct access to the steel surface in mineral media containing more than 20 mM phosphate, a significant reduction of the corrosion rate was observed in the corrosive medium. Under these conditions, a biologically induced surface reaction occurred, resulting in the formation of *vivianite* [$\text{Fe}(\text{PO}_4)_2 \cdot 8\text{H}_2\text{O}$], a crystalline almost insoluble iron(II)-phosphate. The layer of *vivianite* was found to be the reason for the corrosion protection. The surface was always accompanied by an increase in the iron concentration in the medium, but in contrast to biocorrosion processes known so far, the iron release stopped after some days. The other results obtained are the following:

- the species and carbon source of biofilm forming bacteria was are not critical. However, the best results were obtained with *Pseudomonas putida* with Sodium benzoate as carbon source.
- resting or non biofilm forming bacteria were not able to form *vivianite* and bring about corrosion protection
- the increase in the phosphate concentration resulted in an increased corrosion resistance
- the increase of the time of incubation resulted in an increased corrosion inhibition
- when the biofilm was not removed prior to immersion into the corrosive medium, pitting corrosion occurred

To assess the functionality of the process and to understand the formation mechanism of the layers described by Volkland, several experiments have been carried out. Electrochemical impedance spectroscopy has been used as a tool to investigate the occurrence of electrochemical processes [49]. This technique was especially useful because of its low perturbation and the high amount of data that can be obtained on electrochemical processes.

4.2.2 Experimental

To investigate the usefulness of the processes described by Volkland [2], Several experiments were carried out. Bacterial strains of *Pseudomonas putida* (strainno. LMD 29.29, The Netherlands Culture Collection of Bacteria) isolated from garden soil were cultivated in agar. New generation strains were weekly derived from old ones by transfer to new agar plates. Two different phosphate media were used: 30 and 50mM as listed in Table 4.1. The mineral medium was autoclaved at 121°C for 15 minutes before use, and final pH was 7.3 at 20°C. Carbon steel Q-panels were used as material. The cell set-up is given in Figure 4.2.

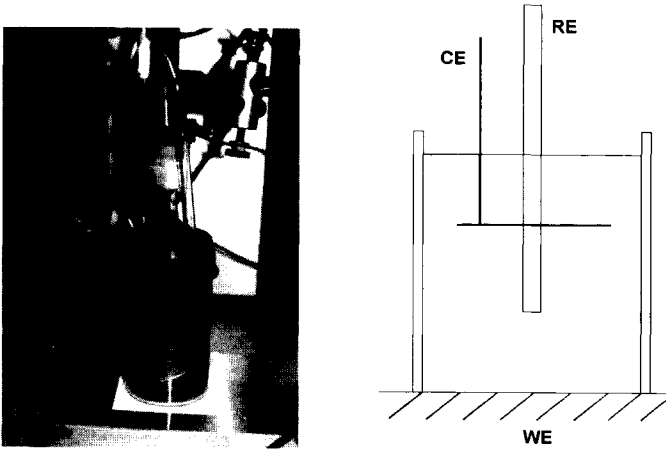


Figure 4.2: Experimental set-up for vivianite formation experiments

Four experimental cycles are reported with EIS monitoring. Table 4.2 shows an overview of the experimental conditions. Solartron equipment was used to perform EIS measurements. Boukamp software [47] was used to model the impedance data. Besides the impedance analysis, visual characterisation was performed with light microscopy and SEM. Furthermore, EDX-analysis was carried out to assess the composition of the layers.

Table 4.1: Composition of medium for the growth of vivianite on carbon steel.

Compounds	MW	Content (g/l)	Content (g/l)
Minerals			
NH_4NO_3	80.04	1.0	1
$\text{MgSO}_4 \cdot 7\text{H}_2\text{O}$	246.5	0.1	0.1
$\text{Ca}(\text{NO}_3)_2 \cdot 4\text{H}_2\text{O}$	236.2	0.07	0.07
trace element solution		5ml	5ml
Phosphate buffer (nutrients)		(30 mM total phosphate content)	(50 mM total phosphate content)
$\text{Na}_2\text{HPO}_4 \cdot 7\text{H}_2\text{O}$	268.1	6.50	10.843
KH_2PO_4	136.1	0.84	1.4
Energy source			
$\text{NaC}_7\text{H}_5\text{O}_2$	144.1	0.865	0.865

Table 4.2: Overview of experiments carried out to investigate the formation of vivianite layers on mild steel

bacteria	experiment duration (hours)	medium	aeration	refreshments
5 inoculated right before experiment	170	50mM	yes	yes
6 no bacteria, refreshments	260	50mM	yes	yes
3 inoculated right before experiment, no refreshments	190	50mM	no	no
7 inoculated one day before experiment	20	50mM	yes	no

Furthermore some qualitative experiments were carried out to determine the character of the formed layers under different conditions. The difference between the layers formed at 30 and 50 mM phosphate concentration was evaluated. Secondly, an experimental series was started to reveal the origin of the layer. Therefore two cells were used containing 30 mM phosphate solution. One was kept sterile while the other one was inoculated with *Pseudomonas putida* 29.

With the exposed samples, weight loss experiments were carried out for two days to investigate the resistance to corrosion of formed layers.

4.2.3 Results

Exploratory Experiments

Initial experiments were carried out to verify the formation process of the vivianite layers. Figure 4.3 shows pictures of a vivianite layer formed after five days in 50mM phosphate medium with bacteria. A black layer was formed and no corrosion occurred.

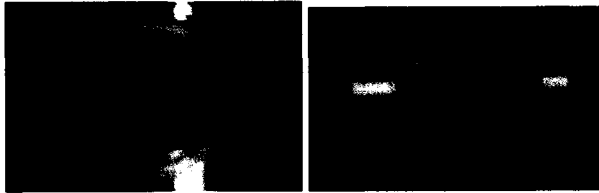


Figure 4.3: Images of the intact, black iron phosphate layer.

The layer was also investigated using SEM/EDX analysis. Figure 4.4 shows two pictures of the layer. The bottom layer is cracked and looks similar to iron phosphates which can be obtained via conventional processes. The white globules on top are also iron phosphates. These globules will eventually grow to form a homogeneous layer as was described by Volkland. However, the layer formed initially is the one that could be used for practical application since it is thin and dense and therefore, in our experiments, we are especially interested in the black layer.

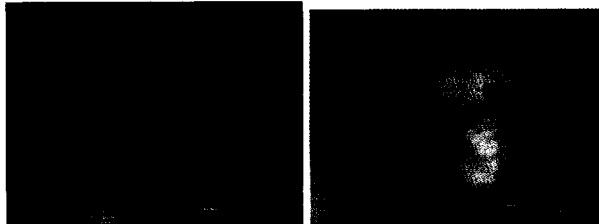


Figure 4.4: SEM pictures of the intact iron phosphate layer.

A second experiment was carried out to assess the expected anti-corrosion properties. Samples were exposed to 30 mM phosphate either with or without bacteria present. After five days, a dark and dull layer had formed on the samples in the bacteria containing solution. No such layer was present on the samples exposed in the sterile medium.

The samples were exposed to 0.1M LiClO_4 solution. A picture of the 16 hours exposed specimen is given in Figure 4.5.



Figure 4.5: Samples exposed to 0.1M LiClO_4 . Left two: untreated samples; middle two: treated in sterile medium; right two: treated in inoculated medium.

After this picture was taken, and the weight loss was determined, the samples were again exposed to the corrosive LiClO_4 medium. After 90 hours a new evaluation of the weight loss was done. The percentages weight loss after 16 and 90 hours are given in Figure 4.6.

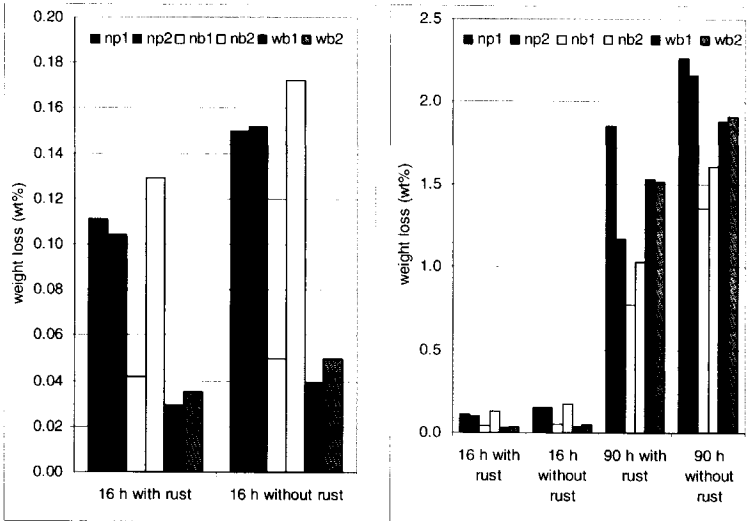


Figure 4.6: Weight loss in wt% for 16 (left) and 90 hours (right) for the three types of samples exposed to 0.1M LiClO_4 . np: no pre-treatment; nb: pre-treated without bacteria; wb: pre-treated with bacteria.

It can be seen that after 16 hours, the corrosion on properly treated samples was lower than on the other four samples. However, the layer turned out not to be stable: after 90 hours, weight loss was the highest for the samples with the good layer. This is in agreement with the comments of Volkland et al. [2] that the layer gives better properties if protected with a coating. This is probably caused by the slight solubility of the iron phosphates which causes the layer to get thinner during exposure. This can be prevented when a coating is applied on top of the layer.

The effect of phosphate concentration is one of the major factors influencing the properties of the layer. Therefore, a simultaneous experiment was carried out in two cells. One containing 30mM phosphate solution and one containing 50 mM phosphate solution. Figure 4.7 shows the layers that are built-up. The one in 30mM solution is much less dense and is easily removed. Figure 4.8 reveals that indeed the layer was not completely covering the surface. The one in 50mM solution is thin, but looks much denser. Figure 4.9 shows the dense layer.

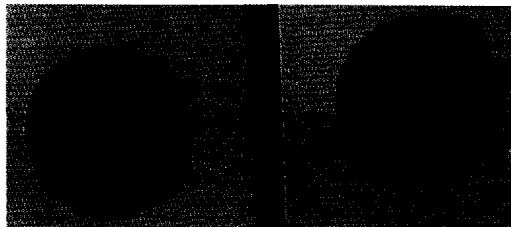


Figure 4.7: Phosphate layer grown in 30 mM (left) and 50 mM (right) phosphate medium

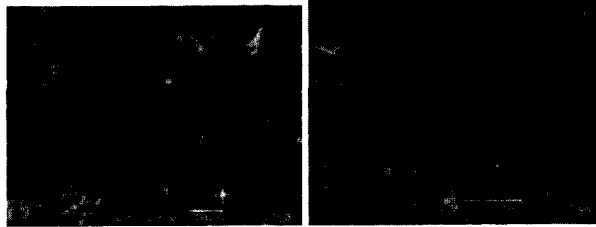


Figure 4.8: SEM pictures of phosphate layer grown in 30mM Phosphate medium

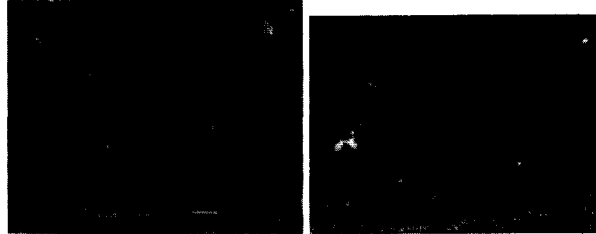


Figure 4.9: SEM pictures of phosphate layer grown in 50mM Phosphate medium

Based on the outcome of these more general experiments, a hypothesis has been derived for the formation of vivianite. The next section discusses this hypothesis. Several experiments were carried out (as listed in Table 4.2) to assess the mechanism of layer formation for the vivianite layer. Electrochemical impedance measurements are used as electrochemical tool to assess this mechanism.

Mechanism Hypothesis

Based on the information derived from the exploratory experiments, a hypothesis can be derived for the mechanism of vivianite formation. This model is verified electrochemically using electrochemical impedance spectroscopy. As described in chapter 3, results of EIS measurements can be modelled via equivalent circuits. The analysis of the electrical equivalent circuits is used to illustrate the variations in the electrochemical responses (charge transfer, charge storage, electrochemical reactions) in time. Each process occurring during the vivianite formation is assigned a time constant. This time constant is expressed in an equivalent circuit element.

Within the hypothesis, the time constants are idealised: pure capacities are used to describe the character of the processes. However, as described in chapter 3, deviations from the ideal behaviour occur in practice and therefore, *Constant Phase Elements (CPE)* are used to fit the circuit elements.

Besides CPEs, in the current, electrochemically active, system, inductive contributions to the impedance are found. These are in general related to reactions involving adsorbed intermediates. In this case, two adsorbed intermediates can cause inductive signals: FePS_{ads} and $\text{Fe}_x(\text{PO}_4)_y$. The inductive character can be explained as follows. At the interface, iron is dissolved, forming ferrous ions. This is an equilibrium reaction quickly resulting in an equilibrium concentration of ferrous ions.



Part of these ions will be complexed with polysaccharides (PS) available from the bacterial activity. This is also an equilibrium reaction, but a much slower one than equilibrium 4.7.



When the potential of the system is increased, equilibrium 4.7 will shift to the right, resulting in an increased concentration of ferrous ions. This increased concentration can lead to a shift of equilibrium 4.8 to the right as well. When the potential is decreased, the equilibria will shift back. However, equilibrium 4.8 is much slower. Therefore, the current resulting from reaction 4.7 will flow with a delay in response relative to the potential. This is characteristic for inductive electrical responses [48].

Initially, when no layers are present yet, only the electrochemical double layer is measured. As soon as the bacteria start to grow and produce EPS, the EPS will interact with dissolving iron to form an organo-metal complex (FePS). The homogeneous layer formation, observed in the exploratory experiments (Figures 4.4, 4.9) suggests that the contribution will be present in series with the double layer, see Figure 4.10. A second reaction occurs: the FePS reacts with present phosphates to form a layer of $FeHPO_4/FeH_2PO_4$. This reaction occurs in series with the formation of FePS, since it is mediated or catalysed by this compound, as is observed by the increased formation rate of iron phosphates.

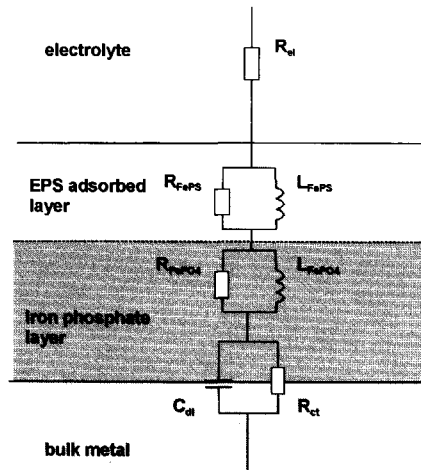


Figure 4.10: Hypothetical circuit model of the electrochemical processes during the initial stage of the vivianite formation

After a certain period, the formation of iron phosphate results in a dense layer, which is reflected in an additional time constant, see Figure 4.11. Since the layer is dense in character, it is expected that the response is parallel to the formation process: when the dense layer has been formed, the area will become inactive.

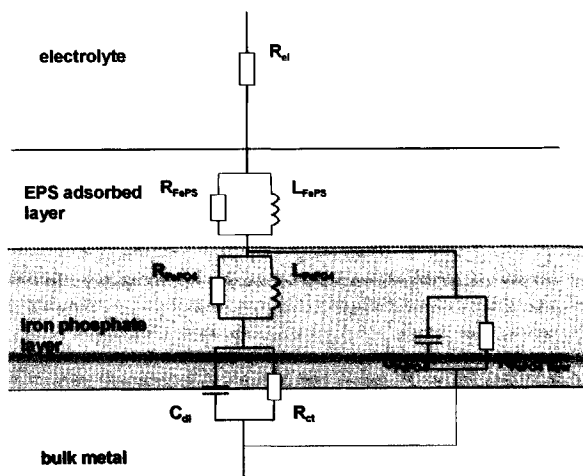


Figure 4.11: Hypothetical circuit model of the electrochemical processes during the vivianite formation, when the iron phosphate starts to form a dense layer

After a certain time period, the formation of FePS will decrease in weight, since the process is not actually occurring on the surface any more. This can be seen from the loose structure of the layer. It will not contribute to the electrochemical impedance any more, see Figure 4.12.

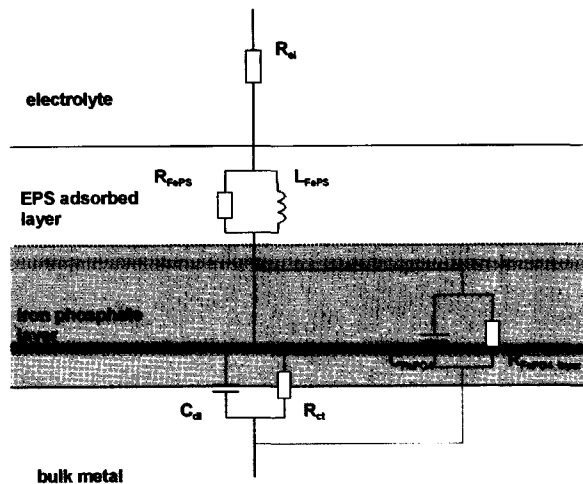


Figure 4.12: Hypothetical circuit model of the electrochemical processes during the vivianite formation, when the FePS forms loosely adhered structures

The process of formation of iron phosphate will fade for the same reason. However, the thick layer that is forming will show up in the impedance signal, see Figure 4.13.

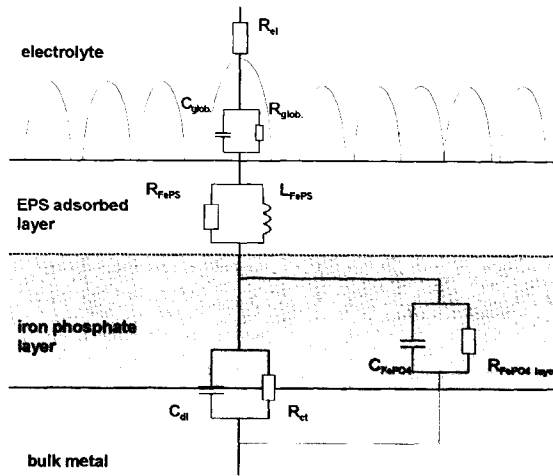


Figure 4.13: Hypothetical circuit model of the electrochemical processes during the vivianite formation, when the vivianite forms in a globular structure

With four experimental cycles, this hypothesis has been validated.

Electrochemical Impedance Spectroscopy

The first EIS-experiment is carried out with bacteria inoculated right before the experiment and refreshments were done after 19, 43 and 67 hours. Before each EIS measurement, the E_{corr} is measured. Figure 4.14 shows the evolution of E_{corr} . After thirty hours, a significant increase in E_{corr} is present. This can be attributed to the formation of the protective vivianite layer. Due to this layer, anodic iron dissolution will decrease, resulting in a higher potential. After a rise in potential of ca. 300 mV, the potential decreases sharply. This implies that the layer is not able to remain its stability. This has to do with the slight solubility of the iron phosphates. After a certain time period, the formation is not fast enough any more to compensate for the slow dissolution. Due to the resulting porosity, anodic dissolution of iron will be possible again.

Some pictures of the intact black layer are shown in Figure 4.15a. Finally, a SEM/EDX analysis revealed that the make-up of the layer was close to the expected composition for iron phosphate. SEM pictures are given in Figure 4.15b to 4.15d.

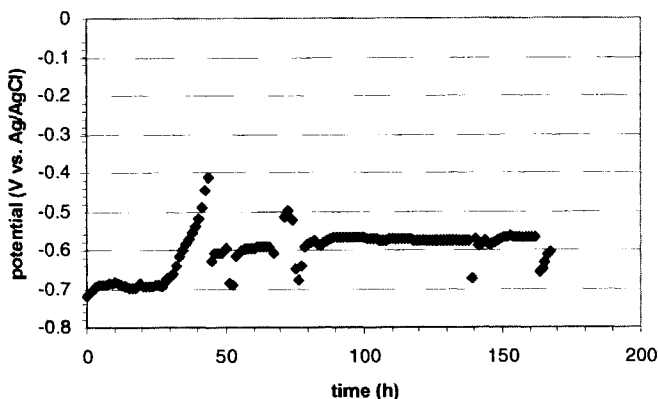


Figure 4.14: OCP of experimental cycle with refreshments and aeration (biomin05).

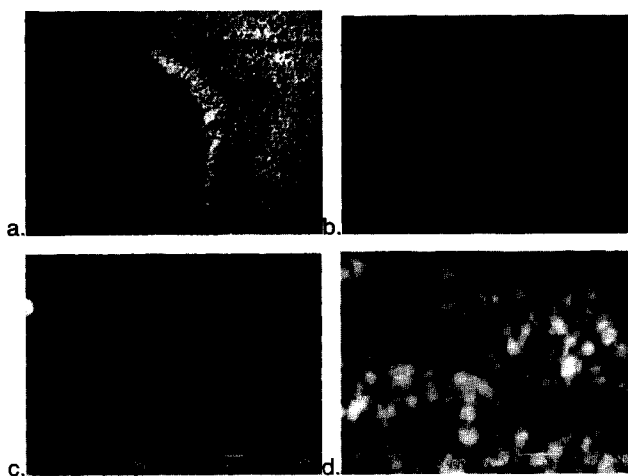
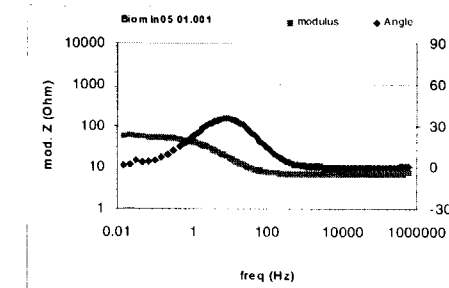
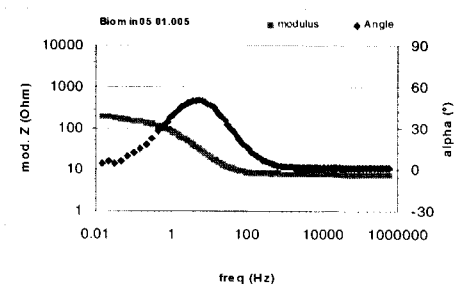


Figure 4.15: Characteristic pictures of sample after exposure. a. thick layer with black phosphate layer on the bottom b. SEM picture of globular layer structure (1000x); c. SEM picture of layer structure (1000x) at cleaned part of sample; d. SEM picture of layer structure (3500x)

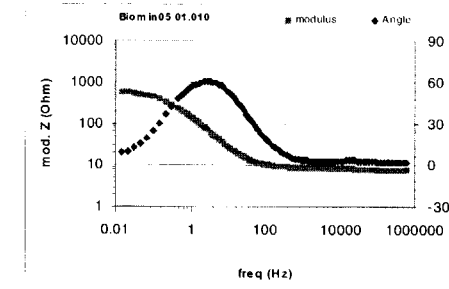
Characteristic Bode-plots are given in Figure 4.16. In these plots, it can be seen that the modulus of the impedance increases, especially in the low frequency part, during the first period. However, the moment the potential drops, also the impedance modulus decreases. Furthermore, the high frequency part of the curves shows an increasingly capacitive behaviour: the phase angle increases markedly. It decreases again towards the end of the cycle.



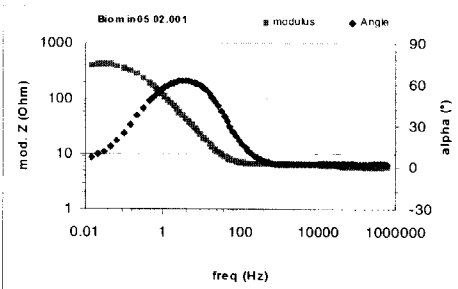
a.



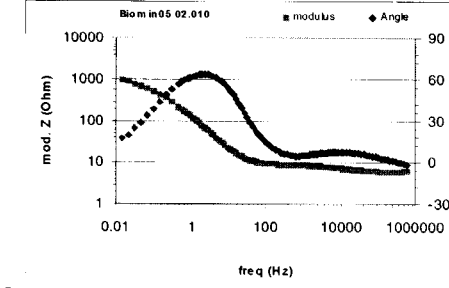
b.



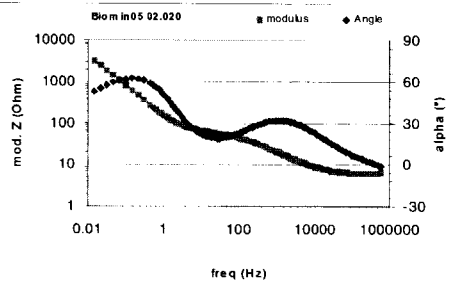
c.



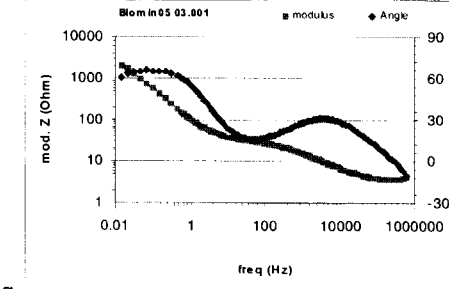
d.



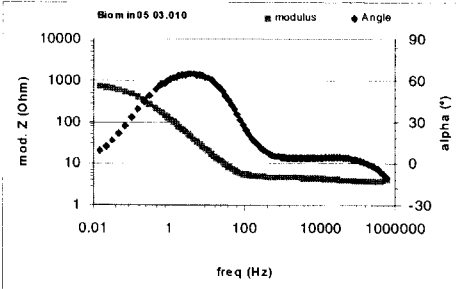
e.



f.



g.



h.

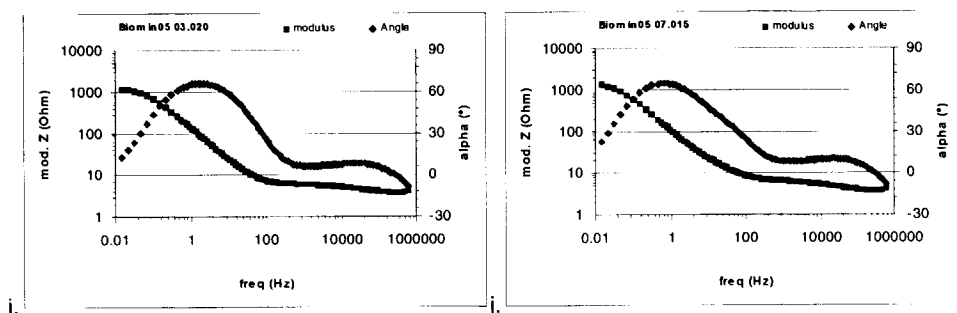
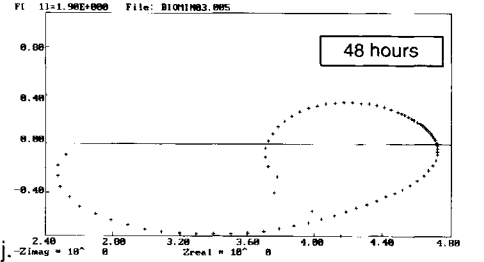
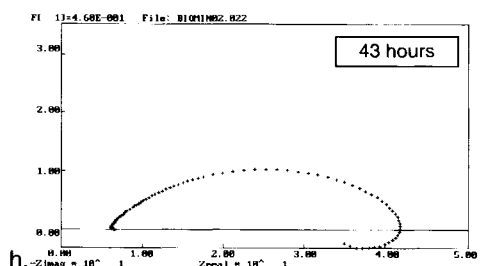
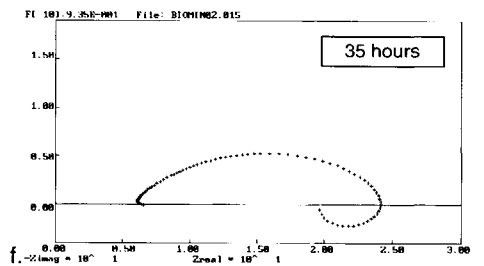
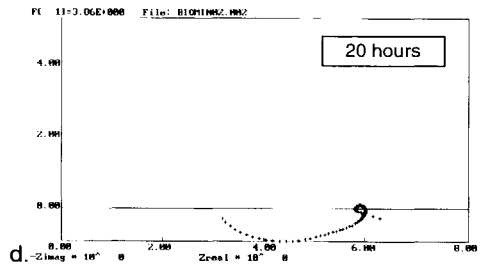
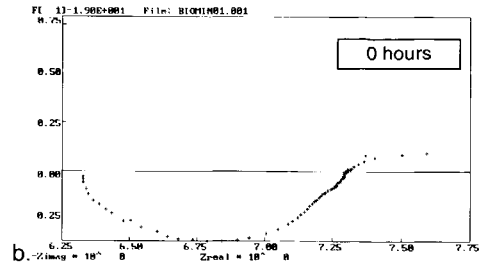
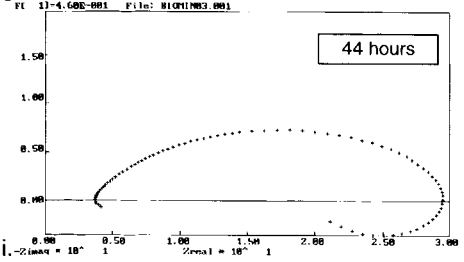
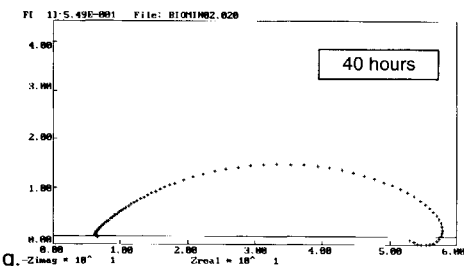
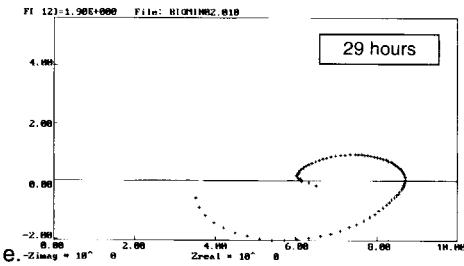
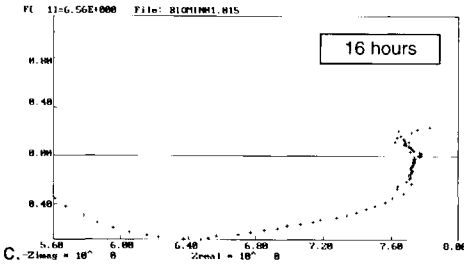
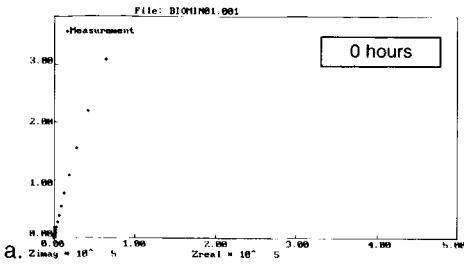


Figure 4.16: Characteristic Bode-plots of experimental cycle with refreshments and aeration. a. 0 hours; b. 4 hours; c. 10 hours; d. 19 hours; e. 29 hours; f. 40 hours; g. 43 hours; h. 53 hours; i. 64 hours; j. 184 hours.

Characteristic Nyquist-plots are given in Figure 4.17. Except for figure a, only the frequency range 1-600,000Hz is shown. Figure 4.17a shows the whole Nyquist-plot. However, in this figure, one time constant dominates the spectrum, masking the other time constants to a large extent, Figure 4.17b. Therefore, to enable a transparent explanation of the changing system, the dominant time constant has been subtracted from the spectrum. This time constant is attributed to the electrochemical double layer. It was shown that the time constant is present as series element and it was therefore allowed to subtract it.

Initially, two inductive loops are present, one resulting from the adsorption of FePS, the second as a result of FePO₄ formation, Figure 4.17b. The equivalent circuit resulting is $R_{el}(R_{ct}Q_{dl})(R_{FePS}L_{FePS})(R_{FePO4}L_{FePO4})$. After a few hours, a high frequency capacitive loop occurs, as a result of the formation of iron phosphate, Figure 4.17c to 4.17e. The equivalent circuit resulting is $R_{el}(R_{ct}Q_{dl})(R_{FePS}L_{FePS})(R_{FePO4}L_{FePO4})(R_{FePO4}C_{FePO4})$. After ca. 30 hours, the FePS formation is not visible in the Nyquist plots any more. The contribution of the capacitive layer increases still further till 40 hours, Figure 4.17f. The equivalent circuit resulting is $R_{el}(R_{ct}Q_{dl})(R_{FePO4}L_{FePO4})(R_{FePO4}C_{FePO4})$. Afterwards, the contribution of this time constant decreases, Figure 4.17g to 4.17k. This is in accordance with the drop in potential, Figure 4.14. The formation of FePS remains present, but less explicitly. It fades away completely after 80 hours, and a second high frequency capacitive loop arises, Figure 4.17l to Figure 4.17r. This time constant can be attributed to the formation of the globular vivianite layer, Figure 4.15d. The equivalent circuit resulting is $R_{el}(R_{ct}Q_{dl})(R_{FePO4}C_{FePO4})(R_{glob}C_{glob})$.



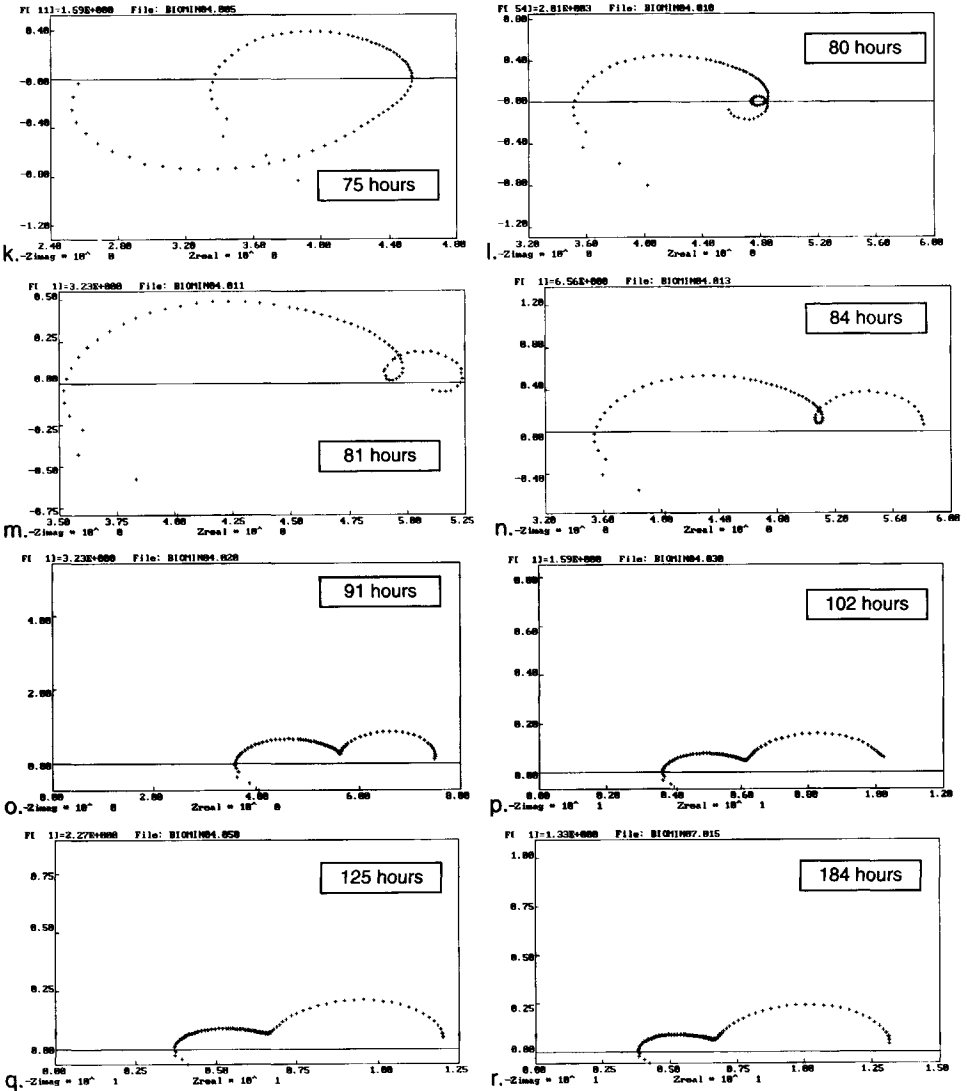


Figure 4.17: Characteristic Nyquist-plots of experimental cycle with refreshments and aeration. Frequencies 1Hz to 600kHz. Double layer contribution subtracted as illustrated in picture a (no subtraction) and b (subtraction). a. 0 hours (all freq.); b. 0 hours (1Hz-600kHz); c. 16 hours; d. 20 hours; e. 29 hours; f. 35 hours; g. 40 hours; h. 43 hours; i. 44 hours; j. 48 hours; k. 75 hours; l. 80 hours; m. 81 hours; n. 84 hours; o. 91 hours; p. 102 hours; q. 125 hours; r. 184 hours;

The development of the circuit elements in time is given in Figure 4.18.

The first time constant, ($R_{ct}Q_{dl}$), is present throughout the whole experimental cycle. The capacitive part ($(Y_{o, dl}, n_{dl})$) of the time constant is constant throughout the experiments. This indicates that the layer thickness of the double layer is constant. The charge transfer resistance R_{ct} increases in the same manner as the OCP. This is a further proof that a resistive layer is forming on the surface that protects the metal from corroding. The sharp decrease after 40 hours is also in accordance with the drop in potential. Afterwards, the R_{ct} remains constant.

The second time constant, ($R_{FePS}L_{FePS}$), which represents the complex formation, is present during the first 80 hours. After 35 hours, it is not possible to make a distinction between this time constant and the third time constant, ($R_{FePO_4}L_{FePO_4}$), present as a result of the reaction of the FePS to iron phosphate. Both constants are increasing in the first part of the experiment. When the potential drop is present, also the formation of FePS decreases rapidly and the formation of iron phosphate cannot be observed separately any more. It can be assumed that the whole process is captured in one time constant.

The fourth time constant, ($R_{FePO_4}C_{FePO_4}$), represents the response of the layer of iron phosphate that is formed. During the initial hours, the resistance increases. Again, this is a confirmation of the resistive character of the iron phosphate layer. The capacitive part of the time constant shows a tendency to the behaviour of a 'coating' layer in the beginning. However, the correlation between n and Y_o is too big (>0.95) to get a continuous fit result. Towards the end, a more stable behaviour is observed. The character in this region is more diffusive (low n -value).

The fifth time constant, ($R_{glob}C_{glob}$), occurs after approximately 80 hours and is the contribution of the globular layer forming on top of the dense iron phosphate layer. The resistance of the layer increases as the layer continues to form. The capacitive contribution is more or less constant. The behaviour of the layer resembles a coating ($n \sim 1$) in the first part. However, as the layer grows, the structure becomes less dense and the n -value decreases.

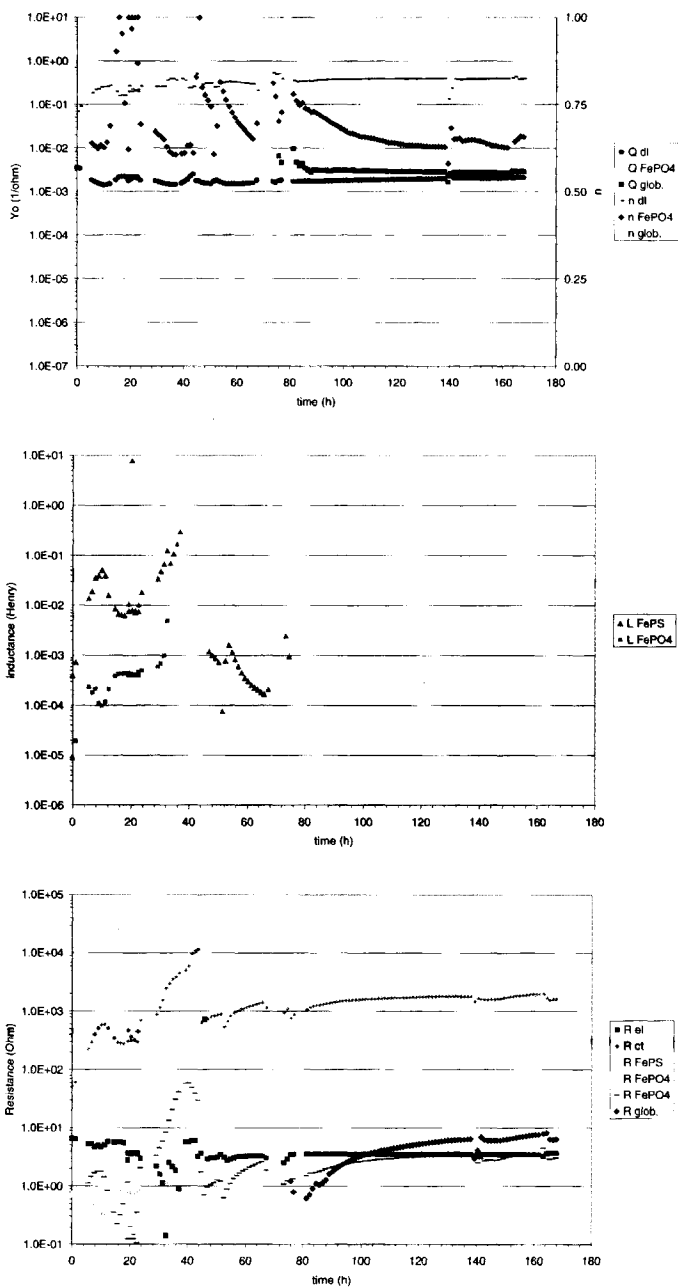


Figure 4.18: Evolution of circuit elements during the experimental cycle: a. Constant phase elements; b. inductances; c. resistances

The second EIS experiment has been carried out under sterile conditions to see whether the formation of the resistive layer could indeed be attributed to the presence of bacterial products. Figure 4.19 shows the OCP measured before each impedance spectrum. A slight increase in potential is present after 20 hours. However, it decreases more rapidly than in the previous experiment and remains at the OCP of steel for the remainder of the experiment. Figure 4.19 shows SEM-pictures of the sample surface after the experiment. It is obvious that no homogeneous layer is formed as was in the presence of bacteria. Partially, a layer is formed with plate-shaped iron phosphates and partially, the structure present in the previous experiments occurs. The plate-structures are the result of too rapid local iron phosphate formation. The thin layer of FePS that was formed in the presence of bacteria was able to homogenise the reaction. In this case, the layer is absent and reaction occurs locally. Furthermore, some bacteria can be observed on the properly phosphated parts. This is due to contaminations which are inevitable during the refreshments.

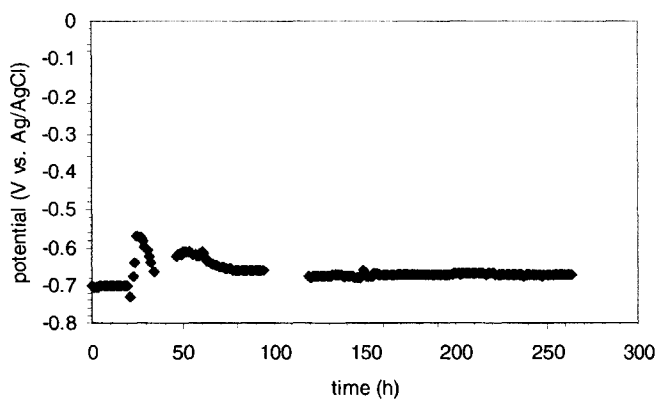


Figure 4.18: OCP of sterile experimental cycle with refreshments and aeration (biomin06).

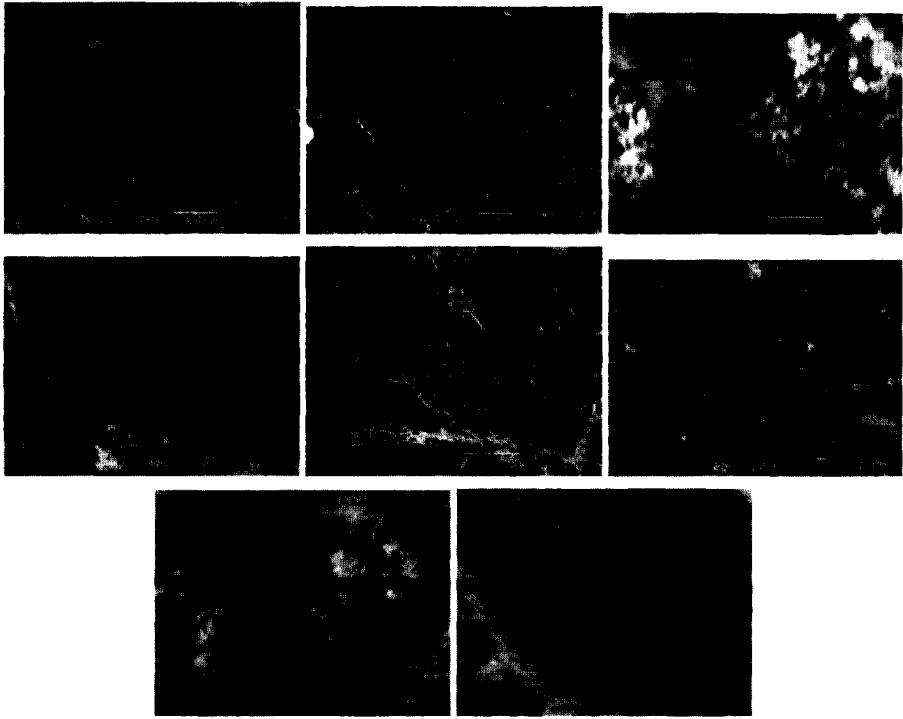


Figure 4.20: Characteristic SEM-pictures of sterile experimental cycle with refreshments and aeration (biomin06).

Figure 4.21 shows characteristic Bode-plots of the EIS measurements. The modulus of the impedance increases during the experiment. Furthermore, the impedance gets slightly more capacitive and after ca. 55 hours, another time constant is revealed in the Bode plots. After 119 hours (Figure 4.21f) no changes are present.

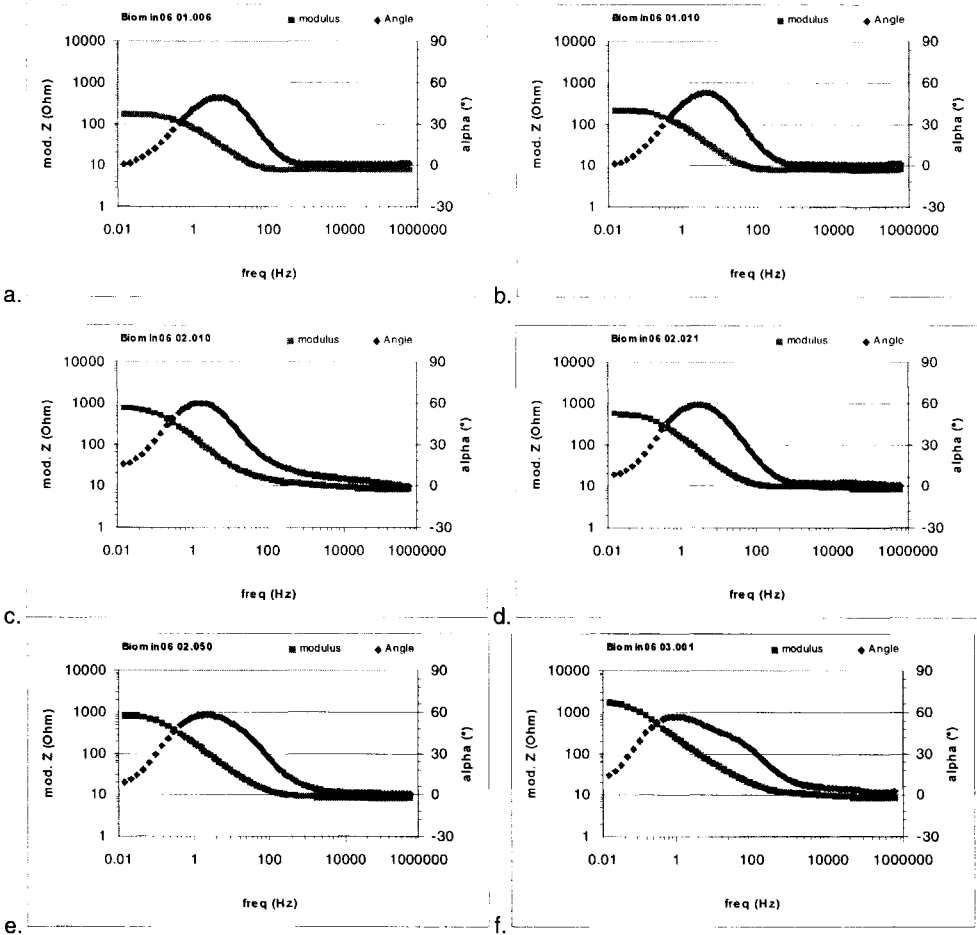


Figure 4.21: Characteristic Bode-plots of sterile experimental cycle with refreshments and aeration (biomin06). a. 6 hours; b. 10 hours; c. 32 hours; d. 55 hours; e. 87 hours; f. 119 hours.

Figure 4.22 shows characteristic Nyquist-plots of the impedance spectra. The plots show the spectra after subtraction of the low frequency time constant attributed to the double layer (R_{ct}, Q_{dl}). The second time constant can be attributed to a thin layer formed homogeneously over the surface, presumably iron phosphate. The third time constant, which is more explicitly present as the experiment continues, is attributed to localised iron phosphate formation, as shown in Figure 4.19. Figure 4.22f shows the relative errors in the fit for equivalent circuit $R_{ct}(R_{ct}, Q_{dl})(Q_{hom.ph.}(R_{hom.ph.}(R_{loc.ph.}, Q_{loc.ph.}))$) confirming the presence of the third time constant.

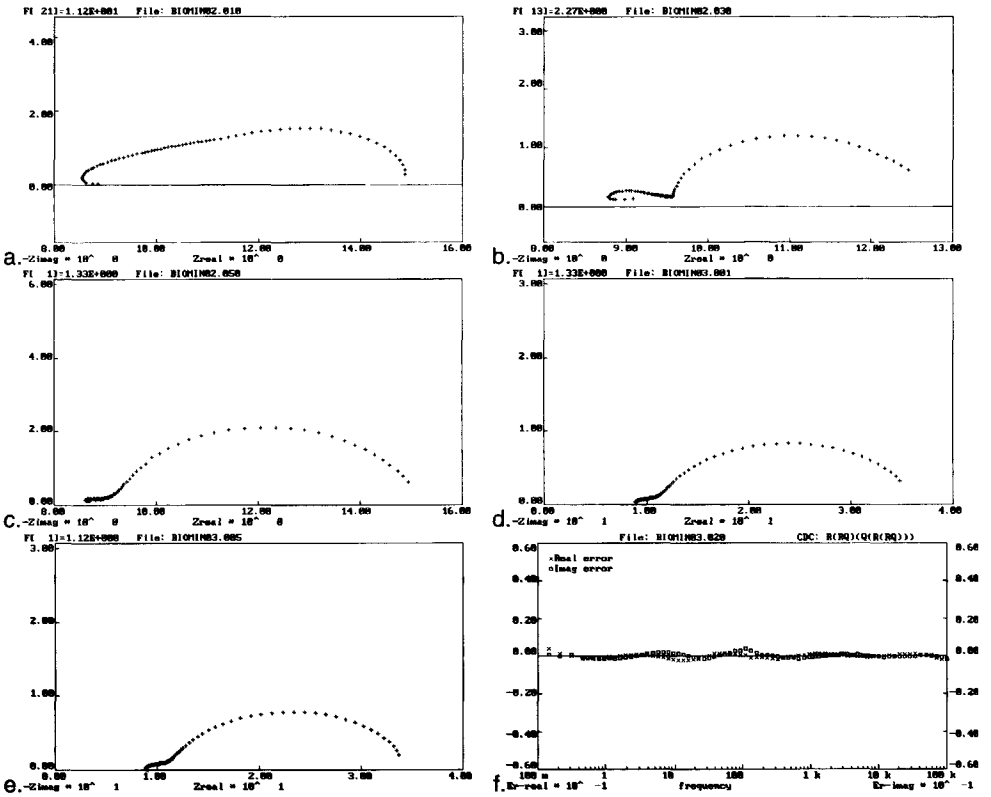


Figure 4.22: Characteristic Nyquist-plots of sterile experimental cycle with refreshments and aeration (biomin06), frequencies 1Hz to 600kHz. Low frequency double layer contribution subtracted. a. 32 hours; b. 65 hours; c. 87 hours; d. 119 hours; e. 124 hours; f. frequency-error plot.

The third experiment is carried out to investigate the effect of aeration and refreshments. The OCP before each EIS measurement is given in Figure 4.23. The potential remains relatively high for an extended period. This is caused by slow dissolution of the iron, which might have something to do with the lower activity of the bacteria (due to absence of oxygen). Figure 4.24 shows a thick layer of phosphate, partially blackish/green, partially white. Underneath the thick layer, a dense layer of phosphate is present as well.

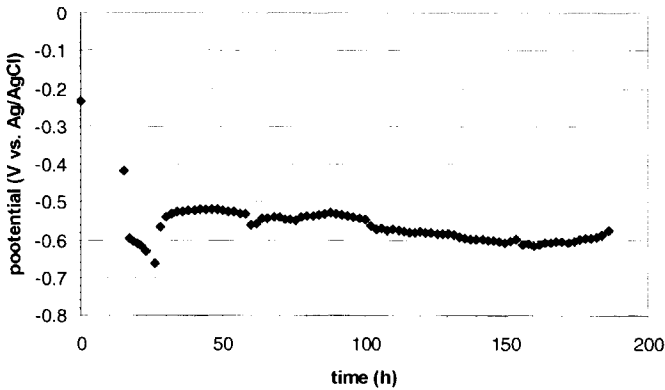


Figure 4.23: OCP of experimental cycle with bacteria, without refreshments and with aeration (biomin03).

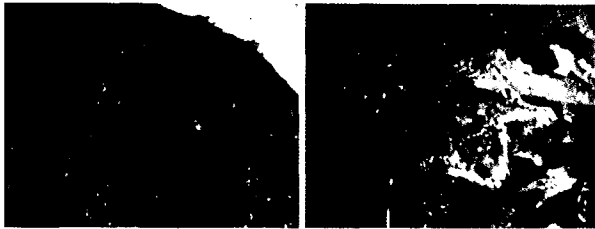


Figure 4.24: Characteristic light microscopy pictures of experimental cycle with bacteria, without refreshments and with aeration (biomin03).

Figure 4.25 shows characteristic Bode-plots of the experiment. Obvious is the very high modulus of the system after a certain exposure time. This is the result of the thick diffusion layer. Furthermore, in the beginning the low frequency part is rather capacitive, indicating a high charge transfer resistance.

Figure 4.26 shows characteristic Nyquist plots. The electrochemical double layer contribution has been subtracted. In this experiment, an inductive loop is clearly present, as was the case with the first cycle with bacteria. This is a further proof of the fact that the bacteria (or their products) are mediating the phosphating process. Figure 4.26d shows the frequency-error plot for fitting the equivalent circuit $R_{el}(R_{ct}Q_{dl})(Q_{ph,1}(R_{ph,1}(R_{ph,f},L_{ph,f})))$.

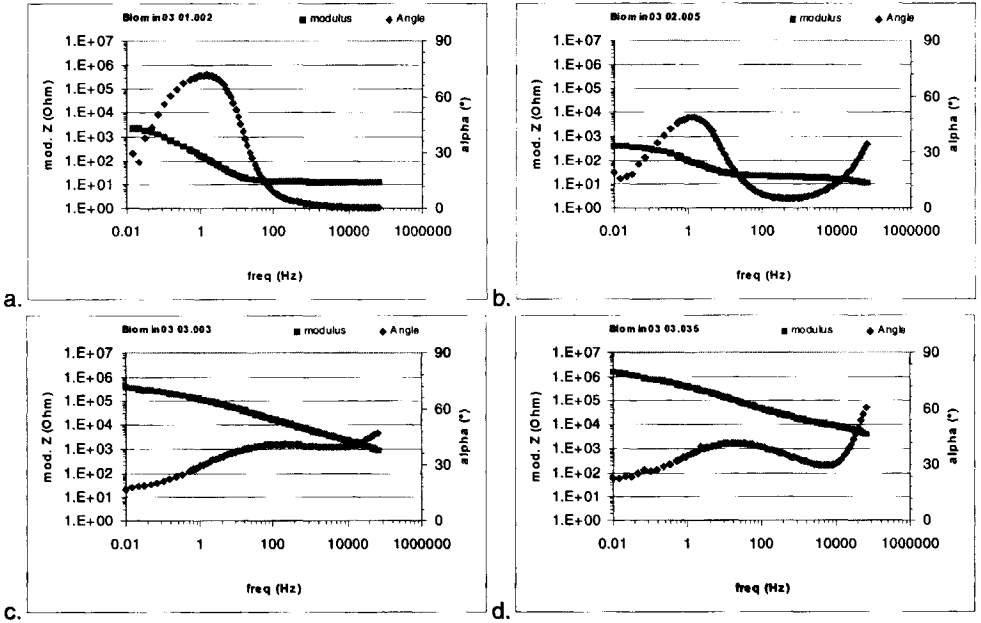


Figure 4.25: Characteristic Bode-plots of experimental cycle with bacteria, without refreshments and with aeration (biomin03). a. 15 hours; b. 23 hours; c. 30 hours; d. 94 hours.

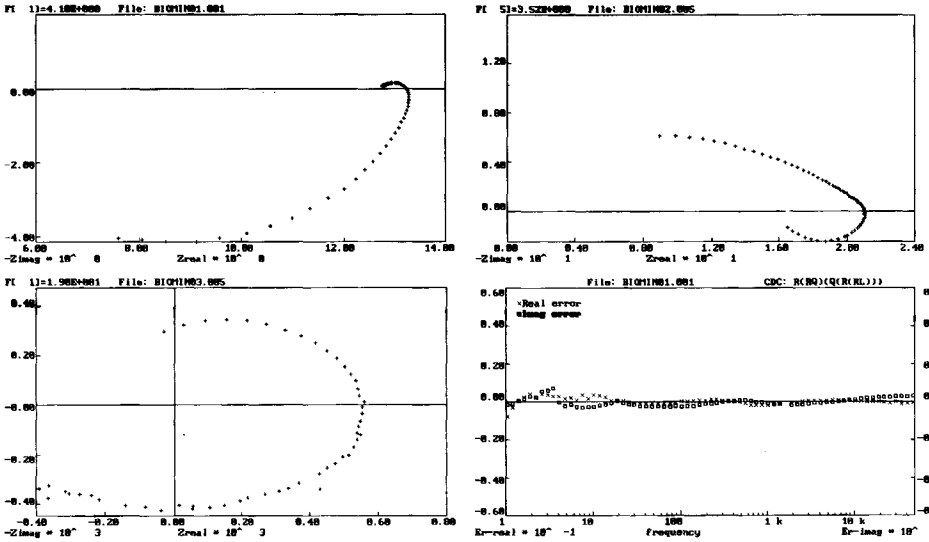


Figure 4.26: Characteristic Nyquist-plots of experimental cycle with bacteria, without refreshments and with aeration (biomin03). Double layer/Charge transfer time constant has been subtracted. a. 0 hours; b. 23 hours; c. 34 hours; d. frequency-error plot.

For the fourth experimental cycle, the bacteria were inoculated one day before the experiment started to enable them to form EPS in advance of the exposure. Figure 4.27 shows the E_{corr} during the experiment. No changes are observed in the potential. It is stable at the E_{corr} of carbon steel. After 20 hours, a black deposit layer had already formed. An increased formation rate is thus possible, however, the electrochemical properties of the layer are less good than those of the layer formed in the first experimental cycle. As can be seen in Figure 4.28, the modulus of the impedance is a factor 10 lower than the values obtained in the first experiment. During the 20 hours of the experiment, no marked changes occurred.

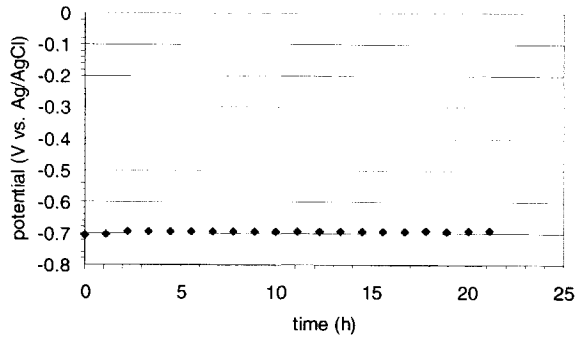


Figure 4.27: E_{corr} of experimental cycle with bacteria inoculated one day before experimental cycle (biomin07).

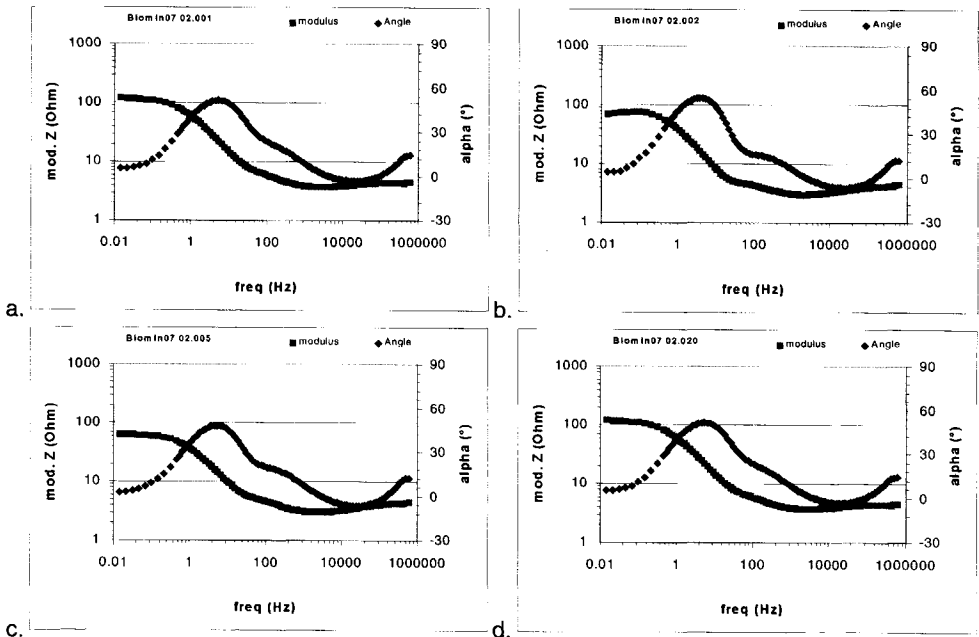


Figure 4.28: Characteristic Bode-plots of experimental cycle with bacteria inoculated one day before experimental cycle (biomin07). a. 0 hours; b. 1 hour; c. 4 hours; d. 21 hours.

Figure 4.29 shows characteristic Nyquist-plots of the impedance spectra. Figures 4.29a and 4.29c are representations of the full spectrum. For 4.29b and 4.29d, the double layer/charge transfer contribution has been subtracted. One remarkable difference with the first experimental cycle is the fact that the capacitive loop, representing the phosphate layer, occurs at lower frequencies. Moreover, it has the character of almost ideal capacitance with an n-value close or equal to unity. The spectra can be fitted with equivalent circuit $R_{ct}(R_{ct}Q_{dl})(R_{ph,l}Q_{ph,l})(R_{ph,f}L_{ph,f})$.

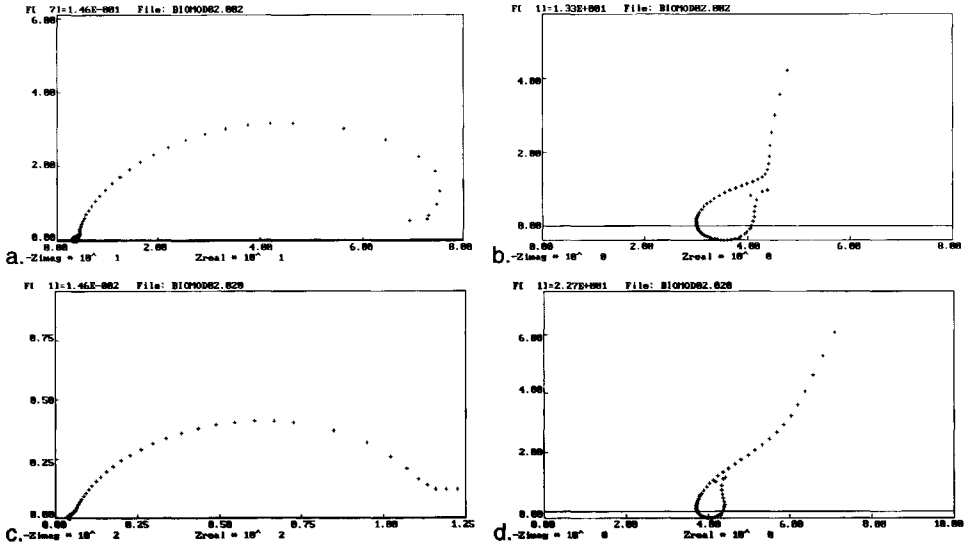


Figure 4.29: Characteristic Nyquist-plots of experimental cycle with bacteria inoculated one day before experimental cycle (biomin07). a. 1 hours; b. 1 hour (double layer subtracted); c. 21 hours; d. 21 hours (double layer subtracted).

Figure 4.30 shows the evolution of the circuit elements in time. As can be seen, no marked changes in the components are present. Q_{dl} is in the same order of magnitude as in the first experiment. R_{ct} is a factor 10 lower than in the first experiment and no clear increase in time is present, regardless of the visually observed phosphate layer. Furthermore, also $L_{ph,f}$ is a factor 10 lower than the inductances present in the first cycle. These differences show that the character of the layer formed in this manner is markedly different from the ones formed in a more quiescent condition.

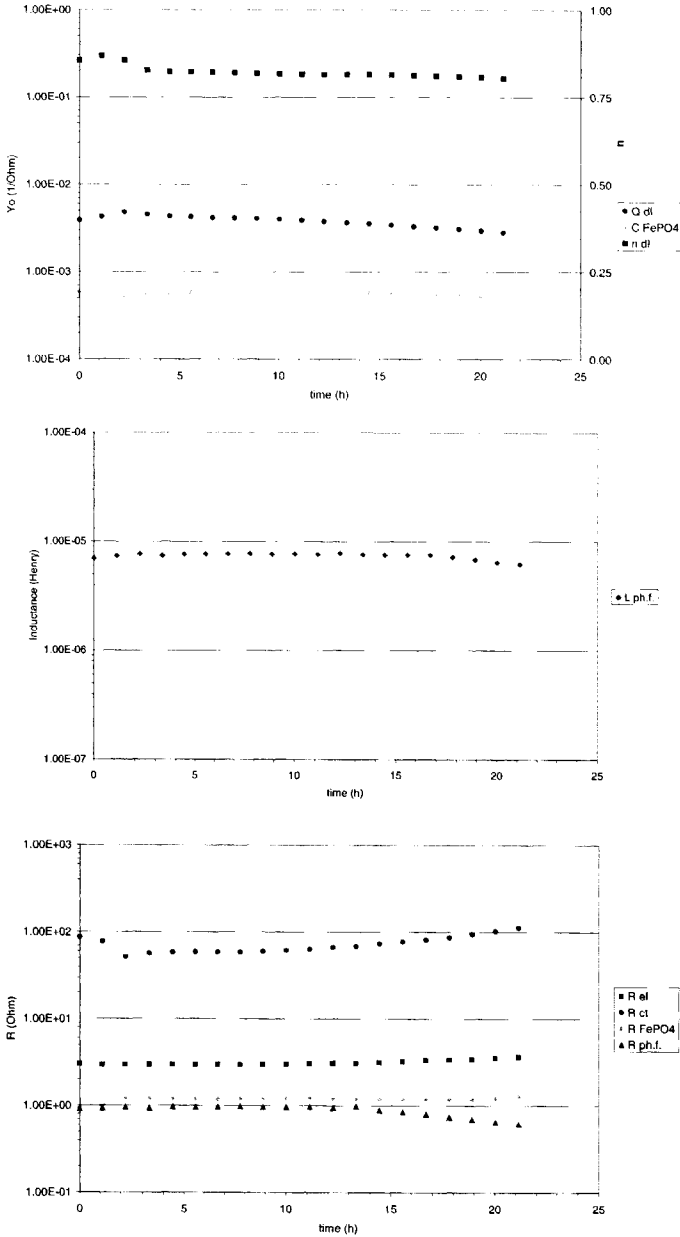


Figure 4.30: Fits of equivalent circuit $R(RQ)(RC)(RL)$, there is no apparent interaction between the time constants. Subtracting them does not result in altering the remaining circuit. (biomin07)

4.2.4 General discussion

Several experimental cycles have been carried out and it was shown to be possible to form protective phosphate layers due to the active contribution of bacteria. The mechanism hypothesis that was formulated has been verified using electrochemical impedance spectroscopy. It was shown (first cycle) that indeed a protective layer can be built up, The resistance against corrosion was increased to a certain maximum after which it decreased again. This indicates that the stability of the layer might not be sufficient yet.

The comparison between the first two cycles shows that indeed the action is due to bacteria and the fact that the bacterial density was low, suggests that the metabolic products are more likely causing the change in phosphate formation than the bacteria themselves. However, production of the metabolic products in advance (cycle 4) did not result in the same quality layer as the first cycle.

4.3 Protective Biofilms

4.3.1 Introduction

The previous section discussed the formation of inorganic layers of biological origin and their possible use as anticorrosion layers. The second possible way to build up protective layers is the formation of *organic layers*. As was suggested in the introduction to this chapter, there is evidence that the presence of biofilms can result in corrosion protection. Especially Jayaraman et al. have reported research in this area [3, 15, 17, 19]. On one hand they ascribe the protective mechanism to the diffusion barrier properties for ions and especially oxygen. Oxygen diffusion is further decreased due to its consumption within the biofilm as the bacteria use it for their respiration. However, this explanation can not explain the complete effect since also fixed biofilms show a protective effect. The explanation for the remainder of the anticorrosive effect of the biofilm can be found in the interaction of the compounds of which the biofilm consists with the metal surface. In this section, the effects of living biofilms are investigated.

4.3.2 Experimental

Three experiments have been carried out in semi-continuous set-up to investigate the possibility of formation of stable biofilms to prevent or deter corrosion. Figure 4.31 shows a schematic set-up of the reactor. The medium, 3.5 g/l yeast extract with 5 g/l glucose added to demineralised water, was continuously refreshed. *Xanthobacter 124X*, isolated from sewage, was used as biofilm, because of its tendency to form very stable biofilms, firmly attached to the bioreactors in which it is used commonly.

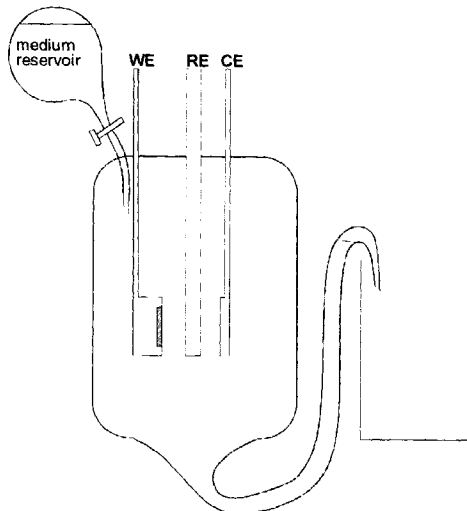


Figure 4.31: Schematical drawing of bioreactor set-up.

Bacterial counting was carried out regularly during the experiments. The effect of the biofilm formation on the electrochemical behaviour was measured in electrochemical potential and polarisation resistance using Corware software.

4.3.3 Results

Figure 4.32 shows the results of the bacterial countings. During all cycles, a stable amount of bacteria in solution was found after a certain time period at approximately 10^8 bacteria/ml.

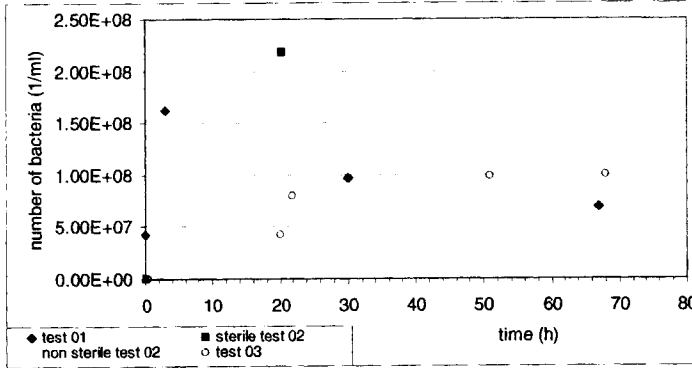


Figure 4.31: Bacterial counts during smi-continuous culture experiments.

Figure 4.33a shows the OCP during the first experimental cycle. Initially the potential increases rapidly to 0.1V vs Ag/AgCl. This is probably due to the formation of a conditioning primary film and the start of biofilm formation, which can be predicted from the fast growth of bacteria during the first few hours (Figure 4.32). After 7 hours, the OCP drops to $-0.6V$ vs Ag/AgCl, a characteristic value of corroding steel in seawater. The R_p plot in Figure 4.33b shows an increase in R_p during the first 7 hours, indicating that a protective layer starts to form. However, also the R_p value drops after 7 hours. The slow subsequent increase is probably due to the formation of corrosion products. Figure 4.34 shows the localised corrosion after the experiment.

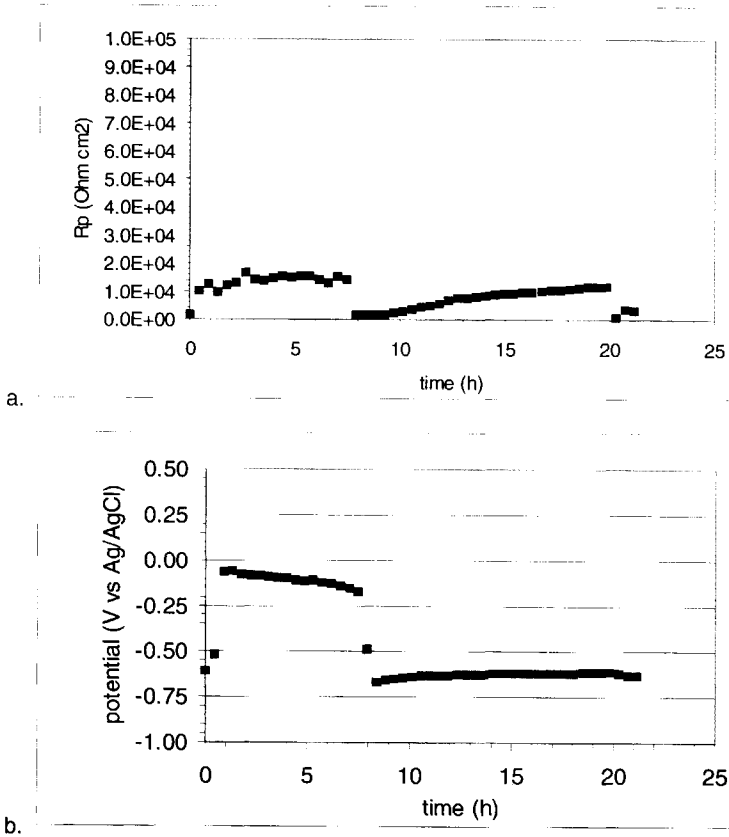


Figure 4.33: a. Development of polarisation resistance R_p for carbon steel during formation of biofilm in semi-continuous culture; b. Corrosion potential development.



Figure 4.34: Pictures of biofilm formed during the 1st experimental cycle

During the second experimental cycle, dilution rate of the medium was increased to decrease the biofilm formation rate, in order to get more homogeneous film formation. Figure 4.35 shows the OCP and R_p values for the second experimental cycle. The initial increase in potential is present, combined with the increase in R_p . However, the stability is low as in the first cycle: after 10 hours, both the OCP and the R_p decrease. Figure 4.36 shows pictures of the inhomogeneous layer after two days of exposure. Compared to the first experiment, a denser layer was formed and less corrosion was present.

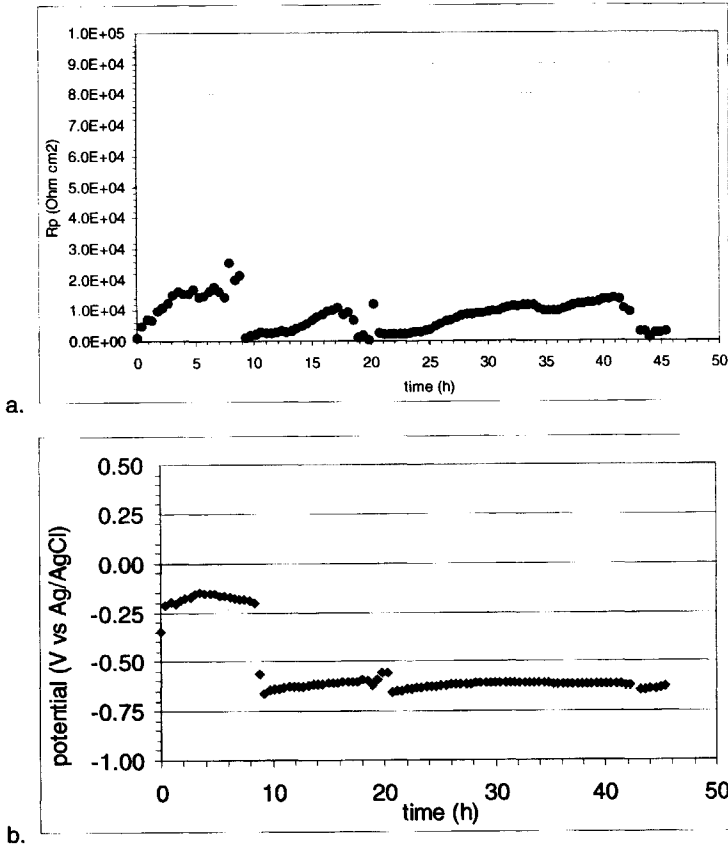


Figure 4.35: a. Development of polarisation resistance R_p for carbon steel during formation of biofilm in semi-continuous culture; b. Corrosion potential development.



Figure 4.36: Pictures of biofilm formed during the 2nd experimental cycle

Figure 4.37 shows the OCP and R_p during the third experimental cycle. Before this cycle, the set-up was improved to prevent contamination with other bacterial species. The OCP shows an irregular behaviour. However, it remains high relative to the previous two series. It is suspected that this has to do with the metabolic activity of the bacteria: when they are active, they use up more oxygen than when they are inactive. The oxygen concentration directly influences the rate of the cathodic reaction and the OCP. The R_p shows a much more stable behaviour. After an initial value comparable to the highest values in the previous experiments, the value increases

threefold after ca. 15 hours. A stable layer is formed, as the R_p remains stable. Figure 4.38 shows pictures of the sample. Pictures a and b give a general impression of the layer: a dark grey layer is present on top of which a globular layer grows. Bacteria are present in small colonies, Figure 3.38c. Figure 3.38d and e show that the layer is almost completely covering the surface. At some small spots, the bare metal is visible (light spots), this might however be caused by drying of the film.

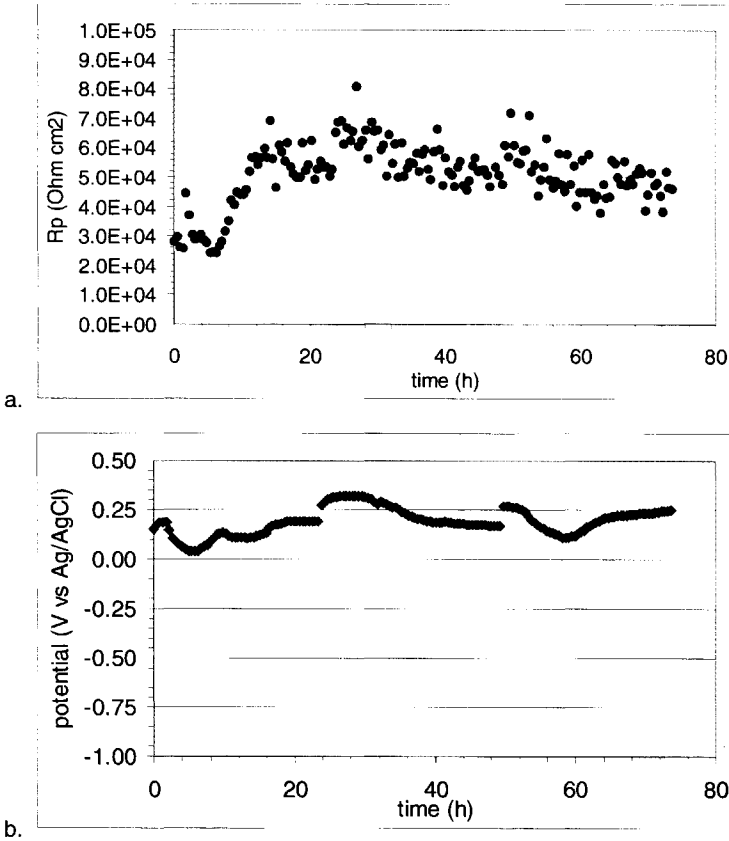


Figure 4.37: a. Development of polarisation resistance R_p for carbon steel during formation of biofilm in semi-continuous culture; b. Corrosion potential development.

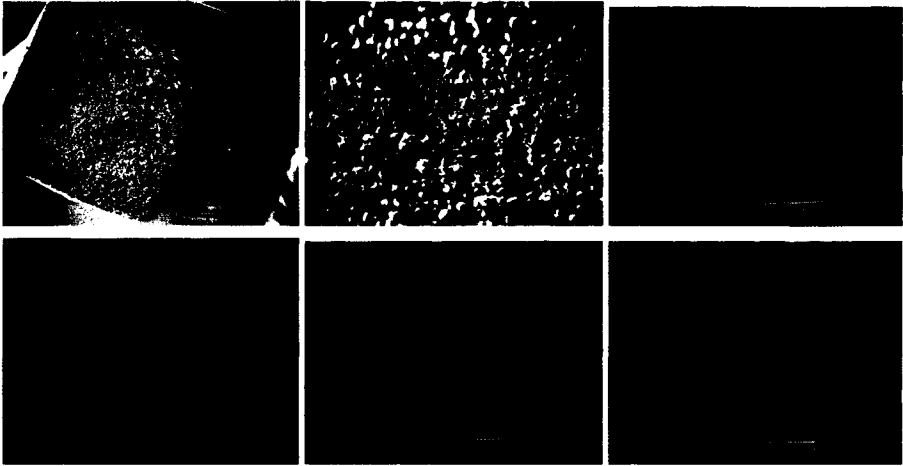


Figure 4.38: Pictures of biofilm formed during the 3rd experimental cycle

4.3.4 General Discussion

The experiments carried out have shown that it is possible to create a stable biofilm, which increases the corrosion resistance. The formed layer contained circa 20wt% carbon. Determining factors for successfully obtaining a stable film were found in bacterial concentration, contamination and refreshment rate (directly influencing the bacterial concentration).

It could be seen clearly that the bacterial colonies were only partially covering the surface. The extracellular polymeric products, building the biofilm, were determining the formation of the protective layer.

4.4 Anticorrosive Bioadditives

4.4.1 Introduction

The idea to use (poly)saccharides as potential anticorrosive compounds arises from the suggestions in the literature that the decrease in corrosion rate of biofilm covered metals was not solely explainable by the barrier properties of the layers and the consumption of oxygen by the biofilm bacteria. Some other mechanism has to be active, since fixed biofilms show a protective effect as well (too large an effect to be explained by the diffusion barrier properties).

The most logical explanation of the anticorrosive effect of the biofilm is the interaction of the compounds of which the biofilm consists with the bare metals. The main components of the biofilm are polysaccharides and polypeptides. Polysaccharides are selected for the investigations. Five different types were produced by bacteria, which were selected for their fast exopolymeric production rate. The electrochemical investigations on these compounds are reported here.

In contrast to the processes described in section 4.2, the way the layer is formed is less important in this case. The main subject of the research is whether a layer is formed and to what extent a protective effect is found. Therefore, the layers are only electrochemically characterised for their corrosion resistance. R_p -measurements are the best technique to provide this information.

4.4.2 Experimental

Five *extracellular polymeric substances (EPS)* were produced by TNO Nutrition and Food, listed in Table 4.3. All are produced by specific *Lactobacillus* species.

Table 4.3: EPS produced for testing on anticorrosive properties.

Bacterial strain	Product type	Amount produced
EPS1	heteropolysaccharide	1.7 g
EPS2	heteropolysaccharide	0.5 g
EPS3	heteropolysaccharide	0.6 g
EPS4	homopolysaccharide	1g
EPS5	homopolysaccharide	1g

Experiments were carried out with the EPS in solution. They were dissolved in a slightly corrosive medium (0.1M LiClO₄) and the corrosivity of the medium with the EPS added was compared to the corrosivity without the addition of EPS. Sample material was plain carbon steel. Samples were embedded in an epoxy matrix.

For the initial investigations, it was decided to use a combination of corrosion potential measurements and polarisation resistance (R_p) measurements for the evaluation of the electrochemical properties. This selection of techniques is based on the simplicity of the evaluation of data arising from the measurements. The corrosion potential measurements are a direct measure of the activity of a system: a lower potential (relative to the reference measurements) implies an active system, a higher potential implies a certain shielding or passivation of the metal surface. R_p -measurements show the resistance of a surface to dissolution processes.

4.4.3 Results

Results are presented in graphical form below in Figures 4.39 to 4.49. Of most of the samples, a photograph of the exposed surfaces is given as well. Furthermore, a SEM and EDX analysis of the formed layers has been performed.

Figure 4.39 shows for a reference measurement a decrease in corrosion potential to -700mV versus Ag/AgCl . The polarisation resistance increases slightly to a stable value of $1500\ \Omega\text{cm}^2$. Figure 4.40 shows a picture of an exposed sample. A lot of loosely attached corrosion products are present and the non-corroded parts of the surface have not changed.

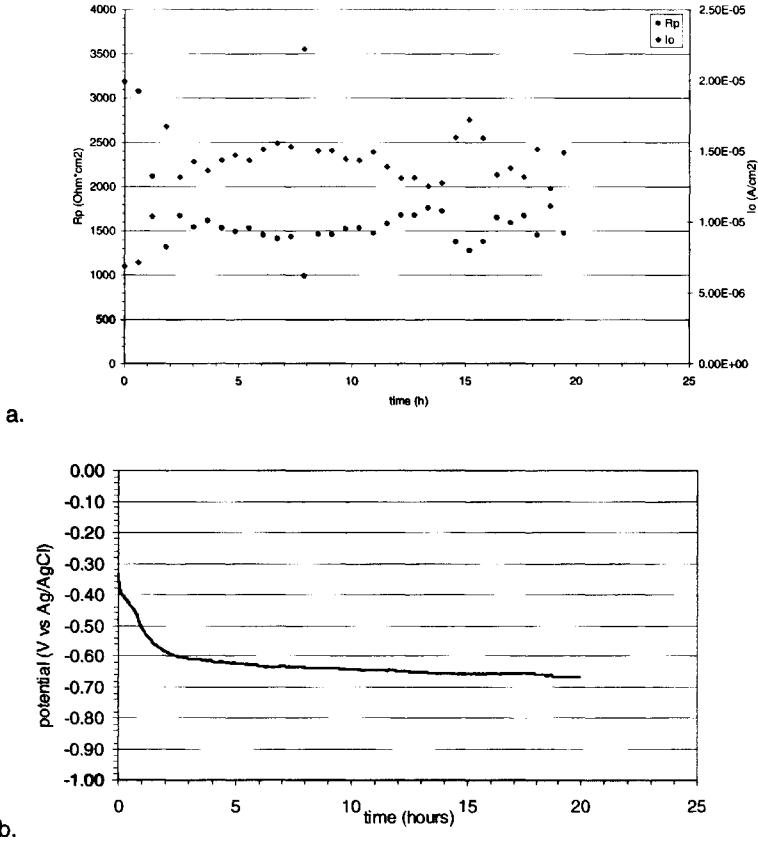


Figure 4.39: a. Development of polarisation resistance R_p and exchange current density i_o for carbon steel in 150ml 0.1 M LiClO_4 ; b. Corrosion potential development

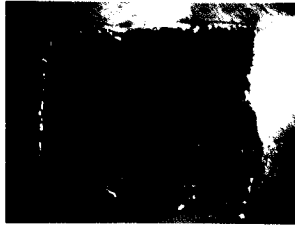


Figure 4.40: Picture of reference sample after exposure

EPS1 (Figure 4.41) shows a short protective effect. The potential was elevated relative to the one in the reference measurement for circa 10 hours. After the exposure a homogeneously deposited layer of organic material was present (Figures 4.42a and b) and no red/brown corrosion products were found. After an extended experimental period, corrosion products started to form (Figure 4.42c). The R_p value shows an initial increase from the starting value of $3000 \Omega/\text{cm}^2$ to $6000 \Omega/\text{cm}^2$. The increase is probably due to the formation of the organic layer. The active area is therefore becoming smaller. After 15 to 20 hours the R_p value collapses to the value of the reference measurement. Afterward the value increases again, probably due to blocking of the surface by both corrosion products and the organic layer.

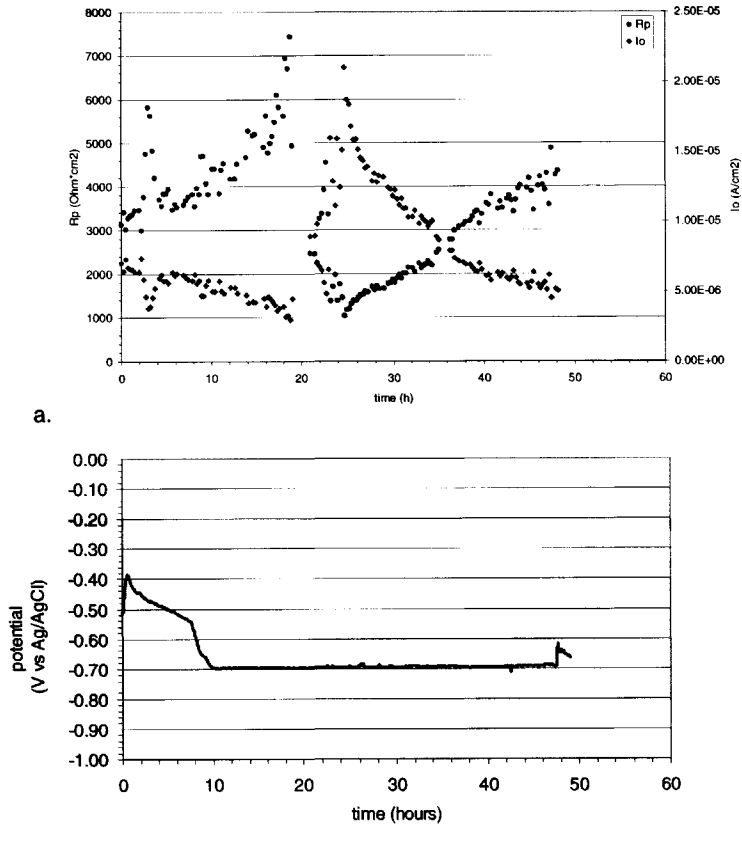


Figure 4.41: a. Development of polarisation resistance R_p and exchange current density i_o for carbon steel in 150ml in 0.1 M LiClO₄ and 0.2g EPS1 in 0.1 M LiClO₄; b. Corrosion potential development

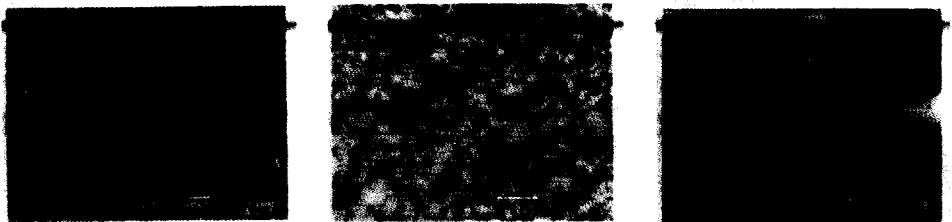


Figure 4.42: SEM picture of EPS1 sample after exposure a. Overview of intact layer; b. intact layer close-up; c. corrosion product

EPS2 shows an initial fast decrease in potential and stabilisation at the value of the reference measurement, see Figure 4.43. The R_p value is doubled relative to the reference ($3500 \Omega/\text{cm}^2$). This is probably caused by the blocking of the surface by the layer as is shown in Figure 4.44.

The active area is smaller than in the reference measurement. The rapid increase in the R_p can be explained by rapid layer formation.

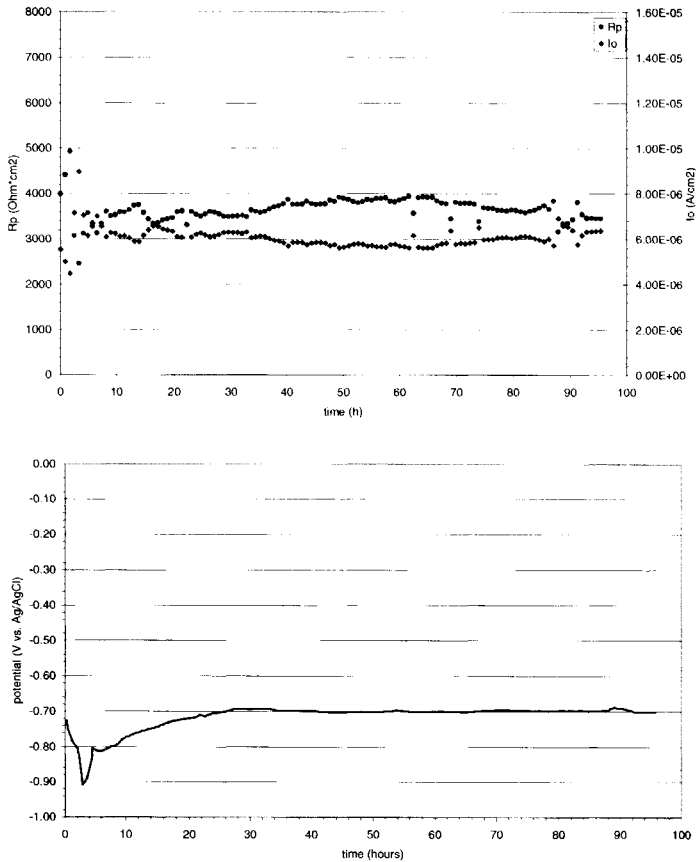


Figure 4.43: a. Development of polarisation resistance R_p and exchange current density i_o for carbon steel in 150ml 0.1 M LiClO₄ and 0.2g EPS2; b. E_{corr} development

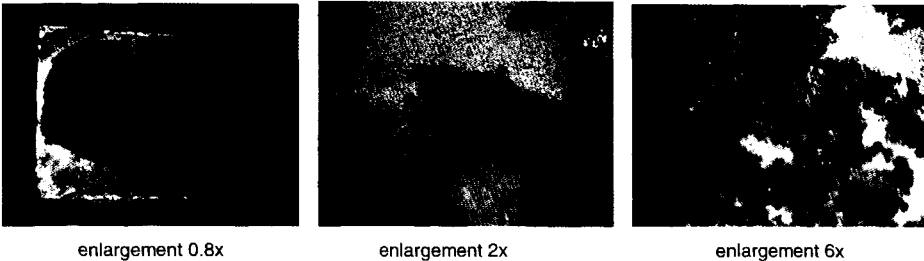


Figure 4.44: Pictures at different enlargements of the sample exposed to EPS2

EPS3 shows a similar behaviour to EPS2, see Figure 4.45. A rapid increase in R_p to $4500 \Omega\text{cm}^2$ and a low and stable potential (100mV more noble than the potential in the reference measurement). Layer formation was not homogeneous either and localised corrosion took place.

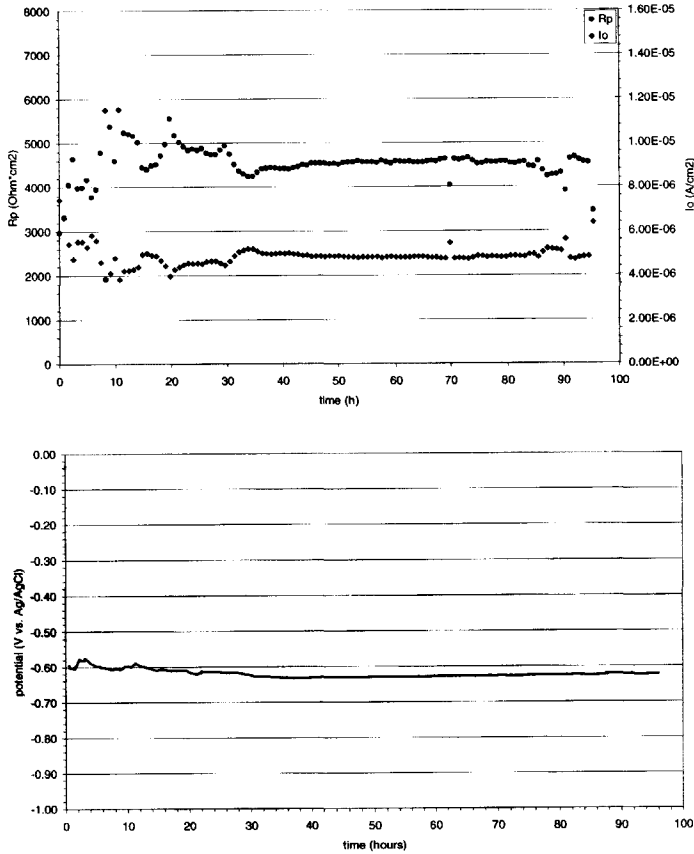
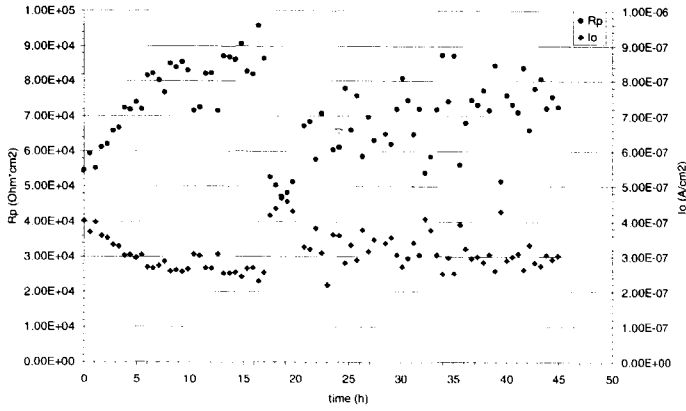
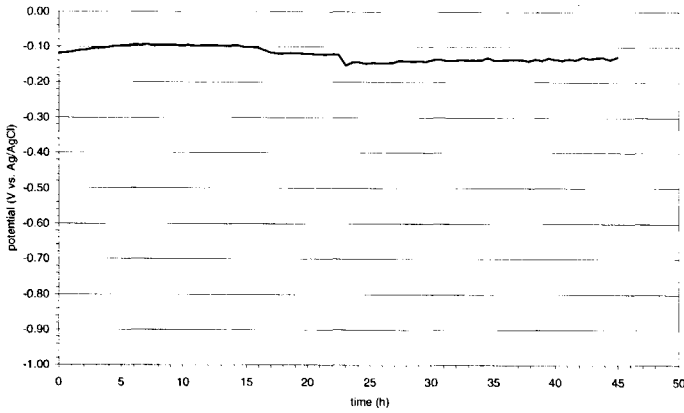


Figure 4.45: a. Development of polarisation resistance R_p and exchange current density I_0 for carbon steel in 150ml 0.1 M LiClO_4 and 0.2g EPS3; b. Corrosion potential development

EPS4 showed behaviour much different from the behaviour of the heteropolysaccharides, see Figure 4.46. The value for the corrosion potential remained much higher (-120mV versus Ag/AgCl) and the R_p value was about $70 \text{ k}\Omega\text{cm}^2$. Furthermore no white deposition layer was formed, but a thin black layer. EDX-analysis showed that the layer did contain ca. 10% carbon and therefore it could be concluded that the layer is of biological origin. As is obvious from Figure 4.47, the formation of the layer was either not uniform or degraded partially. Further studies are needed to reveal the mechanism and character of the formed layer.



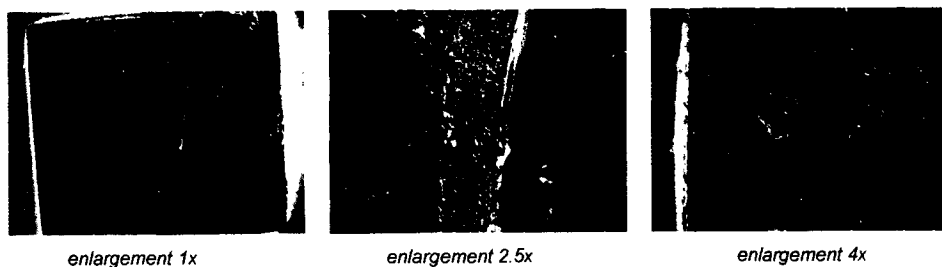
a.



b.

Figure 4.46: a. Development of polarisation resistance R_p and exchange current density I_o for carbon steel in 150ml 0.1 M LiClO_4 and 0.2g EPS4; b. Corrosion potential development

For EPS5 homopolysaccharide, a black deposit, rich in carbon, was deposited as well, see Figure 4.49. However, the effect on the R_p was much less pronounced, Figure 4.48. The plateau in corrosion potential during the first 25 hours could indicate some passivation behaviour.



enlargement 1x

enlargement 2.5x

enlargement 4x

Figure 4.47: Pictures at different enlargements of the sample exposed to EPS4

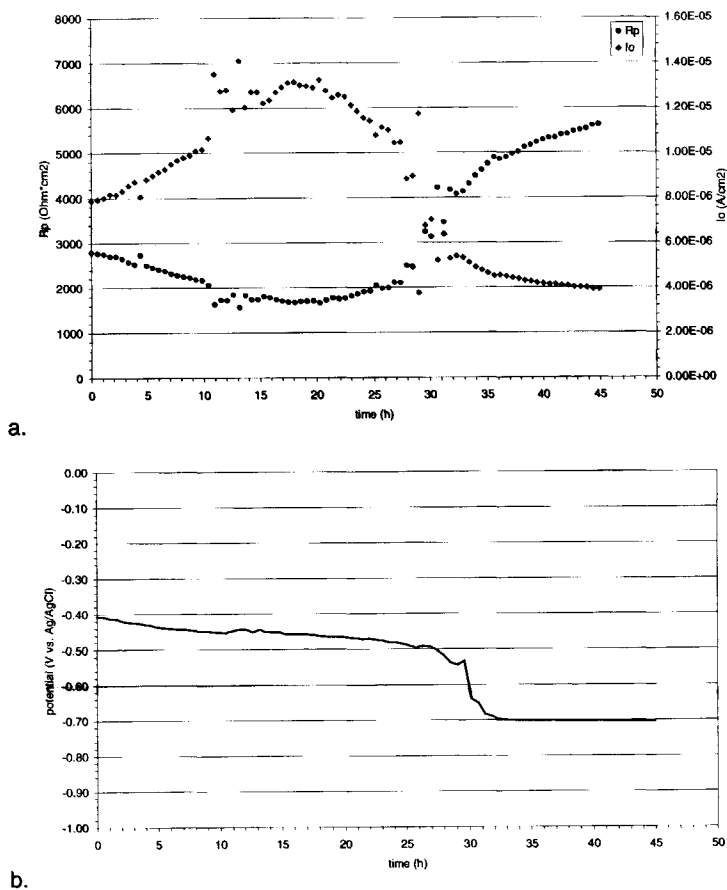


Figure 4.48: a. Development of polarisation resistance R_p and exchange current density I_o for carbon steel in 150ml 0.1 $MLiClO_4$ and 0.2g EPS5; b. Corrosion potential development

As a summary of these results, Table 4.4 lists characteristic values for corrosion potential E_{corr} and the polarisation resistance R_p . All EPS have shown a strong interaction with the carbon steel surface. In most cases not leading to a proper, uniform protective layer, but the surfaces were at least partially protected due to the interactions.

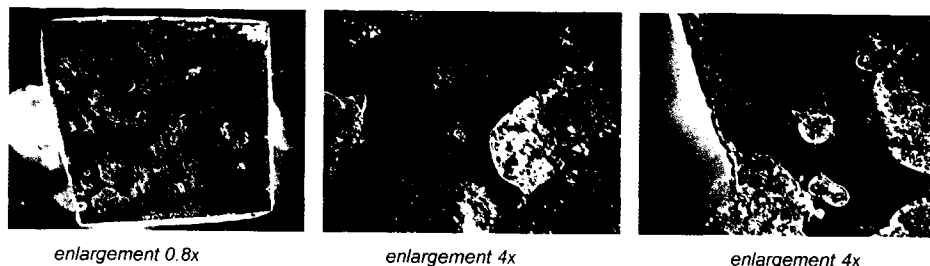


Figure 4.49: Pictures at different enlargements of the sample exposed to EPS5

Table 4.4: Characteristic values for E_{corr} and R_p obtained during the experiments.

Bacteria	Type of EPS	E_{corr} (mV vs. Ag/AgCl)	R_p ($k\Omega/cm^2$)
Reference	-	-700	1500
EPS1	heteropolysaccharide	Plateau at -450, afterwards -700	3,000 - 6,000
EPS2	heteropolysaccharide	-700	3,500
EPS3	heteropolysaccharide	-600	4,500
EPS4	homopolysaccharide	-120	70,000
EPS5	homopolysaccharide	Plateau at -400 Afterwards -700	2,000 - 5,000

4.4.4 General Discussion

As shown with the results presented in this section, bacterial polysaccharides are able to protect carbon steel from corrosion for a certain time period. Increases in the R_p indicate that corrosion resistance can increase 50 times relative to the value without adding the polysaccharides to the solution.

There is an apparent difference between the performance of homopolysaccharides and heteropolysaccharides. The homopolysaccharides build a black deposit layer, resembling a passive oxide layer. The heteropolysaccharides build a thick white layer more resembling a coating.

The results obtained here also showed that there was only a temporary effect. Localised corrosion occurred on all samples. This implies that the layers that formed are not suitable as a final coating layer. A combination with regular coatings is envisaged. The other option is, of course, to use the layers as pre-treatment layers. Due to the compact character of the homopolysaccharide layers, this is the best option for such pre-treatments.

4.5 Conclusions

The work reported in chapter 4 shows that it is possible to use biological processes in corrosion prevention strategies. Three different options were discussed which show possibilities for practical use.

It is apparent that most of the working principles rely on the action of extracellular polymeric substances. The formation of iron phosphates (section 4.2) is homogeneously spread over the surface, most likely due to the presence of bacterial products, which is apparent from the 10 wt% carbon in the layer.

In section 4.3, it was shown that a protective biofilm could be formed, but that the bacterial content should not be too high. Again the extracellular polymeric substances are responsible for the good layer formation.

In section 4.4 the use of extracellular polymeric substances produced *ex situ* was discussed. It was concluded that marked increases (up to 50 times improvement) of the corrosion resistance are possible. Especially homopolysaccharides show promise for practical use.

For the follow up of this work, it can be concluded that, since all options discussed point at the important influence of the bacterial products, the most promising route to follow is the *ex situ* production of bacterial products and to build protective pre-treatment layers with these products. The option to apply the products in coatings still remains possible but is further away from the actual application.

4.6 References

- 1 A. Pedersen, G. Hernandez-Duque, D. Thierry and M. Hermansson, Effects of biofilms on metal corrosion, Proceedings of the 2nd EFC Workshop on Microbial Corrosion, pp. 165-167
- 2 H.P. Volkland, H. Harms, K. Knopf, O. Wanner and A.J.B. Zehnder, Corrosion Inhibition of mild steel by bacteria, Biofouling, Vol. 15 No.4 (2000), pp. 287-297
- 3 A. Jayaraman, J.C. Earthman and T.K. Wood, Corrosion inhibition by aerobic biofilms on SAE 1018 steel, Applied Microbiological Biotechnology, Vol. 47 (1997) pp. 62-68
- 4 A. Pedersen and M. Hermansson, Inhibition of metal corrosion by bacteria, Biofouling, Vol. 3 (1991) pp. 1-11
- 5 V. Scotto and M.E. Lai, Correlation between marine biofilm structure and corrosion behaviour of stainless steel, Eurocorr '96, Nice, September 1996
- 6 W.H. Dickinson, Z. Lewandowski and R.D. Geer, Evidence for surface changes during ennoblement of type 316L stainless steel: dissolved oxidant and capacitance measurements, Corrosion Science, December 1996, pp. 910-920
- 7 K.K.W. Wong and S. Mann, Small scale structures in biomineralisation and biomimetic materials chemistry, Current Opinion in Colloid and Interfacial Science, Vol. 3 No. 1 (1998) pp. 63-68
- 8 A. M. Pritchard, Biofilms: Beneficent or Corrosive?, proceedings of the second COST 520 Workshop, 9-12 June 1999, Sion (Switzerland).
- 9 Comprehensive Treatise of Electrochemistry, Volume 10: Bioelectrochemistry, 1985, Plenum Press, New York
- 10 Wayne H. Dickinson, Frank Caccavo Jr., Bo Olesen and Z. Lewandowski, Ennoblement of stainless steel by the manganese-depositing bacterium *Leptothrix discophora*, Applied and Environmental Microbiology, July 1997
- 11 Z. Lewandowski, W. Dickinson and W. Lee, Electrochemical interactions of biofilms with metal surfaces, Water Science and Technology, Vol. 36 No. 1 (1997) pp. 295-302.
- 12 G.G. Geesey, L. Jang, J.G. Jolley, M.R. Hankins, T. Iwaoka and P.R. Griffiths, Binding of metal ions by extracellular polymers of biofilm bacteria, Water Science and Technology, Vol. 20 No. 11/12 (1988) pp. 161-165.
- 13 P. Linhardt, Manganoxidierende Bakterien und Lochkorrosion an Turbinenteilen aus CrNi-Stahl in einem Laufkraftwerk, Werkstoffe und Korrosion, Vol. 45 (1994) pp. 79-83.
- 14 E. McCafferty and D.C. Hansen, Corrosion inhibition of iron and aluminum by various naturally occurring biological molecules, Advances in Coating Technologies for Corrosion and Wear Resistant Coatings, TMS Annual Meeting, 1995, Warrendale (PA), USA, pp. 183-199
- 15 A. Jayaraman, A.K. Sun and T.K. Wood, Characterization of axenic *Pseudomonas fragi* and *Escherichia coli* biofilms that inhibit corrosion of SAE 1018 steel ST, Journal of Applied Microbiology, Vol. 84 No. 4 (1998) pp. 485-492
- 16 M.A. Khan, R.L. Williams and D.F. Williams, Corrosion behaviour of Ti-6Al-4V, Ti-6Al-7Nb and Ti-13Nb-13Zr in protein solutions, Biomaterials, Vol. 20 No. 7 (1999) pp. 631-637
- 17 A. Jayaraman, E.T. Cheng, J.C. Earthman and T.K. Wood, Axenic aerobic biofilms inhibit corrosion of SAE 1018 steel through oxygen depletion, Applied Microbiology and Biotechnology, Vol. 48 No. 1 (1997) pp. 11-17
- 18 J.S. Potekhina, N.G. Sherisheva, L.P. Povelkina, A.P. Pospelov, T.A. Rakitina, F. Warnecke and G. Gottschalk, Role of microorganisms in corrosion inhibition of metals in aquatic habitats, Applied Microbiology and Biotechnology, Vol. 52 No. 5 (1999) pp. 639-646
- 19 A. Jayaraman, D. Omek, D.A. Duarte, C.C. Lee, F.B. Mansfeld and T.K. Wood, Axenic aerobic biofilms inhibit corrosion of copper and aluminum, Applied Microbiology and Biotechnology, Vol. 52 No. 6 (1999) pp. 787-790
- 20 S. Douglas and T.J. Beveridge, Mineral formation by bacteria in natural microbial communities, FEMS Microbiology Ecology, Vol. 26 (1998) pp. 79-88
- 21 G. Chen, S.V. Kagwade, G.E. French, T.E. Ford, R. Mitchell and C.R. Clayton, Metal ion and exopolymer interaction: a surface analytical study, Corrosion Science, Vol. 52 No. 12 (1996) pp. 891-899
- 22 F.L. Roe, Z. Lewandowski and T. Funk, Simulating microbiologically influenced corrosion by depositing extracellular biopolymers on mild steel surfaces, Corrosion Science, Vol. 52 No. 10 (1996) pp. 744-752

- 23 K.O. Konhauser, Bacterial iron biomineralisation in nature, *FEMS Microbiology Reviews*, Vol. 20 (1997) pp. 315-326
- 24 S.C. Dexter and J.P. LaFontaine, Effect of natural marine biofilms on galvanic corrosion, *Corrosion*, Vol. 54 No. 11 (1998) pp. 851-861
- 25 C.G. Peng and J.K. Park, Principal factors affecting microbiologically influenced corrosion of carbon steel, *Corrosion*, Vol. 50 No. 9 (1994) pp. 669-675
- 26 G. Hernandez, V. Kucera, D. Thierry, A. Pedersen and M. Hermansson, Corrosion inhibition of steel by bacteria, *Corrosion*, Vol. 50 No. 8 (1994) pp. 603-608
- 27 V.K. Gouda, I.M. Banai, W.T. Riad and S. Mansour, Microbiologically induced corrosion of UNS N04400 in Seawater, *Corrosion*, Vol. 49 No. 1 (1993) pp. 63-73
- 28 K. Xu, S.C. Dexter and G.W. Luther, Voltammetric microelectrodes for biocorrosion studies, *Corrosion*, Vol. 54 No. 10 (1998) pp. 814-823
- 29 I.B. Beech, C.W. Sunny Cheung, C.S.P. Chan, M.A. Hill, R. Franco and A. Lino, Study of parameters implicated in the biodeterioration of mild steel in the presence of different species of sulphate-reducing bacteria, *International Biodeterioration and Biodegradation*, 1994, pp. 289-303
- 30 G. Chen, R.J. Palmer and D.C. White, Instrumental analysis of microbiologically influenced corrosion, *Biodegradation*, Vol. 8 (1997) pp. 189-200
- 31 Z. Lewandowski, Wayne Dickinson and Whonchee Lee, Electrochemical interactions of biofilms with metal surfaces, *Water Science and Technology*, Vol. 36 Bo. 1 (1997) p. 295-302.
- 32 W.H. Dickinson, F. Caccavo jr. and Z. Lewandowski, The ennoblement of stainless steel by manganic oxide biofouling, *Corrosion Science*, Vol. 38 No. 8 (1996) pp. 1407-1422
- 33 V. Zinkevich, I. Bogdarina, H. Kang, M.A.W. Hill, R. Tapper and I.B. Beech, Characterisation of exopolymers produced by different isolates of marine sulphate-reducing bacteria, *International Biodeterioration and Biodegradation*, 1996, pp. 163-172
- 34 Phosphating and Metal pre-treatment, D.B. Freeman, 1986, Woodhead-Faulkner Ltd., Cambridge UK
- 35 A. Mollica and A. Trevis, Correlation Between the Formation of Primary Film and Cathodic Modification on Stainless Steels Tested in Sea Water With Flow Rates of 0.3-5.2 m/s, Fourth International Congress on Marine Corrosion and Fouling. Centre de Recherches et d'Etudes Oceanographiques, Boulogne, France, 1976, pp. 351-365
- 36 R. Johnsen and E. Bardal, Cathodic properties of different stainless steels in natural seawater, *Corrosion*, Vol. 41, No. 5 (1985) pp. 296-305
- 37 B. Little and P. Wagner, The Involvement of a Thermophilic Bacterium in Corrosion Processes, *Corrosion*, Vol. 42 No. 9 (1986) pp. 533-536
- 38 S. Dexter and S. Lin, Calculation of seawater pH at polarized metal surfaces in the presence of surface films, *Corrosion*, Vol. 48, No. 1 (1992) pp. 50-60
- 39 S.C. Dexter and H.J. Zhang, Effect of biofilms on corrosion potential of stainless alloys in estuarine waters, 11th International Corrosion Congress, April 2-6, 1990, Florence, Italy, Vol. 4, pp. 4.333-4.340
- 40 S.C. Dexter and G.Y. Gao, Effect of seawater biofilms on corrosion potential and oxygen reduction of stainless steel, *Corrosion*, Vol. 44, No. 10 (1988) pp. 717-724
- 41 K.O. Konhauser and F.G. Ferris, Diversity of iron and silica precipitation by microbial mats in hydrothermal waters, Iceland: Implications for Precambrian iron formations, *Geology*, Vol. 24 (1996) pp. 323-326
- 42 F.G. Ferris, T.J. Beveridge and W.S. Fyfe, Iron-silica crystallite nucleation by bacteria in a geothermal sediment, *Nature*, Vol. 320 (1986) pp. 609-611
- 43 V. Scotto, The influence of marine aerobic microbial film on stainless steel corrosion behaviour, *Corrosion Science*, Vol. 25, No. 3 (1985) pp. 185-194
- 44 V. Scotto and M.E. Lai, The Ennoblement of Stainless Steels in Seawater, a Likely Explanation Coming From the Field, *Corrosion Science*, Vol. 40 No. 6 (1998) pp. 1007-1018
- 45 W.A. Ross, Improvements in preserving the surface of iron, steel, copper, brass and other metals or amalgams from being rusted or oxidised by exposure to water or damp air or perspiration, British patent, 1869
- 46 D.P. Kelly and A.P. Harrison, Genus *Thiobacillus*. In: *Bergey's Manual of Systematic Bacteriology*, Vol. 3 (1989) pp. 1842-1858

- 47 B.A. Boukamp, Manual AC-impedance data analysis system 'Equivalent Circuit', University of Twente, 1989, Enschede, The Netherlands
- 48 H.J.A. Breur, New prospects for rust converting agents in surface tolerant coatings, TNO-report No. CA/96.9930, 1996
- 49 H.J.A. Breur, J.H.W. de Wit, J. van Turnhout and G.M. Ferrari, Electrochemical Impedance Study on the Formation of Biological Iron Phosphate Layers, 5th International Symposium on Electrochemical Impedance Spectroscopy, June 2001, Marilleva, Italy



5 Conclusions and Future Research

The aim of this research was: *investigate the interactions between metals and the environment resulting in fouling and to use the knowledge obtained to develop methods to prevent the effects of fouling or turn fouling into a beneficial deposition process, resulting in methods to protect the materials.*

The research focussed on both biological and inorganic fouling processes. Biofouling sequence and seasonality were investigated with the aim to develop a general fouling model to help equipment users to use appropriate antifouling measures. Scaling and corrosion under scaling deposits were studied with the aim to develop corrosion monitoring strategies to mitigate the scaling. Finally, bacterial deposition processes were investigated in order to develop biological anticorrosion products.

Regarding the biofouling accumulation on surfaces, it can be concluded that:

- The general patterns of biofilm accumulation are valid throughout the year, with local and temporal differences.

The general sequence is bacterial colonisation, microbiological film build-up, and macrofouling, which occurred in all three locations in all experimental cycles. Depending on the time of year, different macrofouling species are present. Furthermore, growth followed s-curve growth kinetics, which is also expected within the general biofouling theory.

- The changes in biofouling development rate can accurately be described using the logistic growth model.

For the Den Helder case, the growth patterns were studied in more detail and it was shown that it is possible to describe the growth curves of eight fouling organisms using a model based on a combination of the logistic growth models for the separate organisms.

Validation of the models through another experimental cycle throughout a fouling season would be very useful. This would help to implement the models in practice.

Regarding the scaling and corrosion in heat exchangers, it can be concluded that:

- Electrochemical impedance spectroscopy is a useful tool to investigate these phenomena.

Strictly speaking, the technique of electrochemical impedance spectroscopy is only valid for stable or slowly changing systems. However, it turned out to be possible to detect pitting and describe the development of the scaling and corrosion processes qualitatively.

- EIS can be used for corrosion monitoring purposes for under deposit and pitting corrosion.

As was stated above, pitting and under deposit corrosion can be detected using EIS. The time constants with which these signals are present can easily be distinguished from the time constants arising from the other electrochemical contributions to the impedance signal. The detection of these time constants can therefore directly be used as a warning signal that corrosion is taking place.

For the practical implementation in accurate monitoring techniques, the measurements should also be carried out in practical cooling water circuits, in the main circuit or in a by-pass circuit. Furthermore, a corrosion detection strategy, simplifying the impedance analysis should be set-up and the measurement cycle should be limited to much less frequencies in order to be able to work with cheaper equipment.

Regarding new biological anticorrosives, it can be concluded that:

- Phosphating of steel can be performed using bacteria and the layers formed indeed show anticorrosive properties.

Phosphating was possible in a sterile medium as well, but in this case the process did not result in a homogeneous layer and much less anticorrosion activity was found. The mediation of the bacteria was necessary in this case to give a proper layer build-up.

- Aerobic bacterial biofilms can prevent corrosion if formed homogeneously, due to the presence of specific extracellular polymeric substances.

It was shown that the polarisation resistance of carbon steel increased markedly when a biofilm was formed on top, covering the surface entirely. The concentration of bacteria in the film is too low to be able to use up the oxygen in the film and therefore, the compounds present in the biofilm must have an active contribution.

- Bacterial extracellular polymers can form protective layers on carbon steel.

Five polysaccharides were tested for their corrosion inhibiting effect and all of them showed an anticorrosive effect. In all cases, a protective layer was formed on the surface during the exposition to a corrosive medium with polysaccharides added.

For the further development of biological anticorrosives, the exopolymers show the largest prospect. It is therefore suggested to focus on this approach for future work.

General Summary

Fouling occurs on almost any surface exposed to aqueous environments. Two of the negative effects which have been discussed within this PhD-thesis are biofouling (bacteria, barnacles, algae and mussels) on surfaces and in heat exchanger tubes in seawater and calcareous deposition (scaling) in fresh water heat exchangers. However, the fouling is not always negative. It has been possible to form anticorrosive layers from bacteria and their products. These types of processes have been captured by the word bioprotection. The research was divided in three separate chapters.

1. Biofouling on surfaces

Even though the general processes leading to a fully developed biofilm are known, much less is known about the influence of seasons and the comparison between different sites. To obtain a better view on these subjects, a study has been carried out in three different European locations, namely Scotland (Millport), Portugal (Cascais) and The Netherlands (Den Helder). The seasonality of the biofouling process has been investigated in order to deduce, in the end, a general model for biological fouling. Such a model can be very useful for users of equipment to estimate the degree of antifouling measures they should take to prevent the fouling process.

During the investigations, it has been possible to describe the biofouling processes of the Dutch location with one simple model (logistic growth). Eight species were dominantly present and for these organisms, modelling was carried out, also taking into account possible interactions between the growth of the different species.

2. Fouling in heat exchangers

Two specific cases of fouling in heat exchangers have been investigated, namely biological fouling in seawater heat exchangers and calcareous deposition processes in fresh water heat exchangers. The main problems arising from these fouling processes are respectively blocking of the tubes and corrosion underneath calcareous deposits.

Copper-Nickel alloys possess sufficient antifouling properties if they are used correctly. However, in practice the antifouling properties are annulled due to the galvanical coupling with other metals or due to cathodic protection systems. In some cases, this cannot be prevented. Therefore, the potential limits within which the alloys can be used to maintain sufficient antifouling properties have been investigated. Both laboratory trials and field experiments were carried out to find these limits.

Calcareous deposition (scaling) is mainly a problem because corrosion can take place underneath the scaling layers. To prevent these corrosion processes, the heat exchangers are cleaned regularly. Because any corrosion can be a problem (due to the localised character of the processes), one should be sure that no corrosion occurs at all. To obtain this knowledge, on-line corrosion monitoring systems are needed to accurately measure the onset of the corrosion. With such systems, cleaning intervals can be extended so that the overall cleaning costs would be decreases markedly. Therefore, these on-line corrosion monitoring systems have been investigated. It has been shown that electrochemical impedance spectroscopy can be a very useful technique in this case.

3. Bioprotection

Microbial growth is in general linked to the negative effects of microbial corrosion. However, from the literature it is known that bacterial biofilms can have a protective effect as well. Practical applications of such protective actions have not yet been achieved.

Three options were investigated to obtain corrosion protection based on bacteria and/or their products:

- **Biological phosphating**

It has been possible to deposit iron phosphates using bacterial processes. Even though no final conclusion can be drawn at this moment, strong clues exist that the bacteria produce a thin layer of organic material which regulates the formation of iron phosphates.

- **Bacterial biofilms**

Cases are known in which bacterial biofilms protect metals from corrosion. This can partially be explained by the use of oxygen by bacteria for their metabolic activity. However, this cannot explain the protective effect completely. It is suggested that some of the compounds present in the biofilm have an active contribution in the protection mechanism. Our research has shown that only a small fraction of bacteria within the biofilm is needed to obtain a protective effect, emphasising the importance of the bacterial products. The main important factor was that a stable, homogeneous biofilm was formed.

- **Biological anticorrosive additives**

Based on the suggestions that part of the protective action of biofilms is due to the compounds in the biofilm, several bacterial products have been investigated. Five different polysaccharides were produced and were tested for their effectivity to protect carbon steel in a corrosive medium. It can be concluded from these experiments that these compounds can have a strong anticorrosive effect. Dense layers are formed on the metal, preventing corrosion of the underlying metal.

Samenvatting

Aangroei in waterige milieus vindt plaats op vrijwel alle oppervlakken die in een dergelijk milieu worden geplaatst. Twee negatieve aangroeiprocessen die binnen dit proefschrift zijn behandeld zijn de biologische aangroei (waaronder bacteriën, zeepokken, algen en mosselen) op oppervlakken en in leidingen in zeewater en de kalkafzetting in zoetwater warmtewisselaars. De aangroeiprocessen zijn niet altijd negatief. Het is namelijk mogelijk gebleken corrosiewerende lagen op te bouwen uit bacteriën en bacteriële producten, deze processen hebben we gevangen onder de algemene term bioprotectie. Het onderzoek is beschreven in drie afzonderlijke hoofdstukken.

1. Biologische aangroei op oppervlakken

Alhoewel bekend is hoe een biologische aangroei laag gevormd wordt, is weinig bekend over de afhankelijkheid van dit proces van het seizoen en de vergelijking tussen verschillende locaties. Om hier een duidelijker beeld van te krijgen is op drie verschillende locaties in Europa, te weten Schotland (Millport), Portugal (Cascais) en Nederland (Den Helder), de seizoensafhankelijkheid van het aangroei proces onderzocht, om uiteindelijk te komen tot een algemeen model voor biologische aangroei. Een dergelijk model kan zeer nuttig zijn voor gebruikers van apparatuur om te bepalen hoe sterk de aangroei is in een bepaalde periode en in welke mate ze aangroeiwering toe moeten passen.

Het is tijdens dit onderzoek mogelijk gebleken met een eenvoudig basismodel (logistic growth) de aangroei processen van de Nederlandse plaats te beschrijven. Een achtal organismen was dominant aanwezig en voor deze organismen is de modellering uitgevoerd waarbij ook de mogelijke interacties tussen aangroei van de verschillende organismen is meegenomen.

2. Aangroei in warmtewisselaars

Twee specifieke gevallen van aangroei in warmtewisselaars werden onderzocht, te weten biologische aangroei in zeewaterwarmtewisselaars van koper-nikkel legeringen en kalkafzettingen in zoetwaterwarmtewisselaars. De belangrijke specifieke problemen in deze twee gevallen zijn respectievelijk het verstopen van de leidingen en corrosie onder de kalkafzettingen.

Koper-nikkellegeringen hebben, bij normaal gebruik, een afdoende aangroeiwerende werking. In de praktijk zijn er echter gevallen waarin de aangroeiwering teniet wordt gedaan doordat er koppelingen met andere metalen aanwezig zijn of door kathodische beschermingsystemen. In sommige gevallen is het niet mogelijk deze zaken te voorkomen. Er is onderzocht bij welke elektrochemische potentialen er aangroei op kan treden, zowel in laboratoriumexperimenten als in veldexperimenten om een veilig gebied af te bakenen waarbinnen koppelingen toegestaan kunnen worden zonder gevaar op aangroei te lopen.

Kalkafzetting in warmtewisselaars is met name een probleem omdat er onder de afzettingen corrosie op kan treden. Om de corrosie tegen te gaan worden de warmtewisselaars regelmatig schoongemaakt. De schoonmaakintervallen kunnen echter niet te lang zijn omdat men er zeker van wil zijn dat er geen corrosie optreedt. Er is daarom behoefte aan on-line corrosie monitoring methoden. Indien het moment waarop corrosie op gaat treden, nauwkeurig is vast te stellen, kan het schoonmaakinterval op veilige wijze vergroot worden. Dit zou een aanzienlijke kostenbesparing met zich meebrengen. Daarom werd er onderzoek gedaan naar de mogelijkheden corrosie onder kalkafzettingen te detecteren. Aangetoond is in dit onderzoek dat elektrochemische impedantiespectroscopie hiervoor een zeer nuttige techniek kan zijn.

3. Bioprotectie

Microbiële aangroei wordt in de meeste gevallen gekoppeld aan het negatieve effect in de vorm van microbiële corrosie. Uit literatuur is echter bekend dat er ook een beschermend effect vanuit kan gaan. Praktische toepassingen zijn er echter nog niet.

Een drietal mogelijkheden werd onderzocht om tot corrosiebescherming met bacteriën en/of hun producten te komen:

- Biologische fosfatering

Het is mogelijk gebleken ijzerfosfaten neer te slaan door middel van bacteriën. Alhoewel geen definitieve uitspraak kan worden gedaan, zijn er sterke aanwijzingen dat de bacteriën een dunne laag organisch materiaal produceren die op een heel gecontroleerde manier de ijzerfosfatering reguleren.

- Bacteriële biofilms

Alhoewel bacteriële biofilms in het algemeen microbiële corrosie veroorzaken, zijn er gevallen bekend waarin aërobe biofilms een anticorrosief effect hebben, dat deels toe is te schrijven aan het verbruik van zuurstof door de metabole activiteit van de biofilm. Dit kan echter niet volledig de corrosiewering verklaren. De stoffen aanwezig in de biofilm hebben een actieve bijdrage. Onderzocht is in hoeverre dit inderdaad het geval is. Gebleken is dat er slechts een kleine fractie bacteriën nodig is in de biofilm om corrosiewerende eigenschappen te verkrijgen. Belangrijk was vooral dat er een stabiele, homogene biofilm gevormd werd.

- Biologische anticorrosieve additieven

Gebaseerd op de aanwijzingen dat bacteriële producten anticorrosieve eigenschappen zouden kunnen hebben, zijn experimenten gedaan met een aantal van deze producten. Gekozen werd voor een aantal verschillende polysacchariden die door TNO Voeding geproduceerd werden. Op basis van deze experimenten, waarbij de activiteit van de stoffen onderzocht is in oplossing, kan geconcludeerd worden dat er daadwerkelijk een sterke anticorrosieve werking van dergelijke stoffen uit gaat. Hierbij wordt er een dichte laag gevormd op het metaal die corrosie weet te voorkomen.

Nawoord

Na circa vijf jaar onderzoek is mijn proefschrift af. Alhoewel dit natuurlijk een individueel stuk werk is, had het niet tot stand kunnen komen als het onderzoek niet in een team was gedaan. Ook de feedback tijdens het tot stand komen van het proefschrift was onmisbaar. Tot slot van dit proefschrift wil ik daarom stilstaan bij de mensen die het mij mogelijk hebben gemaakt dit proefschrift te schrijven.

Allereerst wil ik mijn directe collega's in Den Helder bedanken voor de prettige samenwerking, waarbij ik in het bijzonder Koos Overbeke wil noemen met wie ik niet alleen zeer prettig heb samengewerkt op het gebied van de aangroei en aangroeiwering, maar met wie ik met name ook de kamer heb gedeeld gedurende vier en een half jaar. Het was bijzonder prettig met hem in één kantoor te werken, aangezien we beiden de sociale aspecten die er, in onze ogen, bij het werk horen, naar voren konden brengen.

Daarnaast wil ik voormalig collega Erik van Westing en collega Anton Suurmond bedanken voor het feit dat zij me hebben ingewijd in de geheimen van de elektrochemische impedantiespectroscopie. Deze techniek is zeer belangrijk gebleken voor mijn onderzoek en dankzij de discussies over de fysische interpretatie van impedantiemetingen met Erik en de praktische hulp van Anton met apparatuur en programmatuur, ben ik in staat geweest de techniek op een nuttige wijze in te zetten.

Voor alles wat ik weet van (mariene) biologie ben ik dank verschuldigd aan collega Ritchie Head die me tijdens het eerste jaar op sleeptouw nam binnen het Europese BROS-project waarbinnen hij vanaf het eiland Cumbrae in Schotland me hielp met determinatie en interpretatie van onze gezamenlijke biologische experimenten.

Tot slot hebben vanuit de afdeling oppervlaktetechnologie diverse mensen een bijdrage geleverd aan deelonderzoeken, waarvoor ik hen natuurlijk dankbaar ben. Met name zijn hier nog Gabriele Ferrari en Ritchie Head te noemen voor hun begeleiding bij het schrijven van mijn proefschrift.

Verder wil ik mijn promotoren, Hans de Wit en Jan van Turnhout, bedanken voor het vertrouwen dat ze in mij gesteld hebben. Doordat ik mijn promotiewerk bij TNO in Den Helder heb uitgevoerd, is het contact tussen mij en mijn promotoren vrij onregelmatig geweest. Ondanks dat, heb ik altijd het gevoel gehad dat ze erop vertrouwden dat mijn promotie goed verliep. Daar waar nodig zocht ik contact met hen en konden ze me op de juiste wijze begeleiden.

Tot slot ook een woord van dank voor de hulp die ik, waar dat nodig was, heb gekregen vanuit de vakgroepen Elektrochemie en Corrosie en Polymeertechnologie van de TU Delft en vanuit andere afdelingen binnen TNO, met name Industrie, Voeding en TPD.

Delen van het onderzoek in dit proefschrift zijn tot stand gekomen met cofinanciering van de Europese Commissie (hoofdstuk 2), het Ministerie van Economische Zaken (hoofdstuk 3) en het e.e.t. subsidieprogramma van de ministeries Economische Zaken, VROM en OC&W (hoofdstuk 4). Ik wil deze instanties dan ook bedanken voor de financiële steun.

Curriculum Vitae

Rik Breur werd geboren op 4 juli 1972 in Arnhem. Na twee maanden verhuisde hij met zijn ouders en broer naar Dordrecht waar hij opgroeide (met na vier jaar een broertje erbij). In Dordrecht bezocht hij het Christelijk Lyceum waar hij het Gymnasium deed tot en met de vierde klas, waarna hij een achttal vakken koos waar de klassieke talen niet meer bij pasten.

Na zijn slagen voor het VWO in 1996 startte hij met de studie Materiaalkunde aan de Technische Universiteit Delft. In zijn derde jaar nam hij deel aan het bestuur van studievereniging Tubalkain en organiseerde hij de grote buitenlandexcursie naar het Verenigd Koninkrijk. Verder was hij onder andere actief binnen de orgelfondslustrumcommissie ter viering van het zevende Orgelfonds lustrum.

In zijn vijfde jaar deed Rik een bedrijfstage in België bij het Centre de Recherche Shell Louvain-la-Neuve (CRCSL) waar hij onderzoek deed naar afschuifspanninggeïnduceerde kristallisatie van polyetheen. Aansluitend aan deze stage deed hij zijn afstudeerwerk binnen de vakgroep Polymeertechnologie onder professor Van Turnhout. Dit afstudeerwerk werd uitgevoerd bij TNO Industrie in Den Helder en had als onderwerp het gebruik van roestvormers in oppervlaktetolerante coatings.

In 1992 besloot hij naast de studie Materiaalkunde de studie Chemische Technologie aan te vangen om meer chemische kennis te verkrijgen, met name op het gebied van organische chemie en polymeerchemie. Deze studie heeft Rik (nog) niet volledig volbracht, maar de gewenste bredere chemische kennis op genoemde gebieden is zeker vergaard.

Na zijn studietijd van zes jaar startte hij een promotieonderzoek bij TNO Industrie, wederom in Den Helder waarvan dit proefschrift het resultaat is. Het promotieonderzoek zou zich in eerste instantie vooral richten op microbiële corrosie, maar door de constructie waarin Rik onder TNO contract stond en daarom binnen TNO projecten zijn werk deed, verschoof de aandacht enigszins naar het bestuderen van aangroeiprocessen, het weren van aangroei en het gebruiken van aangroei als beschermende laag.

Op dit moment is Rik werkzaam bij de afdeling Oppervlaktebescherming van TNO Industrie, waar hij met name verantwoordelijk is voor het onderzoek op het grensvlak tussen biologie en materialen en het onderzoek naar organische anticorrosieve coatings.